COMPUTER AIDED THERMAL CREEP ANALYSIS OF CONCRETE CONTINUA

by

Dipl.Ing.

HEIKO GROSS

A thesis submitted for the degree of

Doctor of Philosophy

in the Faculty of Engineering

of the University of London

Imperial College of Science

and Technology, London

February, 1973

ABSTRACT

The work set out in this thesis investigates matrix-theoretically the problem of thermal creep in the structural analysis of concrete continua. Since the structural engineer who is a computer expert is still an outsider, a thorough appraisal of the structural analysis and the validity of the computer techniques contrived for this purpose is made. The interfaces between the mathematics, matrix theory and computer programming involved are discussed.

The insolubility of the differential equations as formulated in the infinitesimal approach to structural analysis is surmounted by the employment of numerical methods in conjunction with a high-speed digital computer. Guidelines for implementing established finite element and finite difference techniques in a mixed method of approach to the computer-aided analysis of elastic, thermoelastic and isothermal or transient thermoviscoelastic axisymmetric stress problems as encountered in the design of prestressed concrete reactor pressure vessels are given.

Three creep testing machines were designed and constructed to ensure the imposition of stable mechanical and thermal boundary conditions during the experimental investigation. The main objective was to record isothermal creep strains developing in concrete specimens subjected to moderate and high stresses and temperatures. The superposition hypothesis as a technique for the reduction of thermal creep strains to linear thermoviscoelastic ones is corroborated experimentally.

The creep curves obtained and other physical characteristics of concrete are fitted by optimal formulae. The theoretical reproduction of relaxation curves is performed to overcome the contrariness between creep and relaxation as regards their suitability as objects of experimental and theoretical investigations. The history-dependent integrals for the computation of thermal relaxation weighting factors are evaluated.

Complex case studies are carried out. To make convincing representation of the numerical results, stress and temperature fields are graphically displayed as contours or isometric surfaces using computer plotting facilities.

ACKNOWLEDGEMENT

The author thanks Professor A.L.L. Baker for the opportunity to undertake this study in the Concrete Structures and Technology Section of the Department of Civil Engineering at Imperial College. His kindness will be remembered.

The author thanks Dr. P.J.E. Sullivan for supervising the project. His constant concern and his valuable guidance are gratefully acknowledged.

The author thanks the members of staff of the Imperial College Computer Centre for their advice and generous allocation of computing time, and the members of staff of the Civil Engineering Departmental Workshop and Concrete Laboratory for their help in constructing the testing machines and in preparing the tests.

The author thanks the authorities of the Building Research Station in the Department of the Environment, U.K., for sponsoring the project.

The author thanks his sister Elke and his brother Uwe for their unfailing encouragement and understanding, his ex-girlfriend Liz for watching over the English style and Miss M. Ming for making such a success of typing the difficult manuscript.

The author thanks Dr. Ing. Th. Jaeger for suggesting studies in England, and his international co-students for creating such a sociable and stimulating working atmosphere.

CONTENTS

ABSTRACT		i
ACKNOWLEDGEMENT		ii
CONTENTS		iii
LIST OF PLATES AND FIGURES		vi
CHAPTER I :	INTRODUCTION	
1.1.	General	1
1.2.	Objectives	2
CHAPTER II :	THE PHENOMENON OF THERMAL CREEP IN CONCRETE	
2.1.	The creep-relaxation duality	5
2.2.	Definition of thermal creep compliance	5
2.3.	Definition of thermal relaxation modulus	6
2.4.	Definition of thermoviscoelasticity	6
2.5.	The superposition hypothesis	7
2.6.	Phenomenological characteristics	8
2.7.	Experimen-theory contradiction	9
2.8.	Conclusions	10
CHAPTER III :	PROPOSED CREEP TESTING MACHINE	
3.1.	Purpose	11
3.2.	Description of design	11
3.3.	Design drawings	21
3.4.	Design criteria	21
3.5.	Proving tests	37
CHAPTER IV :	NON-VISCOUS PROPERTIES OF CONCRETE AT AMBIENT TEMPERATURE	
4.1.	Objective	42
4.2.	Materials	42
4.3.	Fabrication	43
4.4.	Curing	43
4.5.	Shape criteria	44
4.6.	Drying shrinkage	44
4.7.	Moisture loss	46
4.8.	Cold strength	50

CHAPTER V : THERMAL CREEP CHARACTERISTICS OF CONCRETE SPECIMENS

5.1. Objective 53
5.2. Recorded creep strains 53
5.3. Thermoelastic strains 66
5.4. Ultimate thermal strains 67
5.5. Modulus of thermoelasto-plasticity 70
5.6. Modulus of quasi-thermoelasto-plasticity 73
5.7. Ultimate hot cylinder strength 77
5.8. Normalized creep profiles 77
5.9. Thermally induced shrinkage strains 83
5.10. Conclusions 86

CHAPTER VI : SMALL DISPLACEMENT THEORY OF ELASTIC CONTINUA

6.1. Introduction 88
6.2. Three-dimensional continua under spatial deformation 91
6.3. Cylindrical continua under combined torsional and axisymmetric deformation 102
6.4. Conclusions 111

CHAPTER VII : VARIATIONAL ANALYSIS OF COMBINED ELASTIC AND THERMOELASTIC CONTINUA

7.1. Introduction 114
7.2. Principles in the analytic formulation of the thermoelastic problem 119
7.3. Functionals in the analysis of thermoelastic continua 127
7.4. Conclusions 140

CHAPTER VIII: FINITE ELEMENT MATRIX ANALYSIS OF ELASTIC AXISYMMETRIC CONTINUA

8.1. Introduction 141
8.2. The classical deformation modes concept 144
8.3. The natural deformation modes concept 153
8.4. Conclusions 176

CHAPTER IX : COMPUTER AIDED ELASTIC ANALYSIS OF AXISYMMETRIC CONCRETE CONTINUA

9.1. Purpose 178
9.2. Computer programs 178
9.3. Case study 179
9.4. Graphical display of results 181
9.5. Suitability criteria 208
9.6. Outlook 211

CHAPTER X : FINITE DIFFERENCE ANALYSIS OF THERMOVISCOELASTIC AXISYMMETRIC CONTINUA

10.1. Introduction 212
10.2. Transient temperature distribution 214
10.3. Creep-relaxation duality 219
10.4. Convolution integral of strain history 222

CHAPTER XI : THERMOVISCOELASTIC ANALYSIS OF AXISYMMETRIC CONCRETE CONTINUA USING THERMAL RELAXATION WEIGHTING FACTORS

11.1. Objective 227
11.2. Shape optimization of creep profiles 227
11.3. Numeric regression of creep data 236
11.4. Thermal relaxation weighting factors 250
11.5. Computer program THERMO AXICON 254
11.6. Conclusions 257

CHAPTER XII : CONCLUSIONS AND RECOMMENDATIONS FOR FUTURE RESEARCH

12.1. General conclusions 261
12.2. Recommendations for future research 272

APPENDIX I : LIST OF REFERENCES 275
APPENDIX II : FLOW CHART OF COMPUTER PROGRAM 286
APPENDIX III: LIST OF MACHINE PARTS 291
APPENDIX IV : FORMATION OF STIFFNESS MATRICES 295
APPENDIX V : FORMATION OF CONDUCTIVITY MATRIX 303
APPENDIX VI : TABLES OF CREEP DATA AND WEIGHTING FACTORS 305

LIST OF PLATES AND FIGURES

Plate 1	General view of creep testing machine	16
Plate 2	Yoke system and strain measuring device	17
Plate 3	Loading jack, suspensions and weights	18
Plate 4	Control and monitoring units	19
Plate 5	Scanner unit for transducers and thermocouples	20
Fig. 3.1	End elevation of creep testing machine	24
Fig. 3.2	Front elevation of creep testing machine	25
Fig. 3.3	Plan of creep testing machine	26
Fig. 3.4	Fulcrum of lever arm system	27
Fig. 3.5	Front hanger and upper universal joint	28
Fig. 3.6	High temperature resistant yoke system	29
Fig. 3.7	Lower universal joint and link	30
Fig. 3.8	Rear hanger and suspension	31
Fig. 3.9	7" bore three zone furnace	32
Fig. 3.10	Strain measuring device and tranducer	33
Fig. 3.11	Plan of load jack	34
Fig. 3.12	Positioning of collars of device on specimen	35
Fig. 3.13	Mechanical system of creep testing machine	36
Fig. 3.14	Proving test on lever arm system	39
Fig. 3.15	Proving test on transducer	40
Fig. 4.1	Drying shrinkage in concrete test cylinders	45
Fig. 4.2	Scatter of shrinkage readings for Series N	47
Fig. 4.3	Scatter of moisture loss readings for Series N	48
Fig. 4.4	Moisture loss due to air drying	49
Fig. 4.5	Distribution curve for strength of concrete cubes	51
Fig. 4.6	Cylinder strength of concrete for Series J	52
Fig. 4.7	Cube strength of concrete for Series N	53
Fig. 4.8	Cube strength of concrete for Series F	54
Fig. 4.9	Cylinder strength of concrete for Series N	55
Fig. 4.10	Cylinder strength of concrete for Series F	56
Fig. 4.11	Ratio of cylinder to cube strength for Series N and F	57

Fig. 5.1	Low temperature creep for stress/ cold strength ratios of 0.2 and 0.66	61
Fig. 5.2	Low temperature creep for a stress/ cold strength ratio os 0.4	62
Fig. 5.3	High temperature creep for a stress/ cold strength ratio of 0.2	63
Fig. 5.4	High temperature creep for a stress/ cold strength ratio of 0.4	64
Fig. 5.5	High temperature creep for a stress/ cold strength ratio of 0.66	65
Fig. 5.6	Initial and recovered thermoelastic strains	68
Fig. 5.7	Total thermal strains after seven days under load	69
Fig. 5.8	Load-dependent initial thermoelastic strains	71
Fig. 5.9	Relative initial modulus of thermoelasto-plasticity	74
Fig. 5.10	Temperature-dependent cylinder strength	76
Fig. 5.11	Low temperature creep normalized to a stress/ cold strength ratio of 0.2	78
Fig. 5.12	High temperature creep normalized to a stress/ cold strength ratio of 0.2	79
Fig. 5.13	Limits for ultimate thermoelastic strains	80
Fig. 5.14	Limits for ultimate stress/ cold strength ratios	81
Fig. 5.15	Thermoelastic strains normalized to a stress/ cold strength ratio of 0.2	82
Fig. 5.16	Thermal shrinkage strains	84
Fig. 5.17	Temperature-dependent stress-strain curves	85
Fig. 6.1	Direct stress and body pressure components for three-dimensional analysis	93
Fig. 6.2	Shear stress components for three-dimensional analysis	93
Fig. 6.3	Positive displacements and angles of rotation for three-dimensional analysis	95
Fig. 6.4	Transformation of shear stress resultants for three-dimensional analysis	95
Fig. 6.5	Direct stress and body pressure components for axisymmetric analysis	103

Fig. 6.6	Shear stress components for three-dimensional analysis	103
Fig. 6.7	Positive displacements and angles of rotation for the deformation of aplane in polar coordinates	107
Fig. 8.1	Cross-sectional geometry and unit displacement components for the TRIAX 3 element	145
Fig. 8.2	Mode shapes for the elastic and rigid body displacements of the TRIAX 3 element	145
Fig. 8.3	Cross-sectional subdivision and cartesian displacement components for the TRIAX 6 element	154
Fig. 8.4	Cross-sectional subdivision and natural displacement components for the TRIAX 6 element	154
Fig. 8.5	Natural component stress and natural component strain for the TRIM 3 element	161
Fig. 8.6	Natural component stress and total natural strain for the TRIM 3 element	161
Fig. 8.7	Direction cosines for the TRIM 3 element	165
Fig. 8.8	Natural deformation mode $\underline{u}_i$ for the TRIM 6 element	165
Fig. 8.9	Integration over TRIM 6 element using non-dimensional coordinates	165
Fig. 8.10	Natural deformation mode $\underline{u}_i$ for the TRIAX 6 element	170
Fig. 9.1	Silhouette of upper half of concrete pressure vessel	182
Fig. 9.2	Silhouette of longitudinal cross-section of concrete pressure vessel	182
Fig. 9.3	Topological mesh for axisymmetric analysis using TRIAX 3 elements	184
Fig. 9.4	Geometrical mesh for axisymmetric analysis using TRIAX 3 elements	185
Fig. 9.5	Topological mesh for axisymmetric analysis using TRIAX 6 elements	186
Fig. 9.6	Geometrical mesh for axisymmetric analysis using TRIAX 6 elements	187

Fig. 9.7	Contours of elastic radial stresses using TRIAX 3 elements	189
Fig. 9.8	Contours of elastic radial stresses using TRIAX 6 elements	190
Fig. 9.9	Contours of elastic axial stresses using TRIAX 3 elements	191
Fig. 9.10	Contours of elastic axial stresses using TRIAX 6 elements	192
Fig. 9.11	Contours of elastic shear stresses using TRIAX 3 elements	193
Fig. 9.12	Contours of elastic shear stresses using TRIAX 6 elements	194
Fig. 9.13	Contours of elastic hoop stresses using TRIAX 3 elements	195
Fig. 9.14	Contours of elastic hoop stresses using TRIAX 6 elements	196
Fig. 9.15	Contours of elastic major principle stresses using TRIAX 3 elements	197
Fig. 9.16	Contours of elastic major principle stresses using TRIAX 6 elements	198
Fig. 9.17	Contours of elastic minor principle stresses using TRIAX 3 elements	199
Fig. 9.18	Contours of elastic minor principle stresses using TRIAX 6 elements	200
Fig. 9.19	Surface of elastic radial stresses using TRIAX 3 elements	202
Fig. 9.20	Surface of elastic radial stresses using TRIAX 6 elements	202
Fig. 9.21	Surface of elastic axial stresses using TRIAX 3 elements	203
Fig. 9.22	Surface of elastic axial stresses using TRIAX 6 elements	203
Fig. 9.23	Surface of elastic shear stresses using TRIAX 3 elements	204
Fig. 9.24	Surface of elastic shear stresses using TRIAX 6 elements	204
Fig. 9.25	Surface of elastic hoop stresses using TRIAX 3 elements	205

Fig. 9.26	Surface of elastic hoop stresses using TRIAX 6 elements	205
Fig. 9.27	Surface of elastic major principle stresses using TRIAX 3 elements	206
Fig. 9.28	Surface of elastic major principle stresses using TRIAX 6 elements	206
Fig. 9.29	Surface of elastic minor principle stresses using TRIAX 3 elements	207
Fig. 9.30	Surface of elastic minor principle stresses using TRIAX 6 elements	207
Fig. 9.31	Surface polynomial for elastic axial stresses	209
Fig. 10.1	Finite difference approximation to time-dependent thermal gradients	215
Fig. 10.2	Finite difference approximation to time-dependent temperature values	215
Fig. 11.a	Normalized age and time-dependent creep surface fitted by parametric polynomials	230
Fig. 11.b	Thermal creep and relaxation curves fitted by simple exponential functions	232
Fig. 11.1	Rate of change in creep in double logarithmic scale	234
Fig. 11.2	Temperature-dependent parameters of proposed creep formula	237
Fig. 11.3	Stress-dependent parameters of proposed creep formula	239
Fig. 11.4	Thermoviscoelastic characteristics of concrete at 20^{0}C	241
Fig. 11.5	Thermoviscoelastic characteristics of concrete at 40^{0}C	242
Fig. 11.6	Thermoviscoelastic characteristics of concrete at 60^{0}C	243
Fig. 11.7	Thermoviscoelastic characteristics of concrete at 80^{0}C	244
Fig. 11.8	Thermoviscoelastic characteristics of concrete at 110^{0}C	245
Fig. 11.9	Thermoviscoelastic characteristics of concrete at 140^{0}C	246

Fig. 11.10	Thermoviscoelastic characteristics of concrete at 200°C	247
Fig. 11.11	Thermoviscoelastic characteristics of concrete at 250°C	248
Fig. 11.12	Thermoviscoelastic characteristics of concrete at 300°C	249
Fig. 11.13	Thermal relaxation weighting factors in semi-logarithmic scale	251
Fig. 11.14	Temperature distribution after 1 day	255
Fig. 11.15	Temperature distribution after 10 days	255
Fig. 11.16	Temperature distribution after 100 days	256
Fig. 11.17	Temperature distribution at infinity	256

CHAPTER I

INTRODUCTION

1.1. GENERAL

Axisymmetric or spherical concrete structures designed with tensioned or non-tensioned steel reinforcement are used in civil engineering practice as reactor pressure vessels, containers for chemicals, water towers or reservoirs, submarine oil tanks, caissons, bunkers, air-raid shelters, silos, cupolas, lighthouses, industrial chimneys and television aeria masts.

The stress analysis presented in this thesis was developed primarily to suit this type of continuous structures. In addition, however, a first approximate solution may be obtained for stress analysis problems of reactor pressure vessels with boilers contained in the wall and some multi-storey buildings if an axis of revolution is defined. As regards future developments, the design of in-situ built multi-purpose submarine reservoirs may be considered.

With the fast development of prestressed concrete pressure vessels for nuclear power stations in the late 1950's and the growing concern about the safety of building structures against fire hazards, interest has increased in the knowledge of the behaviour of concrete at elevated and high temperatures and its effects on the strain history of loaded structures.

Since the complex configurations of the above mentioned structures render the mixed elliptic and parabolic partial differential equations of the stress analysis problem insoluble in the closed form, techniques for numerical analyses suitable for computer programming are required.

The solution of the problem set out in this thesis is brought about by the development of computer programs in which the thermoviscoelastic, thermoelastic or elastic stresses arising are determined in the space variables using iterative finite element methods and in time using marching finite difference techniques. The change in the structures' stiffness matrix due to ambient or thermal creep effects is accounted for by the employment of thermal relaxation weighting factors

which are arrived at in a rigorous mathematical procedure and valued on the basis of the data obtained from experiments performed for thermal creep compliance.

1.2. OBJECTIVES

The foregoing objectives are achieved by first reviewing the nature of the dialectically interacting phenomena of creep and relaxation in Chapter II and by particularizing the characteristics of the proposed experimental and analytic approach to the thermoviscoelastic problem in concrete continua.

The testing machines built to enable the experimental investigation into the problem of thermal creep are described in Chapter III. The details of their design are documented on twelve size A1 workshop drawings; for the benefit of the reader, however, scaled down versions of the drawings are presented. In these, the machine parts are identified by numbers which refer to a relevant description given in Appendix III.

In Chapter IV, the preliminary tests on the ageing concrete are reported. The development of shrinkage strains, moisture loss and strength characteristics are studied mainly to determine the instant after which age has a negligible effect on the behaviour of the concrete during the tests proper.

The data obtained for the creep deformation of the concrete test cylinders subjected to various stress levels and isothermal temperature regimes between 20 and 600^{0}C, are recorded in Chapter V. The evaluation of the creep tests in form of parameter studies is here carried out to a point, where the reduction of the thermal creep problem to a linear thermoviscoelastic problem is recognized and the applicability of the superposition hypothesis for time-dependent strains may be enjoyed. The original data are listed in Appendix VI.

To prepare the ground for the thermoviscoelastic stress analysis of three-dimensional and axisymmetric continua the small displacement theory and the concept of linear elasticity are recapitulated in Chapter VI. The elliptic partial differential equations which express the structural compatibility under elastic deformation in closed form are

arrived at, but found to be insoluble.

Consequently, in Chapter VII, energy principles in conjunction with variational methods are drawn upon to transform the governing differential equations into integral expressions which may be minimized with respect to the displacement or the temperature field variable, respectively. The uncoupling of the field variables from the sets of space-dependent stiffness and conductivity functions, however, is not possible.

These limitations are surmountable by the implementation of finite element techniques and thus, in Chapter VIII, the classical and the nature deformation modes concepts of the matrix displacement method are expounded. With axisymmetric geometries in mind, ring-shaped elements of triangular cross-section are employed. For continuity, the matrix equations are written in concise symbolic form, leaving the formation of the matrix coefficients for Appendix IV.

For comparison and mutual check of their applicability to the elastic stress problem, two computer programs based on the classical and the natural modes concept, respectively, are implemented in Chapter IX, analysing the behaviour of an axisymmetric concrete pressure vessel subjected to a typical loading case. The resulting stress fields are graphically displayed and evaluated by virtue of contour and surface plotting routines designed for this purpose .

Proceeding from the theory of thermoelasticity, in Chapter X the structural problem is solved in the time variable by employing finite difference techniques. The governing matrix equations are established for the heat conduction problem, the thermoviscoelastic stress analysis problem and the creep-relaxation conversion.

In Chapter XI, the theory of thermoviscoelasticity is reconciled with the experimental data obtained. Formulae for the development of thermal creep strains are originated, permitting the proposed thermal relaxation weighting factors to be determined numerically. Considering the axisymmetric concrete pressure vessel described, the thermoviscoelastic stress fields arising from the enforced compatibility of differential

thermal expansions due to transient temperature fields are analysed and displayed for various time instants. The flow chart of the underlying computer program is given in Appendix II.

The conclusions drawn and the recommendations made for future research form the objective of Chapter XII. The references drawn upon are listed in Appendix I.

CHAPTER II

THE PHENOMENON OF THERMAL CREEP IN CONCRETE

2.1. THE CREEP-RELAXATION DUALITY

The natural phenomena of creep and relaxation manifest themselves in evolutionary processes, i.e. the responses they describe when material is acted upon by external agents develop as functions of time and history ([34], [40], [45], [47], [49], [76], [91], [92], [108], [109], [113]). Like other evolutionary processes in the real world, they are incapable of being formulated in exact scientific language as suitable rheological models are not yet available ([13], [14], [15], [16], [38], [65], [94], [114], [iii]).

The complexity of the problem of thermoviscoelasticity has its origin in the duality of the creep and relaxation phenomena ([28], [45], [55], [63], [69], [73], [90], [110], [iv], [v]). Strictly speaking, the thermoviscoelastic process unfolds dynamically in conformity with the dialectic interaction between the polarized responses from creep and relaxation which are highly interdependent. In other words, the effects emerging from the two phenomena occur simultaneously. Consequently, the true analysis of structures should incorporate concepts for both the variation of strains under prescribed stress system ([9], [10], [33], [34], [39], [56], [59], [66], [108]) and the variation of stresses under prescribed strain systems ([55], [64], [69], [105], [106]) However, such an analysis is impracticable.

Realizing, though, that in real life any process is dynamic, i.e. a time and history-dependent response between action and reaction systems, the standard tool of dialectics may be utilized to analyse the movements of the creep and relaxation processes within their boundaries. This implies that for mathematical and experimental ease, the creep and relaxation phenomena are uncoupled by suppressing the one, viz. keeping constant its representative statical entity, in order to investigate the other ([45], [47], [90]).

2.2. DEFINITION OF THERMAL CREEP COMPLIANCE

With the dependence on feasible testing procedures in

mind, thermal creep compliance may be conveniently defined as the temperature, age and time-dependent strain occurring after the instantaneous application of a fixed load to a concrete specimen or structure at time zero, in excess of the strain detected in an unloaded and heated companion specimen or structure ([23], [54], [61], [67], [72], [74], [93], [96], [97], [98], [100], [103]).

More accurately, really, thermal creep should be reckoned as the strain in excess of the shrinkage strain strains due to the coefficient of thermal expansion elastic strain which changes in time according to the dependence of the elasticity on the prevailing temperature and the time under load ([9], [76]). For analytic purposes, the former definition suffices.

2.3. DEFINITION OF THERMAL RELAXATION MODULUS

With relaxation being coupled to creep by the dialectic principle, its definition follows logically from the inverse of the above formulation. In other words, thermal relaxation constitutes the temperature, age and time-dependent reduction in stress, occurring after the instantaneous imposition of a fixed strain onto a concrete specimen or structure at time zero ([76], [106], [110]).

Changes in stress due to prescribed geometric displacements, or redistributions of stresses within composite sections of concrete and steel due to prescribed strain conditions, which may represent either constant strains or compatible deformations, thus constitute genuine relaxation problems ([17], [21], [33], [52], [68], [70], [90], [95], [105], [106], [107]).

Also, relaxation responses develop much faster than creep responses, hence substantiating that stress analyses based on relaxation functions are more suitable for the life-like reproduction of the structure's behaviour ([45], [90], [106]).

2.4. DEFINITION OF THERMOVISCOELASTICITY

The theory of thermoviscoelasticity comprises the analytic investigation into temperature, age and time-dependent material responses brought about by both the phenomenon of creep and relaxation, under the exclusion of plastic i.e. non-

linear stress-dependent effects ([35], [38], [45], [69], [70], [73], [76], [89], [105], [110]). The external agents which are the creep-inducing stress and the relaxation-inducing strain, thus activate initial responses which are elastic.

If linear thermoviscoelastic strains are mentioned, it implies that not only the initial but also the time-dependent responses are linear in the stress variable ([33], [38], [60], [70], [76], [89]). As a result, all strain responses may be superimposed, rendering the sequence of load applications immaterial.

2.5. THE SUPERPOSITION HYPOTHESIS

As regards the ascertainment of stress and strain fields for service loads, the structural analysis is based on the small displacement theory and the concept of linear elasticity, thus inviting the employment of the superposition hypothesis ([32], [33], [70], [89], [102], [106], [110]). It states that the total effect of prescribed statical disturbances on any force or displacement component may be obtained by the superposition of the individually determined contributions ([25], [60]). The superposition is justified owing to the linearity of all equilibrium, constitutive and compatibility equations.

These equations are independent of the time of load application and the duration under load, in this way rendering the time variable unnecessary for the application of the hypothesis to elastic structures. Thus, whenever sets of simultaneous linear equations are encountered, the time-invariant superposition hypothesis forms an underlying premise.

If histories of linear thermoviscoelastic strains which by definition are proportional to the creep-inducing stress, are analysed, the superposition hypothesis is broadened inasmuch as various states of loading and deformation may be superimposed also with reference to their initiation ([25], [38], [45], [60], [70], [76], [106]).

Considering the effect of each statical disturbance on any force or displacement component, thus the time of the perturbation and its duration must be accounted for in order to analyse the total effect due to the sum of all causes correctly.

A severe limitation of the superposition hypothesis which also has a bearing on the type of tests to be performed, is constituted by its impossibility to superimpose history - dependent transient thermal effects. In order not to violate the superposition hypothesis, transient thermal conditions must be treated as step-wise quasi-isothermal. In other words, if a transient thermoviscoelastic solution is required at a time instant t, it must be assumed that the strain in each individual element of the body has developed under isothermal conditions; the value being given by the temperature T(t) momentarily existing in that element.

It follows that data obtained from tests on creep or relaxation under transient temperature regimes, though useful for the verification of theoretical results, do not lend themselves directly to mathematically rigorous stress analyses.

2.6. PHENOMENOLOGICAL CHARACTERISTICS

Although it is desirable to base the constitutive equation of concrete on the understanding of the processes in the microstructure of the cement paste ([11], [12], [14], [18], [19], [31], [50], [57], [71], [75], [87], [88]), for the purpose of structural analysis, the complex behaviour of concrete first requires a research programme carried out which investigates thermal creep and relaxation on the phenomenological level ([43], [47]).

This implies that the thermoviscoelastic response functions will only be formulated in terms of their main physical variables temperature, age, time and, if creep strains are investigated, stress/ cold strength ratio. In this way, experimental data of practical nature are produced which enable the completion of realistic design analyses.

Experiments on thermoviscoelasticity must be carried out under conditions which make it possible for the researcher to analyse the theoretical model for its evolution ([43], [47]). Depending on whether the analytic approach requires the knowledge of strain or stress histories, experiments on isothermal creep or relaxation need to be devised.

2.7. EXPERIMENT-THEORY CONTRADICTION

From previous research and analysis ([45], [76], [90], [106]) it is known that a flagrant contradiction exists between the experimental and the matrix-theoretical access to the thermo-viscoelastic stress problem in structures. In brief, structural analyses favour the incorporation of the relaxation phenomenon, while test rigs are almost incapable of simulating it realistically :

(1) Considering the creep-relaxation duality, the evolutionary process of creep is determined more easily than the one of relaxation. This is mainly due to the fact that, while dead loads are applied to procure creep-inducing stresses, the strain can easily be detected either visually using microscopes or kinematically using mechanical devices in conjunction with electronic displacement transducers.

In contrast, since relaxation-inducing strains require the imposition of time-invariant distances between the bearing plates of the specimen, the question arises as where to place the load cell ([64], [106]).

(2) Using finite element stress analyses ([1-8], [27], [29], [30], [44], [45], [46], [51], [68], [77], [86], [90], [101], [115], [116]), the method corresponding to creep investigations is the flexibility or force method. It is elegant, since the sizes of matrices to be stored in the computer memory are small and determined only by the number of redundancies in a structure. A reduced stress system which is in equilibrium with the forces and a system of self-equilibrating stresses which do not disturb the equilibrium of this system must be found.

Then, by determining the redundancies, i.e. the indeterminate generalized forces, the true stress system which satisfies the compatibility requirements is arrived at.

The main if not fatal difficulty is to know how many redundancies exist in a structure and thus the flexibility method requires a sound skill and knowledge about structures.

In consequence, the relatively simpler finite element matrix displacement method which reproduces the phenomenon of thermoviscoelasticity by employing relaxation functions has

been preferred in this thesis.

2.8. CONCLUSIONS

In the long run, the obstacles complicating the incorporation of thermoviscoelastic effects into the theory of structures requiring relaxation functions are less severe than those precluding the performance of reliable relaxation tests.

As regards the experimental investigation into the problem of thermoviscoelasticity, therefore, the author designed machines for creep testing ([43]).

In conclusion, it may be pertinent to recollect the characteristics that the proposed creep testing machine and the fitted mathematical model should exhibit, in order to reproduce the thermoviscoelastic process is a meaningful manner :

(1) The energy which maintains the system, e.g. the gel water flow, the propagation of microcracks, etc., at its initial and final values, must be supplied by an external source.

(2) The energy needed to impose a dynamic step change in stress on the system must be activated by a force which is absolutely constant throughout an individual test.

(3) A time-dependent strain response imposed by an external load step function to a thermoviscoelastic solid at its initial stable state, propagates along a natural exponential-like path towards a final stable state. Thus it should be attempted to describe the differential creep as a simple approximate function of time in a double logarithmic scale.

(4) To enable a justified fit of approximating functions to the creep responses, continuous recording of the developing strains and the prevailing test temperature must be ensured.

(5) The creep-relaxation conversion which must be performed in order to obtain the required information about the complementary relaxation responses, must be mathematically rigorous so as to keep the theoretical model for the thermoviscoelastic problem consistent.

CHAPTER III

PROPOSED CREEP TESTING MACHINE

3.1 PURPOSE

Three identical creep testing machines, each with a design load of ten tons, were built to perform tests for the purpose of investigating the strength and creep characteristics of a good-quality structural concrete at moderately high and elevated temperatures.

In order to obtain these characteristics, the testing machines are provided with facilities for accurate strain and temperature measurements on concrete specimens subjected to thermoviscoelastic, thermoviscoplastic and failure-procuring conditions.

The specimens used are of the cylindrical shape Ø 60 x 180 mm and compressed by virtue of a yoke system which is capable of applying load step functions of any magnitude up to a resultant force of ten tons. An electrically heated furnace housing the yoke system enables the specimens to be exposed to temperatures up to 700 ^{0}C, generating thermal conditions of either stationary or transient nature.

3.2. DESCRIPTION OF DESIGN

3.2.1. MAIN FRAME

Structurally, the rig of the testing machine - figures (3.1) to (3.3) and plate 1 - constitutes a three-dimensional steel frame consisting of four upright posts of hollow square cross-sections and three horizontal plates welded at the top, the bottom and an intermediate level between them. To ensure linear straining under load, the two frontal posts are always kept under compression, while the posts at the rear expand as the working load increases.

3.2.2. LEVER ARM

This structural member - figures (3.1) to (3.4) and

figure (3.8) - provides the facility to multiply the effect of the weights on the pan according to a leverage of 1 : 15. The slotted weights - plate 3 - each have a mass varying between 57 and 58 kg ; the design load of 10 tons thus corresponds to a set of about 12 weights piled up onto the weight-pan, requiring a minimum length of the suspension of 120 mm. The lever arm is supported at its fulcrum by a mounting fixed to the front edge of the top plate. The distance between the fulcrum and the front hanger measures 60 mm, hence the length of the effort arm amounts to 900 mm. A screwed arm with a movable counterweight, forming an extension of the front end of the lever arm, enables the lever system to be brought into statical equilibrium at zero load conditions.

3.2.3 GRIPPING STEEL

The machine parts transmitting the mechanical force from the short arm of the lever system to the concrete specimen - figure (3.5) to (3.7) and plate 2 - are specified as the front hanger, the upper universal joint, the upper pulling rod, the yoke system, the lower pulling rod, the lower universal joint and the lower link to the intermediate plate. The hanger is pivoted on the frontal knife-edge of the lever arm, whereas the lower link is studded to contrive a shortening or an extension of the gripping steel if required.

The yoke system is available in two versions of which the first is machined in a high temperature resistant titanium alloy. Due to unexpected weaknesses exhibited by this material, a sturdier version in incoloy alloy is employed where the working load exceeds 5 tons. The models only differ in the cross-sections of the studs and the material and both deform the specimens on the basis of a tension-compression conversion.

3.2.4. FURNACE

The environmental conditions to which the individual concrete specimens are exposed, are generated by a 7" bore

three zone furnace - figure (3.9) with a safe operating temperature of 700°C. Geometrically, it is a thickwalled hollow cylinder with end caps, which efficiently houses the shackle system plus specimen as to minimize the consumption of electric power during testing. Each zone possesses a resistance of approximately 50 ohms and the recommended upper voltage input is 170 volts. The temperature in the furnace is controlled by a platinum resistance thermometer placed next to the heating coils. The furnaces are built by Donaldson Furnaces Ltd.

3.2.5. FURNACE SLIDING ASSEMBLY

This assembly - figure (3.2) and plate 2 - enables the furnace to be lowered as to expose the yoke system when positioning or removal of the specimen is desired. It consists of the column, the sliding bracket, on which the furnace bearing ring is welded, the pulley and the counter-weight; the latter hangs inside the left front post and facilitates the vertical movement of the furnace.

3.2.6. LOADING JACK

A movable platform - figure (3.11) and plate 3 - was devised to enable the weights to be piled up; then these may be speedily lowered onto the weight-pan to effect an instantaneously applied fixed load on the specimen at time zero. The main items of the loading jack include the supporting frame, the weight bearing ring, the two jactuators, the couplings, the motor, the reversing switch and the speed control.

3.2.7. THERMOCOUPLES

To pick up the temperature existing at the surface of the specimen during testing, thermocouples are employed. They consist of two wires of different alloys, chromel and alumel, joined at each end. Owing to the different of temperature at the junctions, an electric current is caused to flow in the circuit. The output from the thermocouples is transformed to an equivalent voltage and thus reproducible

on the continuous plotter designed by Kent Ltd. Reference is made to plate 4.

3.2.8. TERMPERATURE CONTROLLERS

Control units - plate 4 - have been developed by CNS Instruments Ltd. to program constant temperatures and variable heating rates for three zone furnaces. The power input is controlled by a resistance thermometer which forms one arm of an a.c. Wheatstone bridge. The voltage is compared with the eqivalent value of a predetermined set temperature and the resultant error is fed into a silicon transistor amplifier to operate a relay; a preceding calibration ascertains the relationship between the set-point adjustment and the furnace temperature. The connected voltmeters and ammeters read the electric variables maintaining the programmed boundary conditions.

3.2.9. SAFETY DEVICE

A sensing thermocouple is inserted in the furnace to contrive an intermittent cut-out of the mains supply when a certain pre-set temperature is attained. The output from the sensing element assigns an error signal to a silicon transistor amplifier which actuates a triggered relay. This feature is useful in that it prevents damage to the testing machine, if a hazardous breakdown of the thermometer sets free the uncontrolled heating of the furnace. The safety device called 'Mini' is a temperature controller designed by Pye Ether Ltd.

3.2.10. TRANSDUCER

The mechanical strain measuring device - figure (3.10) and plate 2 - transfers the relative movement registered between its collars via potentiometer legs outside the furnace, where the deformation is recorded by a displacement transducer of the type ER/± 0.2 by Sangamo Controls Ltd. Originally, the collars were fixed to the bearing plates, but in aiming to eliminate the end face disturbances, their clamping directly to the body of the specimen was considered

more appropriate. For details see figure (3.11). The d.c./d.c. transducer is fed by a d.c. supply and produces a d.c. output signal which is fed direct to the digital voltmeter. Its basic element is a linear variable differential transformer; when the primary winding of the transformer is fed with a high frequency a.c. supply, the movement of the transducer spindle, i.e. the transformer core, will result in an output signal from the series opposing secondary winding.

3.2.11. DIGITAL VOLTMETER

Initially, only this unit and the power pack, both designed by Sangamo Controls Ltd., were available to exploit the performance capabilities of the displacement transducers. Catering for multi-channel working, the digital voltmeter - plate 4 - provides facilities to manually select any channel and to show its information on the digital display unit, which has binary coded output.

3.2.12. SCANNER UNIT

In the course of testing, this unit was acquired to contrive an unattended, automatic testing performance, once initiated. The scanner unit - plate 5 - incorporates the facilities of the digital voltmeter, but in addition enables the recording of information from a number of measuring points, transducers as well as thermocouples, at regular intervals of time. The impulses instructing the scanner are derived from a digital clock. Also, high frequency pulse 1 MHz are available when it is required to skip the interrogation and print out of channels where recording is not desired.

3.2.13. MICRO STRAIN METER

This unit - plate 4 - has been designed by Peekel Ltd., to measure developing strains via strain gauges by virtue of two - and four-arm bridges. It enables the transducer readings to be verified by comparing them with the strain gauge readings obtained for the same specimen.



PLATE 1. GENERAL VIEW OF CREEP TESTING MACHINES



PLATE 2. YOKE SYSTEM AND
STRAIN MEASURING DEVICE



PLATE 3. LOADING JACK, SUSPENSIONS AND WEIGHTS



PLATE 4. CONTROL AND MONITORING UNITS



PLATE 5: SCANNER UNIT FOR TRANSDUCERS AND THERMOCOUPLES

Strain gauges operate reliably only at ambient temperature; with increasing temperatures their electric resistance changes, resulting in the production of meaningless measurements.

3.3. DESIGN DRAWINGS

The design features of the testing machine are documented on twelve size A1 workshop drawings. For the benefit of the reader, however, a set of twelve small size drawings are produced, which appear as size A4 illustrations in figures (3.1) to (3.12). Reference is made to Appendix III.

3.4. DESIGN CRITERIA

3.4.1. MAIN FRAME

(1) Simplicity - to convey aesthetical design features ; to reduce the number of items required; to minimize the time and labour spent on cutting, welding and assembling

(2) Critical height - to make certain that the suspension can be designed long enough to account for a pile of 12 weights with a total height of 1200 mm and that a sufficient clearance is left underneath the pan for the accommodation of the loading jack ; to locate the yoke system and the furnace at a height convenient for operation ; to allow sufficient sliding travel for the furnace when positioning or removal of the specimen is desired ; to ensure stability of the compressive front posts against buckling

(3) Optimal size of bottom plate - to reduce the space required for the erection of the rig ; to guarantee stability of the rig against tilting ; to provide sufficient space between the front posts for the assembly of the furnace

(4) Clamped ends of posts - to guarantee stability of the frame against torsional and bending moments

3.4.2. LEVER ARM

(5) Lightness - to facilitate static equilibrium at zero load conditions ; to reduce the weight at the top of the rig in general

(6) Precision - to procure a leverage of exactly 1 : 15 ; to ensure exact fit of the knife-edges of the pivots into the vees of the fulcrum and the hangers

3.4.3. SUSPENSION

(7) Double tubing - to enable the single weights to be piled up before the total set is slid down onto the weight-pan to effect the instantaneous application of a fixed load

(8) Cylindrical joint - to contrive in conjunction with the rotation about the knife-edge the free swinging of the suspension in all directions

3.4.4. FRONT HANGER

(9) Cylindrical joint - to stimulate the rotation vertically to the knife-edge of the front pivot with the intention of overcoming any inaccuracy caused by a relative angle between the knife-edges of the main and the front pivot; to ease the self-alignment of the hanger with the line of action of the stress resultant working on the specimen

(10) Compactness - to minimize the absolute distance between the main and the front pivot and hence the total length of the lever arm

3.4.5. UNIVERSAL JOINTS

(11) Ball bearing - to ensure that no bending and twisting moments are transmitted from the lever system to the parts which are in actual contact with the specimen

(12) Compactness - to provide for the insertion of the end caps of the furnace without increasing the total height of the gripping steel, i.e. the distance between the lever and the intermediate plate ; to make possible the undisturbed sliding of the furnace

(13) Location outside the furnace - to materialize the design of the universal joints in the less expensive bright mild steel

3.4.6. YOKE SYSTEM

(14) Stability - to eliminate the amplification of any random dislocation of the joints and bearings

(15) Alignment - to guarantee pure compression in the longitudinal direction of the specimen

(16) Compactness - to devise a yoke system that fits despite its high design load into the furnace of given inside diameter

(17) Temperature resistant alloys - to maintain the rigidity of the yoke system at elevated temperatures

(18) Simplicity - to avoid any unnecessary drilling, cutting and screwing of the very hard titanium and incoloy alloys

(19) Economic use of alloys - to reduce the expenses on the alloys which are high-priced

3.4.7. STRAIN MEASURING DEVICE

(20) Mechanical system - to achieve least sensitivity of the device against shock; to ensure that the relative displacements are transmitted correctly, irrespective of the temperature inside the furnace

(21) Potentiometer legs - to enable the relative displacements to be measured at a location where the transducer is not affected by the heat

(22) Alignment of transducer - to accomplish the measurement of the relative displacements in the extension of the centre-line of the specimen

(23) Reliability of connections - to guarantee the transmission of the true displacements

(24) Mechanical safety device - to make a compression of the specimen correspond to an expansion of the transducer armature as to prevent the transducer from being damaged when a failure of the specimen occurs

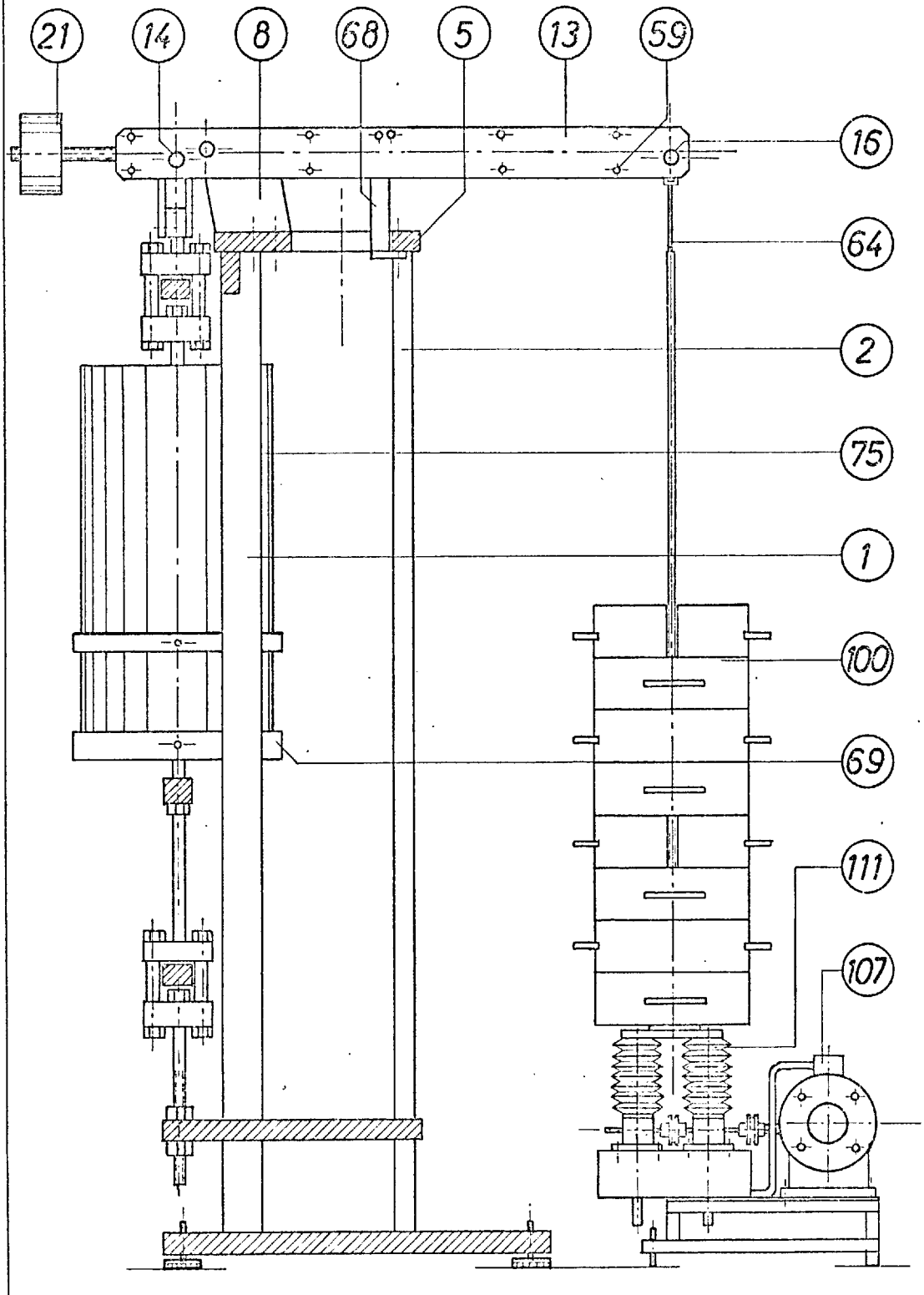


FIG. 3.1. END ELEVATION OF CREEP TESTING MACHINE

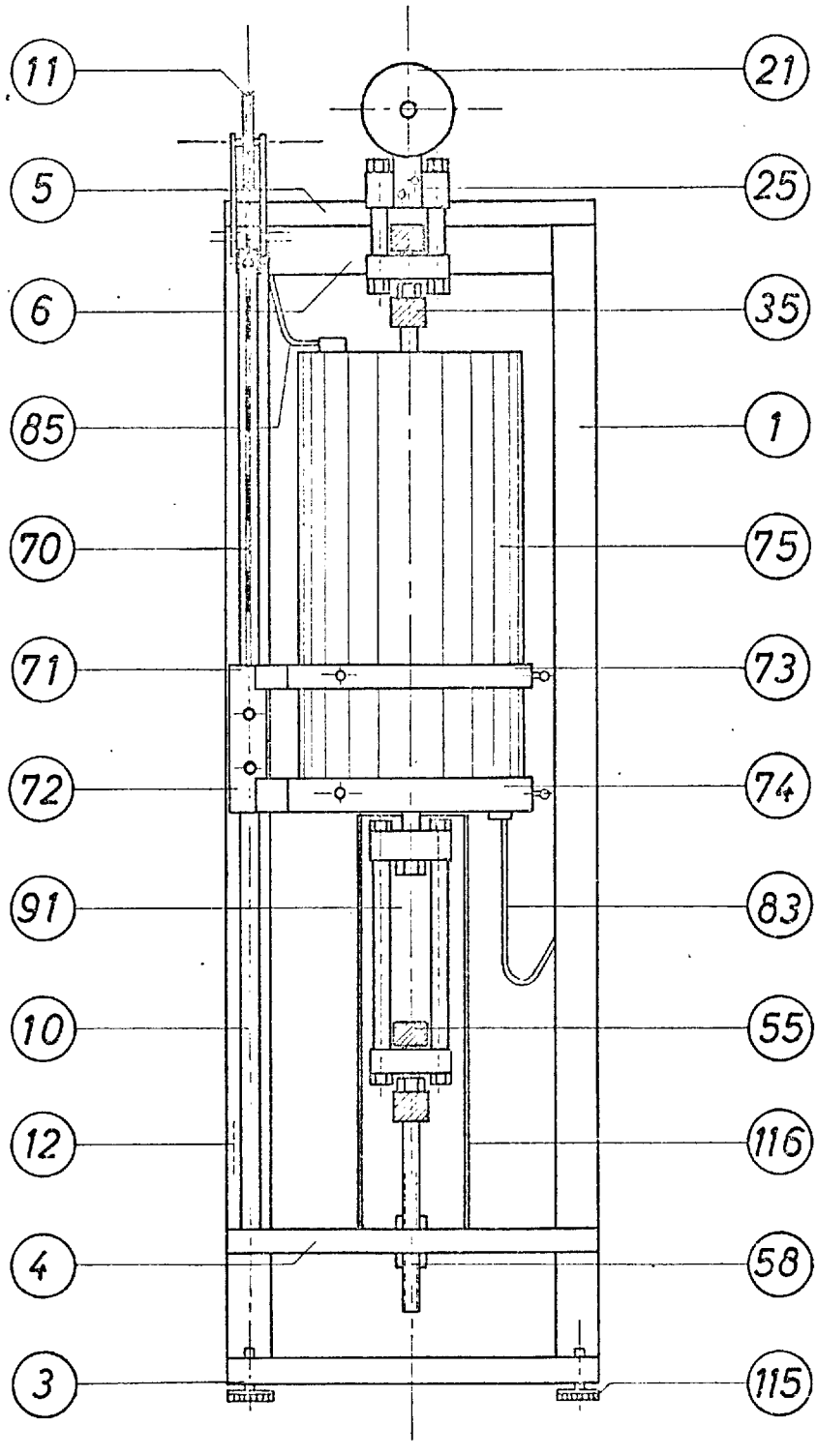


FIG. 3.2. FRONT ELEVATION OF CREEP TESTING MACHINE

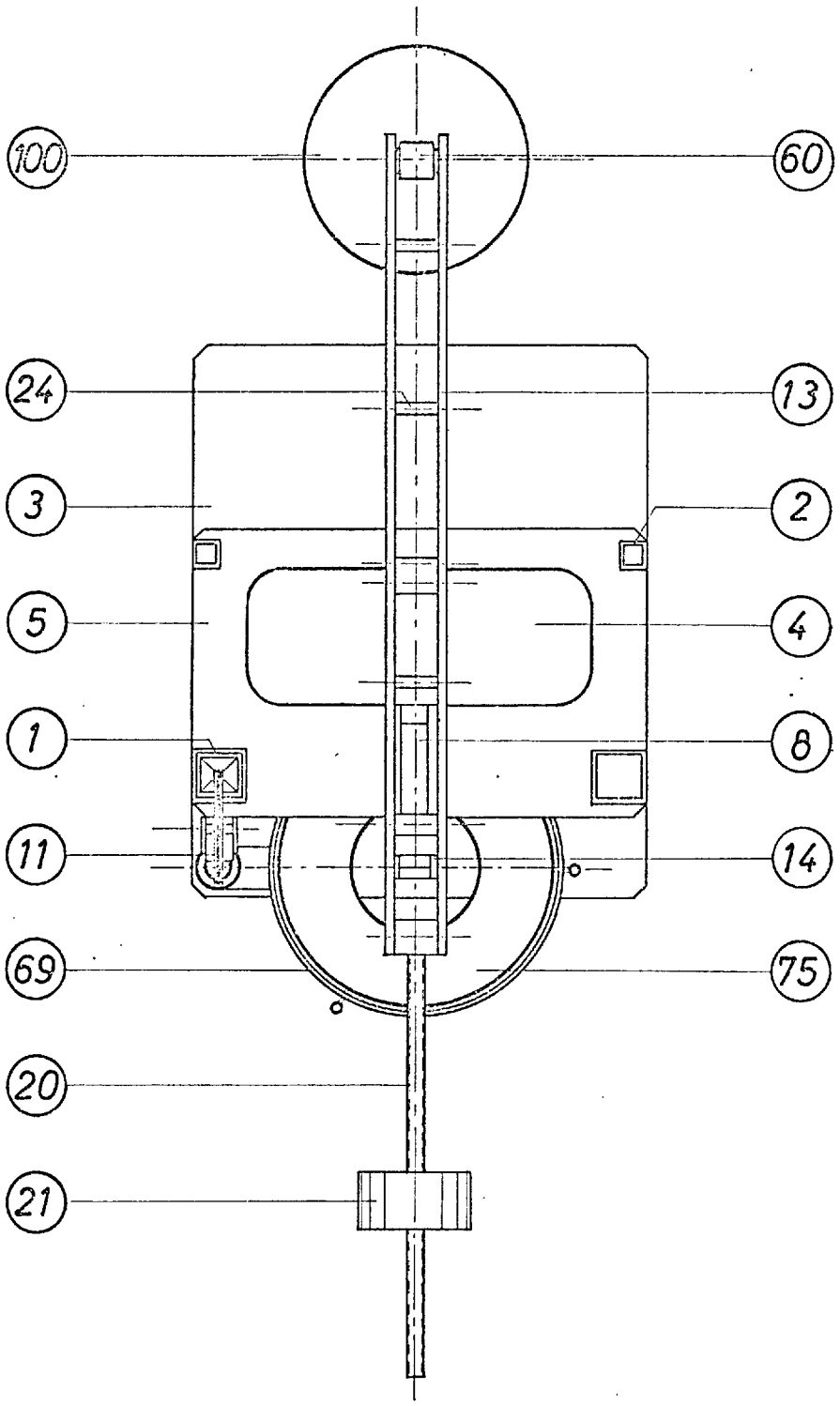


FIG. 3.3. PLAN OF CREEP TESTING MACHINE

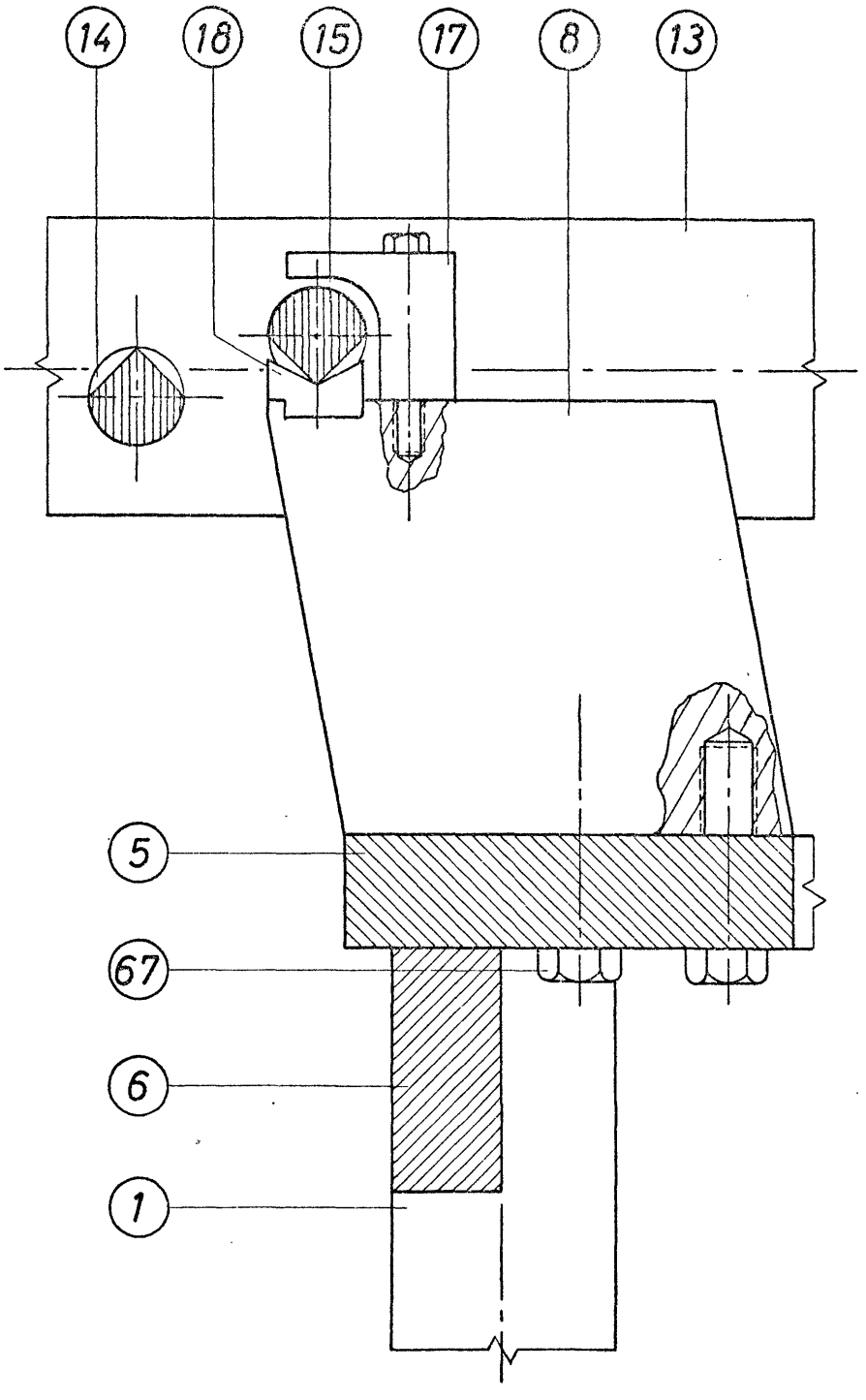


FIG. 3.4. FULCRUM OF LEVERARM SYSTEM

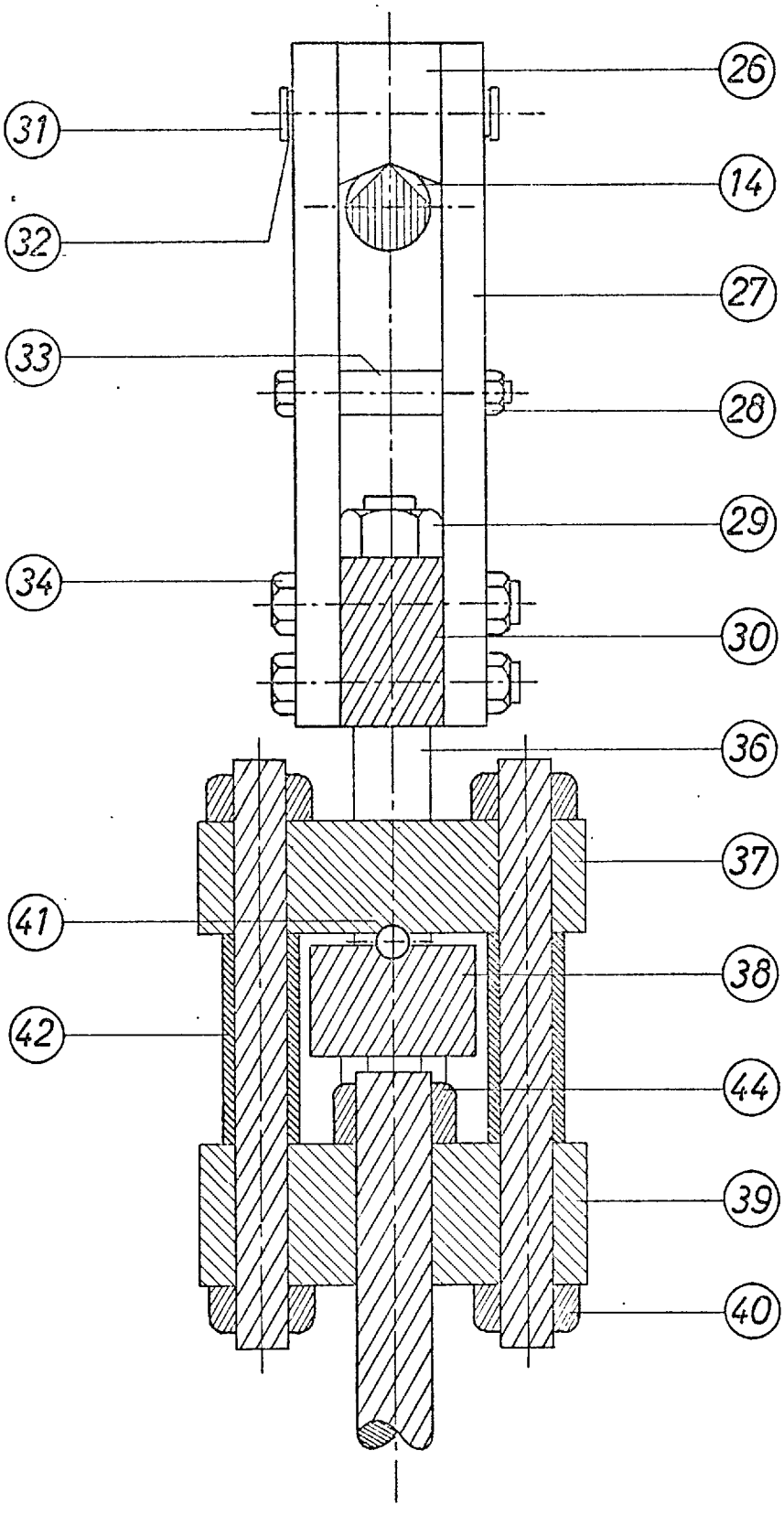


FIG. 3.5. FRONT HANGER AND UPPER UNIVERSAL JOINT

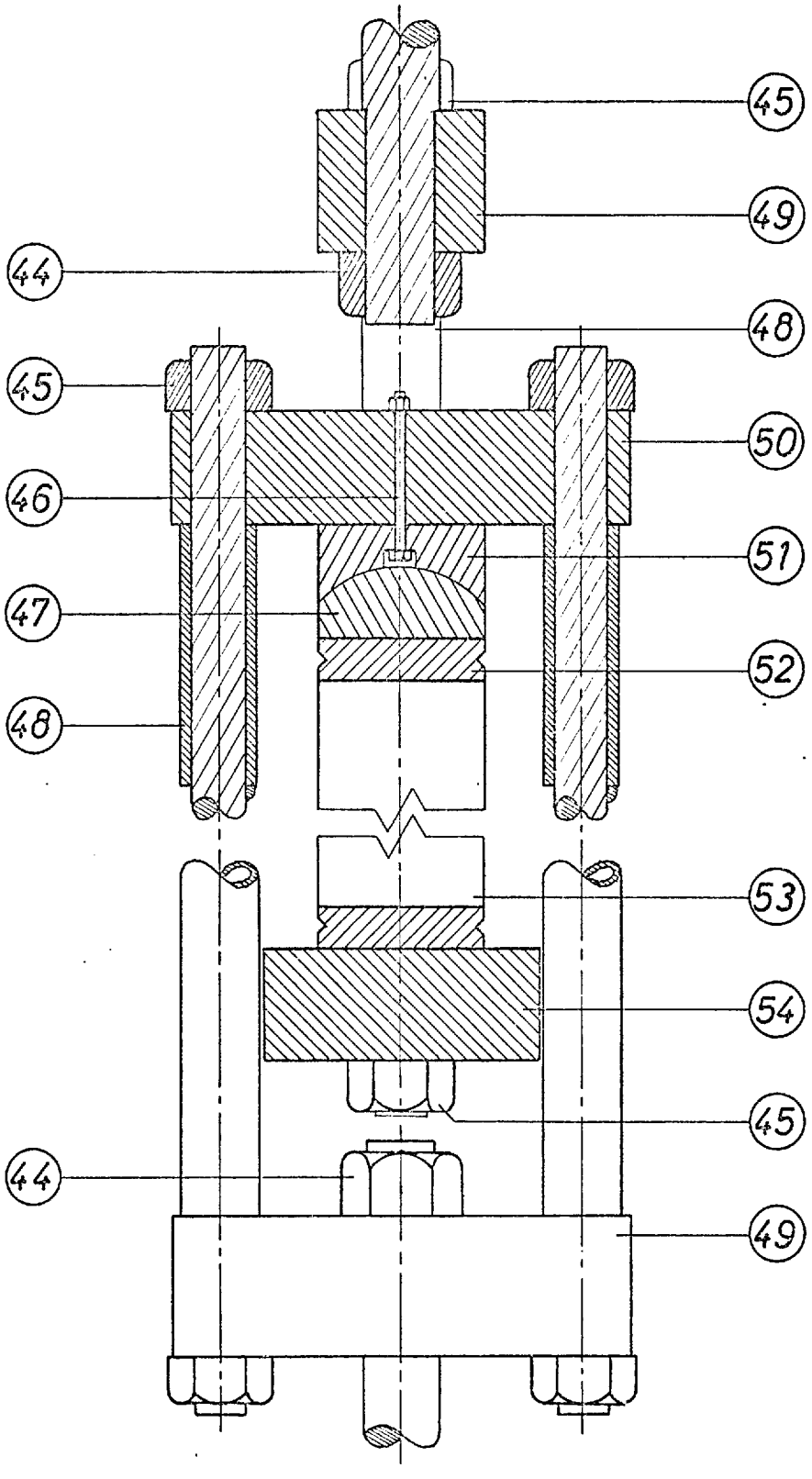


FIG. 3.6. HIGH TEMPERATURE RESISTANT YOKE SYSTEM

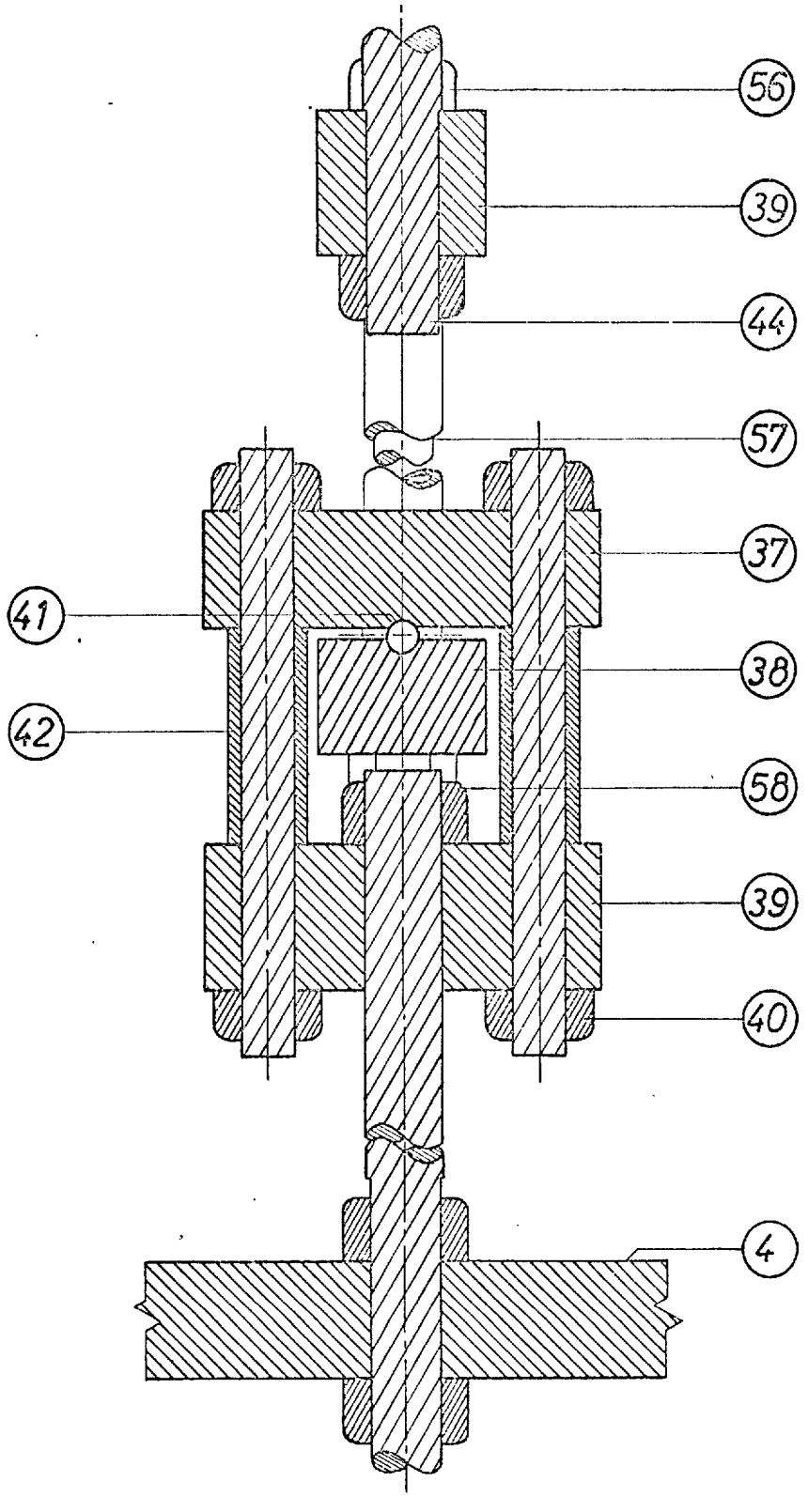


FIG. 3.7. LOWER UNIVERSAL JOINT AND LINK

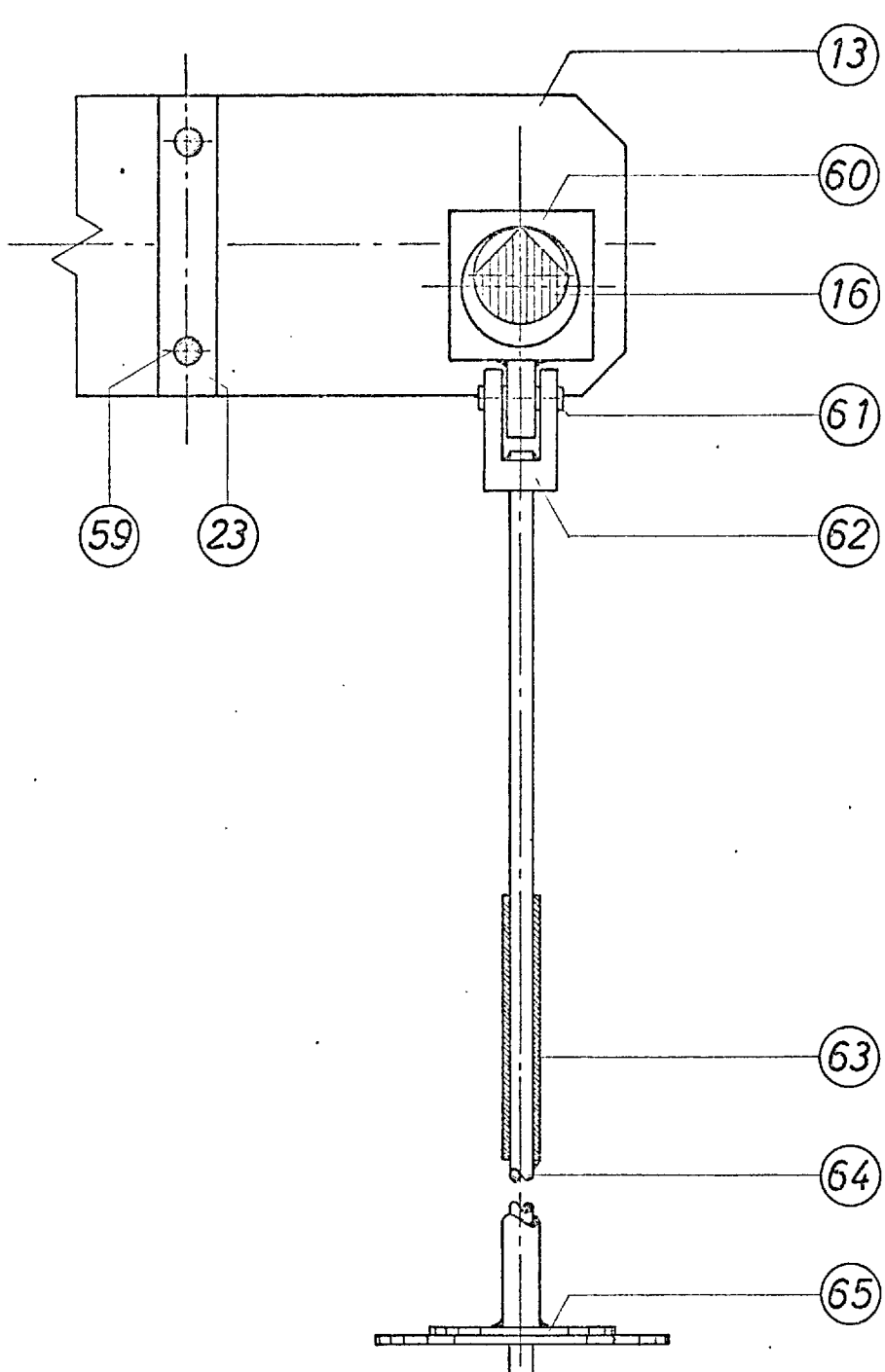


FIG. 3.8. REAR HANGER AND SUSPENSION

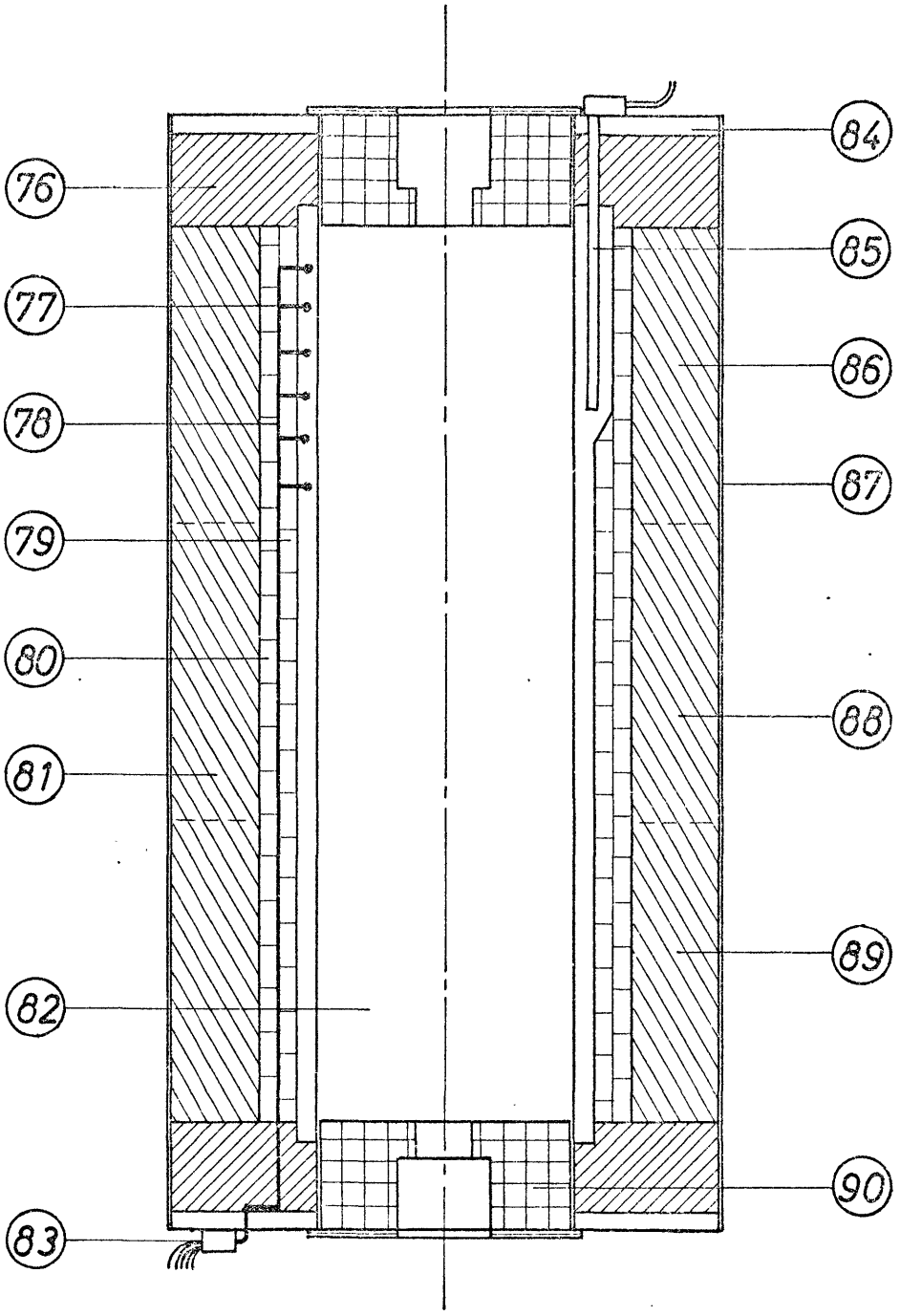


FIG. 3.9. 7" BORE THREE ZONE FURNACE

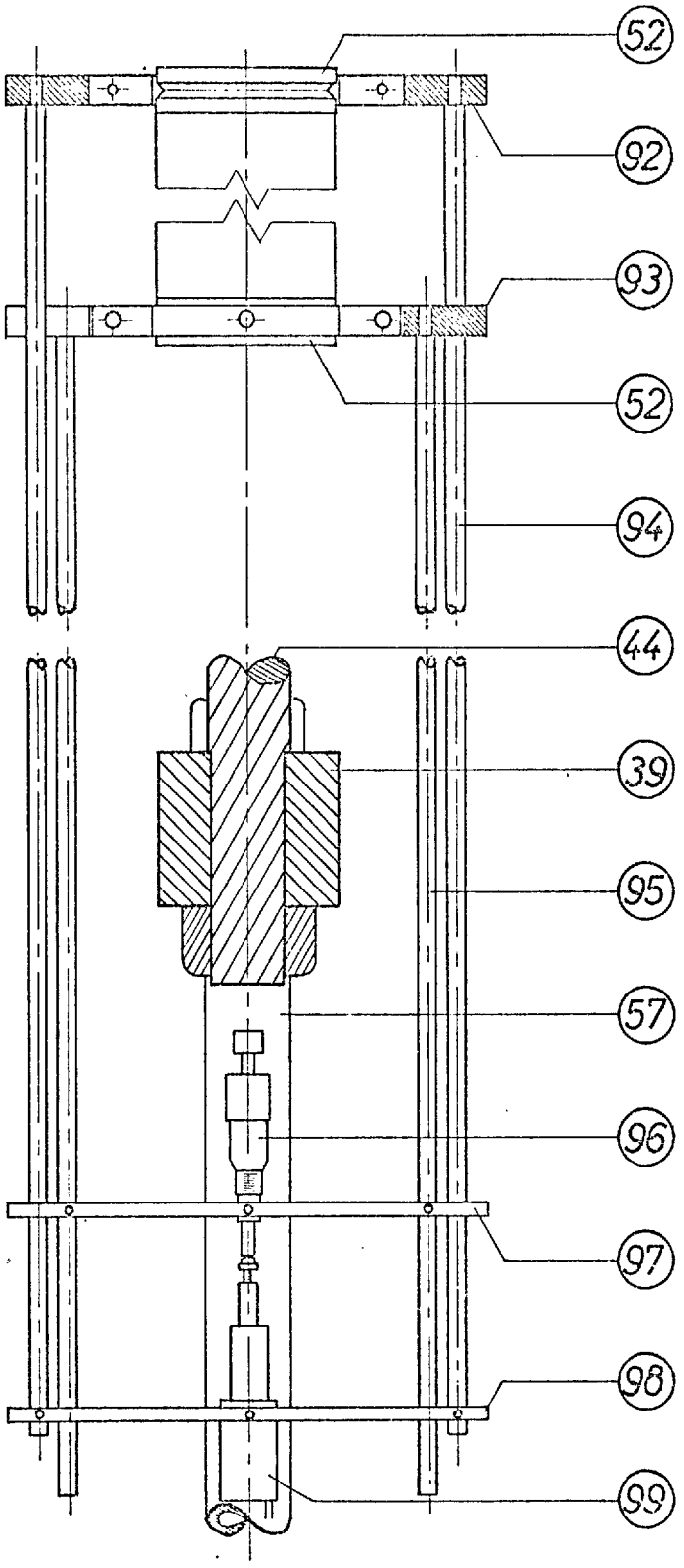


FIG. 3.10. STRAIN MEASURING DEVICE AND TRANSDUCER

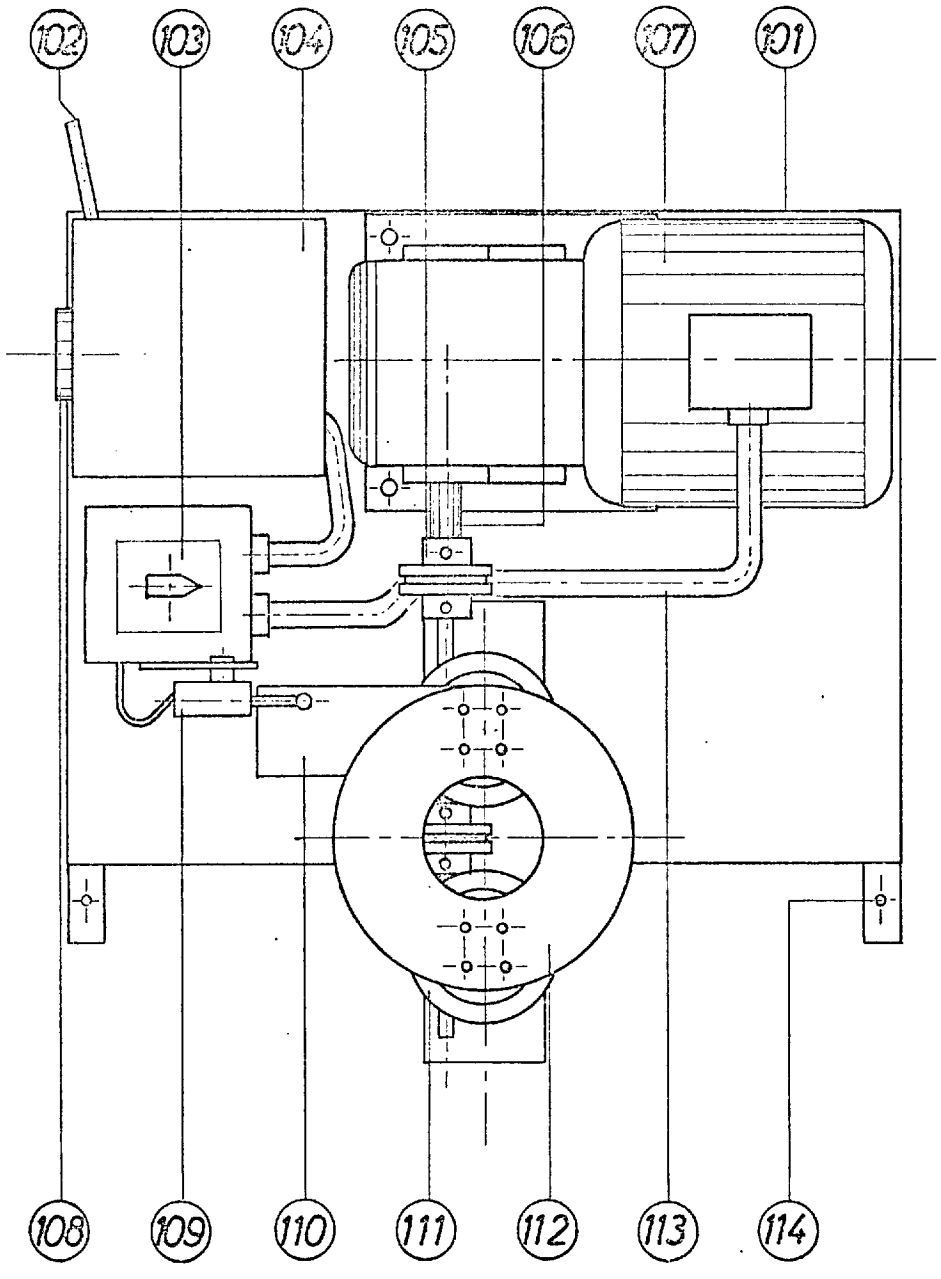


FIG. 3.11. PLAN OF LOADING JACK

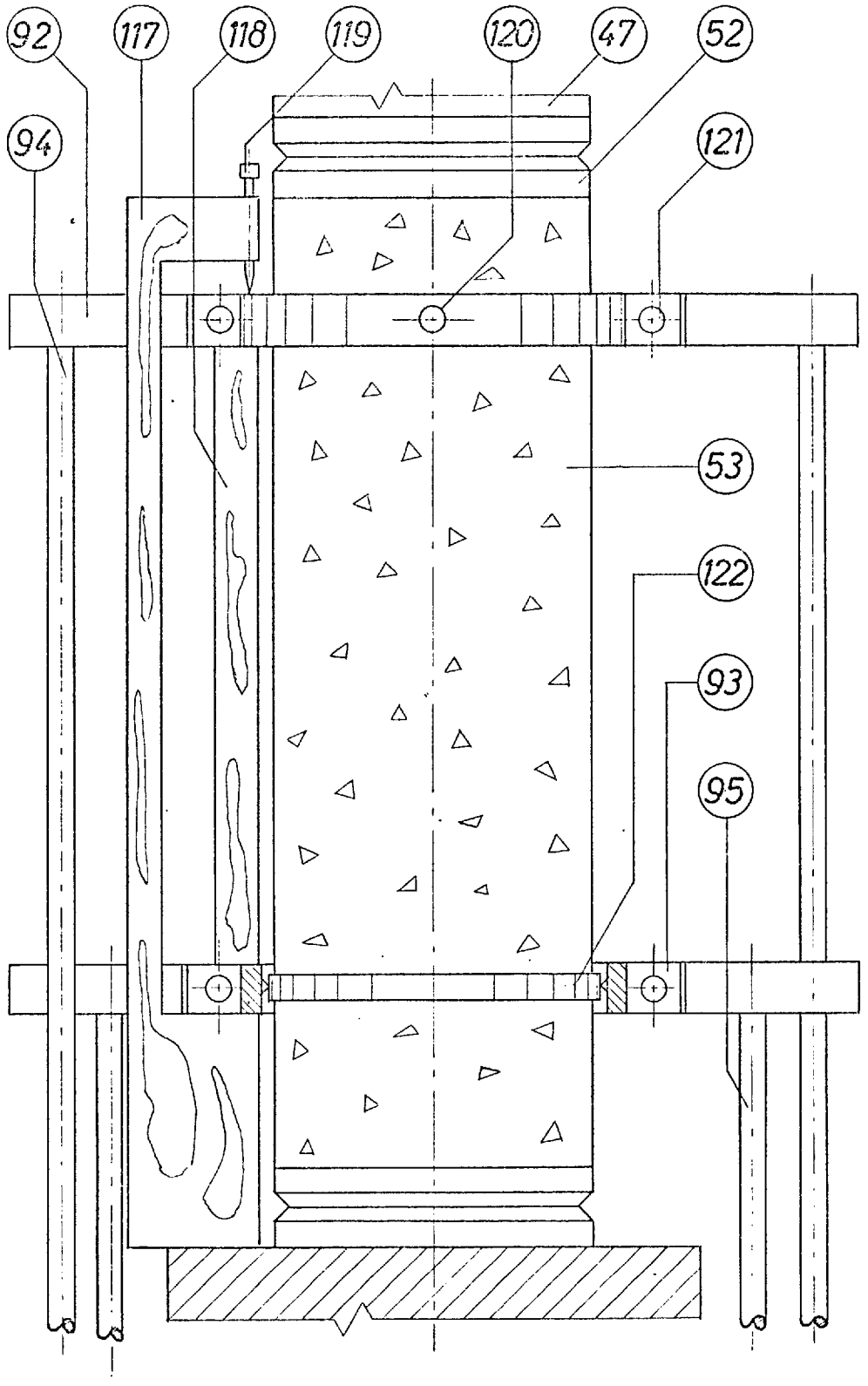


FIG. 3.12. POSITIONING OF COLLARS OF DEVICE ON SPECIMEN

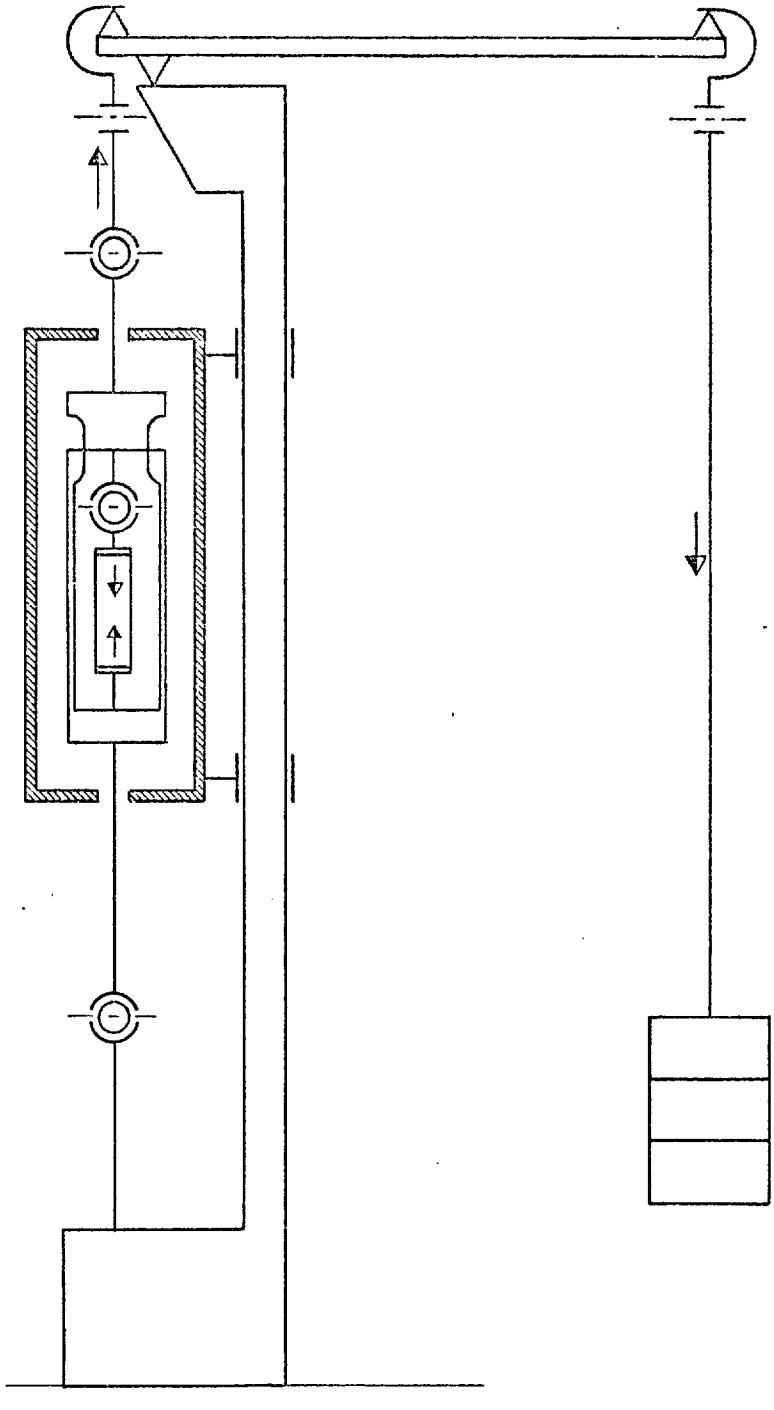


FIG. 3.13. MECHANICAL SYSTEM OF CREEP TESTING MACHINE

3.5. PROVING TESTS

3.5.1. LOADING SYSTEM

To calibrate the loading system, repeatability must be checked for elastic strains occurring in a load cell, which is axially compressed both in an Amsler compression machine and the proposed creep testing machine.

Eight 20 mm strain gauges were fixed at equal distances around the equator of a Ø 60 x 180 mm steel tube, alternately showing in the axial and the circumferential direction. While the load was increased gradually, strain readings were taken on a Peekel strain indicator. Figure (3.14) illustrates that the characteristic load-strain curve of the load cell is reproducible in the creep testing machine; the perfect functioning of its lever arm system is thus demonstrated.

3.5.2. TRANSDUCER

Transducer readings appear on the screen of the digital voltmeter in units of mV; hence the aim is to calibrate the transducers such that a measured strain of 20μ corresponds to 1 mV.

As strains exceeding 20000μ were not expected to develop during high temperature creep tests, the transducers were calibrated within the corresponding interval of 0.0 to 0.1 in. The transducers were mounted on a jig, while the travel of each spindle was controlled by a micrometer head. Then the span of the relevant transducer channel was turned until zero deviation was attained between the decimal numbers recorded at naught and at three quarters of the interval, both by the micrometer head and the digital voltmeter.

An example is given in table 3.1. Starting from electrical zero, the armature was moved in an out. The maximum deviation was 4/1000 = 0.4%, thus falling outside the tolerance of 0.2% as specified by the manufacturers of the transducers.

Table 3.1. Calibration of Transducer I

Micrometer Head (in.)	Digital Voltmeter (mV)	Error (mV)
0.0	0	0
0.025	249	-1
0.050	498	-2
0.075	750	0
0.100	1004	+4

3.5.3. STRAIN MEASURING DEVICE

Unlike the load cell described above, the steel tube and the concrete cylinder used for the proving tests on the strain measuring device were equipped with four strain gauges, fixed vertically at equal distances around the equatorial circumference. The strain gauges yielded the average axial compression within the 30 mm centre strip of the test specimens, whereas the transducer recorded the relative displacement between the centres of the two platens of the yoke system - figure (3.10).

The stress-strain curves based on the transducer readings were highly unreliable; they diverged from the curves recorded by the Peekel strain indicator, which developed in conformity with the known moduli of elasticity of 200 KN/mm^2 and 30 KN/mm^3, respectively, for steel and concrete.

The operation of the strain measuring device was considered unsatisfactory, with the result that the collars of the potentiometer legs were fixed to the concrete specimen itself at a distance of 5 in., leaving 30 mm each end to avoid the immediate influence of the end restraints. Reference is made to figure (3.12). The results recorded by the transducer then coincided with those obtained from the strain gauge readings throughout the elastic range and were only slightly higher at higher loads. This may be explained by the higher probability of microcracks forming in the larger testing volume considered.

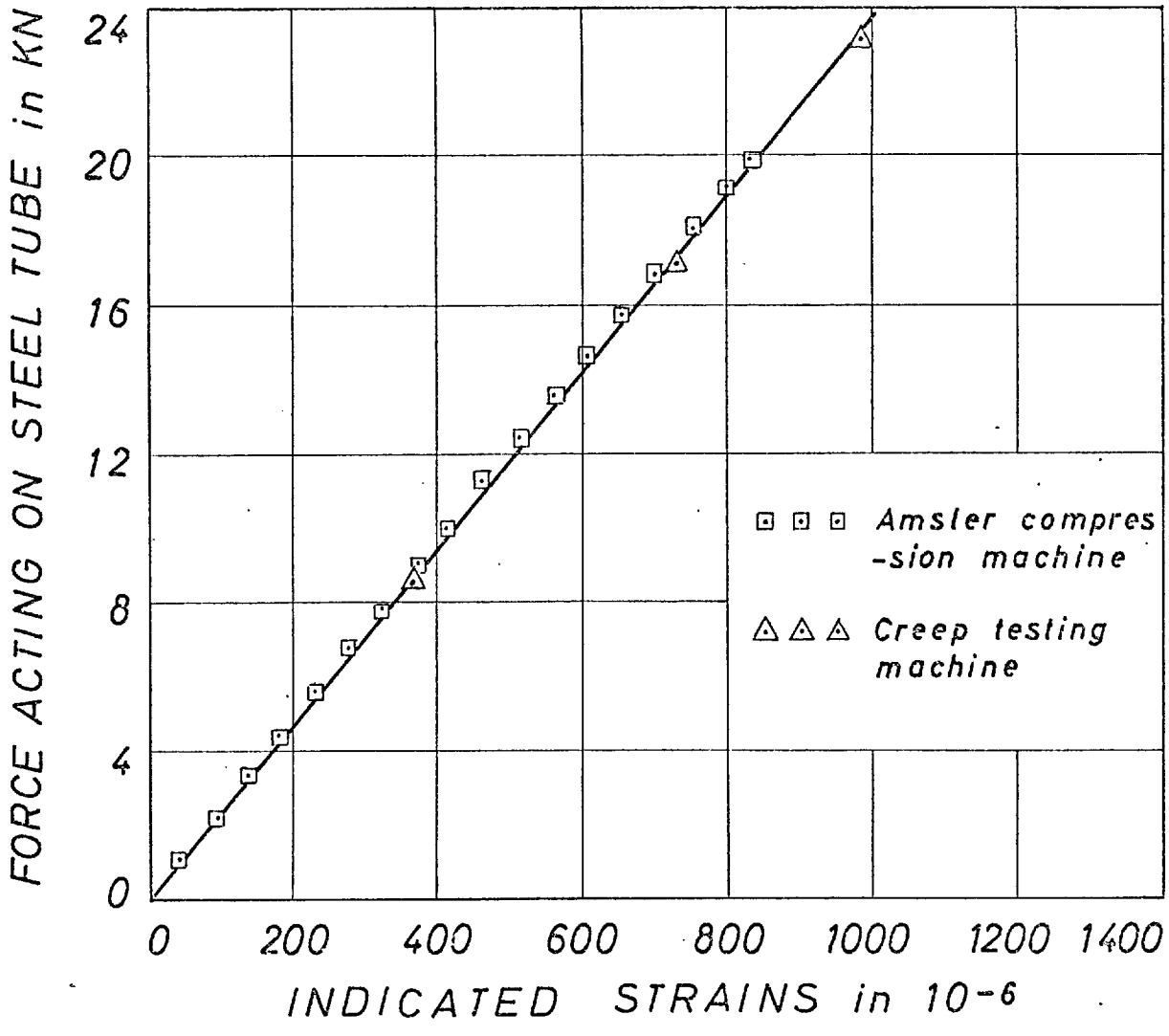


FIG. 3.14. PROVING TEST ON LEVER ARM SYSTEM

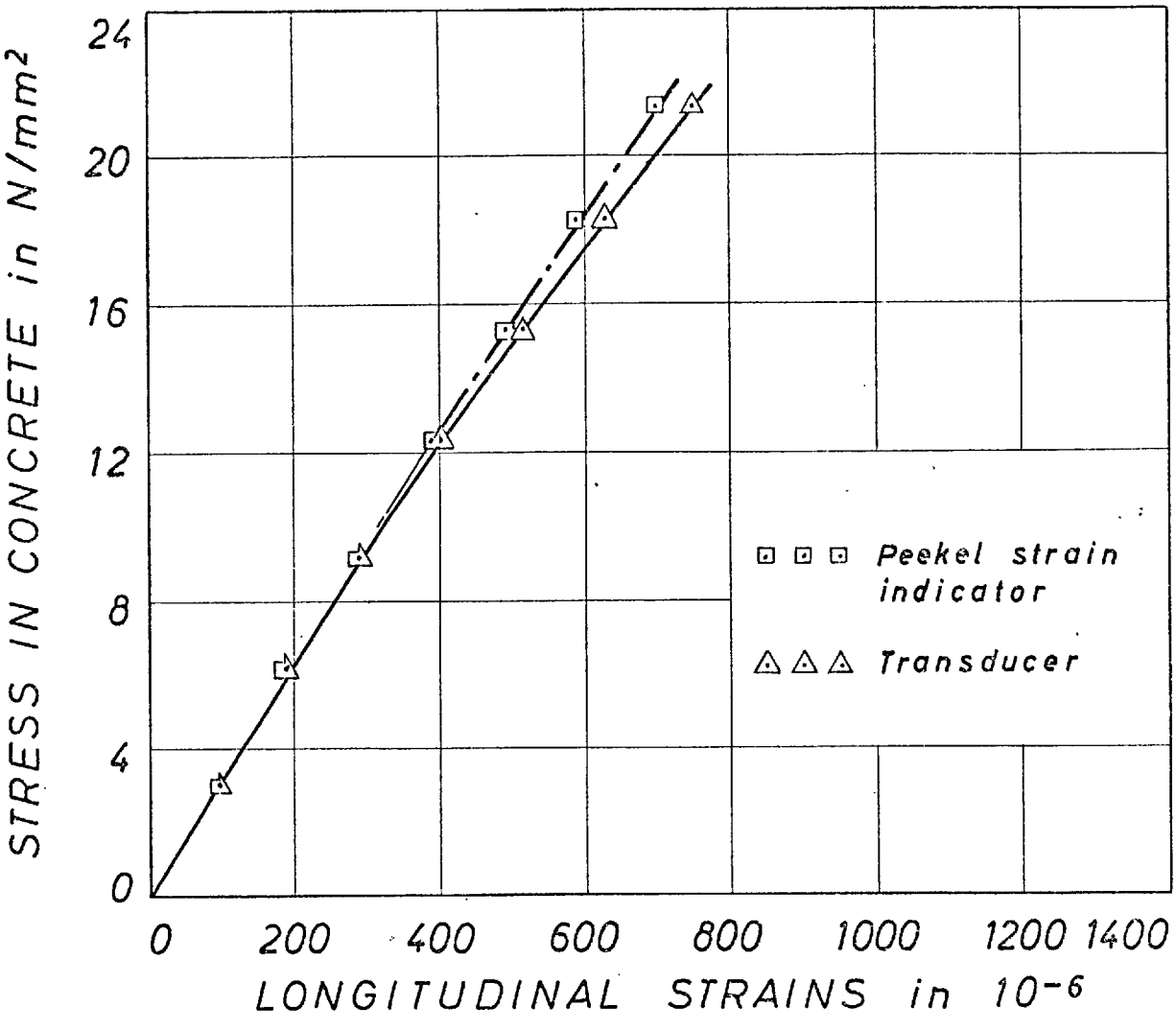


FIG. 3.15. PROVING TEST ON TRANSDUCER

The overlapping of the two stress-strain curves is shown in figure (3.15).

The performance of proving tests at high temperatures using strain gauges is futile due to the change in electric resistance of the gauge wires. Under steady state conditions, the thermal expansion of the displacement transmitting rods, which are unequal in length, does not interfere with the measuring of the creep strains, as it occurs and settles in the heating period prior to testing. Thus, no further calibration is required. However, if the thermal conditions are of transient nature, the differential thermal expansion of the rods must be investigated. This may be done by comparing the measured strains of a heated steel tube of known properties with the predicted ones.

To check strain readings obtained for higher temperatures, the ascertained initial modulus of thermoelastoplasticity was compared with moduli found by other authors.

CHAPTER IV

NON-VISCOUS PROPERTIES OF CONCRETE AT AMBIENT TEMPERATURE

4.1. OBJECTIVE

The purpose of the experimental project was to perform thermal creep tests on concrete cylinders at a time after casting, when the phenomena of drying shrinkage, moisture loss and strength of concrete had ceased to affect the test results appreciably.

The objective of this subsidiary investigation, therefore, was to observe the functional behaviour of these phenomena prior to testing. It was decided to manufacture cylindrical specimens of a good-quality structural concrete, to be tested later than six months after casting. A 28-day cube strength of 40 N/mm^2 was anticipated ; more important, the final strength of the test cylinders was hoped to fall below 45 N/mm^2, to satisfy the capacity of the testing machines at higher stress/strength ratios.

4.2. MATERIALS

One concrete mix was used throughout this investigation. Both the two sands and the coarse aggregate were Thames River deposits. The relevant sieve sizes are entered in table 4.1, in which the mix proportions are listed. The water/cement ratio was 0.60, while the ratio of the total aggregate to cement worked out at 4.55. Water in the materials was not allowed for, as they were dried in blast air.

Table 4.1. Mix Proportions

Particulars	Weight
Ordinary Portland Cement	1.00
Fine Sand (100 - 25 B.S.)	0.65
Coarse Sand (25 B.S. - 4.8 mm)	1.55
Coarse Aggregate (4.8 - 9.5 mm)	2.39
Water	0.60

4.3. FABRICATION

The concrete mix was manufactured in a 0.05 m^3 counter-rotating Eirich pan mixer in batches of 0.012 m^3 approximately. The coarse aggregate, the sands and the water were first mixed together for a period of four minutes. Then the cement was added and mixing continued for a further two minutes. Slump and compaction factor tests were conducted ten minutes after discharging the concrete from the mixer. Their average values amounted to 1.25 in. and 94% respectively.

Each batch consisted of six test cylinders Ø 60 x 180mm, six smaller size control cylinders Ø 50 x 150 mm and six 102 mm cubes for strength and weight control. The concrete was placed in two layers and compacted on a table vibrator operating at 500 rpm, until the majority of the air bubbles had escaped, ensuring that segregation did not take place.

Three series of specimens were cast : Series J in July, Series N in November and Series F in February such that all test cylinders could be tested for creep at an age between six months and one year. To produce Series J, N and F, seven,nine and six mixes were manufactured respectively, as about 130 test cylinders were needed.

4.4. CURING

All specimens, cylinders and cubes, were cured under wet hessian for one day before being demoulded. The specimens of Series J were water stored for 27 days. Its cubes were crushed at an age of 28 days, while the cylindrical specimens continued to mature under damp hessian for up to 50 days. Thereafter they were left in air at 50% RH and 20^{0}C.

The curing for specimens of Series N and F differed in that they were water stored only up to the seventh day and kept under damp hessian for four weeks.

The alteration in the curing procedure was undertaken firstly to allow the concrete to mature under more realistic conditions, secondly, to accelerate the testing procedure by causing the processes of drying shrinkage and moisture loss

to level off at an earlier time instant after casting. Thirdly, it was intended to reduce slightly the strength of the matured concrete, in order not to strain the capacity of the testing machine.

4.5. SHAPE CRITERIA

To reduce the restraining effect caused by the machines' bearing plates, cylinders of a height equal to three times the diameter were fabricated. In this way, as large a part of the test specimens as possible is left unaffected by the end restraints. For this reason and due to the more uniform stress distribution on horizontal planes, rather than cubes or prisms, cylinders yield greater consistency of results for nominally similar specimens.

Cylinders are cast and tested in the same position, thus representing the mechanical action in a structural compression member more realistically than specimens of square cross-section.

With a uniform load distribution being desirable during testing, the cylinders' end faces were ground to a smooth finish on a grinding machine. To avoid later wetting of the specimens, this treatment was applied immediately after their removal from the water tank.

4.6. DRYING SHRINKAGE

Since it has become engineering practice to separate the effects of creep on concrete from those due to drying shrinkage, the latter phenomenon was observed on some test cylinders of Series N and F. One specimen from each of the total 16 batches was equipped with three pairs of gauge points, positioned at interval of 2/3Π around the circumference. The distance between the gauge points of each pair measured 100 mm.

The reading were taken on a Demec strain gauge and entered in figure (4.1). It displays the profile of shrinkage strains developing in the cylinders after exposure to air.

After 140 days, the strains had reached a value of 600μ or 0.06%, still unfolding at a rate of 30/600 = 5% per

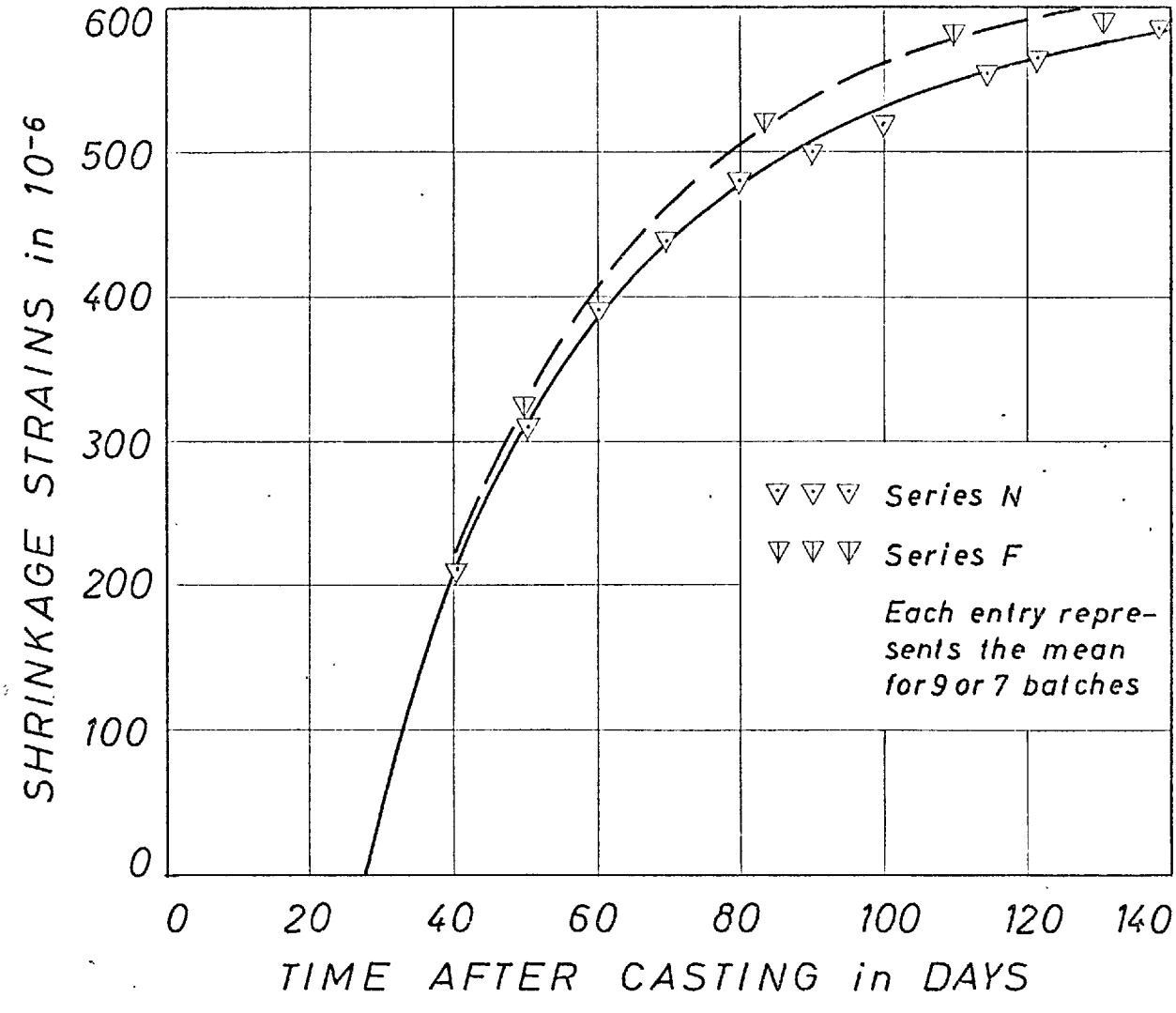


FIG. 4.1. DRYING SHRINKAGE IN CONCRETE TEST CYLINDERS

month. For ages greater than six months, however, the effect of drying shrinkage on the maturity of concrete becomes negligible, as the rate of increase has dropped to 2/620 = 0.3% per month.

4.7. MOISTURE LOSS

Drying shrinkage is essentially a function of the free water retained in the concrete. To support this argument, the moisture loss in all 96 test specimens and still existing control specimens of Series N and F was measured continuously as from the moment of air drying.

For a comparative study, the shrinkage strains pertaining to the cylinders of Series N were plotted once more versus time in figure (4.2), which shows the scatter and the 95%-confidence limits. The mean profile of the moisture loss in g and its 95%-confidence limits, which are plotted versus time in figure (4.3), overlap almost completely with the relevant profiles in figure (4.2).

Thus the existence of a direct affinity between the phenomena of drying shrinkage and moisture loss is probable.

In figure (4.4), the relative reduction in weight due to moisture loss is compared for the three types of specimens of Series N and F. Clearly, the final moisture loss is a linear function of the surface-volume ratio. For visual assessment, the surface-volume ratio and the weight loss are entered in table 4.2 ; the reference values being those for the test cylinders.

Table 4.2 Shape-dependent Characteristics

	Cube	Lg. Cyl.	Sm. Cyl.
Surf.-vol. ratio in 1/cm	0.591	0.793	0.932
Surf.-vol. ratio in %	74	100	118
Weight loss (N) in %	69	100	112
Weight loss (F) in %	70	100	109

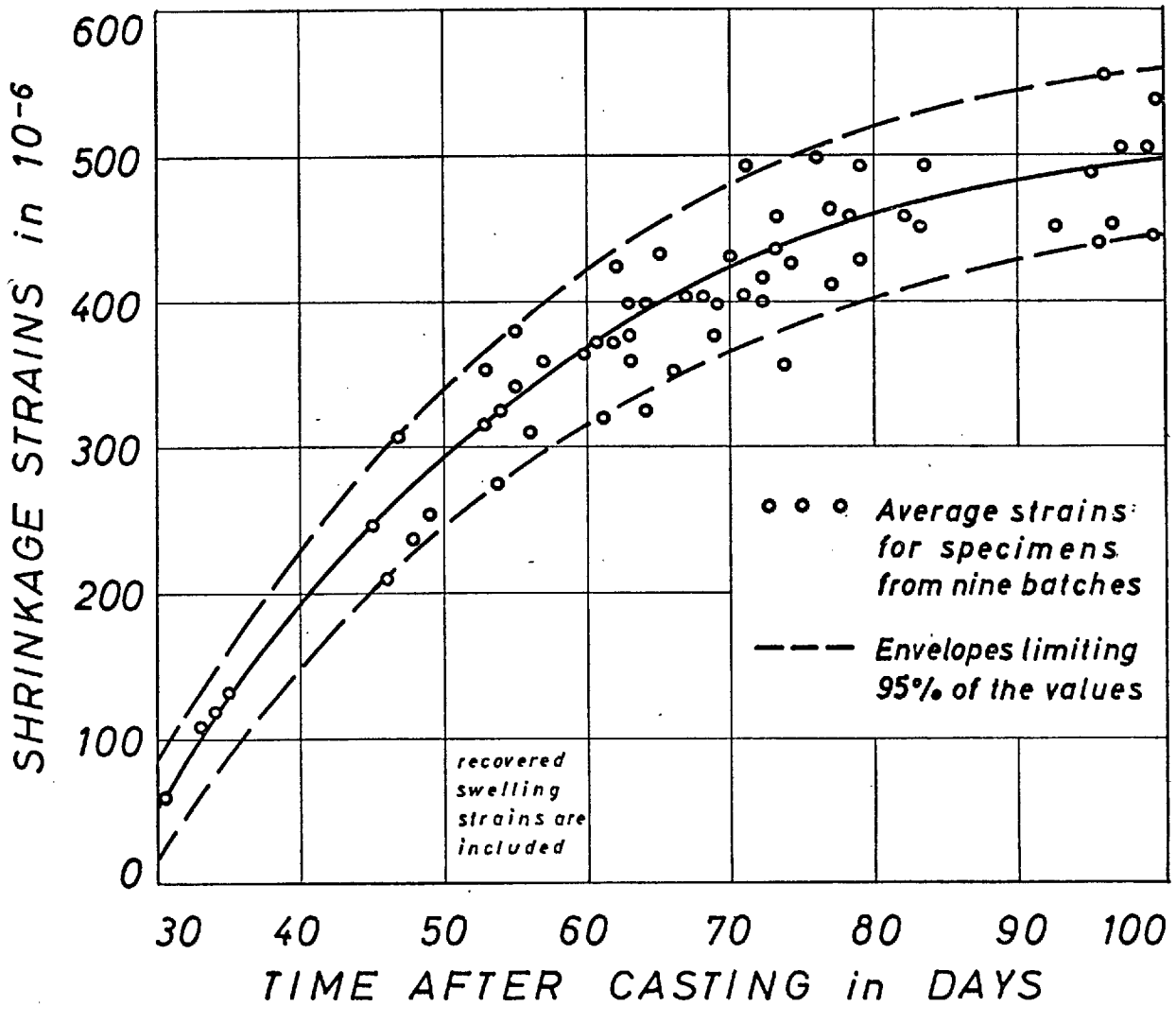


FIG. 4.2. SCATTER OF SHRINKAGE READINGS FOR SERIES N

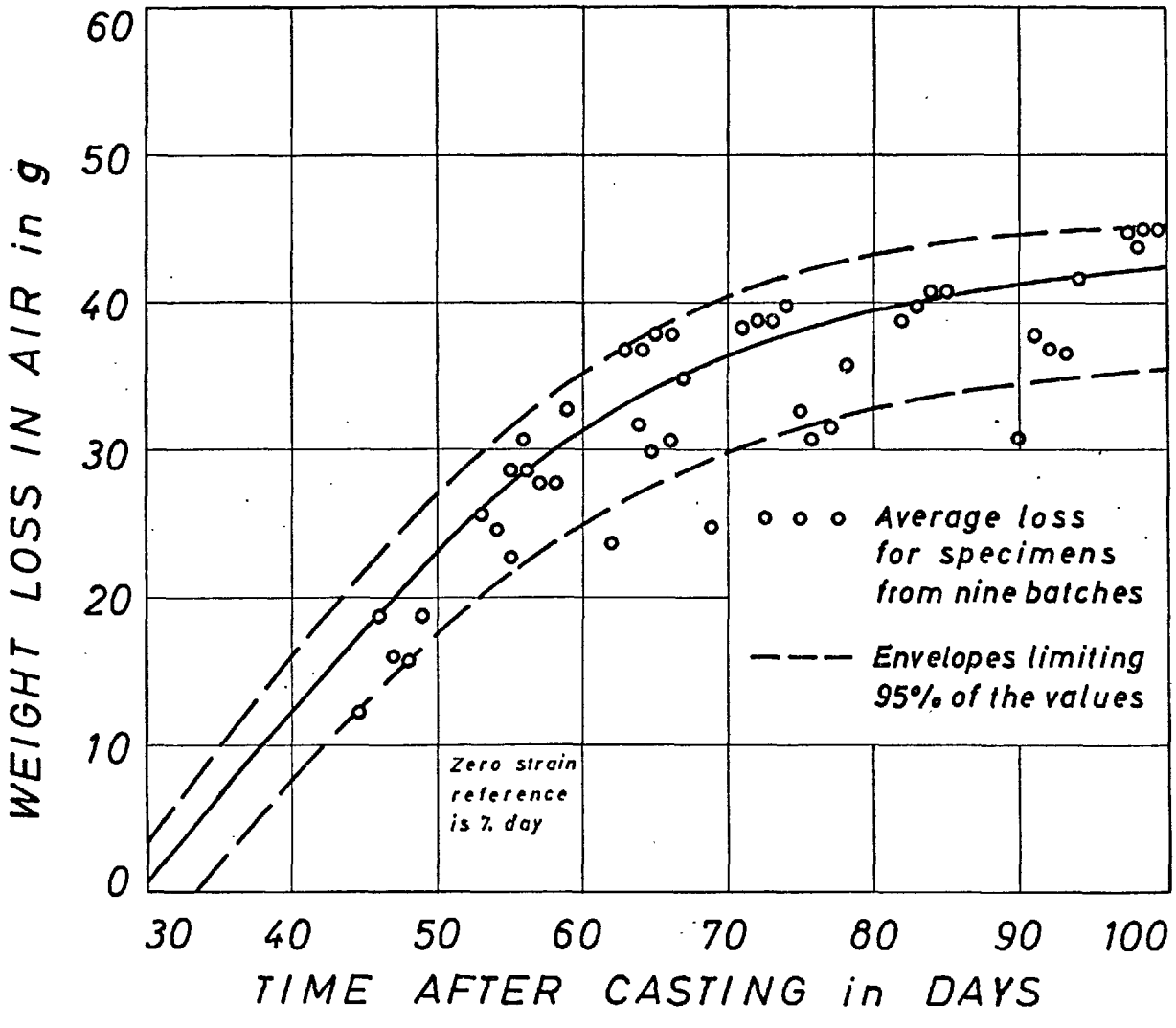


FIG. 4.3. SCATTER OF MOISTURE LOSS READINGS FOR SERIES N

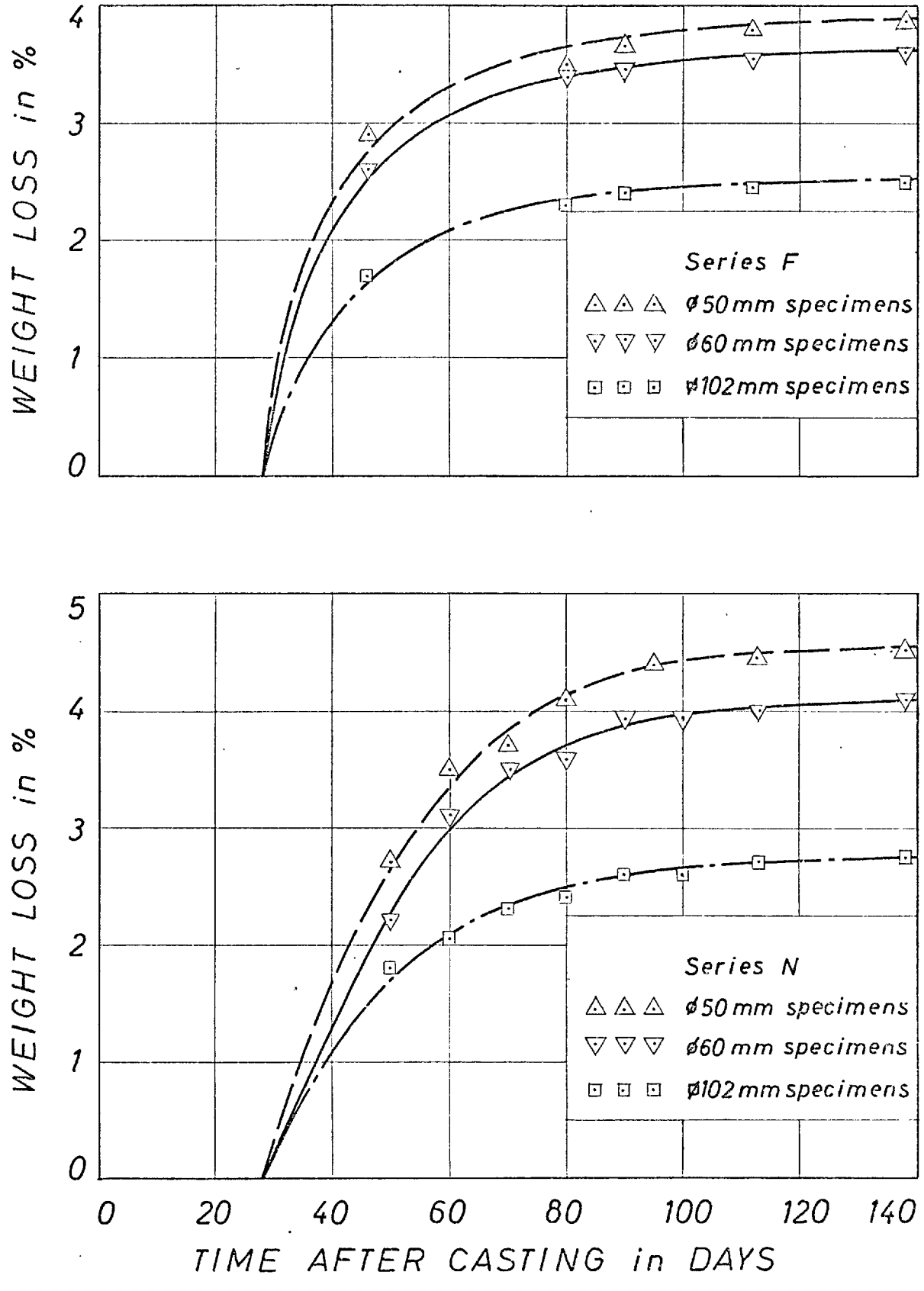


FIG. 4.4. MOISTURE LOSS DUE TO AIR DRYING

Evaluating the results in figures (4.1) to (4.4) numerically, it can be said that the ratio of shrinkage strains to relative weight loss for the test cylinders invariably comes to 1.5%, as it varies along the profiles between 0.0134 and 0.0146 for Series N and between 0.0129 and 0.0166 for Series F.

From table 4.2, the weight losses for the control specimens fall slightly below their predicted values. This may be explained by the fact that these specimens, thought stored in the same room, matured on the concrete floor, which naturally exhibits a lower temperature than the wooden table on which the large cylinders were kept.

4.8. COLD STRENGTH

To assess how probable it is in the long run that specimens have a strength between two limits considered, a distribution curve was drawn from the results of the 21 cubes of Series J, tested at an age of 28 days. The 102 mm cubes reached an average strength of 38.7 N/mm^2.

The area under the curve in figure (4.5) between any two values, represents the number of specimens falling within the domain. The values along the abscissa are measured in terms of the average strength and the standard deviation for the whole sample. Although the number of specimens is limited, a good reproduction of the normal distribution curve is obtained.

In table 4.3, the cube and cylinder strengths at different ages are compared for Series J. Clearly, the strength of concrete does not increase within the period of four to seven months ; as also illustrated in figure (4.6), the average cylinder strength establishes itself at 45 N/mm^2.

Table 4.3. Cube and Cylinder Strengths of Concrete

	Cube	Lg. Cylinder		Sm. Cylinder	
Age in d	28	130	132	165	192
Strength	38.7	44.2	45.2	44.8	45.1
No. of spec.	21	4	7	7	7
Deviation	3.33	5.11	6.04	2.79	5.71

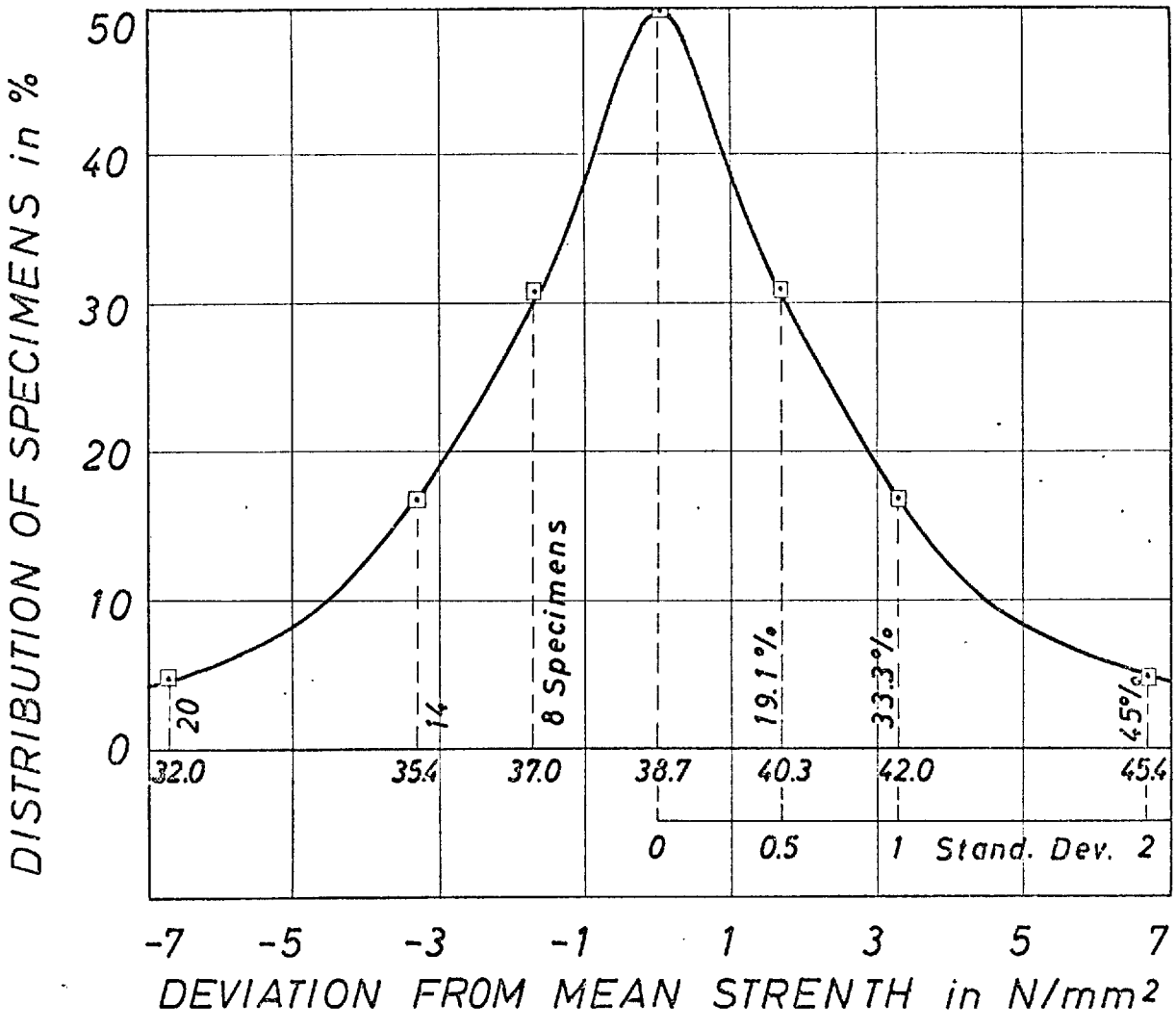


FIG. 4.5. DISTRIBUTION CURVE FOR STRENGTH OF CONCRETE CUBES

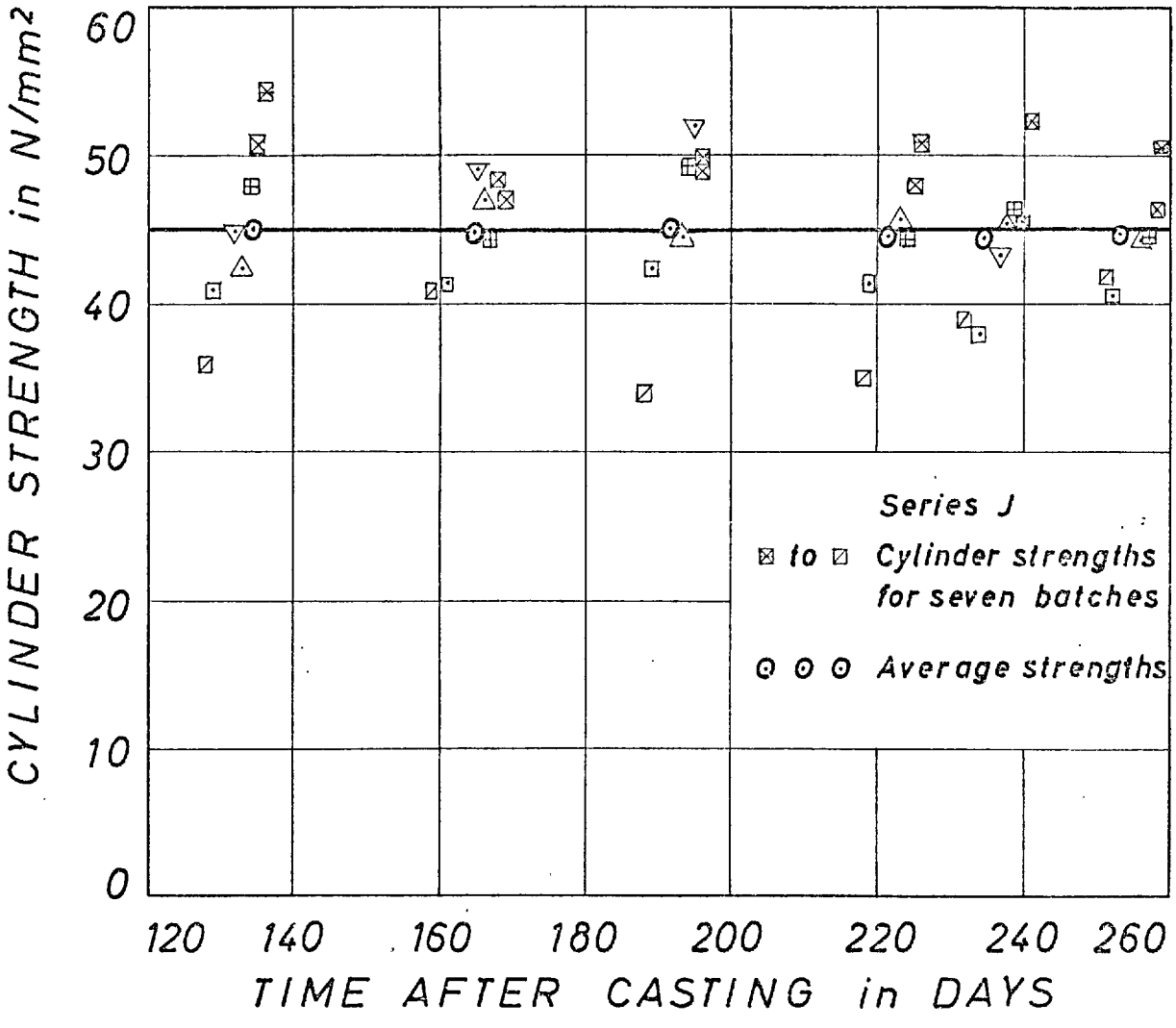


FIG. 4.6. CYLINDER STRENGTH OF CONCRETE FOR SERIES J

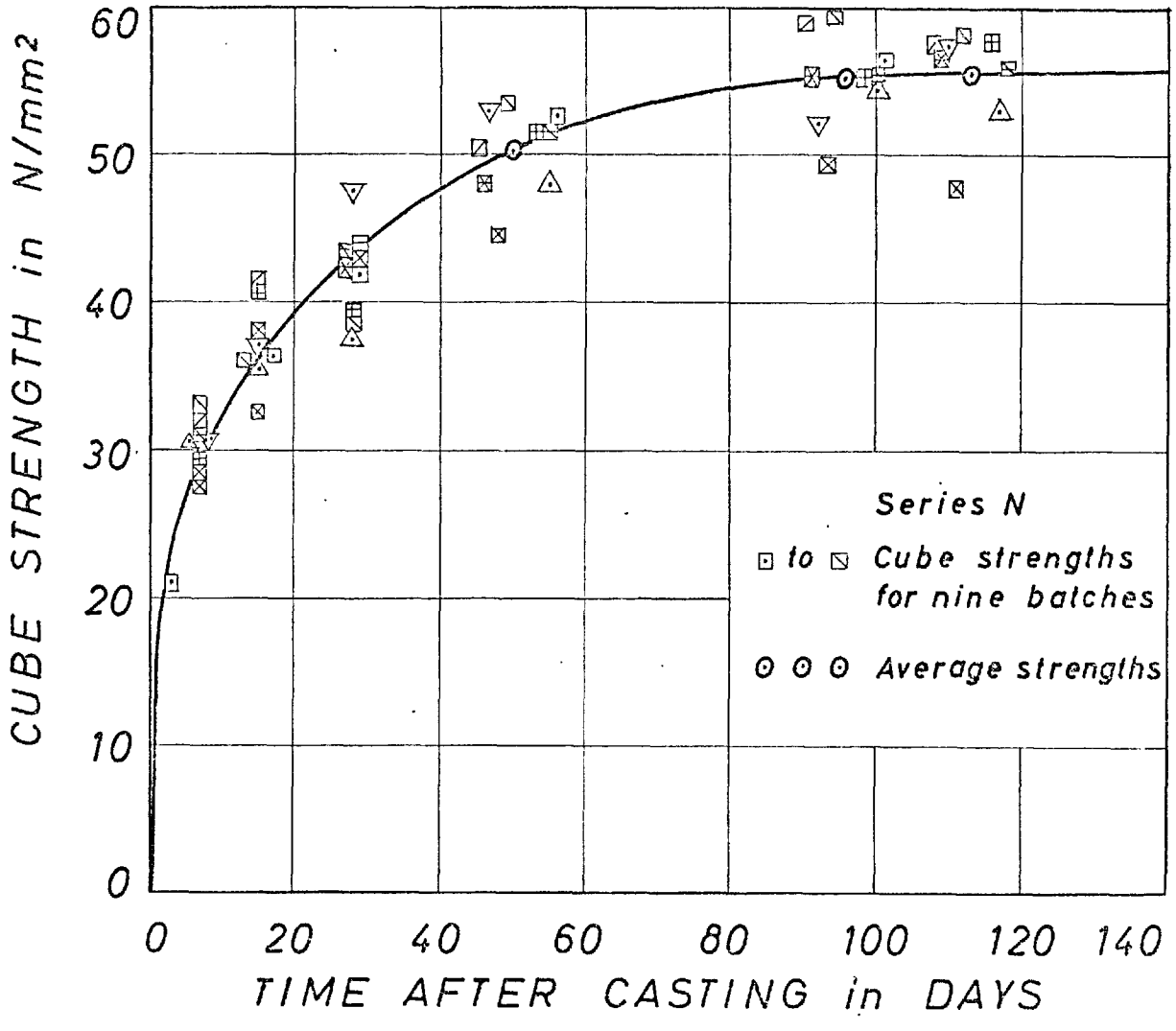


FIG. 4.7. CUBE STRENGTH OF CONCRETE FOR SERIES N

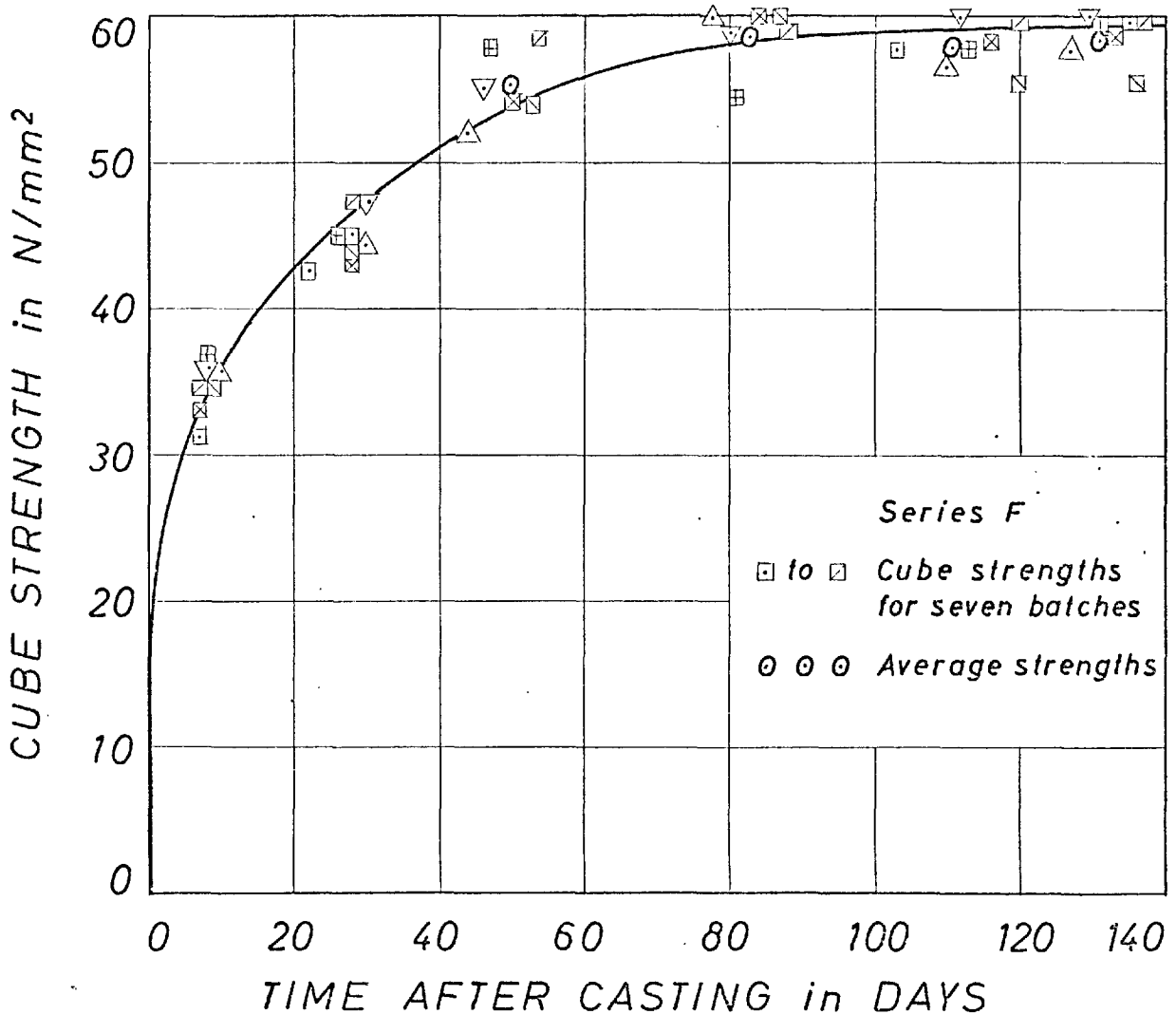


FIG. 4.8. CUBE STRENGTH OF CONCRETE FOR SERIES F

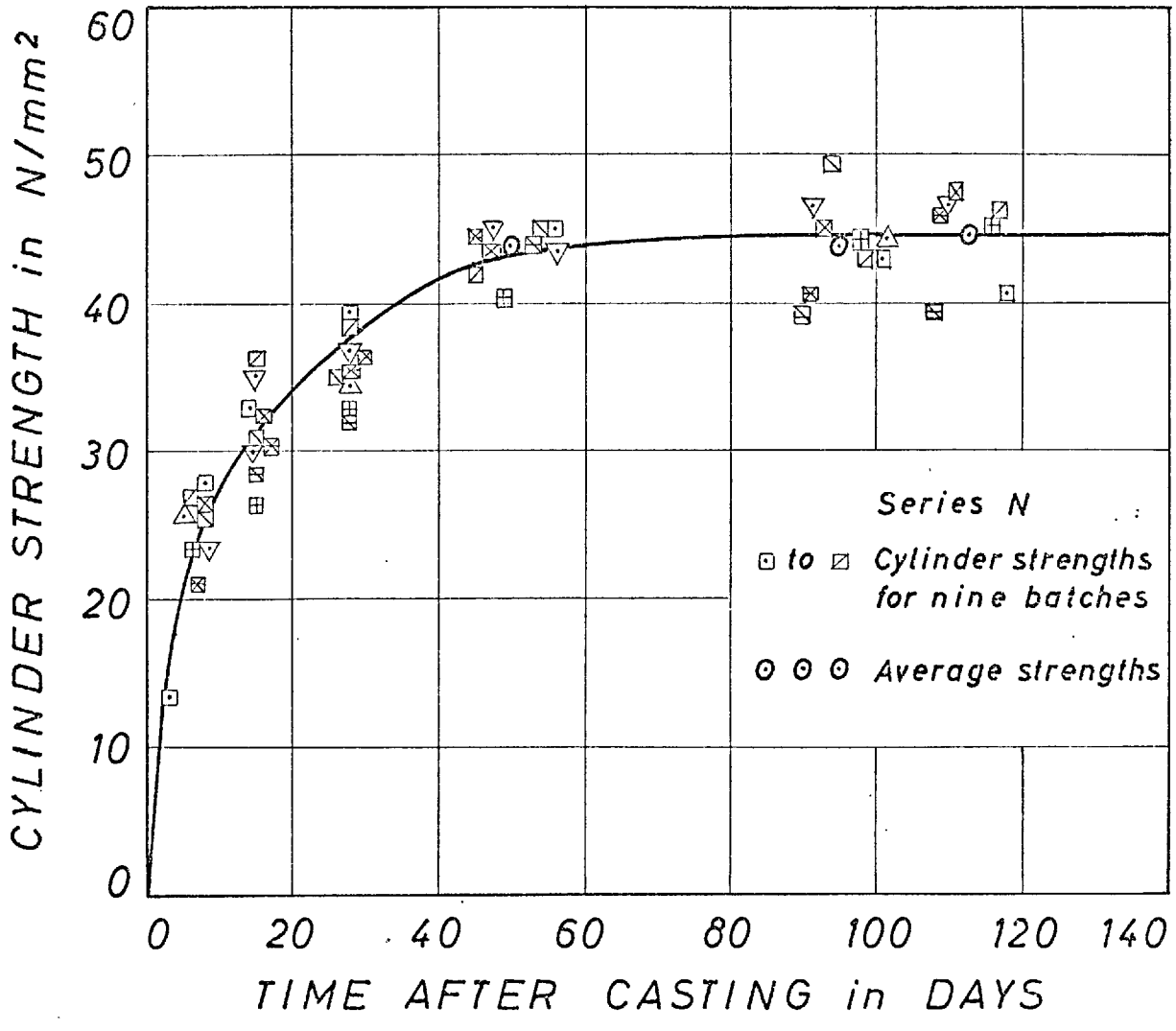


FIG. 4.9. CYLINDER STRENGTH OF CONCRETE FOR SERIES N

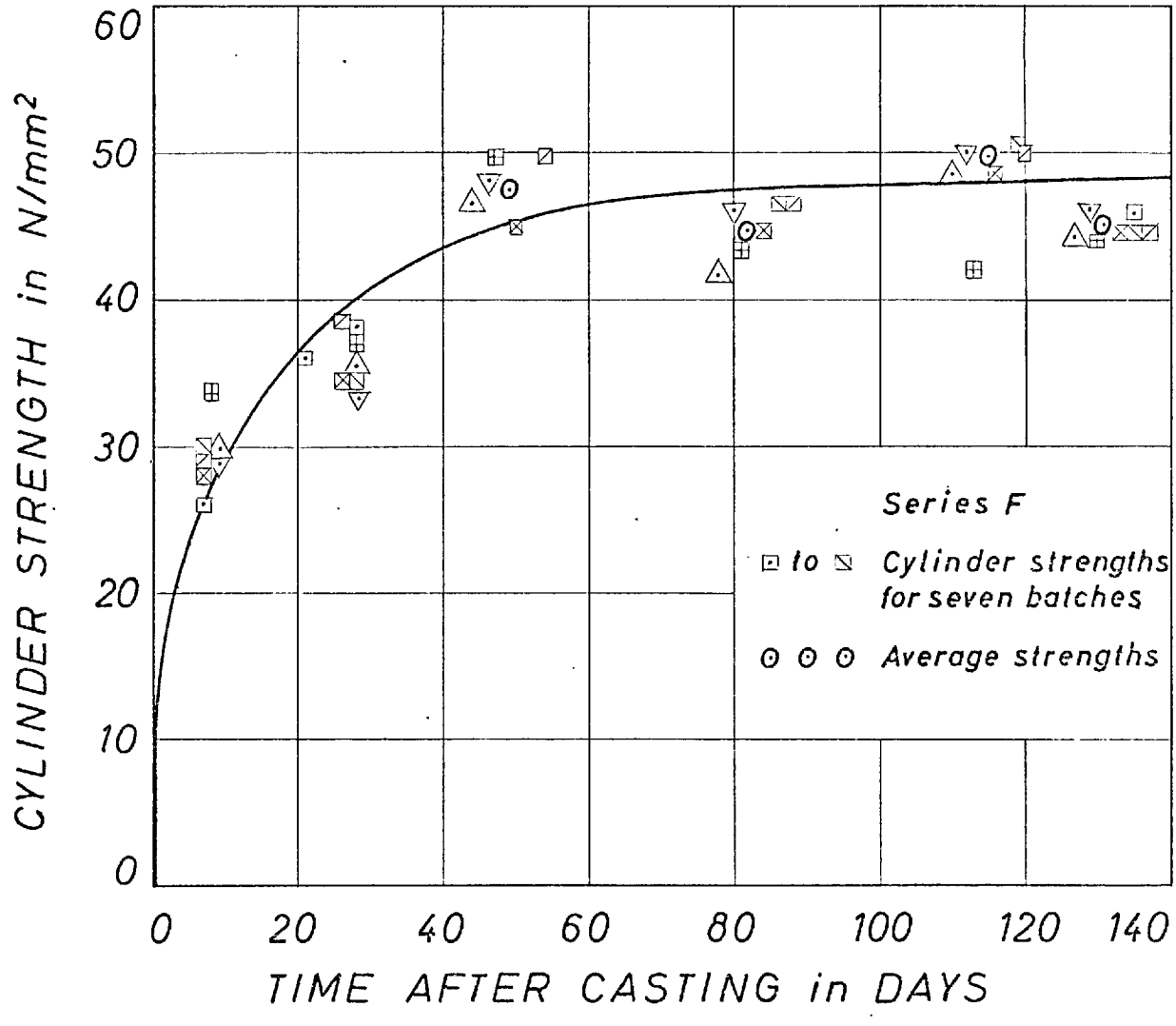


FIG. 4.10. CYLINDER STRENGTH OF CONCRETE FOR SERIES F

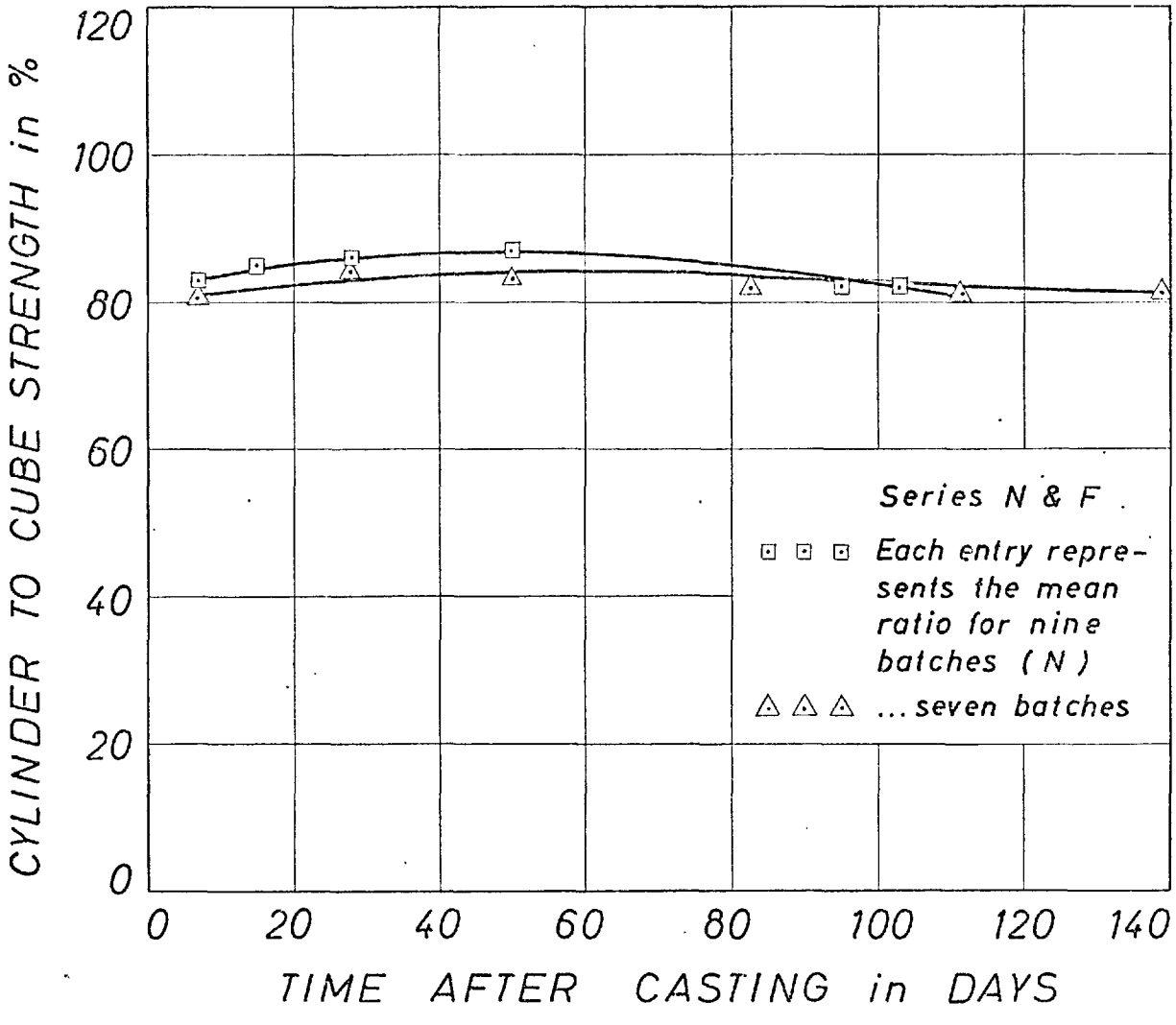


FIG. 4.11. RATIO OF CYLINDER TO CUBE STRENGTH FOR SERIES N & F

Comparing the values in col. 2 and 3 of table 4.3, the slightly lower strength (-6%) of the larger cylinders is noticed. The reason may be the higher probability with which a local weekness may occur in larger specimens.

Figures (4.7) and (4.8) show the cube strength for Series N and F as a function of time. The 28-day strength is 43 and 45 N/mm^2 respectively ; at 140 days after casting, the values amount to 55.5 and 59 N/mm^2.

For comparison, figures (4.9) and (4.10) describe the corresponding increase in cylinder strength. Here, the 28-day strength reaches 37 and 38 N/mm^2, while the values at 140 days are 45 and 48 N/mm^2. All curves have levelled off completely, thus indicating that no increase in strength is anticipated for the period after four months.

Finally, the ratio of cylinder strength to cube strength is plotted against the time scale for Series N and F, invariably falling between 81 and 87%. The profiles of the curves in figure (4.11) are slightly convex-up with the peak occurring at 50 days. From figures (4.7) to (4.10), 90% of the final strength is gained by this time.

Tentatively, the lower surface-volume ratio of the control cylinders against the control cubes stimulates a faster gain of strength initially. Once, however, the levelling off commences, the cubes retain a moisture which is higher by 1.5% (Series F) and 2% (Series N). Thus the hydration process in the cubes has advanced more strongly thereafter.

Neglecting any possible increase in strength after 140 days, the ratio of 28-day strength to final strength for the control cubes of Series N and F, works out at 77.5 and 76.5% respectively, while the corresponding ratio for the control cylinders amounts to 82 and 79%.

CHAPTER V

THERMAL CREEP CHARACTERISTICS OF CONCRETE SPECIMENTS

5.1. OBJECTIVE

As the present research aims to investigate the long-term temperature-dependent behaviour of concrete continua, it should be mentioned that concrete is the main load bearing material in the construction not only of building structures, but of prestressed concrete pressure vessels as well.

One aspect of the philosophy of safety common to both types of structures is that, while the structural stability is guaranteed, the safeguards against potential hazards like fire and thermal overload require exceptional attention.

However, fire and thermal overload are distinct. For fire, steep temperature gradients and the change in moisture content within short periods are characteristic. Thus the short-term high-temperature creep must be investigated. Thermal overload in pressure vessels, in contrast, requires research into long-term low-temperature creep.

To study the behaviour of concrete exposed to such severe environmental conditions, this chapter collects the author's experimental results concerning thermal creep characteristics and other temperature-dependent properties of concrete. Here, the evaluation of test data is restricted to phenomenological aspects; i.e. their visual assessment is pursued only to a point, where the ground for the development of the proposed theory is prepared.

The structural analysis is expounded in Chapter VI to X, while the analytic concept for the embodiment of the phenomenon of thermal creep is reconciled with the test results in Chapter XI.

5.2. RECORDED CREEP STRAINS

Except for the residual strength of concrete cylinders after heat testing, the data reported in this chapter were

obtained from experiments conducted on the creep testing machines designed by the author and described in Chapter III.

To investigate the phenomenon of thermal creep, some 45 tests were performed, including tests which failed at high temperatures, and confirmatory tests. Checking the continuity of results, it became apparent that for temperature up to 100°C and a stress/ cold strength ratio of s = 0.4, the recorded creep strains were falsified due to an electronic instability of the transducers. The five tests concerned were carried out during the calibration of the newly developed instrumentation.

Having established a uniform temperature distribution throughout the concrete cylinders by preheating them for one day at the relevant temperatures, a fixed compressive load equivalent to a stress/ cold strength ratio of 0.2, 0.4 or 0.66 was applied.

On average, the activation of the load consumed one minute, thus justifying that strains occurring immediately after its full imposition were in the first instant called thermoelastic. All cylinders were between six and twelve months old when tested and their average compressive old strength worked out at $c'_{uy} = 42$ N/mm^2.

The basic information acquired is at hand in form of creep profiles displayed in figs. (5.1) to (5.5), the parameter being the test temperature. The profiles are drawn directly from test results, hence most of the subsequent findings are deduced from them. Low temperature responses for s = 0.2 and 0.66 are charted in fig. (5.1), and for s = 0.4 in fig. (5.2). The strains developing at high temperatures are plotted in figs. (5.3), (5.4) and (5.5), the corresponding stresses being associated with ratios of 0.2, 0.4 and 0.66.

Of all cylinders, only those subjected to both high temperatures and a stress equalling a ratio of 0.4 were recruited from specimens of Series J; the others pertained to Series N.

The original test data are given in tables A6.1 to A6.3 of Appendix VI.

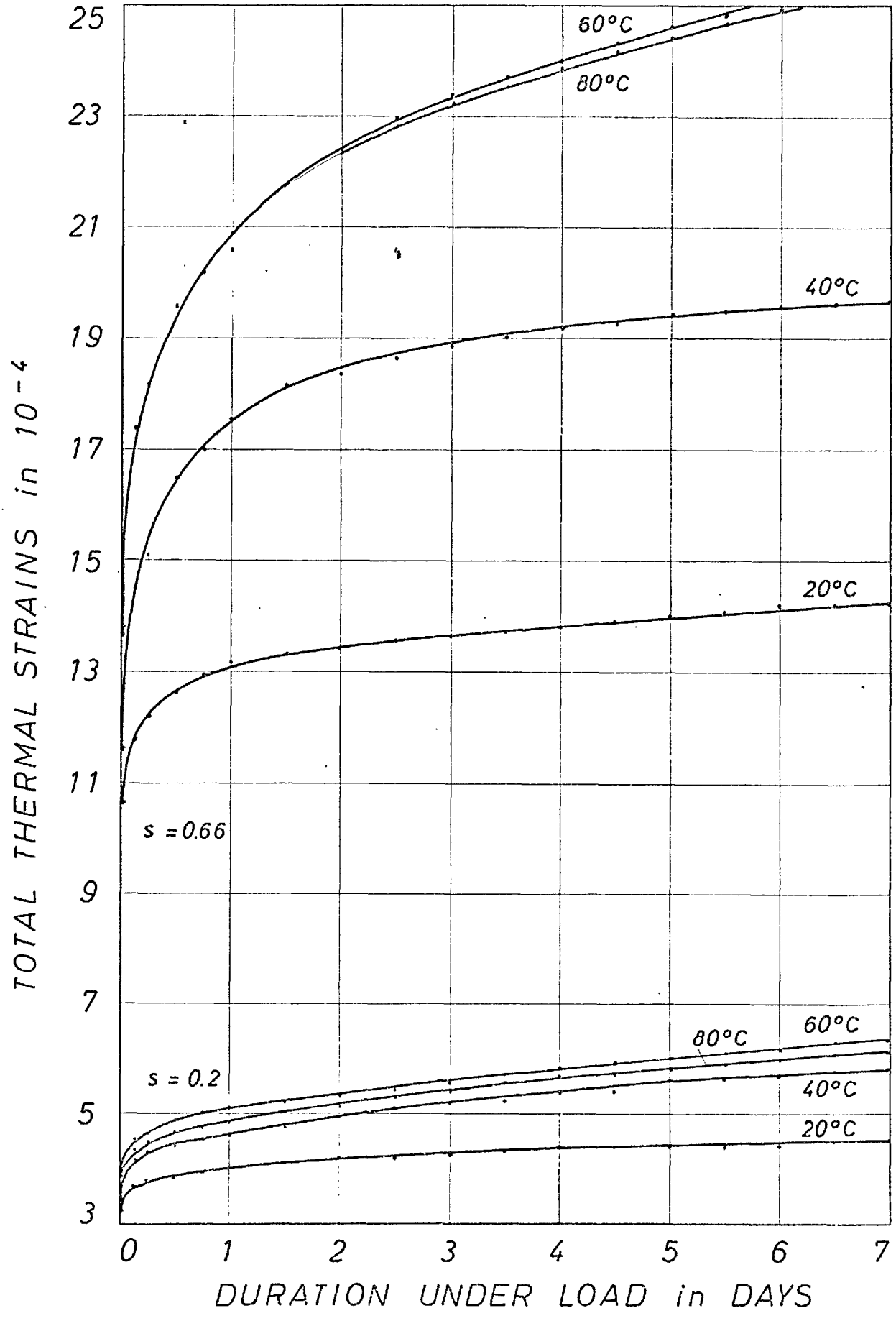


FIG. 5.1. LOW TEMPERATURE CREEP FOR STRESS / COLD STRENGTH RATIOS OF 0.2 & 0.66

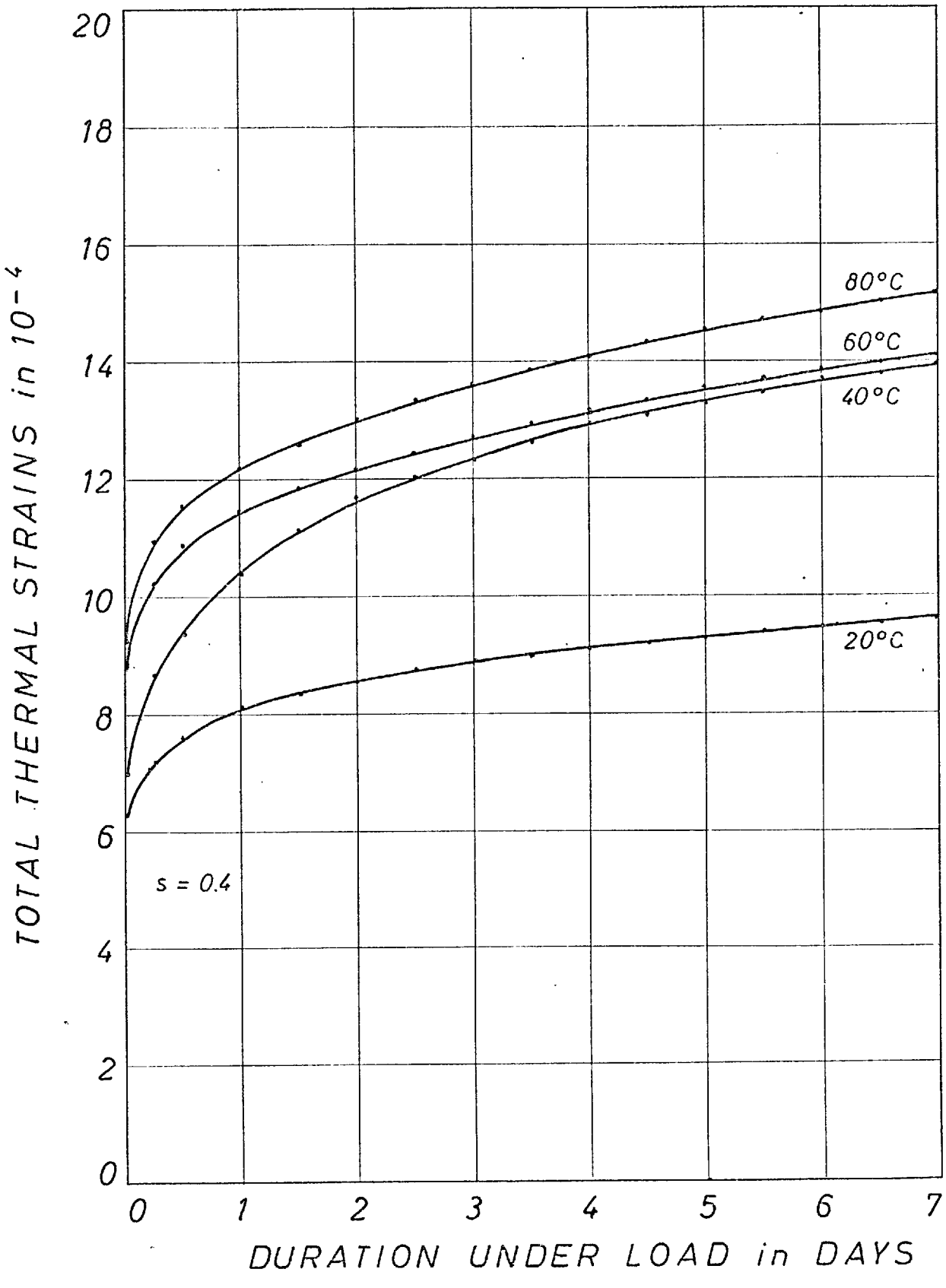


FIG. 5.2. LOW TEMPERATURE CREEP FOR A STRESS / COLD STRENGTH RATIO OF 0.4

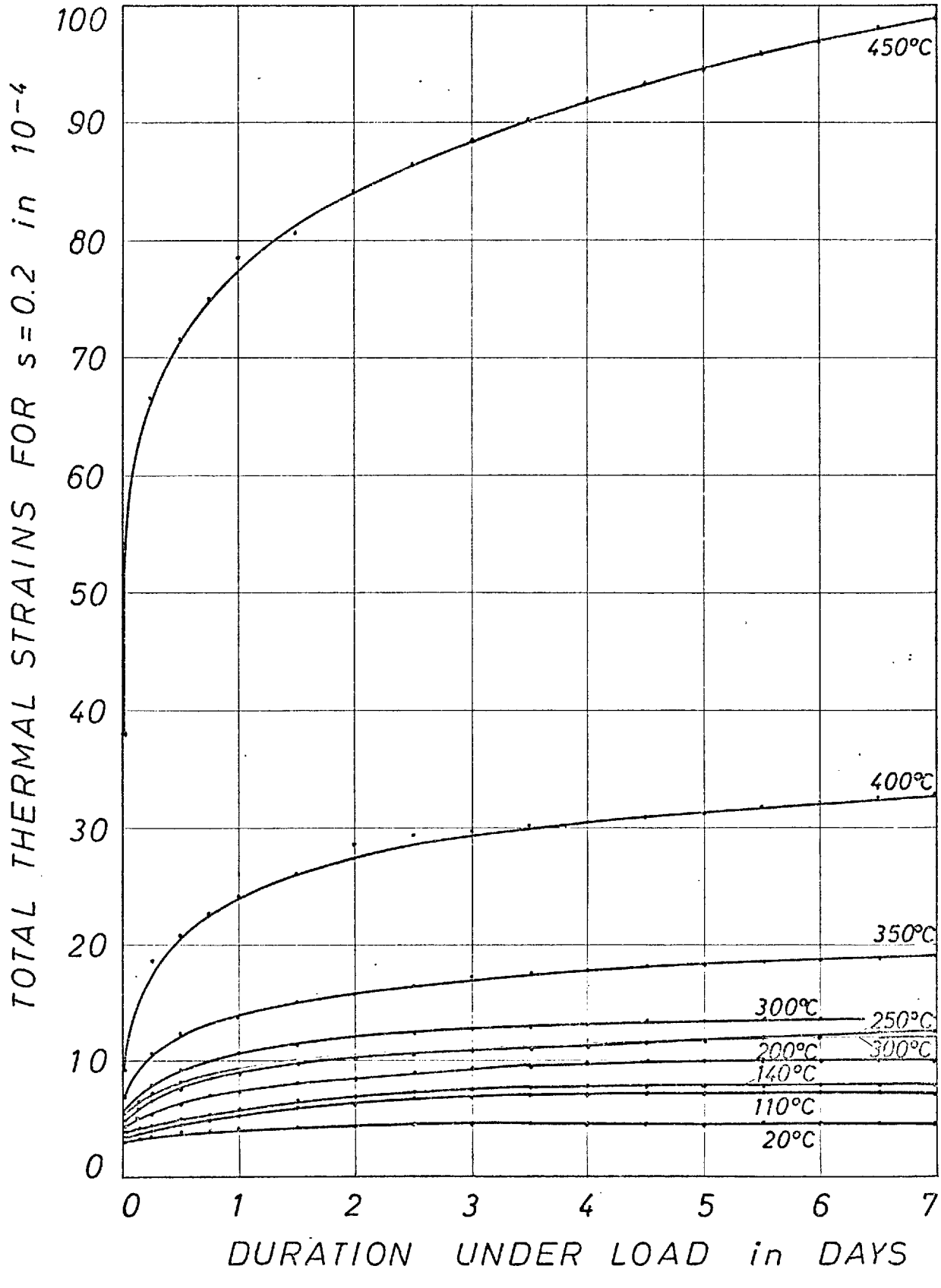


FIG. 5.3. HIGH TEMPERATURE CREEP FOR A STRESS / COLD STRENGTH RATIO OF 0.2

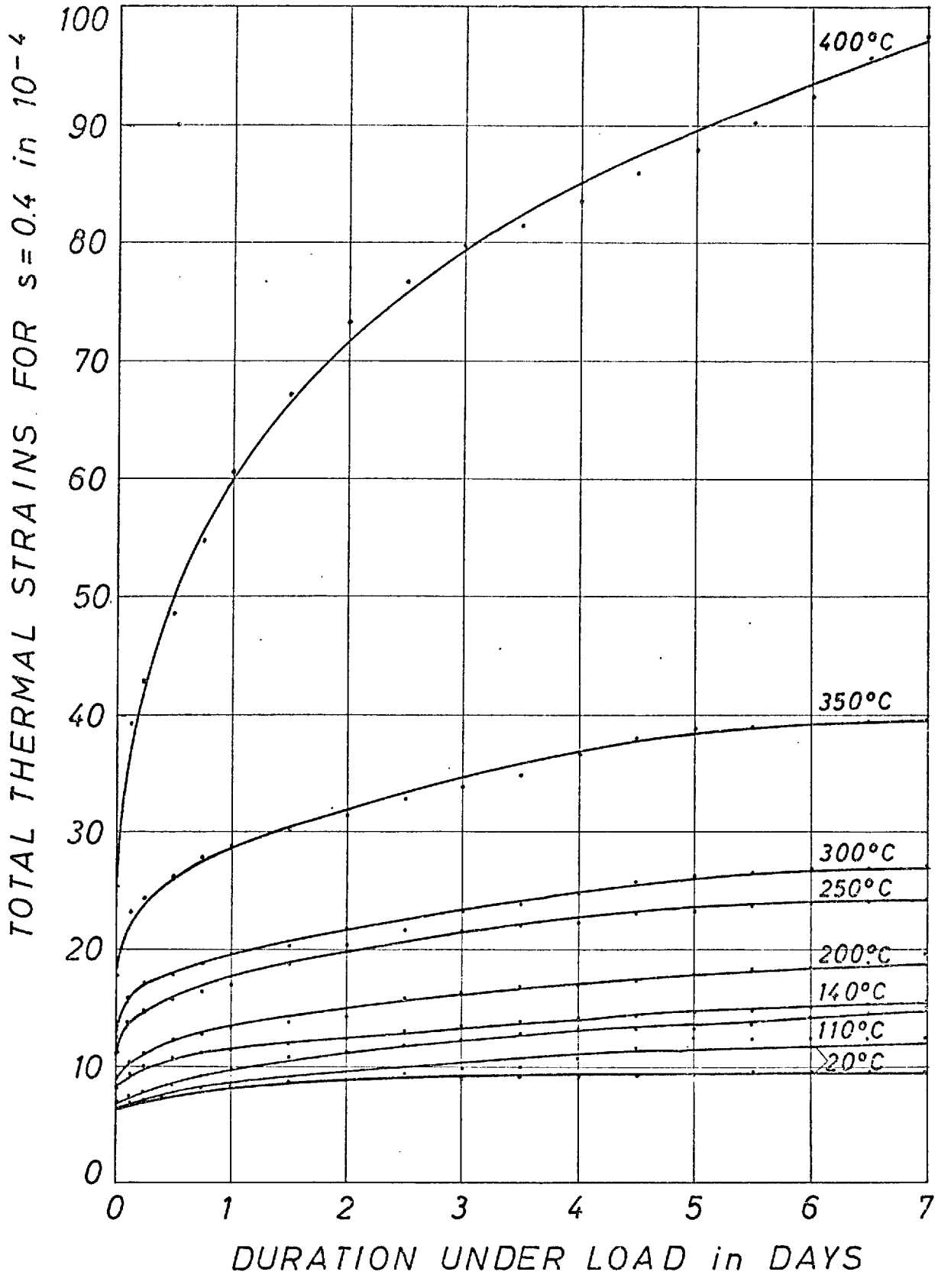


FIG. 5.4. HIGH TEMPERATURE CREEP FOR A STRESS / COLD STRENGTH RATIO OF 0.4

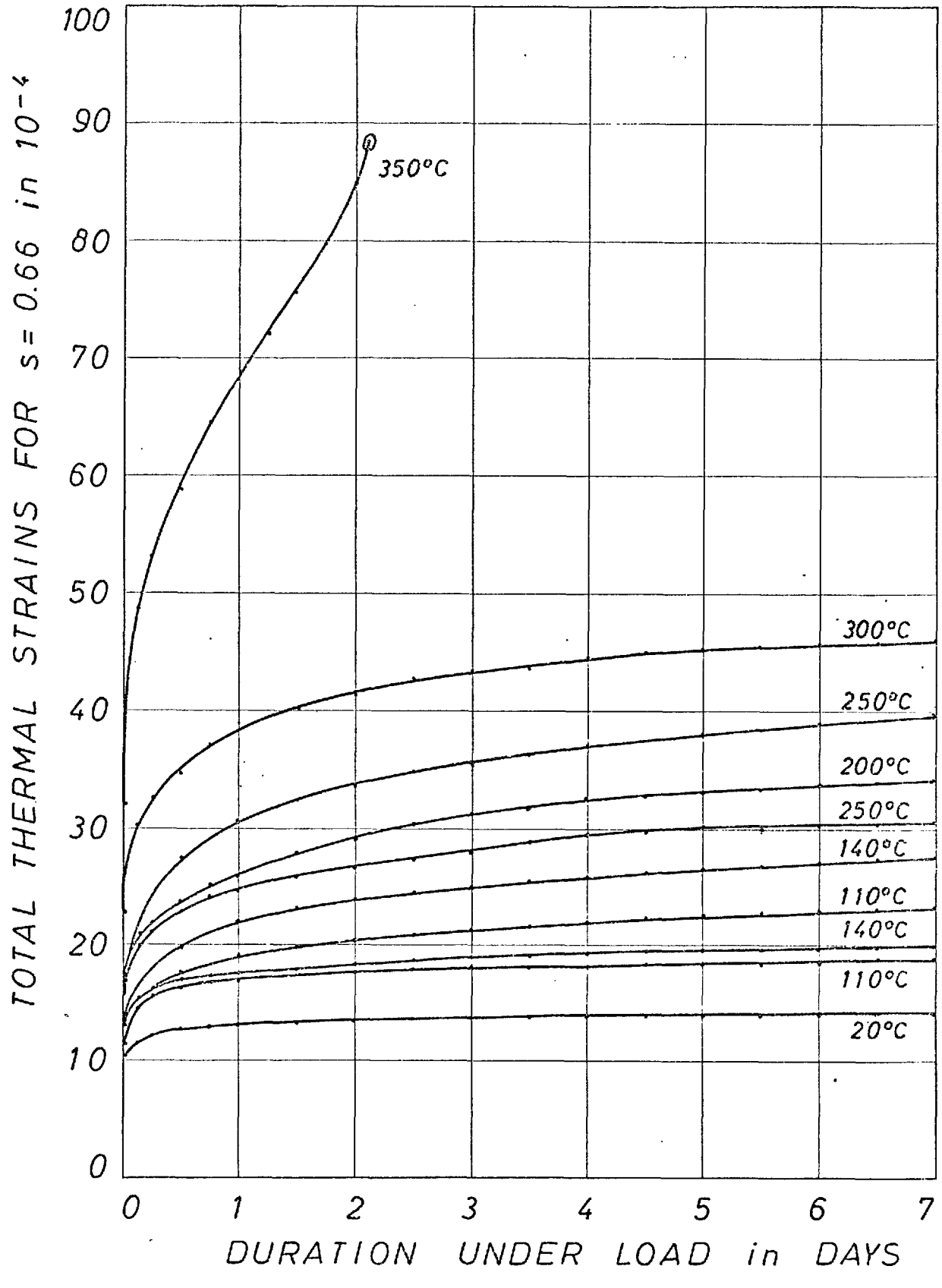


FIG. 5.5. HIGH TEMPERATURE CREEP FOR A STRESS / COLD STRENGTH RATIO OF 0.66

5.3. THERMOELASTIC STRAINS

Since in figs. (5.1) to (5.5) the steep initial gradients of the creep profiles largely bar the pinpointing of the values for the initial strains, a parameter study is carried out in fig. (5.6) to show the effect of the stress/ cold strength ratio on the formation of thermoelastic strains.

Scrutinizing fig. (5.6) with the intention of finding a regularity in the stress-dependence, an approximate linearity is observed - at least for the lower temperatures. Since the deformations due to the lower stresses have a greater likelihood of being linear, the tests carried out at s = 0.2 were taken as the basis of normalization. Thus the straight lines from 0 to s = 0.2 were extrapolated to give a pseudo-elastic deformation at 0.4 and 0.66.

Scaling all thermoelastic strain readings, as if they were taken at s = 0.2, a normalized profile common to the results obtained for the three different stress/ cold strength ratios may be drawn, as done in fig. (5.15). Independent of the load level, a local peak in the strains is registered at 60^0C. The fitting of a single, monotonically increasing function to the test data is thus precluded, leaving as the simplest solution the superposition of a tri-linear function.

As the stress-dependent test data exhibit absolute linearity in the strains recorded at the base temperature T = 20^0C, the author proposes a formula for the determination of thermoelastic strains in which the reference strain $\varepsilon_{0.2}(20^0C)$ appears as a factorizing parameter

$$\varepsilon_{0.2}(T) = \varepsilon_{0.2}(20^0C)\ (1.0 + 0.00833\ (T - 30))\ (30 \leq T \leq 60)$$

$$\varepsilon_{0.2}(T) = \varepsilon_{0.2}(20^0C)\ (1.25 - 0.00250\ (T - 60))\ (60 \leq T \leq 110)$$

$$\varepsilon_{0.2}(T) = \varepsilon_{0.2}(20^0C)\ (1.125 - 0.00349\ (T - 110))\ (110 \leq T \leq 350) \qquad (5.1)$$

where $\varepsilon_{0.2}(20^0C)$ = 320 μ and the term ambient is applicable to temperatures up to 30^0C.

As seen from fig. (5.6), for s = 0.2, the highest endurable temperatures is 452°C. Thus, the initial strains experienced for thermal conditions close to that temperature embody large, unpredictable plastic components; their mathematical consideration proves unreliable.

Analysing the thermoelasto-plastic domain of strains in fig. (5.8), the following approximate field function may be arrived at for test temperature higher or equal to 200°C

$$\varepsilon(s,T,0) = \left(\frac{s}{0.1}\right)^{1+e(s,T)} \left(\varepsilon_{0.1}(200^{0}C) + 15.4\ (0.01\ T - 2)^{4}\right) \quad \text{(in } \mu\text{)} \qquad (5.2)$$

where $e(s,T) = 1.5\ (0.001\ T - 0.18)$

For s = 0.1, the exponent e(s,T) becomes zero, rendering the solution of formula (5.2) thermoelastic. $\varepsilon_{0.1}(200^{0}C)$, which amounts to 210 μ, and strains for T = 200°C may be determined using formula (5.1).

5.4. ULTIMATE THERMAL STRAINS

Ultimate design methods for the analysis of concrete structures take into consideration the largest possible strains withstood by concrete. Consequently, ultimate values attained by temperature-dependent strains for various load levels would be of interest. An answer may be elicited from figs. (5.6), (5.7) and (5.13).

Fig. (5.6) infers that concrete of the specified mix and age fails under loads imposing initial strains greater than about 40.10^{-4} = 0.4%. Deviating from the conventional definitions in structural mechanics however, ultimate values in thermal analyses are in addition temperature-dependent, thus justifying that the extremal value of the temperature- and stress-dependent strain field is coined maximum ultimate strain.

In other words, for higher temperature and lower stress/ cold strength ratios, even larger values than 0.4% may be expected for the initial strains. By tentative

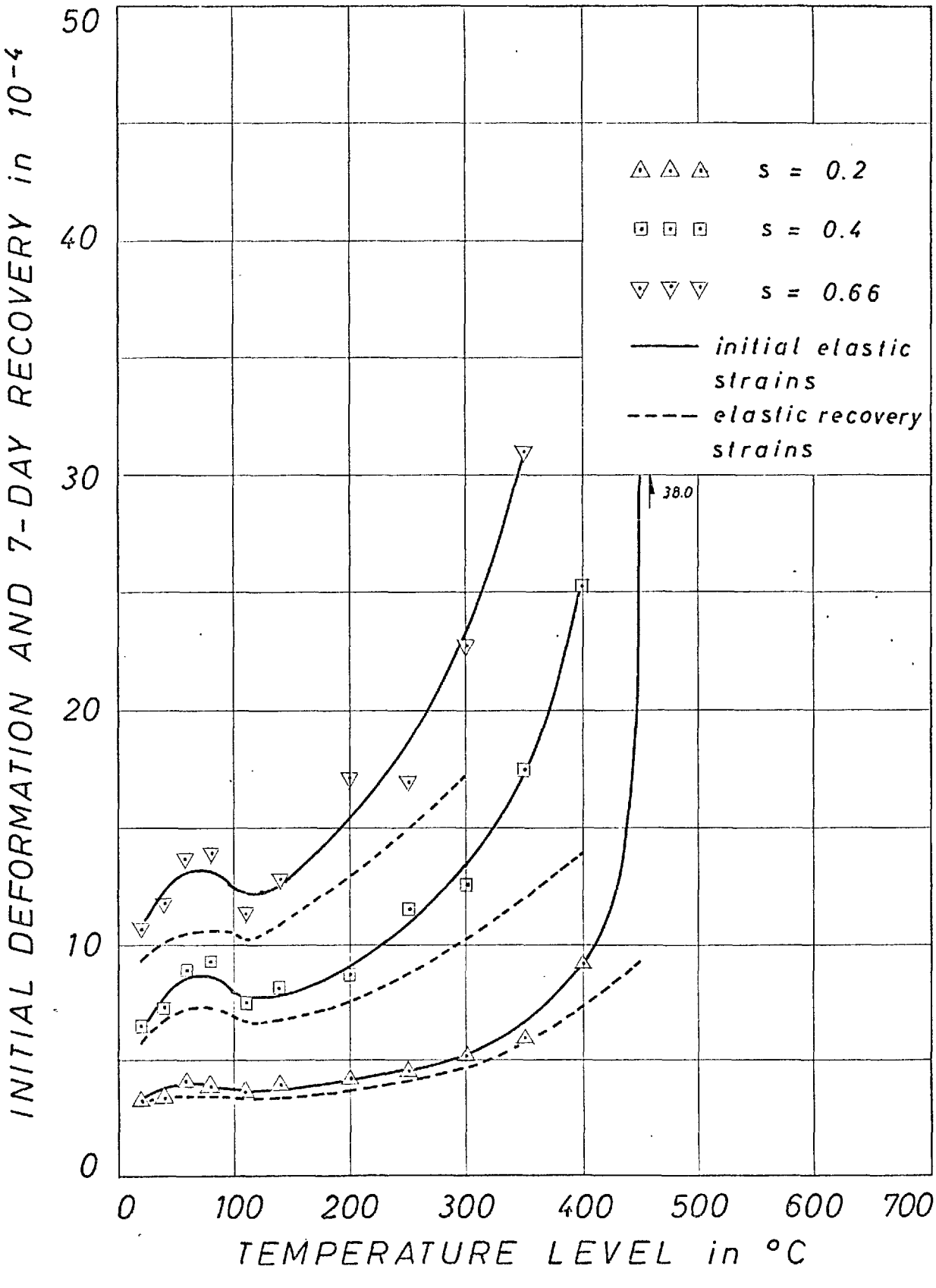


FIG. 5.6. INITIAL & RECOVERED THERMO-ELASTIC STRAINS

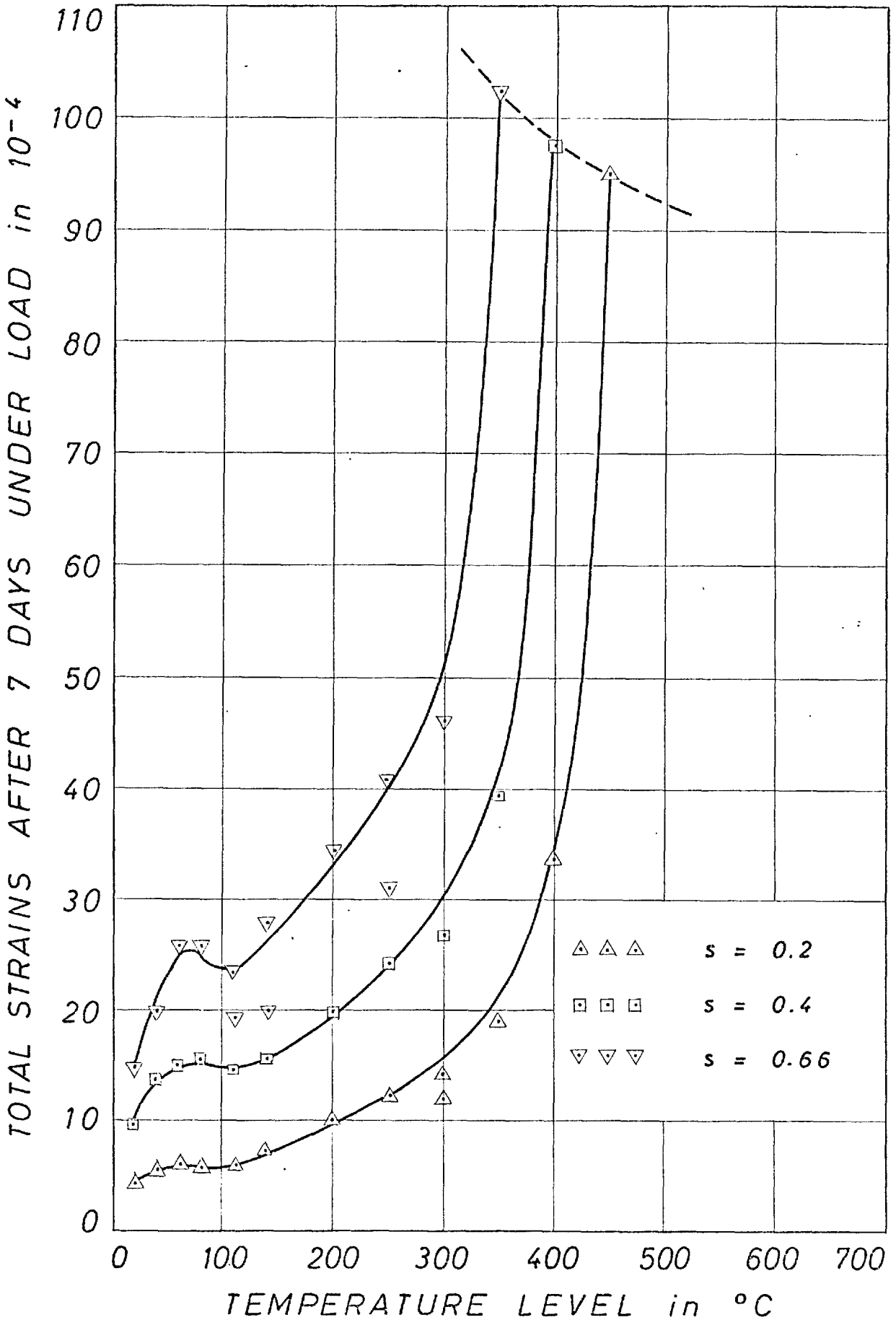


FIG. 5.7. TOTAL THERMAL STRAINS AFTER SEVEN DAYS UNDER LOAD

extrapolation along the confidence limits drawn from experiments in fig. (5.13), for s = 0.1 and T = 600°C a thermoelastoplastic strain of about 1% may be predicted. This value presumably coincides with the maximum ultimate thermoelasto-plastic deformation, as concrete ceases to take any significant stress when heated to temperatures beyond 600°C.

Thus it may be concluded that

$$\varepsilon(T,t=0)_{max} \tilde{=} 1\% \qquad (5.3)$$

As regards ultimate creep strains, fig. (5.7) indicates that within the domain $0.2 \leq s \leq 0.66$, the 7-day creep strains do not exceed values of about 1%, irrespective of the test temperature. Since by extrapolation along the creep profiles in figs. (5.3) to (5.5) the estimated maximum increase in strain beyond seven days is limited to about 20%, the ultimate total creep strain at infinity may be expected to settle at

$$\varepsilon(T,t=\infty)_{max} \tilde{=} 1.2\% \qquad (5.4)$$

The applicability of statement (5.4) outside the investigated stress domain is presumed but not guaranteed.

5.5. MODULUS OF THERMOELASTO-PLASTICITY

Once the initial thermoelastic strains are recorded, the modulus of thermoelasticity is determined by dividing the stress by the strain.

Before proceeding, however, it should be stated up to which stresses the corresponding deformations may be termed thermoelastic. For this reason, the initial strains registered in fig. (5.6) are plotted versus the stress/ cold strength ratio, as depicted in fig. (5.8). The parameter is the test temperature. Reference is also made to the stress-strain curves in fig. (5.17).

For low temperatures, the modified constitutive relationship is clearly linear. Fig. (5.8) infers that for a good-quality concrete the domain of thermoelasticity extends from zero load to two third of the ultimate

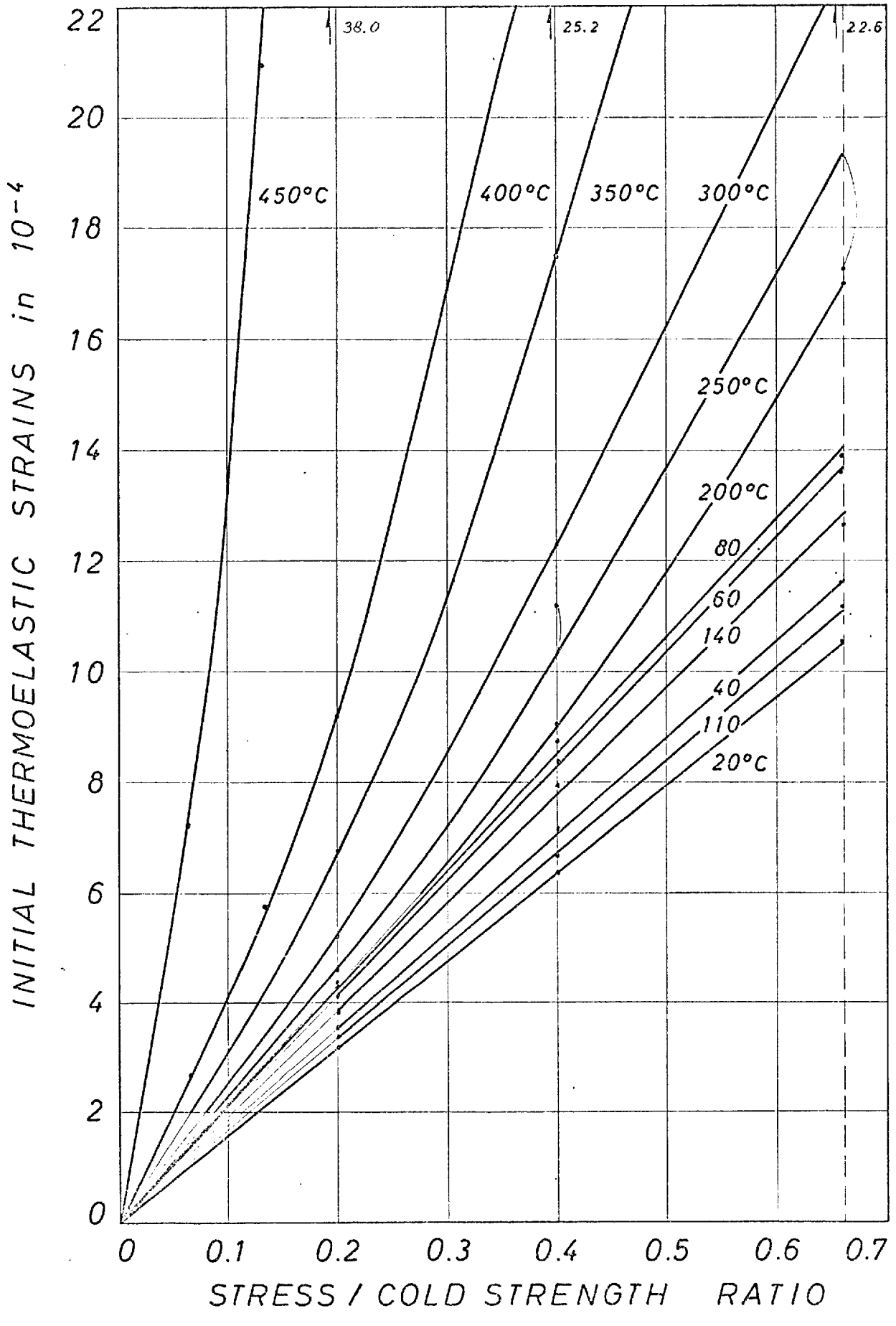


FIG. 5.8. LOAD-DEPENDENT INITIAL THERMOELASTIC STRAINS

cold strength and from ambient temperature up to 140°C.

With the environmental conditions becoming more severe, a transition from thermoelastic to thermoplastic behaviour takes place. From fig. (5.8), the boundary of the thermo-elastic domain is marked by the data pairs (s,T) = (0.66,140°C), (0.4,200°C), (0.2,300°C) and (0.1,400°C). For values beyond, the non-linearity builds up.

This borne in mind, the profiles in fig. (5.9), which are constructed from the inverse of the instantaneous strain responses, define the mechanical modulus for the thermo-elastic range investigated. Since the transition to plastic behaviour is gradual and temperature-dependent, the uncoupling of the elastic and plastic domains proves impracticable.

There is reason to believe that particularly at high temperatures and high stress/ cold strength ratios, the non-linearity illustrated by the family of modified stress-strain relations in fig. (5.8) is brought about not only by plastic deformations but by viscous components as well; despite the certainty that the initial strains were recorded within two minutes after the load-application.

For a stress/ cold strength ratio of s = 0.2, errors in the initial strain readings due to viscous effects are reduced, since in the corresponding test procedures the load was applied within 20 sec. Adhering to the definition of thermoelasto-plasticity, here only the profile for s = 0.2 is approached mathematically. Save in the vicinity of 60°C, where the associated value drops to 80% of the initial one, an inversed quadratic parabola may be fitted to the test results entered in fig. (5.9).

Arithmetically, the author's formula for the obtainment of the relative modulus of thermoelasto-plasticity for virgin concrete of the given mix and age reads

$$m_{0.2} = 4.81\ (452 - T)^{\frac{1}{2}} \qquad \text{(in \%)} \qquad (5.5)$$

where $m_{0.2}$ is defined by $E_{ini}(T)/E_{ini}(20^{0}C)$ and $E_{ini}(20^{0}C)$ = 28.1 KN/mm^2.

To emphasize the usefulness of formula (5.5), a comparison between recorded and fitted values is carried out in table 5.1.

Table 5.1. Relative modulus of thermoelastic-plasticity

T	20	110	140	200	250	300	350	400	450
$m_{0.2_{rec}}$	100	89	85	76	69	62	48	35	8
$m_{0.2_{fit}}$	100	91	85	76	68	59	49	35	7

(in %)

5.6. MODULUS OF QUASI-THERMOELASTIC-PLASTICITY

If it is argued that in practical design one cannot afford to distinguish between truly instantaneous load-applications and those which consume infinitesimal time intervals like to two minutes, a more general modulus of thermoelasto-plasticity which tolerates small viscous contributions to the initial deformations may be called into existence.

The vertices of the parabolas to be fitted to the temperature-dependent moduli in fig. (5.9) represent the ultimate temperatures associated with the individual stress levels and are thus located along the abscissa. To determine them, the limiting stress/ cold strength ratios are plotted against the test temperature in fig. (5.14). Since the load is applied by weights of finite magnitude, only upper and lower bound solutions can be produced. Upper bound values symbolize the collapse the specimens, while for lower bound values the corresponding load is still endured.

The data from the failure tests were not sufficient to warrant a rigorous analysis of the results. Instead, the limiting profile in fig. (5.14) is plotted and approximated by a tri-linear function.

$$s_{ult}(T) = 1.0 - 0.001\,(T - 20) \quad (20 \leq T \leq 350)$$

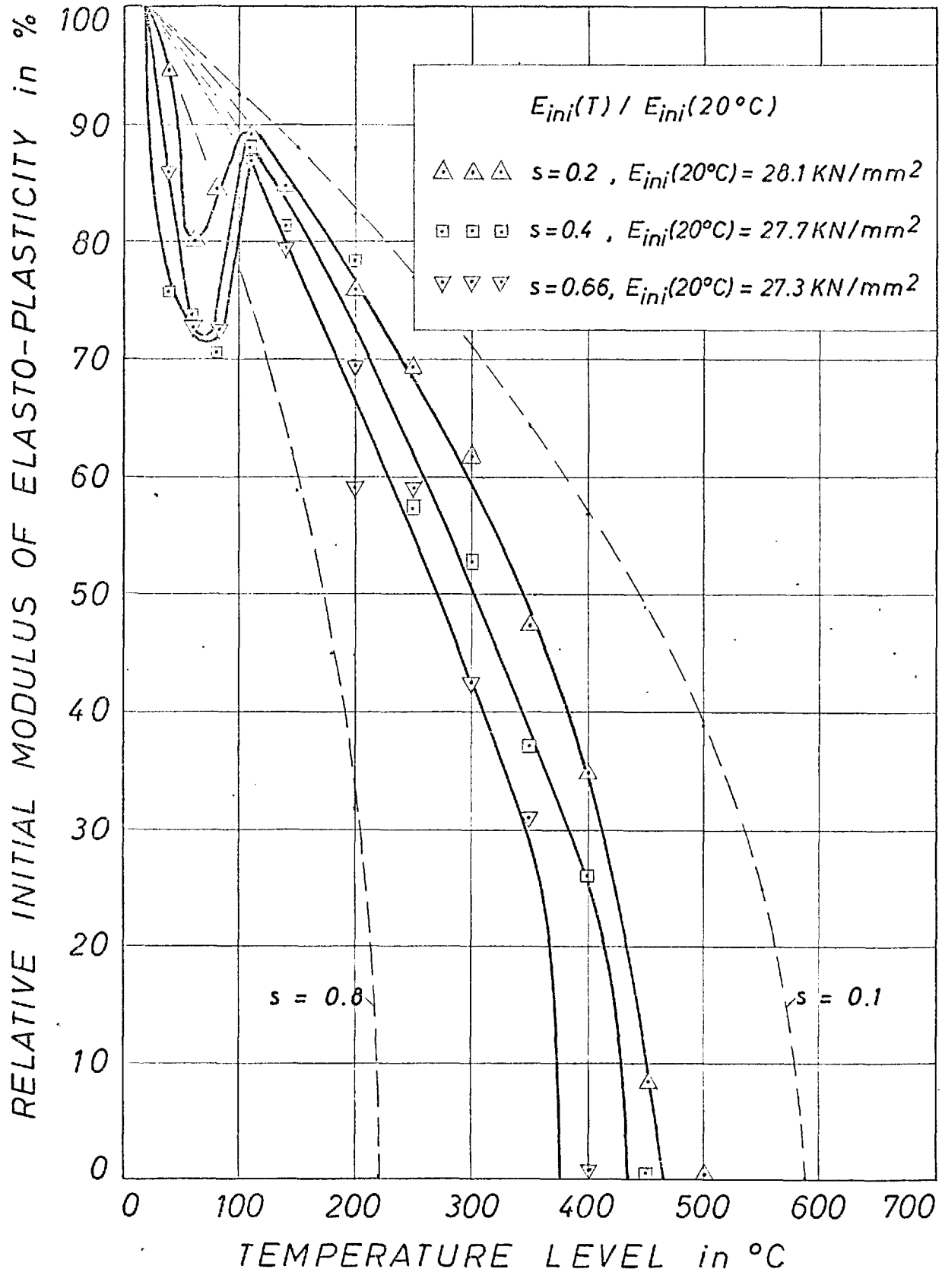


FIG. 5.9. RELATIVE INITIAL MODULUS OF THERMOELASTO-PLASTICITY

$$s_{ult}(T) = 0.66 - 0.00457\,(T - 350)\quad(350 \leq T \leq 452)$$

$$s_{ult}(T) = 0.2 - 0.000746\,(T - 452)\quad(452 \leq T \leq 700) \tag{5.6}$$

The ultimate temperatures endured, i.e. the vertices of the parabolas, are arrived at by inverting eqs. (5.6)

$$\begin{aligned} T_{ult}(s) &= 1000\,(1.0 - s) + 20 \quad (0.66 \leq s \leq 1.0) \\ T_{ult}(s) &= 219\,(0.66 - s) + 350 \quad (0.2 \leq s \leq 0.66) \\ T_{ult}(s) &= 1340\,(0.2 - s) + 452 \quad (0.02 \leq s \leq 0.2) \end{aligned} \tag{5.7}$$

Relying on the experimentally corroborated values in figs. (5.9) and (5.14), the author suggests the following formula for the determination of the stress and temperature-dependent relative modulus of quasi-thermoelasto-plasticity

$$m_s = a(s)\,(T_{ult}(s) - T)^{\frac{1}{2}} \tag{5.8}$$

where $T_{ult}(s)$ is given by eqs. (5.7) and the parameter $a(s)$ is obtainable from the simple expression

$$a(s) = 100\,(T_{ult}(s) - 20)^{-\frac{1}{2}} \tag{5.9}$$

To illustrate the general applicability of formula (5.8), some experimental and empirical values for $s = 0.4$ and 0.66 are compared in table 5.2. Also, eq. (5.5) is identically satisfied.

Table 5.2. Relative modulus of quasi-thermoelasto-plasticity

T	20	110	140	200	250	300	350	400
$m_{0.4\ rec}$	100	88	82	78	59	53	37	26
$m_{0.4\ fit}$	100	88	83	72	64	53	38	13
$m_{0.66\ rec}$	100	88	80	69	59	42	30	-
$m_{0.66\ fit}$	100	85	80	67	55	39	0	-

(in %)

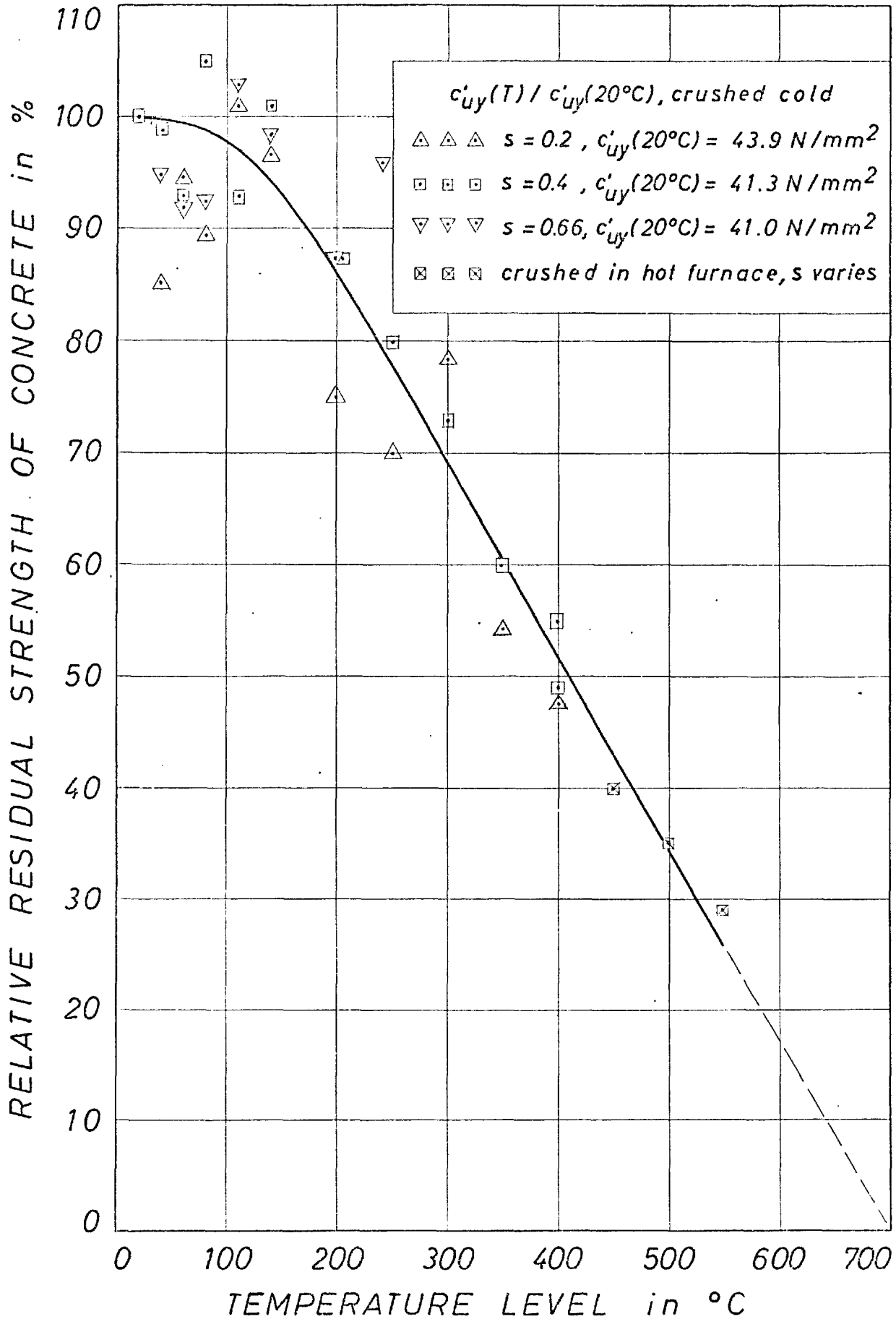


FIG. 5.10. TEMPERATURE-DEPENDENT CYLINDER STRENGTH

Based on formula (5.8), the temperature-induced deterioration of concrete can be predicted for various stress/ cold strength ratios. Examples are shown in fig. (5.9) for s = 0.1 and 0.8.

5.7. ULTIMATE HOT CYLINDER STRENGTH

The temperature-dependent ultimate strength of concrete was tested on cylindrical specimens, after gently cooling and removal from the furnaces. Thus, unless premature failure occurred in the furnace, the specimens were crushed cold to yield the residual hot strength.

The results in fig. (5.10) seem to indicate that in contrast to the modulus of thermoelasto-plasticity, the ultimate strength is quite independent of the load level at which the preceding tests were conducted. Also, the continuity of the strength's profile beyond 400°C infers that the hot strength is independent of whether the specimens are crushed hot in the furnace or at ambient temperature after cooling.

As revealed by the entries in fig. (5.10), the reduction in the ultimate residual strength does not exceed 10%, as long as the temperature is kept below 150°C . For higher temperatures the author found the simple linear relation

$$n_{7\text{-day}} = (120 - 0.171\ T) \quad (150 \leq T \leq 700) \qquad (5.10)$$

where n is defined by the ratio $c'_{yu}(T)$ c'_{yu} (20°C) and the reference to c'_{yu} (20°C) = 42 N/mm^2.

For heating periods shorter or longer than one plus seven days, formula (5.10) may not apply.

5.8. NORMALIZED CREEP PROFILES

One of the purposes of monitoring thermal creep strains at various stress/ cold strength ratios is to investigate the extent of the applicability of the superposition hypothesis in the thermal analysis of concrete structures. Normalizing the profiles displayed in figs. (5.1) to (5.5) to a reference stress/ cold strength ratio of, say, 0.2, an

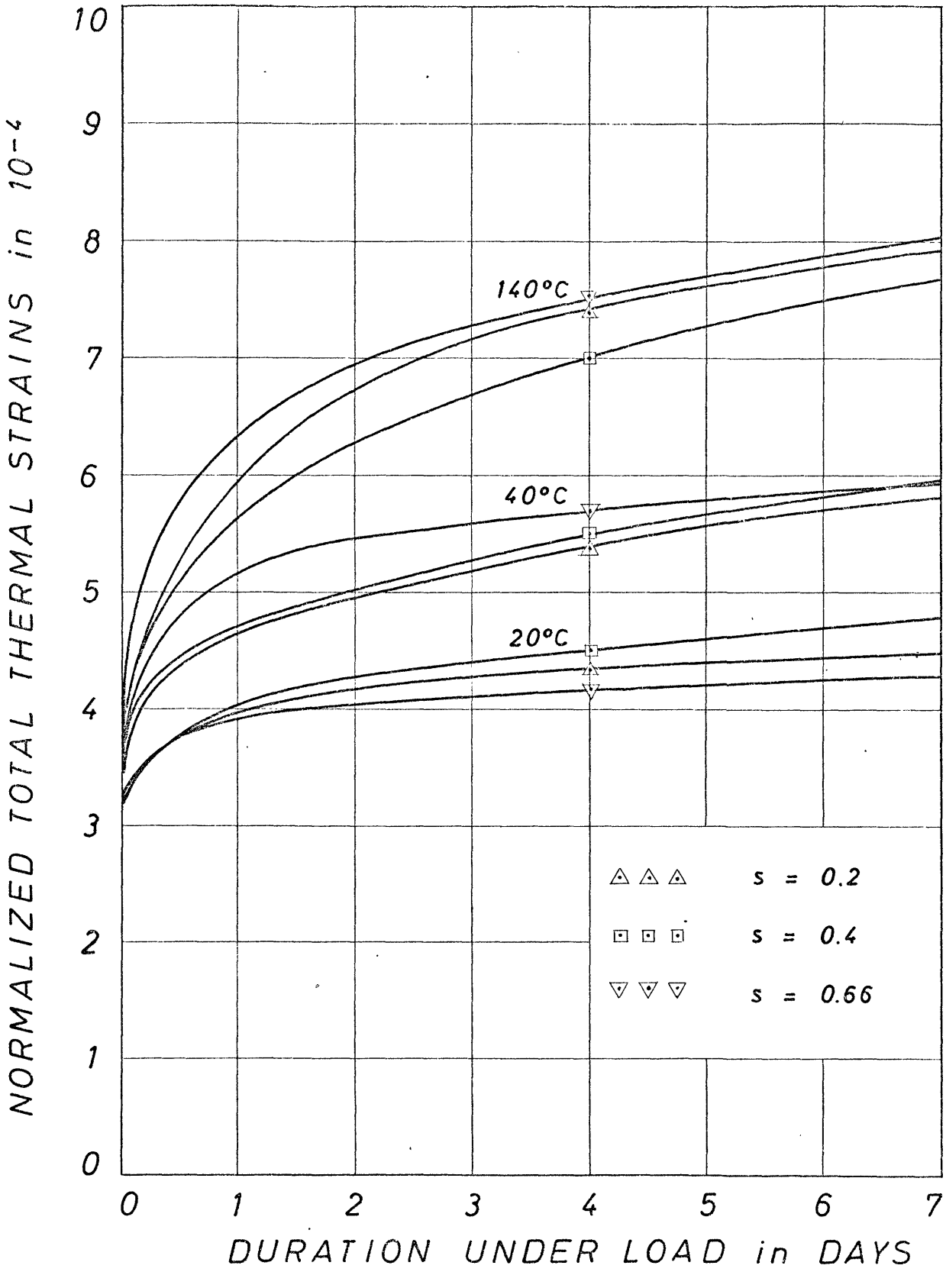


FIG. 5.11. LOW TEMPERATURE CREEP NORMALIZED TO A STRESS LEVEL OF 0.2

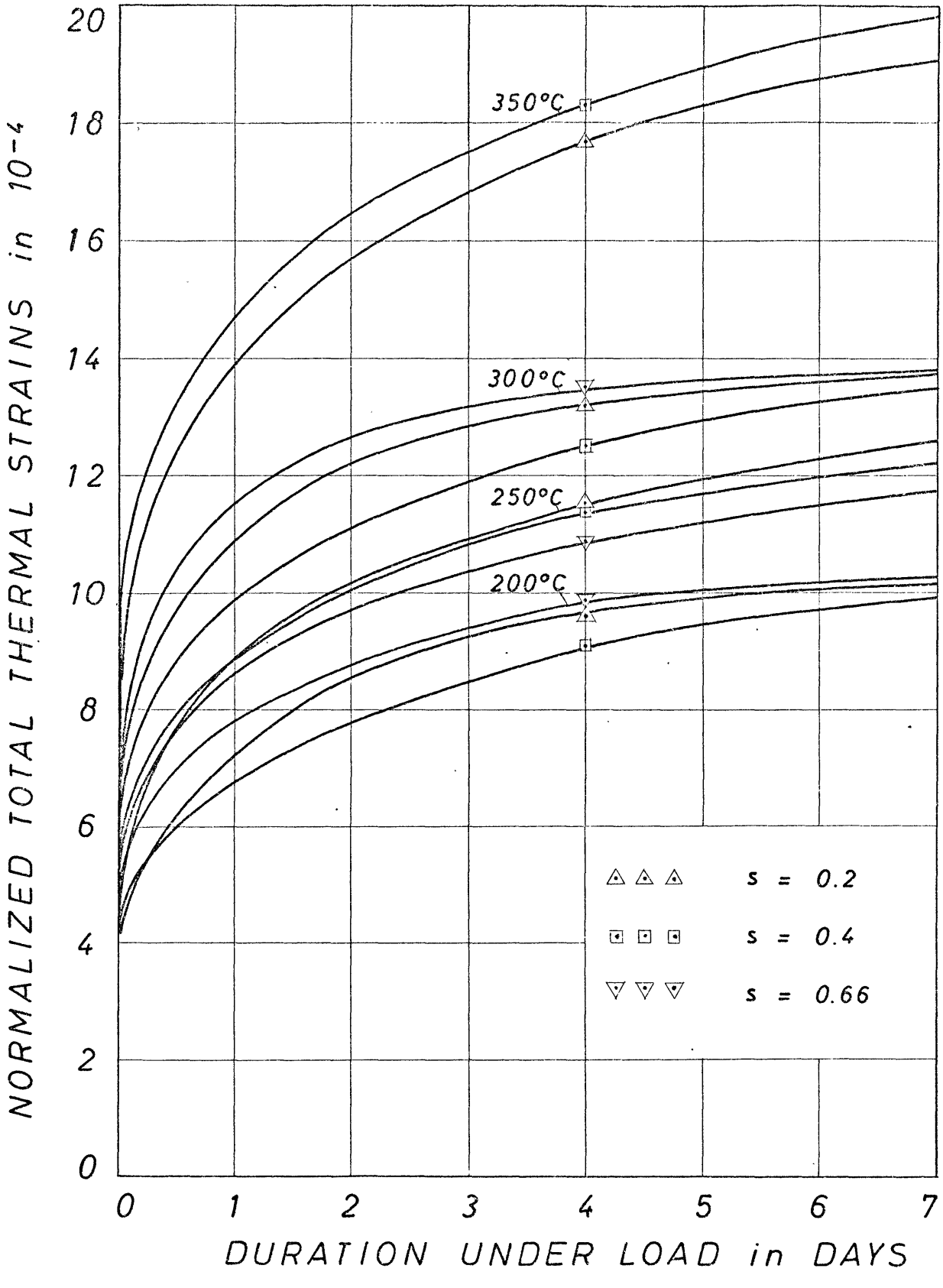


FIG. 5.12. HIGH TEMPERATURE CREEP NORMALIZED TO A STRESS LEVEL OF 0.2

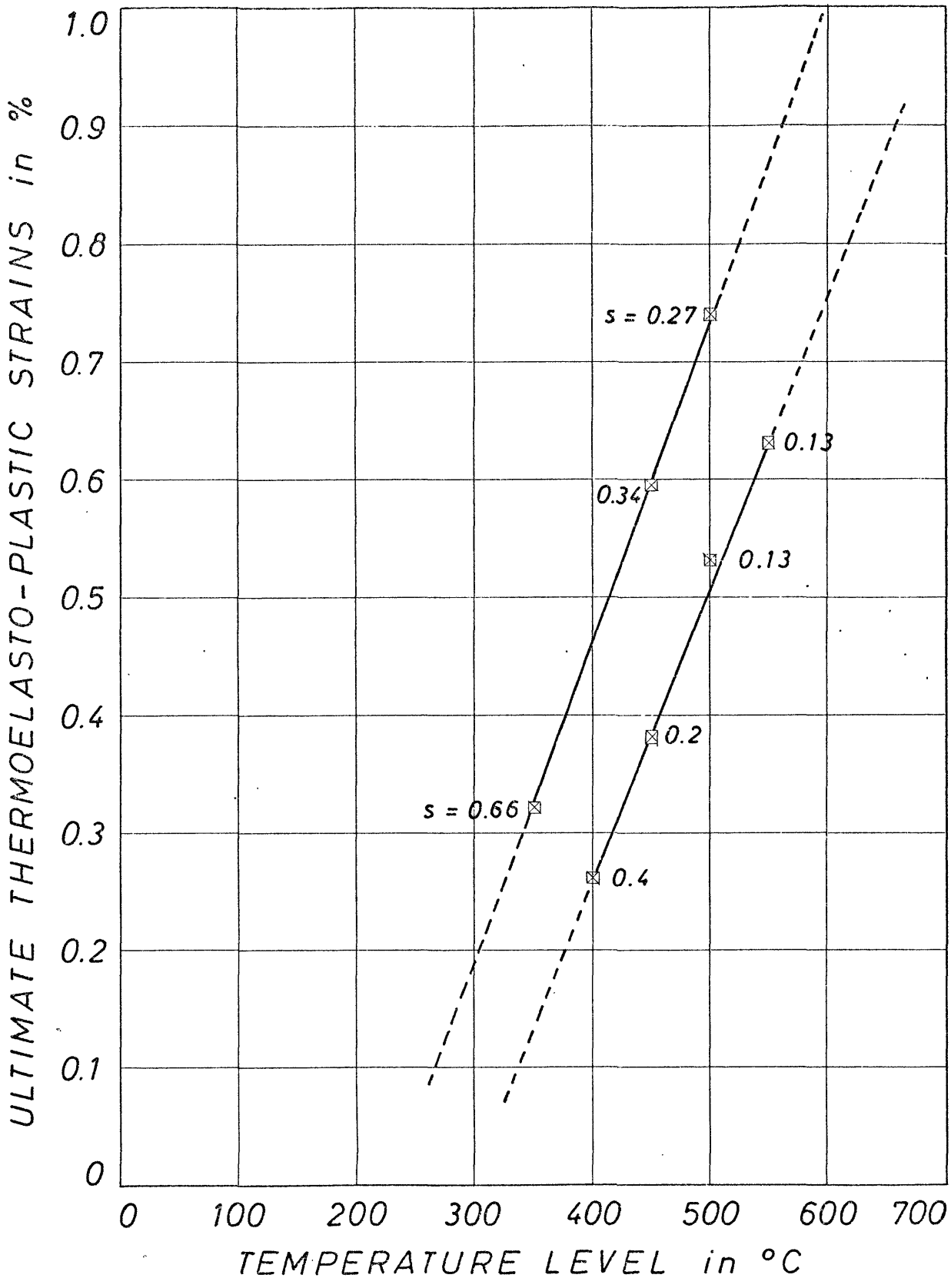


FIG. 5.13. LIMITS FOR ULTIMATE THERMO-ELASTO-PLASTIC STRAINS

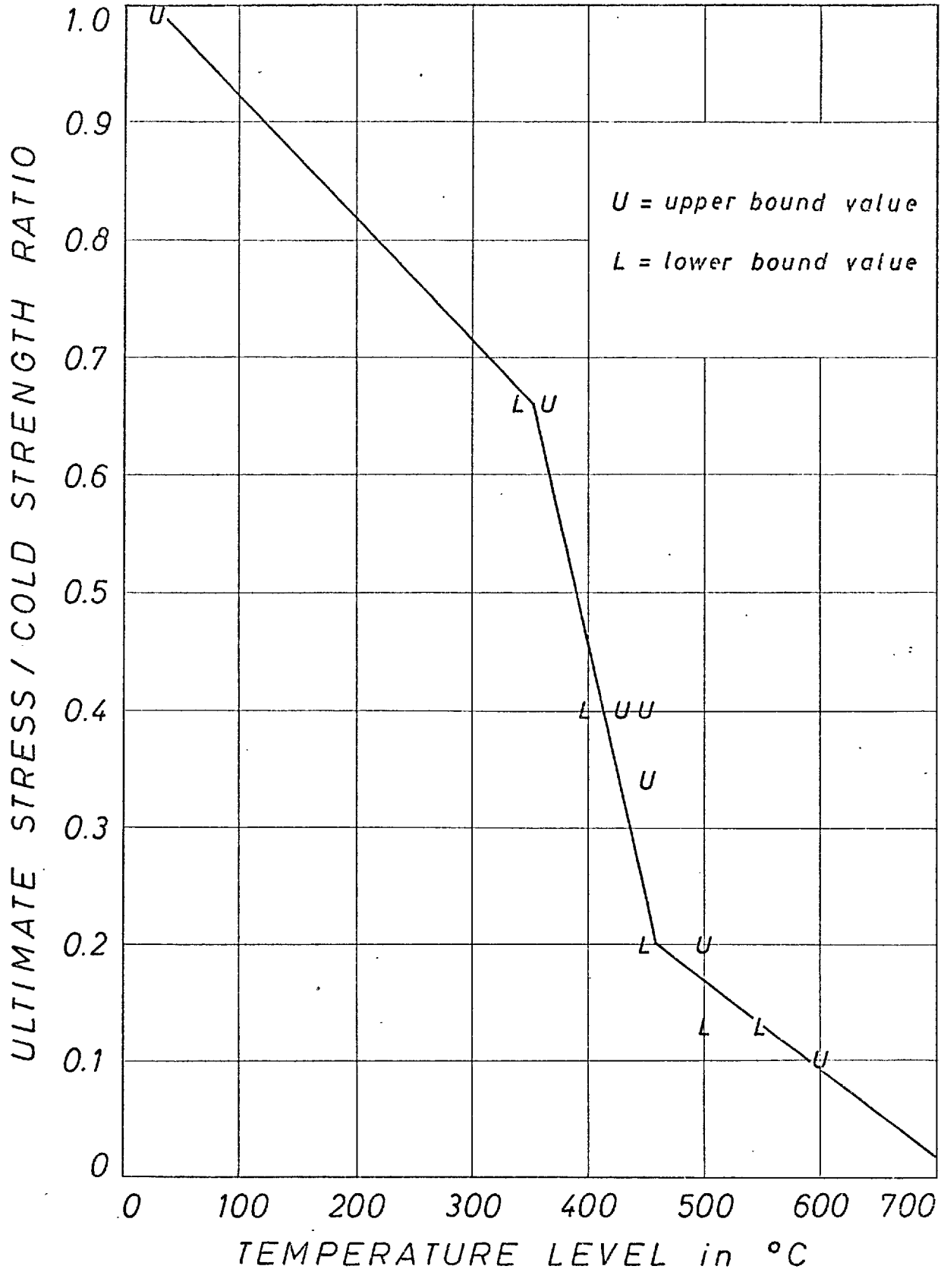


FIG. 5.14. LIMIT FOR ULTIMATE STRESS / COLD STRENGTH RATIO

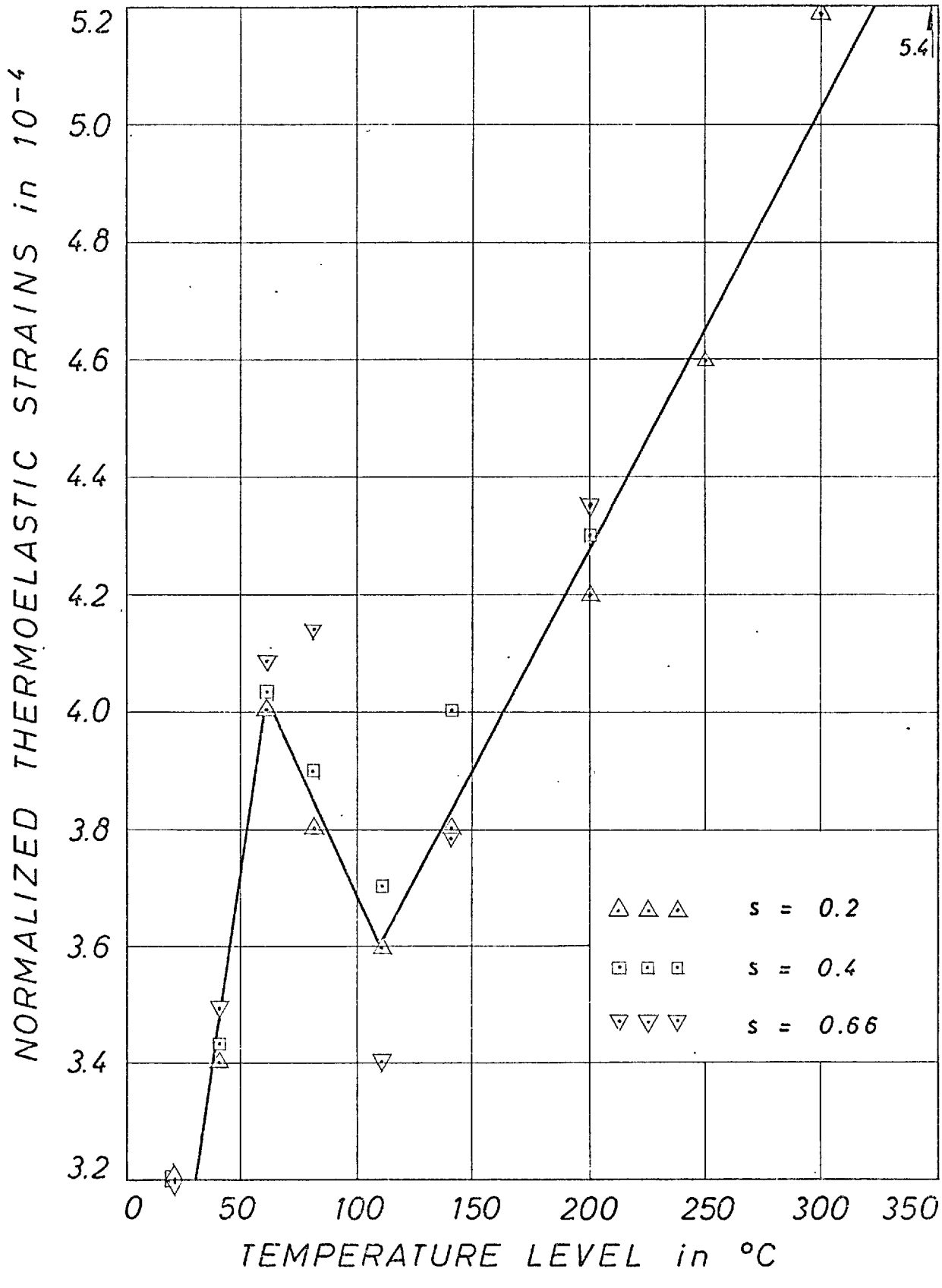


FIG. 5.15. THERMOELASTIC STRAINS NORMALIZED TO A STRESS LEVEL OF 0.2

overlapping of curves obtained for equal temperatures would verify that the problem of thermal creep may be reduced to a problem of linear thermoviscoelasticity.

In commencing to standardize the recorded data, it is realized that it is total creep strains which must be compared - and not just the viscous strains. Within the investigated range, the initial strains are not purely thermoplastic. The tentative substantiation for comparing total strains then is derived from the observation that thermoplastic strains and thermal creep strains complement each other; a higher relative thermoplastic proportion in the initial strains has the tendency to reduce the build-up of potential viscous strains. Secondly, however small the loading period, for higher loads and temperatures, finite creep contributions influence the initial strain readings.

Apart from noticeable deviations for temperatures between 60 and 80°C, the stress-normalized curves in figs. (5.11) and (5.12) exhibit errors from the corresponding common mean of less than ± 10%. Definite incongruity in the superposition of normalized creep profiles is encountered for highest endurable temperatures; more exactly, strains recorded at 450°C for s = 0.2, at 400 C for s = 0.4 and 350°C for s = 0.66 defy the comparison with test results obtained for equal temperatures but lower stress/ cold strength ratios.

The results compiled in figs. (5.11) and (5.12) thus offer the convincing evidence that the superposition hypothesis is applicable to thermal creep analyses of good-quality concrete, below the mechanical and thermal conditions described.

5.9. THERMALLY INDUCED SHRINKAGE STRAINS

As may be observed in figs. (5.6), (5.7) and (5.15), a local maximum at 60°C interrupts the continuity of the otherwise increasing strain profile in temperature. Tests were carried out to measure the drying shrinkage at various temperatures, in an attempt to separate between the basic and the drying components.

The tests on thermal shrinkage matched with the total creep tests in that the monitoring of the strain developments

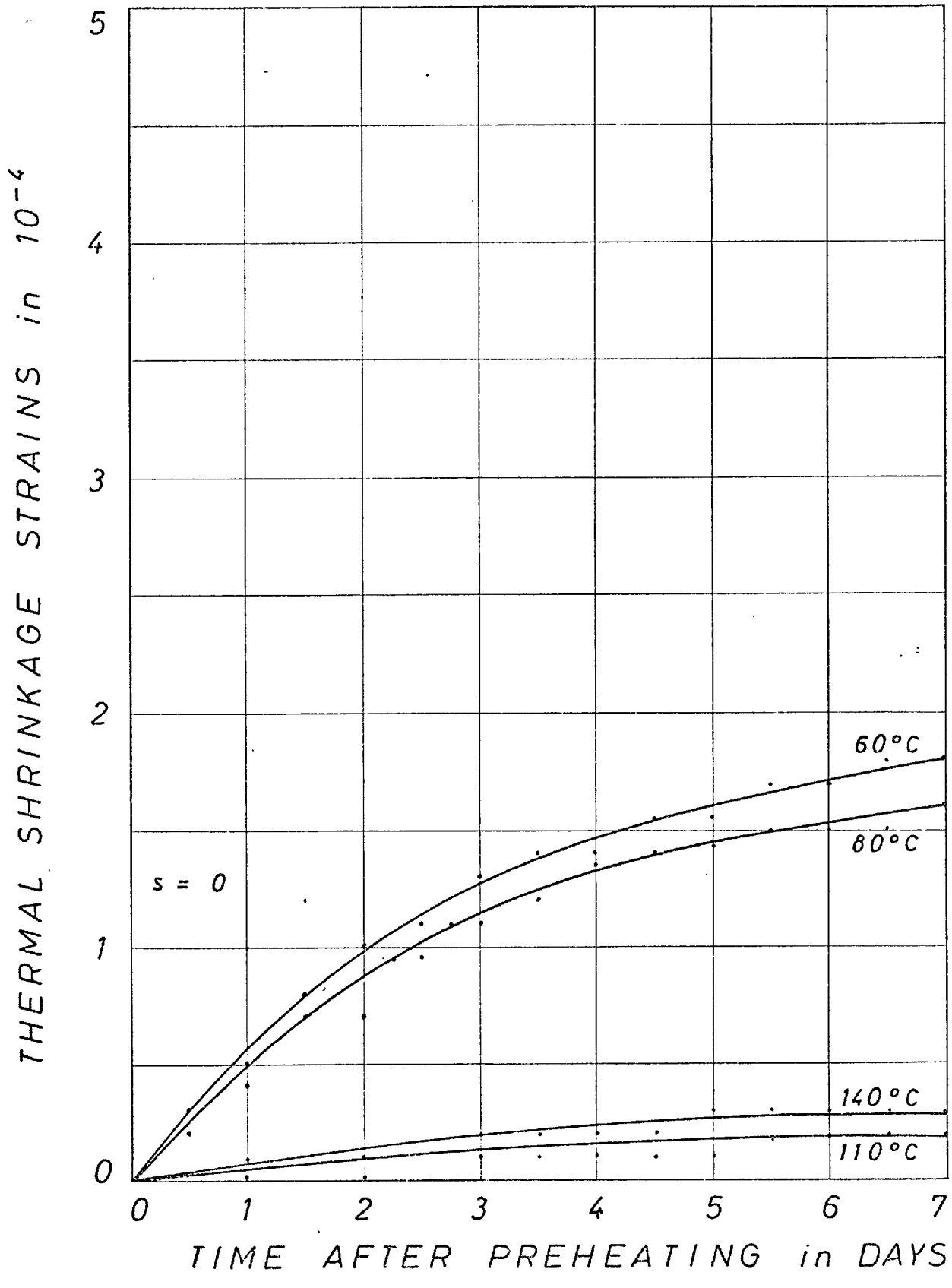


FIG. 5.16. THERMAL SHRINKAGE

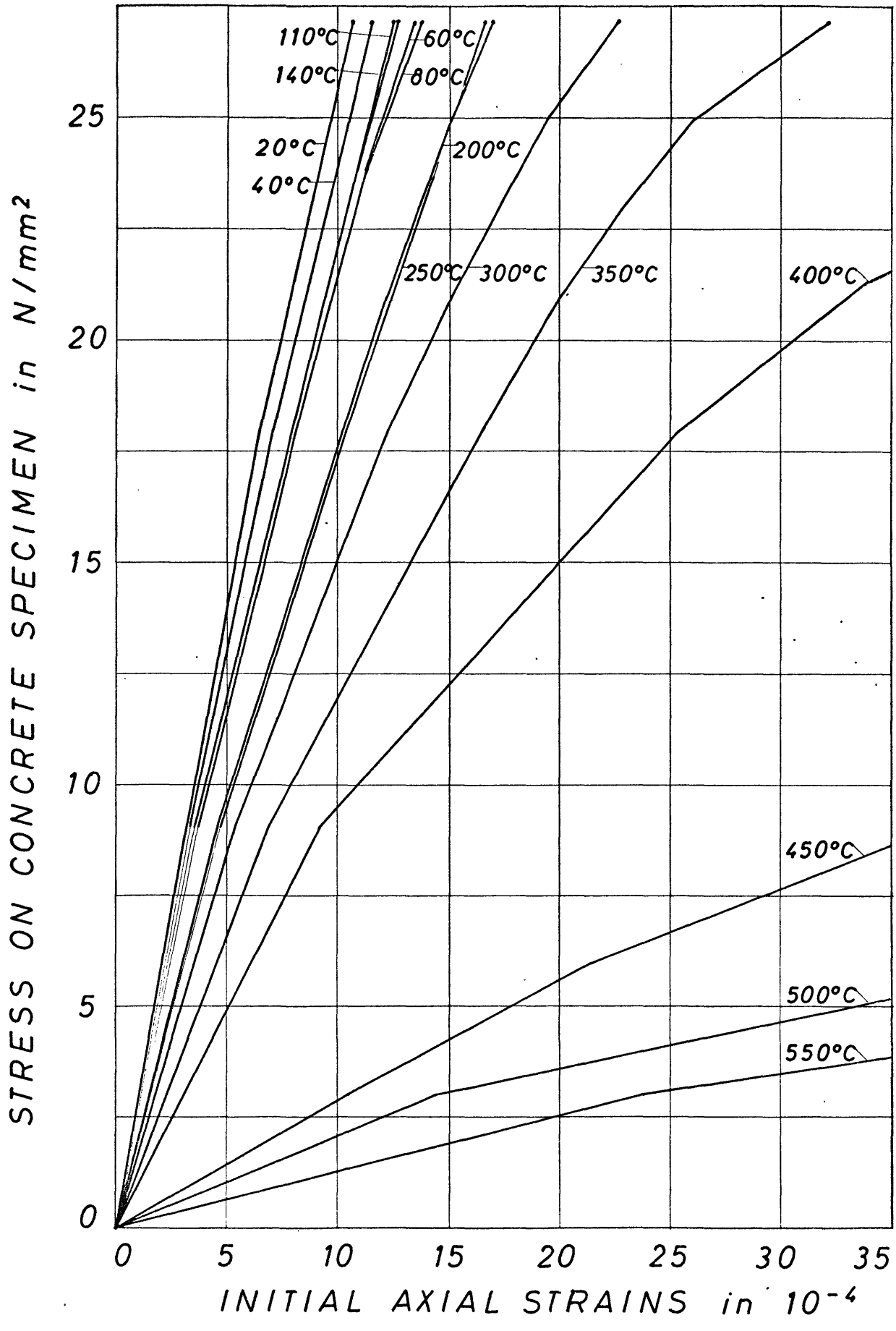


FIG. 5.17. TEMPERATURE-DEPENDENT STRESS-STRAIN CURVES

commenced after a preheating period of one day. They differed in that no load was imposed onto the concrete cylinders.

The thermally induced shrinkage strains recorded for the set temperatures 60, 80, 110 and 140°C are entered in fig. (5.16). Outside the extension of the local peak, i.e. for 110 and 140°C, no significant shrinkage strains were detected. For temperatures of 60 and 80°C, however, finite strain readings of 180 and 160 μ were taken at the end of the seventh day after preheating.

Naturally, thermal shrinkage strains cannot be scaled in the stress variable. Given a time instant, a fixed component must be subtracted from the total strains measured for the various underlying stress/ cold strength ratios, before normalization can commence. Since, however, the resulting differences for s = 0.2 fall below the values which could be expected by extrapolation based on the continuity of viscous strains in the temperature variable, the scaling of total strains for temperature 60 and 80°C excluding thermal shrinkage leads to results which are worse still.

The tentative answer is that for low stresses the domains of thermoviscous and thermal creep strains intersect; i.e. the theoretically separable components partially activate the same potential deformations and thus may not be fully superimposed. Consequently, the observation of thermal shrinkage strains appears to be of mainly phenomenological interest and does not simplify the analytic regression of the test data.

As a result, the deviation of 20% from the linear behaviour in stress found for temperatures of 60 and 80°C is accounted for in the subsequent analytic formulations.

5.10. CONCLUSIONS

On the basis of test results, the author contrived practical formulae for the stress-dependent ultimate temperature of concrete, for the thermoelastic strains occurring in virgin concrete, for the modulus of thermoelasto-plasticity and for the ultimate hot cylinder strength.

The major conclusion is that for conditions milder than $s = 0.66$ and $T = 300^{0}C$, the total creep strains are linear in the stress variable. Within these limits, therefore, the phenomenon of thermal creep in concrete, which according to general terminology comprises stress and temperature-dependent non-linearities in strains developing under sustained loads, may be reduced to the problem of linear thermoviscoelasticity which submits to the mathematically rigorous treatment using the superposition hypothesis.

CHAPTER VI

SMALL DISPLACEMENT THEORY OF LINEAR ELASTIC CONTINUA

6.1. INTRODUCTION

6.1.1. OBJECTIVE

The linear elastic analysis of three-dimensional solids and of combined twisted an axisymmetrically deformed solid cylinders is a problem of 18 unknown functions to be evaluated. Subdividing an elastic continuum into a large number of infinitesimal unit volume elements, the necessary conditions are satisfied, if for each such element 18 equations can be established in order to find the magnitudes of nine local stress components, six local strain components and three local displacement components pertaining to the corresponding three-dimensional or cylindrical global fields.

The sufficient conditions are satisfied, if the overall functions can be found to guarantee the geometrical compatibility within the whole continuum ; in other words, attempts to reassemble the fictitious elements after loading must always be successful. No gaps or dislocations are allowed to form between the interelement faces.

6.1.2. ASSUMPTIONS AND IMPLICATIONS

In the following the assumptions are stated under which the small displacement theory of linear elasticity shall be derived. Also, the implications these bear onto the detailed derivation are discussed.

(1) The variation of shear stresses within an element is by one order of magnitude smaller than the actual shear stresses - thus the interelement faces do not undergo any appreciable warping and may be assumed to remain plane.

(2) The validity of linear elasticity holds - thus complete reversibility of deformations is assured.

(3) The initial geometry remains unchanged after loading - thus linear equations of equilibrium are established, the super-position principle applies, the succession of given

states of stress is of no importance and subscripts in comma notation may be conveniently interchanged.

(4) The induced deformations are infinitesimal - thus elongations of elementary sides are very small compared to the original dimensions, tangents of angles of rotations may be replaced by the angles themselves and their cosines are approximately unity.

(5) The solid consists of an isotropic elastic material - thus its mechanical properties can be sufficiently described by the two constant values of the modulus of elasticity and the Poisson's ratio.

(6) The solid expands volumetrically in conformity with a constant coefficient of thermal expansion - thus no thermally induced shear stress components exist.

(7) The thermally induced direct stress components are brought about by the action of fictitious negative forces which suppress the development of thermal strains - thus a negative sign must be assigned to the stresses due to confined expansion.

(8) The heat propagates in conformity with the coefficients of thermal conductivity, specific heat and density which are independent of direction and temperature - thus these coefficients appear as proportionality constants unaffected by differentiation.

In the following, the assumptions shall be referred to as ass. (6.1.2.i), i=1,8.

6.1.3. TENSOR NOTATION

For the sake of brevity a vectorial treatment of quantities shall be favoured throughout the present and the following chapter. Summations of directed quantities and/or their partial derivatives shall be understood as vectorial summations of scalar magnitudes in the relevant unit basic directions x_i, i=1,2,3 of the continuum.

By introduction of subscripts which shall be attached to directed quantities any set of three equations for the truly spatial case can be reduced to a single general equation.

With the exception of the equations of moment equilibrium, cylindrical geometry precludes the formulation of such general equations, since a state of unpreferred directions is no longer given.

Considering a unit volume element subjected to the action of a direct quantity, the first subscript i of that quantity designates the x_i-constant face, whereas the second subscript j denotes the direction j of its line of action. Comma notation shall be used to indicate the direction with respect to which the quantity is partially derived.

Here and in the following, the subscript i indicates that expressions are established for any direction x_i, i=1,2, 3 and the consecutive subscripts i,j,k,i,.. are understood to follow in a positive cyclic order 1,2,3,1,.., unless stated otherwise.

6.1.4. DIFFERENTIAL OPERATIONS

A number of Laplace's equations and some other definitions shall be utilized in deriving the small displacement theory of elastic bodies in an efficient and concise manner and are therefore listed in the following.

Applying tensor notation to Laplace's potential deformation equations for a spatial continuum, for a twisted as well as axisymmetrically deformed cylindrical continuum and for a merely axisymmetrically deformed cylindrical continuum, respectively, the following definitions hold

(1) $$\Delta u_i = u_{i,ii} + u_{i,jj} + u_{i,kk} = 0$$

(2) $$\Delta u_i = u_{i,ii} + \frac{1}{r} u_{i,i} + u_{i,jj} + u_{i,kk} = 0$$

where it should be noted that $u_{k,kk}$ is expanded by the term $\frac{1}{r} u_{i,k}$

(3) $$\Delta u_i = u_{i,ii} + \frac{1}{r} u_{i,i} + u_{i,jj} = 0$$

Similarly, the potential temperature distribution equations corresponding to definitions (1) to (3) form as

$$(4) \qquad \Delta\Theta = \Theta_{,ii} + \Theta_{,jj} + \Theta_{,kk} = 0$$

$$(5) \qquad \Delta\Theta = \Theta_{,ii} + \frac{1}{r}\Theta_{,i} + \Theta_{,kk} + \Theta_{,jj} = 0$$

$$(6) \qquad \Delta\Theta = \Theta_{,ii} + \frac{1}{r}\Theta_{,i} + \Theta_{,jj} = 0$$

Also, the total direction strain due to mechanical action, as corresponding to definitions (1) to (3) respectively, can be defined in tensor notation

$$(7) \qquad \varepsilon = u_{i,i} + u_{j,j} + u_{k,k}$$

$$(8) \qquad \varepsilon = u_{i,i} + \frac{1}{r}u_i + u_{j,j} + u_{k,k}$$

$$(9) \qquad \varepsilon = u_{i,i} + \frac{1}{r}u_i + u_{j,j}$$

Finally, the definition of the potential strain equation for an axisymmetrically deformed cylindrical continuum takes the form

$$(10) \qquad \Delta\varepsilon = \varepsilon_{,ii} + \frac{1}{r}\varepsilon_{,i} + \varepsilon_{,jj} = 0$$

In the following,the definitions shall be referred to as def. (6.1.4.i), i=1,10.

6.2. THREE DIMENSIONAL CONTINUA UNDER SPATIAL DEFORMATION

6.2.1. EQUILIBRIUM OF FORCES AND COUPLES

Considering an elastic solid continuum in static equilibrium under prescribed mechanical boundary conditions, the internal state of stress within any unit volume element of the continuum is defined by a stress tensor which is a bundle composed of nine double subscribted stress components

$$\sigma_{ij} \qquad i,j = 1,2,3 \qquad (6.1)$$

(9 unknowns, 0 equations)

Body pressure is present due to the action of self-weight and does not vary appreciably within an arbitrary unit volume element. Locally, therefore, the body pressure may be defined by the three body force components X_i which are treated as external forces acting in the directions x_i of

the space.

Figure (6.1) depicts the direct stress components and the body pressure components acting on a unit volume element, whereas figure (6.2) shows the corresponding shear stress components. Adding up the stress resultants in any direction x_i, the equilibrium of forces in tensor notation is established

$$(\sigma_{ii} + \sigma_{ii,i}\, dx_i)\, dx_j dx_i - \sigma_{ii}\, dx_j\, dx_k + (\sigma_{ji} + \sigma_{ji,j}\, dx_j) \cdot$$

$$dx_k\, dx_i - \sigma_{ji}\, dx_k\, dx_i + (\sigma_{ki,k}\, dx_k)\, dx_i\, dx_j - \sigma_{ki}\, dx_i\, dx_j$$

$$+ X_i\, dx_i\, dx_j\, dx_k = 0$$

which immediately reduces to

$$\sigma_{ii,i} + \sigma_{ji,j} + \sigma_{ki,k} + X_i = 0 \,.$$

Using subscript summation convention, the set of equations of force equilibrium may be represented even more compactly by

$$\sigma_{ij,i} + X_j = 0 \qquad i,j = 1,2,3 \qquad (6.2)$$

(9 unknowns, 3 equations)

Realizing that the components of the direct stress resultants do not form leverarms about the origin of the local space triad, the equilibrium of couples in any direction x_i is established under consideration of the corresponding shear stress resultants

$$(\sigma_{jk} + \sigma_{jk,j}\, dx_j)\, dx_k\, dx_i\, \frac{dx_j}{2} + \sigma_{jk}\, dx_k\, dx_i\, \frac{dx_j}{2} -$$

$$(\sigma_{kj} + \sigma_{kj,k}\, dx_k)\, dx_i\, dx_j\, \frac{dx_k}{2} + \sigma_{kj}\, dx_i\, dx_j\, \frac{dx_k}{2} = 0$$

which can be simplified to give

$$2\,\sigma_{jk} - 2\sigma_{kj} + \sigma_{jk,j}\, dx_j - \sigma_{kj,k}\, dx_k = 0$$

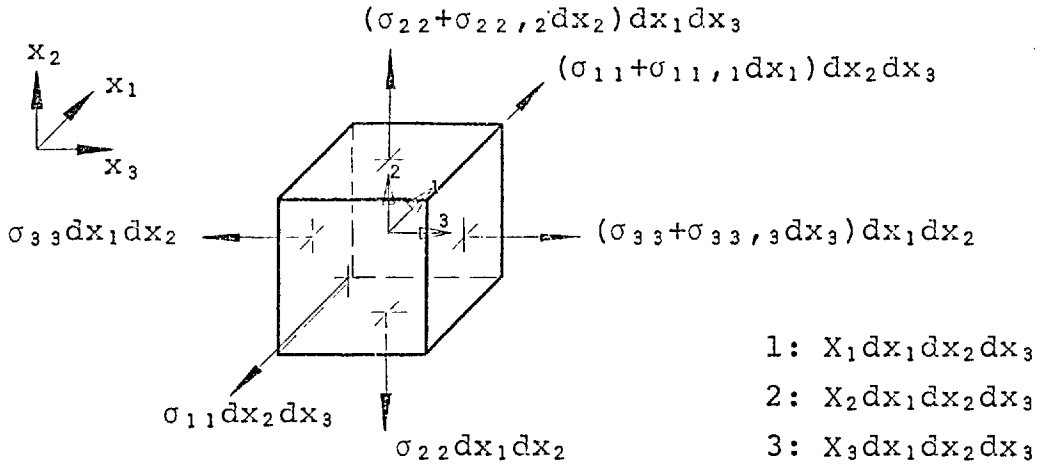


Fig. 6.1. Direct stress and body pressure components for three-dimensional analysis

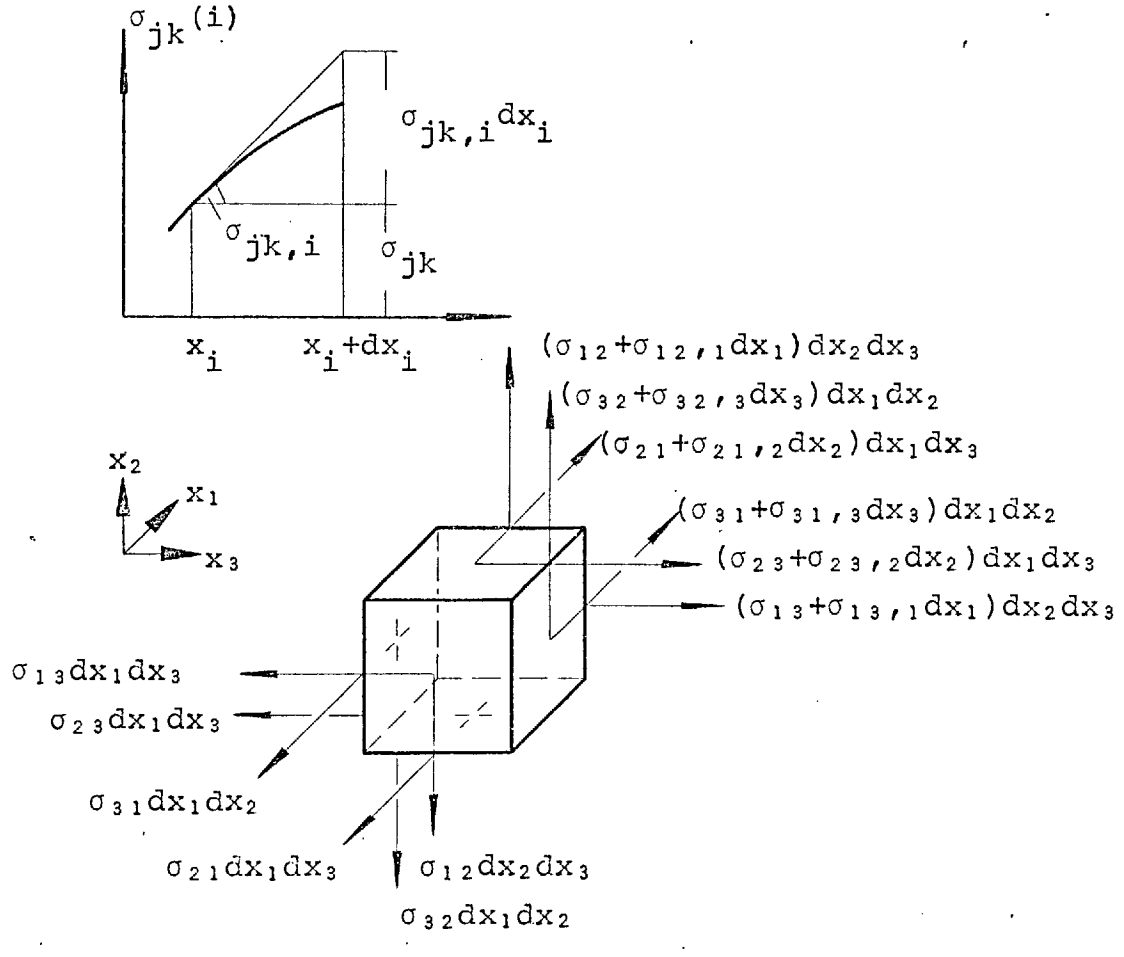


Fig. 6.2. Shear stress components for three-dimensional analysis

Under ass. (6.1.2.1), the set of equation of couple equilibrium may be represented by

$$\sigma_{jk} = \sigma_{kj} \tag{6.3}$$

(9 unknowns, 6 equations)

From eqs. (6.2) and (6.3) and ass. (6.1.2.2) and (6.1.2.3), an infinitesimal volume element under any combination of mechanical boundary conditions is in static equilibrium, if

$$\sigma_{ij,i} + X_j = 0 \tag{6.4}$$

where $\sigma_{ij,i}$ is now symmetric.

If a unit volume element on the boundary of the continuum is subjected to a prescribed surface traction, of which the line of action is given by the surface normal n, this surface traction may be defined by the spatial components F_i which are treated as external forces acting under the direction cosines $n_{,i}$ from the surface normal. The equation of force equilibrium at the surface for any direction x_i thus becomes

$$n_{,i}\sigma_{ii} + n_{,j}\sigma_{ij} + n_{,k}\sigma_{ik} = F_i$$

More compactly this equation reads

$$n_{,i}\sigma_{ij} = F_j \tag{6.5}$$

where σ_{ij} is symmetric.

6.2.2. STRAIN-DEFORMATION RELATIONS

To any state of internal stress there exists a conjugate state of strain. Thus, the corresponding six strain components are defined by

$$\varepsilon_{ij} \tag{6.6}$$

(15 unknowns, 6 equations)

Figure (6.3) depicts the positive displacements and angles of rotations for an arbitrary face of a deformed unit volume element. If an overbar indicates that the barred

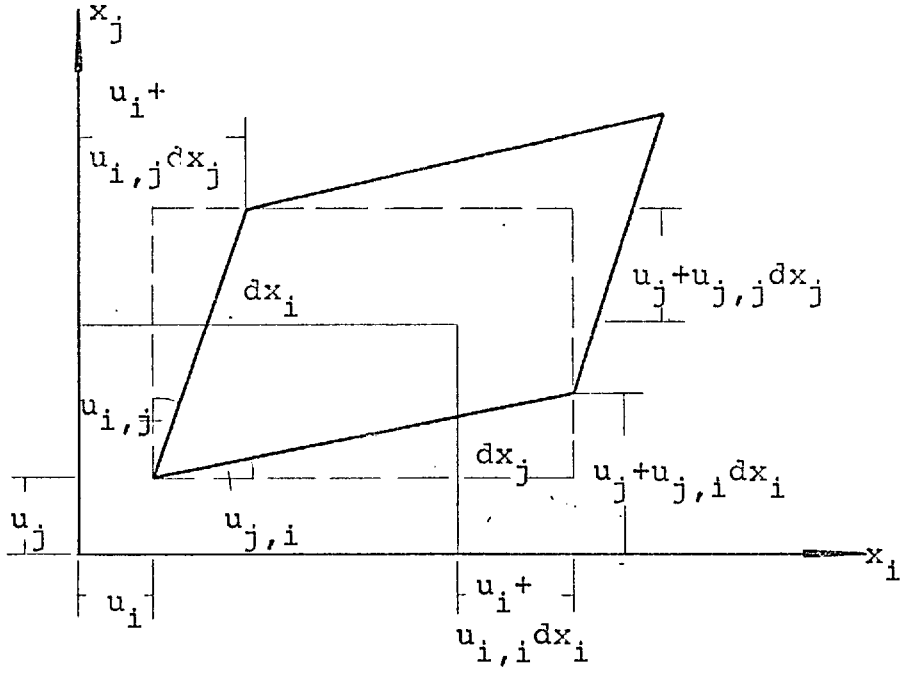


Fig. 6.3. Positive displacements and angles of rotation for three-dimensional analysis

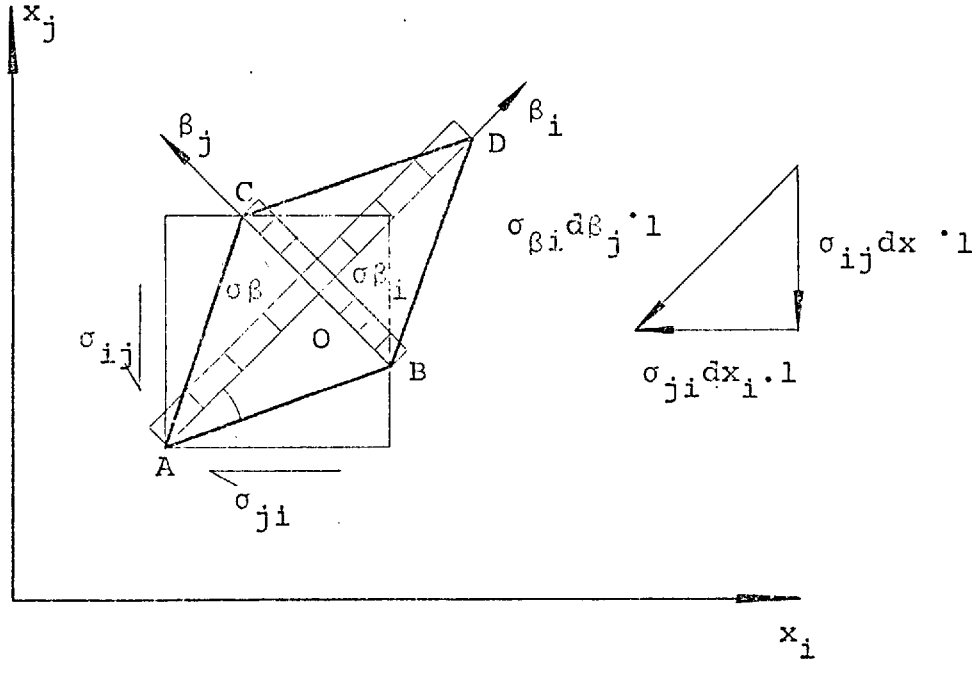


Fig. 6.4. Transformation of shear stress resultants for three-dimensional analysis

quantity pertains to the deformed element, the length of any elementary side after loading takes the value

$$\bar{dx}_i = \frac{dx_i(1 + \varepsilon_{ii})}{\cos(u_{j,i})} = \frac{dx_i + (u_i + u_{i,i}dx_i - u_i)}{\cos(u_{j,i})}$$

Under ass. (6.1.2.4) the above equation reduces to

$$\bar{dx}_i = dx_i\ (1 + u_{i,i})$$

Thus, the direct strain and displacement components are linked as follows

$$\varepsilon_{ii} = u_{i,i} \tag{6.7}$$

(18 unknowns, 9 equation)

In the presence of a temperature field, thermal volumetric deformation following ass. (6.1.2.6) leads to an alternative definition of direct strains

$$\varepsilon_{ii} = \alpha\theta \tag{6.8}$$

where α is the coefficient of thermal expansion.

The total shearing strain of a deformed elementary face is defined by the sum of the two relevant angles of rotation

$$\varepsilon_{ij} = \frac{u_{j,i}\ dx_i}{dx_i(1 + \varepsilon_{ii})} + \frac{u_{i,j}\ dx_j}{dx_j(1 + \varepsilon_{jj})}$$

Under ass. (6.1.2.4) the strain-deformation relations in shear become

$$\varepsilon_{ij} = u_{i,j} + u_{j,i} \tag{6.9}$$

As will be explained in section 7.1.3, the formulation of virtual work principles favours the more convenient definition

$$\varepsilon_{ij} = \tfrac{1}{2}(u_{i,j} + u_{j,i}) \tag{6.10}$$

(18 unknowns, 12 equations)

6.2.3. CONSTITUTIVE RELATIONSHIPS

Constitutive relationships generally include interactions between stresses, strains, time and temperature, but under ass. (6.1.2.2) and (6.1.2.5) the degenerate to simple elastic laws. Direct stresses and strains are linked through the modulus of elasticity E and the Poisson's ratio μ

$$\varepsilon_{ii} = \frac{1}{E} \left(\sigma_{ii} - \mu \left(\sigma_{jj} + \sigma_{kk}\right)\right) \qquad (6.11)$$

(18 unknowns, 15 equations)

From volume change after loading

$$V + dV - V = \sum_{i}^{3} dx_i \left(1 + u_{i,i}\right) - \sum_{i}^{3} dx_i$$

the total direct strain ε is obtained by equating

$$\frac{dV}{V} = \sum_{i}^{3} u_{i,i}$$

and its magnitude must be equal to the sum of eqs.(6.11)

$$\varepsilon = \frac{\sigma}{E} (1 - 2\mu) \qquad (6.12)$$

where ε follows def. (6.1.4.7) and σ its analogue.

To find the stress-strain relations in shear, a short digression from the conventional definitions of strains is necessary, inasmuch as shear strain components, pertaining to the cartesian basic vectors of a deforming unit square element, need to be expressed in terms of direct strain components acting along the axes of the forming rhombus.

Figure (6.4) illustrates the relation between the original shear stress resultants σ_{ij} and the direct stress resultants $\sigma_{\beta i}$ in the transformed coordinate system. The equations of force equilibrium for the partial elements ABD and ABC take the form

$$\sigma_{\beta i}\, d\hat{}_{\beta j} \cdot 1 = \sigma_{ij}\, dx_i \sqrt{2} \cdot 1$$

$$\sigma_{\beta j}\, d\hat{}_{\beta i} \cdot 1 = \sigma_{ij}\, dx_j \sqrt{2} \cdot 1$$

and under ass. (6.1.2.4) reduce to

$$\begin{aligned} \sigma_{\beta i} &= \sigma_{ij} \\ \sigma_{\beta j} &= -\sigma_{ij} \end{aligned} \tag{6.13}$$

In the transformed rectangular coordinate system β_i, β_j, x_k eqs. (6.11) read

$$\varepsilon_{\beta i} = \frac{1}{E} (\sigma_{\beta i} - \mu (\sigma_{\beta j} + \sigma_{kk}))$$

$$\varepsilon_{\beta i} = \frac{1}{E} (\sigma_{\beta j} - \mu (\sigma_{\beta i} + \sigma_{kk}))$$

and after substitution of eqs. (6.13) take the form

$$\begin{aligned} \varepsilon_{\beta i} &= \frac{1}{E} ((1 + \mu)\, \sigma_{ij} - \mu\sigma_{kk}) \\ \varepsilon_{\beta j} &= -\frac{1}{E} ((1 + \mu)\, \sigma_{ij} - \mu\sigma_{kk}) \end{aligned} \tag{6.14}$$

Now the tangent of the angle OAB of the deforming unit square element can either be defined by the expression

$$\tan (\tfrac{\pi}{4} - u_{j,i}) = \frac{\tan \frac{\pi}{4} - \tan (u_{j,i})}{1 + \tan \frac{\pi}{4} \tan (u_{j,i})}$$

which under ass. (6.1.2.3) reduces to

$$\tan (\tfrac{\pi}{4} - u_{j,i}) = \frac{1 - u_{j,i}}{1 + u_{j,i}} \tag{6.15}$$

or by the expression

$$\tan (\tfrac{\pi}{4} - u_{j,i}) = \frac{\frac{1}{2} d\beta_j (1 - \varepsilon_{\beta j})}{\frac{1}{2} d\beta_i (1 - \varepsilon_{\beta i})}$$

which under ass. (6.1.2.3) reduces to

$$\tan (\tfrac{\pi}{4} - u_{j,i}) = \frac{1 + \varepsilon_{\beta j}}{1 + \varepsilon_{\beta i}} \tag{6.16}$$

Substituting eqs. (6.14) into eq. (6.16) and subsequently equating with eq. (6.15), the following general expression is derived

$$\frac{1 - u_{j,i}}{1 + u_{j,i}} = \frac{1 - \frac{\mu}{E}\sigma_{kk} - \frac{1 + \mu}{E}\sigma_{ij}}{1 - \frac{\mu}{E}\sigma_{kk} + \frac{1 + \mu}{E}\sigma_{ij}} \qquad (6.17)$$

where $\frac{\mu}{E}\sigma_{kk} << 1$

It may be stated that in a triaxial state of stress the stress component σ_{kk} does not influence appreciably the formation of the elementary angles of rotation in the $x_{i,j}$-plane, and thus its contribution to the shear stress component σ_{ij} is negligible. In other words, the stress-strain equations in shear are uncoupled from those in extension.

Comparing the coefficients of eq. (6.17), the following definition is arrived at

$$u_{j,i} = \frac{1 + \mu}{E}\sigma_{ij}$$

With eq. (6.10) the corresponding set of equations for an arbitrary unit volume element takes the form

$$\varepsilon_{ij} = \frac{1 + \mu}{E}\sigma_{ij} \qquad (6.18)$$

(18 unknowns, 18 equations)

Using eq. (6.12), eqs. (6.11) and (6.18) may be inverted to yield

$$\begin{aligned} \sigma_{ii} &= \frac{E}{1 + \mu}\left(\varepsilon_{ii} + \frac{\mu}{1 - 2\mu}\varepsilon\right) \\ \sigma_{ij} &= \frac{E}{1 + \mu}\varepsilon_{ij} \end{aligned} \qquad (6.19)$$

Substituting eqs. (6.7) and (6.12) into the first and eq. (6.9) into the second of eqs. (6.19), the following stress-deformation equations are established

$$\begin{aligned} \sigma_{ii} &= a\,(u_{i,i} + b\,(u_{j,j} + u_{k,k})) \\ \sigma_{ij} &= a\,\frac{c}{d}\,(u_{i,j} + u_{j,i}) \end{aligned} \qquad (6.20)$$

Considering thermal volumetric expansion, substitution of eq. (6.8) into the first of eqs. (6.19) leads under ass. (6.1.2.7) to the following definition of thermal stress

$$\sigma_{ii} = - ae\alpha\theta \qquad (6.21)$$

The constants, which for brevity are used in eqs. (6.20) and (6.21) and the following, are given by the expressions below

$$a = \frac{E(1 - \mu)}{(1 + \mu)(1 - 2\mu)} \quad b = \frac{\mu}{1 - \mu} \quad c = 1 - 2\mu \qquad (6.22)$$

$$d = 2(1 - \mu) \qquad e = \frac{1 + \mu}{1 - \mu} \quad G = \frac{E}{2(1 + \mu)}$$

For the 18 unknown functions to be evaluated an equal number of equations is available, and thus the necessary conditions are satisfied.

6.2.4. COMPATIBILITY EQUATIONS

The six strain components ε_{ij} must be derived from three displacement function u_i and therefore cannot behave independently. To substantiate geometrical continuity, compatibility equations must exist between the magnitudes of the strain components.

Mathematically, a solid continuum under triaxial states of stress is an elliptic system, since any disturbance at one point of the body such as an imposed displacement, an applied force or a change in internal stress can affect the conditions at all other points. If a set of Laplace's equations which mathematically are elliptic partial differential equations could be derived, all compatibility requirements would be met.

In proceeding to derive the compatibility equations, eqs. (6.20) and (6.21) are substituted into the equations of force equilibrium (6.4)

$$a((u_{i,i} + b(u_{j,j} + u_{k,k}))_{,i} + c(u_{j,i} u_{i,j} + c(u_{k,i} + u_{i,k})_{,k}$$

$$- e\alpha\theta_{,i}) + X_i = 0 \qquad (6.23)$$

Expansion leads to

$$a(u_{i,ii} + b(u_{j,ji} + u_{k,ki}) + \frac{c}{d}(u_{j,ij} + u_{i,jj} + u_{k,ik} + u_{i,kk}) - e\alpha\Theta_{,i}) + X_i = 0$$

After rearranging the terms, eqs. (6.23) may by virtue of ass. (6.1.2.3) first be written as

$$a(u_{i,ii} + \frac{1}{d}(u_{j,ij} + u_{k,ik}) + \frac{c}{d}(u_{i,jj} + u_{i,kk}) - e\alpha\Theta_{,i}) + X_i = 0$$

and then as

$$a\frac{c}{d}((u_{i,ii} + u_{i,jj} + u_{i,kk}) + \frac{1}{c}(u_{i,ii} + u_{j,ji} + u_{k,ki}) - \frac{de}{c}\alpha\Theta_{,i}) + X_i = 0$$

If the mathematical abbreviation grad div u_i is introduced to reflect the rate of change of the normal strain vector as given by def. (6.1.4.7) with respect to the direction x_i and if def. (6.1.4.1) is utilized, the governing elliptic partial differential equation of the combined elastic and thermoelastic stress analysis in space is established. Substituting for the constants according to expressions (6.22), thus

$$G(\Delta u_i + \frac{1}{1-2\mu}\ \text{grad div}\ u_i - \frac{2(1+\mu)}{(1-2\mu)}\alpha\Theta_{,i}) + X_i = 0 \qquad (6.24)$$

where the temperature field satisfies Laplace's equation following def. (6.1.4.4).

This equation has an infinite number of solutions since the displacements are free to take any prescribed values along the spatial limits. Mathematically, the sufficient conditions are satisfied.

6.2.5. SPECIAL CASES

With the absence of thermal strains, eqs. (6.24) reduce to

$$G(\Delta u_i + \frac{1}{1-2\mu}\ \text{grad div}\ u_i) + X_i = 0 \qquad (6.25)$$

If, furthermore, the influence of the body forces on the overall deformation is neglected, the governing compatibility equation for a spacial elastic continuum takes the compact form

$$\Delta u_i + \frac{1}{1-2\mu} \text{ grad div } u_i = 0 \qquad (6.26)$$

6.2.6. LIMITATIONS

Although it has been repeatedly proposed in the past to express the overall displacement field in terms of so-called stress functions that are in accordance with the given statical boundary conditions and obey Laplace's potential deformation equation, the partial differential equations (6.24) to (6.26) remain isoluble.

The classical approach to the closed solution of a spatial elasticity problem collapses, since any attempt to described the corresponding displacement fields such that they do not violate the internal compatibility and satisfy the prescribed boundary conditions will fail even for the simplest geometries.

6.3. CYLINDRICAL CONTINUA UNDER COMBINED TORSIONAL AND AXISYMMETRICAL DEFORMATION

6.3.1. EQUILIBRIUM OF FORCES AND COUPLES

Considering an infinitesimal volume element of cylindrical geometry, the stress tensor (6.1) is now composed of the normal and the shear stress components depicted in figure (6.5) and figure (6.6) respectively. The summation of the stress resultants in each direction x_i of the cylindrical coordinate system thus states the internal mechanical conditions under which the equilibrium of forces is satisfied. Upon dividing each term concerned by the quantity $dx_i dx_j d\phi$, the set of expanded equilibrium equations for the general axisymmetric case may be presented in the following tensor notation formulation

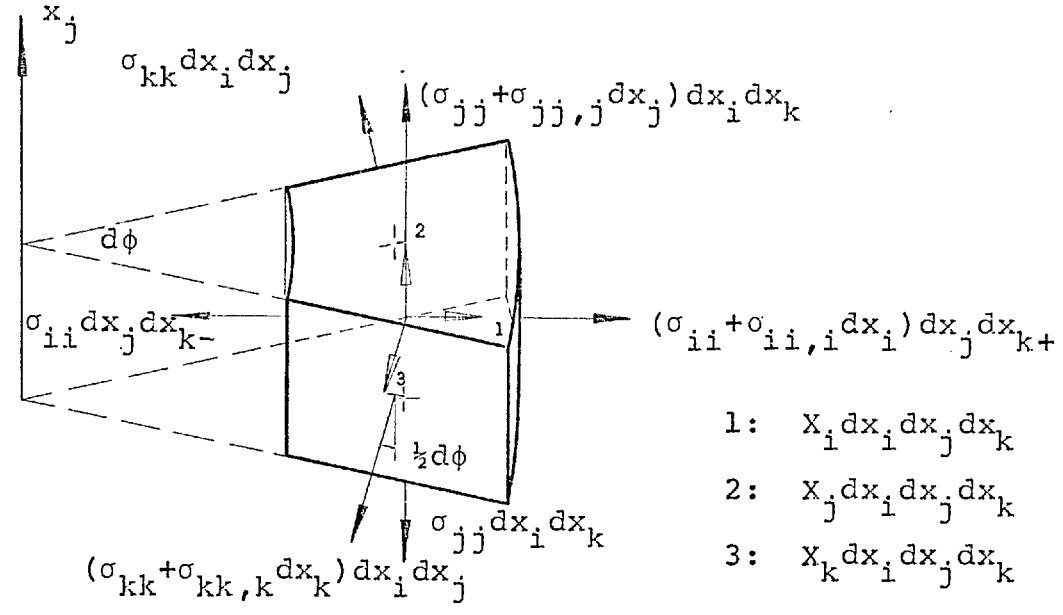


Fig. 6.5. Direct stress and body pressure components for axisymmetric analysis

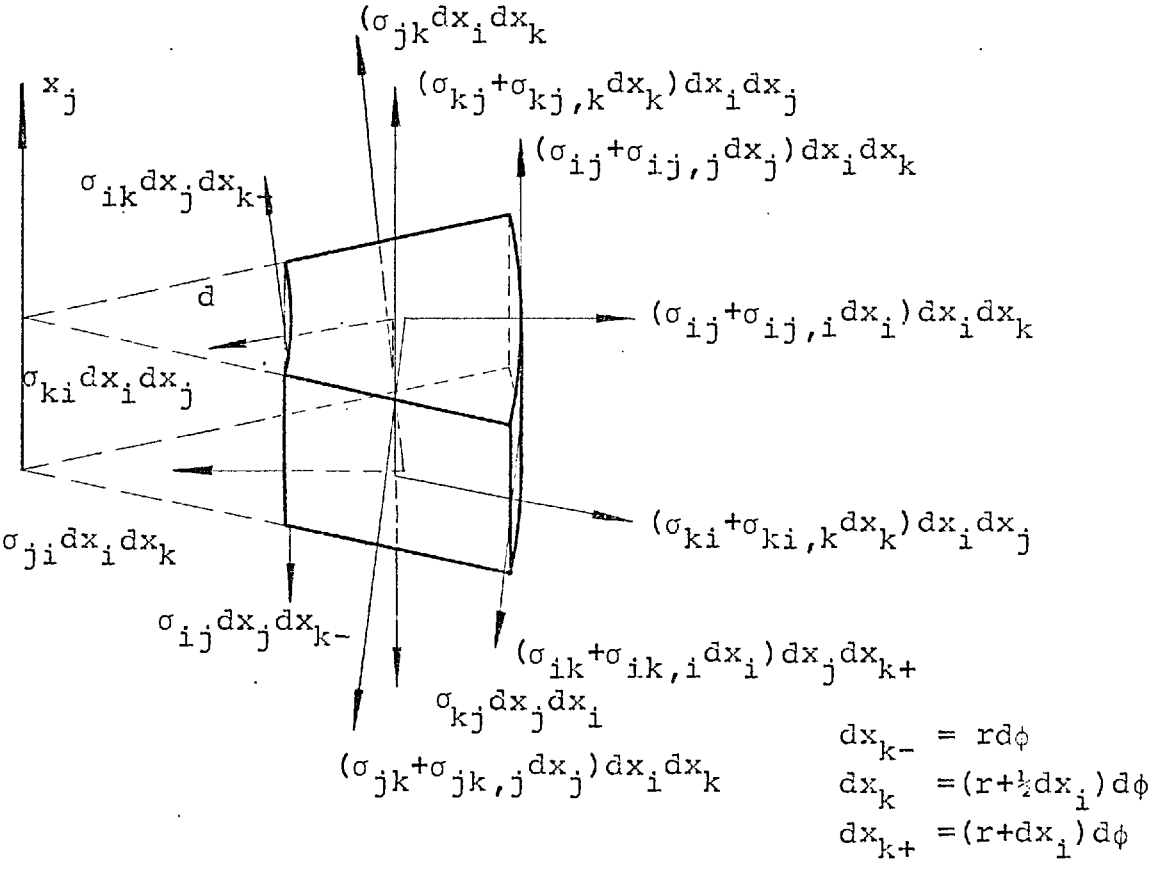


Fig. 6.6. Shear stress components for axisymmetric analysis

$$\frac{\sigma_{ii}}{dx_i} \cdot r + \sigma_{ii} + \sigma_{ii,i} + \sigma_{ii,i}dx_i - \frac{\sigma_{ii}}{dx_i} \cdot r + \frac{\sigma_{ji}}{dx_j}\frac{dx_i}{2} + \sigma_{ij,j}.r$$

$$+\sigma_{ji,j}\frac{dx_i}{2} - \frac{\sigma_{ji}}{dx_j}.r - \frac{\sigma_{ji}}{dx_j}\frac{dx_i}{2} + \frac{\sigma_{ki}}{d\phi}dx_i + \sigma_{ki,k}.r + \sigma_{ki,k}\frac{dx_i}{2}$$

$$- \frac{\sigma_{ki}}{d\phi}dx_i - \sigma_{kk} + X_i \cdot r + X_i\frac{dx_i}{2} + \frac{\sigma ji}{dx_j} = 0$$

$$\frac{\sigma_{jj}}{dx_j} + \frac{\sigma_{jj}}{dx_j}\frac{dx_i}{2} + \sigma_{jj,j}.r + \sigma_{jj,j}\frac{dx_i}{2} - \frac{\sigma_{jj}}{dx_j}.r - \frac{\sigma_{jj}}{dx_j}\frac{dx_i}{2} + \frac{\sigma_{kj}}{d\phi}$$

$$+ \sigma_{kj,k}.r + \sigma_{kj,k}\frac{dx_i}{2} - \frac{\sigma_{kj}}{d\phi} + \frac{\sigma_{ij}}{dx_i}.r + \sigma_{ij} + \sigma_{ij,i}.r + \sigma_{ij,i}dx_i$$

$$- \frac{\sigma_{ij}}{dx_i}.r + X_j.r = 0$$

$$\frac{\sigma_{kk}}{d\phi} + \sigma_{kk,k}.r + \sigma_{kk,k}\frac{dx_i}{2} - \frac{\sigma_{kk}}{d\phi} + \frac{\sigma_{jk}}{dx_j}.r + \frac{\sigma jk}{dx_j} + \sigma_{jk,j}.r +$$

$$\sigma_{jk,j}\frac{dx_i}{2} - \frac{\sigma_{jk}}{dx_j}.r - \frac{\sigma_{jk}}{dx_j}\frac{dx_i}{2} + \frac{\sigma_{ik}}{dx_i}.r + \sigma_{ik} + \sigma_{ik,i}.r +$$

$$\sigma_{ik,i}dx_i - \frac{\sigma_{ik}}{dx_i}.r + X_k.r = 0$$

Once equal terms of opposite signs are cancelled, the equilibrium equations can be reduced even further. Realizing that the terms containing the differential dx_i are by one order of magnitude smaller than the others, their influence on the equilibrium of forces may be neglected. An infinitesimal element of cylindrical geometry is thus found to be in static equilibrium under any combination of torsional and axisymmetric boundary conditions, if

$$(\sigma_{ii}.r)_{,i} + (\sigma_{ji}.r)_{,j} + (\sigma_{ki}.r)_{,k} - \sigma_{kk} + X_i.r = 0$$

$$(\sigma_{ij}.r)_{,i} + (\sigma_{jj}.r)_{,j} + (\sigma_{kj}.r)_{,k} + X_j.r = 0$$

$$(\sigma_{ik}.r)_{,i} + (\sigma_{jk}.r)_{,j} + (\sigma_{kk}.r)_{,k} + X_k.r = 0$$

(9 unknowns, 3 equations) (6.27)

Eqs. (6.27) correspond to eqs. (6.4). As opposed to the truly three-dimensional case, however, the equilibrium equations for cylindrical geometries cannot be contracted to one general equation, since a state of unpreferred directions is not given.

A local state of equilibrium must also be maintained between the couples which originate from the action of shear stress resultants on lever arms about the centroid of the infinitesimal element. After dividing each contribution to the couple equilibrium by the quantity $0.5\ dx_i dx_j dx_k$, the following equations are obtained.

$$2\sigma_{jk} - 2\sigma_{kj} + \sigma_{kj,k}\ dx_j - \sigma_{kj,k}\ dx_k = 0$$

$$2\sigma_{ki} - \sigma_{ik}\ \frac{dx_{k+}}{dx_k} + \sigma_{ki,k}\ dx_k - \sigma_{ik,i}\ dx_i\ \frac{dx_{k+}}{dx_k} = 0$$

$$\sigma_{ij}\ \frac{dx_{k+}}{dx_k} + \sigma_{ij}\ \frac{dx_{k-}}{dx_k} - 2\sigma_{ji} + \sigma_{ij,i}\ dx_i \frac{dx_{k+}}{dx_k} - \sigma_{ji,j} dx_j = 0$$

With ass. (6.1.2.1) and the expressions given in fig. (6.5), the set of equations of couple equilibrium may be contracted to the general equation

$$\sigma_{ij} = \sigma_{ji} \qquad (6.28)$$

(9 unknowns, 6 equations)

Thus the subscripts in eqs. (6.27) may be conveniently interchanged.

6.3.2. STRAIN-DEFORMATION RELATIONS

The stress tensor has reduced to six components and so has the strain tensor. Using the formulae obtained in eqs. (6.7) and (6.9) for the strains occurring in a cartesian plane, the three strain components in a longitudinal plane the three strain components in a longitudinal plane through the axis of revolution are immediately identified as

$$\varepsilon_{ii} = u_{i,i}$$

$$\varepsilon_{jj} = u_{j,j} \qquad (6.29)$$

$$\varepsilon_{ij} = u_{i,j} + u_{j,i}$$

(18 unknowns, 9 equations)

From fig. (6.7), the strain in the tangential direction depends not only on the displacement u_k but also on the radial displacement u_i. Separating the effect of the radial deformation, the increase $u_i d\phi$ in the arc length $\overset{\frown}{AD}$ determines the tangential strain as

$$\varepsilon_{kk}\ (u_i) = \frac{u_i}{r}$$

The difference in translational deformation between the elementary sides $\overline{AB}$ and $\overline{CD}$ with respect to the tangential direction amounts to

$$(u_k - u_{k,k}\, dx_k) = u_{k,k}\, dx_k$$

Consequently, the tangential strain due to a torsional displacement u_k can be inferred as

$$\varepsilon_{kk}\ (u_k) = u_{k,k}$$

The total tangential strain components is thus obtained by superposition

$$\varepsilon_{kk} = \frac{u_i}{r} + u_{k,k} \qquad (6.30)$$

(18 unknowns, 10 equations)

Considering the shearing strains in the circular plane, the angle between the directions of the deformed arc $\overset{\frown}{A'D'}$ and the initial arc $\overset{\frown}{AD}$, as shown in figure (6.7), is $u_{i,k}$. Similarly, the angle between the sides $\overline{A'B'}$ and $\overline{AB}$ is found to be $u_{k,i}$. However, only the angle $u_{k,i} - \frac{u_k}{r}$ contributes to the shearing strain, since $\frac{u_k}{r}$ represents the rigid body rotation about the axis of revolution. The angle

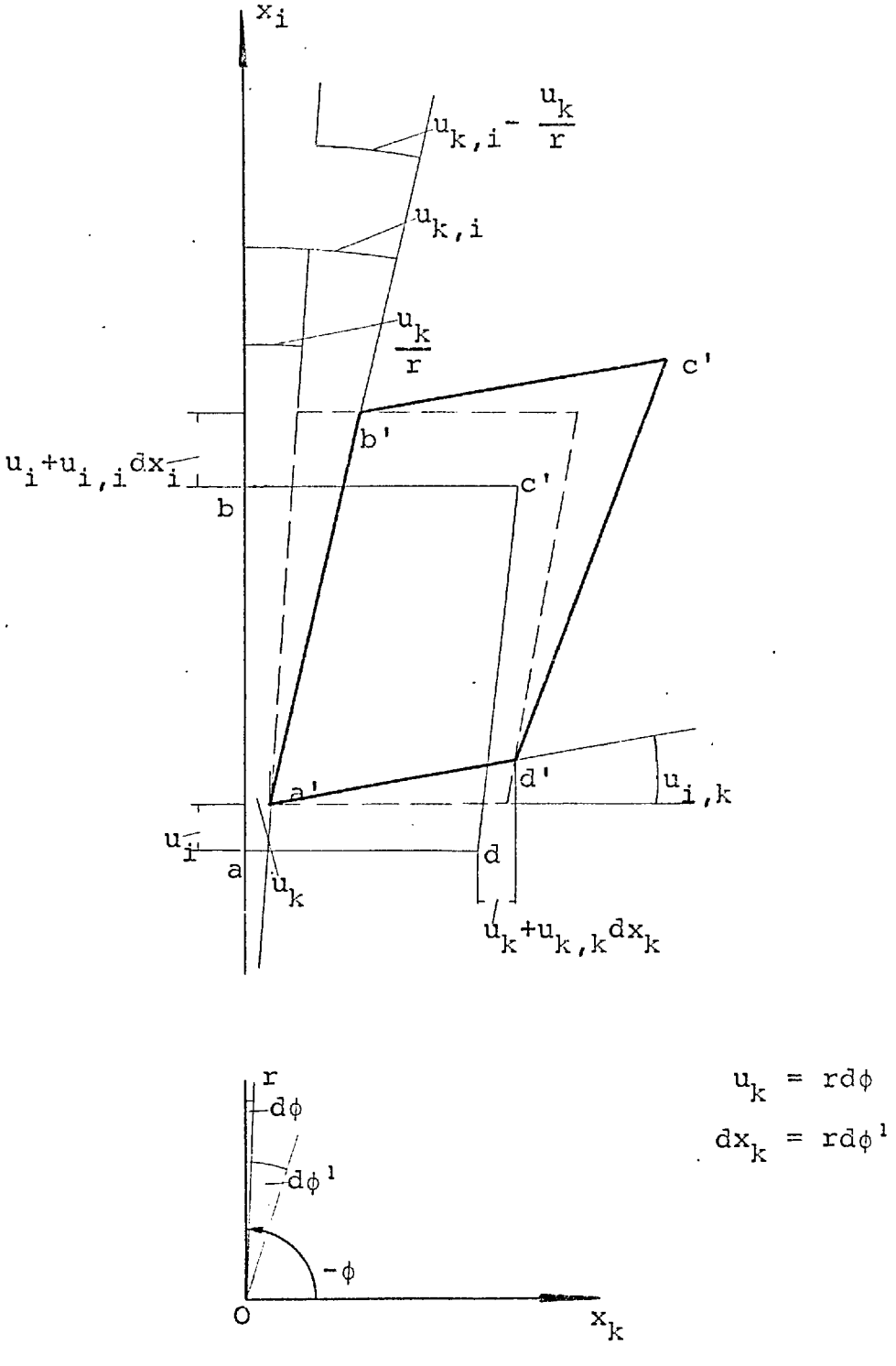


Fig. 6.7. Positive displacements and angles of rotation for the deformation of a plane in polar coordinates

defining the total shear strain in the circular plane thus adds up to

$$\varepsilon_{ik} = u_{i,k} + u_{k,i} - \frac{u_k}{r} \tag{6.31}$$

(18 unknowns, 11 equations)

With the absence of rigid body rotations in the circumferential surface of the cylinder, the total strain here becomes

$$\varepsilon_{jk} = u_{j,k} + u_{k,j} \tag{6.32}$$

(18 unknowns, 12 equations)

6.3.3. CONSTITUTIVE RELATIONSHIPS

Assuming that apart from mechanical stresses thermal stresses build up due to the presence of temperature gradients the stress-strain relationships for the twisted, as well as axisymmetrically deformed cylindrical continuum are obtained by subsituting eqs. (6.29) to (6.32) into eqs. (6.19) and by considering eqs. (6.20) and (6.21)

$$\begin{aligned}
\sigma_{ii} &= 2G(u_{i,i} + \frac{\mu}{c}\varepsilon - \alpha\theta) \\
\sigma_{jj} &= 2G(u_{j,j} + \frac{\mu}{c}\varepsilon - \alpha\theta) \\
\sigma_{kk} &= 2G(\frac{u_i}{r} + u_{k,k} + \frac{\mu}{c}\varepsilon - \alpha\theta) \\
\sigma_{ij} &= G(u_{i,j} + u_{j,i}) \\
\sigma_{jk} &= G(u_{j,k} + u_{k,j}) \\
\sigma_{ki} &= G(u_{i,k} + u_{k,i} - \frac{u_k}{r})
\end{aligned} \tag{6.33}$$

(18 unkowns, 18 equations)

In eqs. (6.33), ε follows def. (6.1.4.8), whereas the definitions of the constant c and the shear modulus G are found amongst the expressions (6.22).

For the 18 unknown functions the required number of 18 equations is available, and thus the necessary conditions are satisfied.

6.3.4. COMPATIBILITY EQUATIONS

Compatibility is guaranteed when the stress components in the equations of force and couple equilibrium are expressed in terms of the unknown displacement function. Substituting therefore the definitions of the stress components in the form of eqs. (6.33) into eqs. (6.27), the corresponding derivations of eqs. (6.27) will complete the expansion of the compatibility equations in the three unequal directions of the cylindrical continuum. Dividing throughout by the radius r and applying ass. (6.1.2.3), thus

$$G(2u_{i,ii} + u_{i,jj} + u_{i,kk} + \frac{2u_{i,i}}{r} - \frac{2u_{k,k}}{r} - \frac{2u_i}{r^2} + (u_{j,j} + u_{k,k} + \frac{2\mu}{c}\varepsilon - \alpha\theta),i) + X_i = 0$$

$$G(u_{j,ii} + 2u_{j,jj} + u_{j,kk} + \frac{u_{j,i}}{r} + (\frac{u_i}{r} + u_{i,i} + u_{k,k} + \frac{2\mu}{c}\varepsilon + 2\alpha\theta),j) + X_j = 0$$

$$G(u_{k,ii} + u_{k,jj} + 2u_{k,kk} + \frac{3u_{i,k}}{r} + \frac{u_{k,i}}{r} - \frac{u_{k,i}}{r} + (u_{j,j} + u_{i,i} + \frac{2\mu}{c}\varepsilon - 2\alpha\theta),_k) + X_k = 0$$

Differentiating the total direct strain, the components of which comply with def. (6.1.4.8), with respect to all directions x_i, the following equivalences are procured

$$u_{j,ji} + u_{k,ki} = \varepsilon,_i - u_{i,ii} - \frac{u_{i,i}}{r} + \frac{u_i}{r^2}$$

$$u_{i,ij} + u_{k,kj} = \varepsilon,_j - u_{j,jj} - \frac{u_{i,j}}{r}$$

$$u_{i,ik} + u_{j,jk} = \varepsilon_{,k} - u_{k,kk} - \frac{u_{i,k}}{r}$$

Substituting the expressions for the mixed, second derivatives into the expanded equations and using def. (6.1.4.2), the compatibility conditions for the twisted as well as axisymmetrically deformed cylindrical continuum are established

$$\begin{aligned} G(\Delta u_i + \frac{3u_{k,k}}{r} - \frac{u_i}{r^2} + \frac{1}{c}\varepsilon_{,i} - 2\alpha\theta_{,i}) + X_i &= 0 \\ G(\Delta u_j + \frac{1}{c}\varepsilon_{,j} - 2\alpha\theta_{,j}) + X_j &= 0 \\ G(\Delta u_k + \frac{2u_{i,k}}{r} - \frac{u_{k,i}}{r} + \frac{1}{c}\varepsilon_{,k} - 2\alpha\theta_{,k}) + X_k &= 0 \end{aligned} \qquad (6.34)$$

where the temperature field satisfies def. (6.1.4.5) and the constant c is known from eqs. (6.22).

Eqs. (6.34) are elliptic partial differential equations and thus fulfill the sufficient condition for the applicability of the small displacement theory in the elastic analysis of cylindrical continua. Like eqs. (6.24), they have an infinite number of solutions, since the displacements are free to take any prescribed values along the limits of the cylindrical domain.

6.3.5. SPECIAL CASES

Restricting the attention to axisymmetric deformations, the circumferential displacement component u_k disappears and differentiations with respect to the tangential direction vanish. Thus eqs. (6.34) reduce to

$$\begin{aligned} G(\Delta u_i - \frac{u_i}{r^2} + \frac{1}{c}\varepsilon_{,i} - 2\alpha\theta_{,i}) + X_i &= 0 \\ G(\Delta u_i + \frac{1}{c}\varepsilon_{,j} - 2\alpha\theta_{,j}) + X_j &= 0 \end{aligned} \qquad (6.35)$$

where the Laplace's operator and the total direct strain follow def. (6.1.4.3) and (6.1.4.9) respectively and the temperature field satisfies def. (6.1.4.6).

Differentiating eqs. (6.35) with respect to the radial and the axial direction respectively, and subsequently adding all terms, one single equation is formed

$$- \frac{u_{i,i}}{r^2} + \frac{u_i}{r^3} + \frac{1}{c}\frac{1}{r}(\varepsilon_{,i}.r)_{,i} - 2\frac{1}{r}\alpha(\theta_{,i}.r)_{,i}$$

$$+ \frac{1}{c}\varepsilon_{,jj} - 2\alpha\theta_{,jj} = 0$$

Since ε and θ comprise functions depending on the radius, the differentiation of their derivatives with respect to the radial direction x_i, $\varepsilon_{,i}$ and $\theta_{,i}$ must take into account the presence of the radius.

Neglecting the first two terms because of their small contribution and expanding the differentiations with respect to x_i, the potential normal strain equation for the mechanically and thermally loaded axisymmetric continuum is clarified to a point where the employment of Laplace's operators enable it to be contracted to

$$\Delta\varepsilon - 2c\alpha\Delta\theta = 0 \qquad (6.36)$$

The operators used are given by def. (6.1.4.10) and (6.1.4.6) respectively.

6.3.6. LIMITATIONS

The governing elliptic partial differential equations (6.34) to (6.36) are insoluble since mechanical, thermal and geometrical boundary conditions cannot be described in an analytic form. Thus, although the mathemtical formulation of the general solution to complex elasticity problems in axisymmetric continua exists, the displacement functions are incapable of complying with the disturbances caused by the action of conventional forces, prestressing strains and imposed displacements.

6.4. CONCLUSIONS

6.4.1. MATHEMATICAL SOLUBILITY

Looking at the Laplace-type partial differential equations (6.24) and (6.34) with the intention of solving them for the displacement fields, their elliptic nature is recognized. The mathematical property takes its name from the shape of the conical sections, which the boundaries of the disturbances describe when propagating from a perturbation point.

The most general solution for such equations consists of a Fourier series solution which, however, is of mathematical use only and practically of no or little meaning, since an infinite number of solutions exists, unless some specific physical boundary conditions are defined. These conditions are no more than restrictions of the analytical kind imposed on the general equations such that appropriate physical phenomena can be identified.

Thus, a general mathematical solution to the elasticity problem in spatial continua exists, but it does not apply.

6.4.2. PHYSICAL INSOLUBILITY

It is only when boundary conditions due to statical disturbances are used that the usefulness of the compatibility equations (6.24) and (6.34) , governing the thermoelastic behaviour of truly spatial and cylindrical continua, can be enjoyed.

Physically, the elliptic property of a thermoelastic continuum subjected to a skleronomical state of stress signifies that a disturbance propagating from one point of the structure can affect any other point. The final values of the influence coefficients are obtained, once the structure has fully relaxed in compliance with its elasticity.

The disturbances may be excited due to the action of conventional external forces, prestressing strains and imposed displacements; unfortunately, however, they are incapable of being laid down in an analytic form. Even the boundary conditions of simplified problems in space, as expressed for instance by eqs. (6.25) to (6.26) and eqs. (6.35)

to (6.36), defy the description in a closed mathematical form.

Thus it must be realized that spatial elasticity problems exceed the analytic applicability of the small displacement theory.

6.4.3. PHILOSOPHICAL COLLAPSE

As it can be seen from eqs. (6.24) to (6.26) and eqs. (6.34) to (6.36), the general compatibility equations can be reduced to fit special problems when appropriate boundary conditions are employed. It verifies that a general physically meaningful solution to the differential equations of the elastic analysis in space is not possible.

Philosophically, this implies that the development of the small displacement theory has arrived at the ultimate concept of its analytic approach which collapses due to the impossibility of obtaining a general meaningful solution. It does not mean that the compability equations and thus the small displacement theory of linear elasticity in spatial continua are unnecessary or obsolete developments.

Merely it indicates a quality in the nature of the ultimate state of a theory, as these equations on the one hand reflect the most general and adequate synthesis in elasticity and thermoelasticity and on the other hand must be restricted to very special non-spatial cases to apply.

The major conclusions are that the spatial compatibility equations are at the same time general and particular and thus would have presented a genuine state of scientific instability, if the theory of linear elasticity had not been reconstructed from new fundamentals as it is shown in the following chapters.

CHAPTER VII

VARIATIONAL ANALYSIS OF COMBINED ELASTIC AND THERMOELASTIC CONTINUA

7.1 INTRODUCTION

7.1.1. OBJECTIVE

Since there is a clear existence of contradictions between the small displacement theory of linear elastic analysis in spatial continua and the limitations that confront it, it is endeavoured to derive a theory that verifies the findings already obtained and supersedes the small displacement theory by offering new possibilities to the elastic analysis.

To proceed, the elastic theory which in Chapter VI has been based on the equilibrium of forces and couples that behave in conformity with the elastic law is coupled with the conception of energy. This link clearly indicates that the principle of conservation of energy, as known from physics, shall lead to general governing equations also in the statical analysis, especially since the variational theory sets out to derive it on the basis of mechanical work done along displacements.

The necessary conditions in proving the equivalence of the variational and the small displacement theory, is that the principle of virtual work or an extension of it arrives at analytic compatibility equations identical with those obtained in Chapter VI.

The sufficient condition for the applicability of the variational theory of elasticity is satisfied, if the principle of virtual work in its analytic formulation or an extension of it yields an explicit solution to the unknown spatial displacement fields.

7.1.2. ASSUMPTIONS AND IMPLICATIONS

In the following, the assumptions are stated under which the energy principles shall lead to the variational theory of linear elasticity and thermoelasticity. At the same time, the inferred implications are discussed.

(1) The displacements are fictitious; their occurrence is possible but not necessary - thus the applied forces, by doing work along these displacements, do not have the tendency to set the mechanical system into motion.

(2) The displacements are differentially small - thus in the formulation of virtual work the forces can be considered independent of the displacements.

(3) The displacements are kinematically compatible with the geometrical configuration of the system comprising shape, biactions and support reactions - thus any ambiguity in defining the continuous displacement field is avoided.

(4) In the process of doing virtual work along virtual displacements, the external forces retain their initial magnitudes - thus the state of statical equilibrium is not violated.

(5) The internal forces are developing slowly inside the unit volume elements - thus the mechanical action gives rise to internal deformations which are linearly dependent on them.

(6) A mechanical system is in statical equilibrium, if the work done by the externally imposed forces vanishes for any possible virtual displacement - thus the virtual work theorem is defined.

(7) Considering the occurrence of virtual displacements, the external work done by the real forces is equal to the increase in the internal strain energy - thus the link between the virtual work theorem and the energy concept is established.

(8) The principle of virtual work is valid for solids deforming in conformity with the linear elastic law - thus definitions (1) to (8) of section 6.7.2. apply.

In the following, the assumptions shall be referred to as ass. (7.1.2.i), i = 1,8.

7.1.3. SET THEORY

Generally, the spatial stress tensor (6.1) and the conjugate strain tensor (6.6) and also the analoguous definitions for a twisted as well as axisymmetrically deformed cylindrical continuum are expressed by sets of functions which may be assembled in the following column arrays

$$\underline{\sigma} = \{\sigma_{ii}, \sigma_{jj}, \sigma_{kk}, \sigma_{ij}, \sigma_{jk}, \sigma_{ki}\} \tag{7.1}$$

$$\underline{\varepsilon} = \{\varepsilon_{ii}, \varepsilon_{jj}, \varepsilon_{kk}, \varepsilon_{ij}, \varepsilon_{jk}, \varepsilon_{ki}\} \tag{7.2}$$

where the functions of the shear strain components ε_{ij} follow definitions (6.9) or (6.31), (6.32) and the third of (6.29), respectively.

The work done per unit volume then amounts to $\varepsilon^t\sigma$. However, it is convenient to make the transformation of stresses and strains identical such that in any new coordinate system there is

$$\begin{aligned} \underline{\sigma}^1 &= \underline{C}^t\, \underline{\sigma}\, \underline{C} \\ \underline{\varepsilon}^1 &= \underline{C}^t\, \underline{\sigma}\, \underline{C} \end{aligned} \tag{7.3}$$

In order to keep the work done unchanged under transformation, the following definitions of stress and strain tensors are accepted

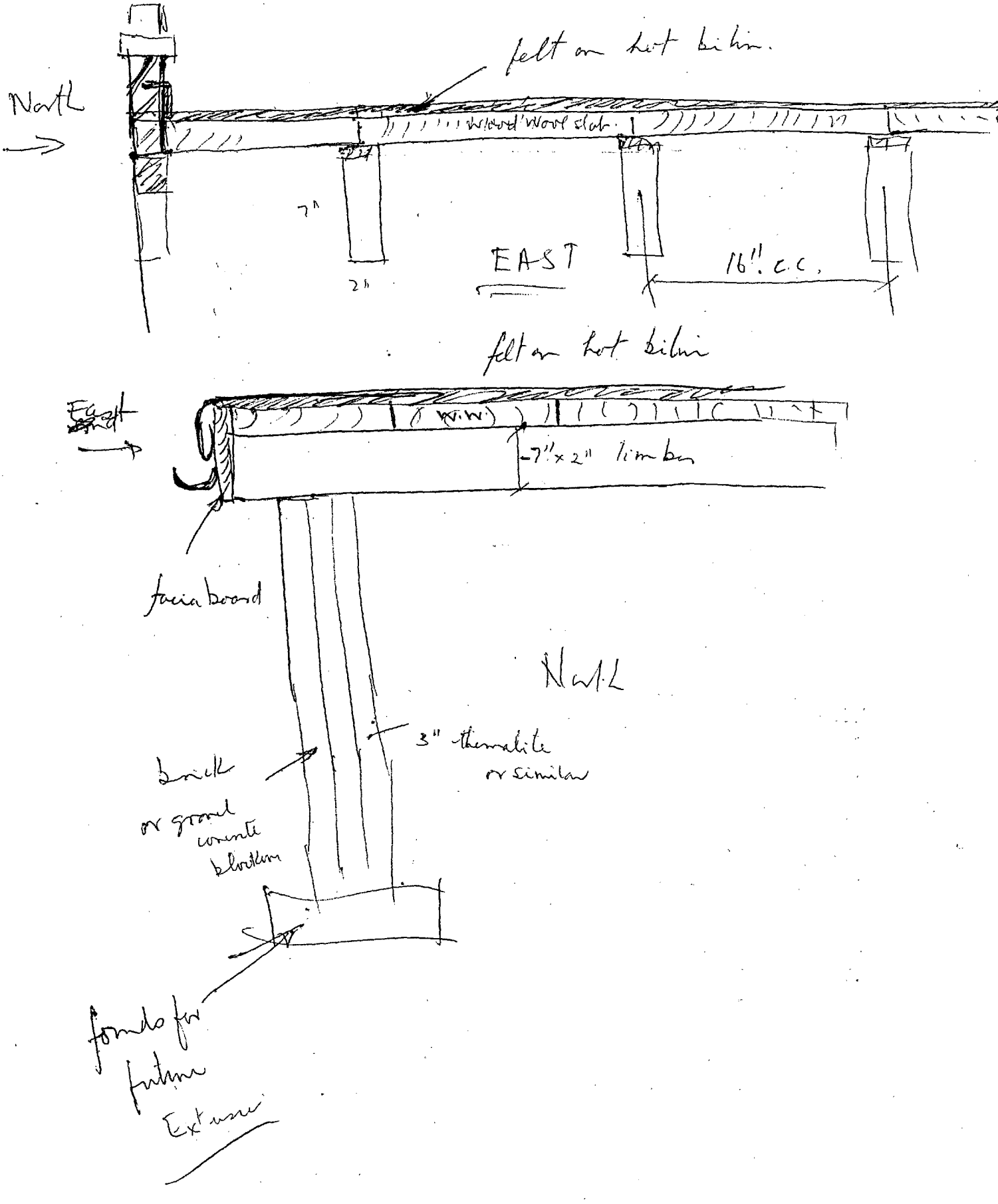
$$\underline{\sigma} = \{\sigma_{ii}, \sigma_{jj}, \sigma_{kk}, \sqrt{2}\sigma_{ij}, \sqrt{2}\sigma_{jk}, \sqrt{2}\sigma_{ki}\} \tag{7.4}$$

$$\underline{\varepsilon} = \{\varepsilon_{ii}, \varepsilon_{jj}, \varepsilon_{kk}, \sqrt{2}\varepsilon_{ij}, \sqrt{2}\varepsilon_{jk}, \sqrt{2}\varepsilon_{ki}\} \tag{7.5}$$

where the shear strain functions now follow definition (6.10) or the analoguous definitions in cylindrical coordinates.

Considering truly spatial deformation, the equations of internal equilibrium (6.4), the equations of equilibrium

0272 671099


felt on hot bitin.
North
Wood Wool slab
7"
2"
EAST
16" c.c.
felt on hot bitin
North
7" x 2" timber
fascia board
North
3" thermalite or similar
brick or ground concrete block
footing for future Extension

at the boundary (6.5) and the strain-deformation equations (6.7) and (6.10) may be expressed by using the following sets of functions

$$\underline{D}\,\underline{G} + \underline{X} = \underline{O} \tag{7.6}$$

$$(\underline{D}n)\,\underline{\sigma} = \underline{F} \tag{7.7}$$

$$\underline{\varepsilon} = \underline{D}^{t}\underline{u} \tag{7.8}$$

where for all cases $\underline{D}$ is conveniently given by the same differential operator matrix

$$\underline{D} = \begin{bmatrix} (\,)_{,i} & 0 & 0 & \sqrt{2}(\,)_{,j} & 0 & \sqrt{2}(\,)_{,k} \\ 0 & (\,)_{,j} & 0 & \sqrt{2}(\,)_{,i} & \sqrt{2}(\,)_{,k} & 0 \\ 0 & 0 & (\,)_{,k} & 0 & \sqrt{2}(\,)_{,j} & \sqrt{2}(\,)_{,i} \end{bmatrix} \tag{7.9}$$

Analysing an axisymmetric continuum which is subjected to torsion and axisymmetric loading, the differential operator matrix $\underline{D}$ enables the equations of internal equilibrium (6.27) to be formulated in sets as well

$$\underline{D}\,(r\underline{\sigma}) - \sigma_{kk}\underline{e} + r\underline{X} = 0 \tag{7.10}$$

where $\underline{e}$ is defined by the column vector $\{1 \;\; 0 \;\; 0\}$.

Since the state of unpreferred directions is not given for cylindrical geometry, the derivation of the strain-deformation relations (6.29) to (6.32) demands the consideration of the total distortional angles. Furthermore, the strain components (6.30) and (6.31) incorporate special terms and thus the differential operator (7.9) does not apply to the analogues of eqs. (7.7) and (7.8).

The multiple use of the differential operator matrix in the formulation of various equilibrium, as well as train-deformation equations, proves the advantage of a conveniently chosen definition of strains.

7.1.4. CALCULUS OF VARIATION

The calculus of variation deals with the transformation of insoluble differential equations of boundary value problems to equivalent functionals. A functional may be an integral operation which assigns a value to each of a certain class of functions. Using the tensor and comma notation convention, it could take the form

$$I = \int f(x_i, u_i, u_{i,i} \ldots u_{i,ni})\, dv \qquad (7.11)$$

The central problems is to find those functions u_i etc. in a prescribed class of functions f for which the given functional I has a minimum.

In a boundary value problem the admissible functions are specified by a boundary condition. A necessary and sufficient condition that the admissible functions minimize the functional (7.11) is the vanishing of its variation for all admissible varied functions $u_i + \beta \partial u_i$, provided that the following Euler equation is simultaneously satisfied

$$\frac{\partial f}{\partial u_i} - \left(\frac{\partial f}{\partial u_{i,i}}\right)_{,i} - \left(\frac{\partial f}{\partial u_{j,i}}\right)_{,i} - \left(\frac{\partial f}{\partial u_{k,i}}\right)_{,i} + \ldots +$$

$$+ (-1)^n \left(\frac{\partial f}{\partial u_{k,ni}}\right)_{,ni} = 0 \qquad (7.12)$$

The necessary condition for an admissible function u to furnish an extreme value of a functional I can be derived immediately. A function ∂u shall be called admissible variation if, for a sufficiently small β, $u + \beta \partial u$ is an admissible function. Thus, for β real and positive, the following unequality holds

$$I(u + \beta \partial u) \geq I(u)$$

If ∂u is an arbitrary admissible variation which satisfies the only condition that it vanishes at the boundary of the given region, then $I(u + \beta \partial u)$ is a function of β only, since a determinate integration is carried out over the domain

of u and ∂u. The admissible function u + β∂u converges to the extremizing function when β is equal to naught; here, therefore, the functional I(u + β∂u) as a function of must have an extreme value.

From differential calculus then, the derivative of the functional must vanish when β is equal to zero, thus

$$\partial I(u,\partial u) = I(u + \beta\partial u),_{\beta}\Big|_{\beta = 0} \tag{7.13}$$

where the functional ∂I which depends on ∂u as well as on u is called the first variation of the functional I.

Although a necessary condition, the vanishing of the first variation is only sufficient in conjunction with the existence of an absolute extreme value as furnished by the Euler equation (7.12).

7.2. PRINCIPLES IN THE ANALYTIC FORMULATION OF THE THERMOELASTIC PROBLEM

7.2.1. PRINCIPLE OF CONSERVATION

The more general principle of conservation is an axiom neither capable nor in want of a proof; its validity in the theoretical or experimental reproduction of a natural phenomenon must be justified by agreement with past experiences- which is the case.

The principle of conservation may be formulated by utilizing Green's theorem which states that any net change $a_{,i}$ of a scalar quantity a in a unit element can only be brought about by a net change penetrating through the element surface. For direction x_i this goes to prove that

$$a_{,i}dx_i dx_j dx_k = n_{,i}a\ ds \tag{7.14}$$

Integrating over the whole volume and the surface of the continuum, Green's theorem is established

$$\int a_{,i}\ dv = \int n_{,i}a\ ds \tag{7.15}$$

where $n_{,i}$ designates the direction cosines of the surface normal under which the net change is penetrating into the body.

7.2.2. PRINCIPLE OF VIRTUAL WORK

Widening the field of applicability of the principle of conservation of energy to a stress analysis problem, where mechanical work is done along displacements under preservation of the static equilibrium of the structure, the principle of virtual work can be introduced.

Employing Green's theorem, proof can be given to the existence of the virtual work principle. Let the virtual work theorem take the form

$$\int F^t u \, ds + \int X^t u \, dv = \int \sigma^t \varepsilon \, dv \tag{7.16}$$

In this integral equation the stress functions are assumed to be in statical equilibrium with the body forces and the surface tractions, whereas the strain functions are in compatibility with the displacements. Stress and strain fields are virtual systems which are totally unconnected.

In proceeding to prove the validity of eq. (7.16), the quantity a is replaced by the product of the two scalars b and c. The expanded Green's theorem (7.15) thus becomes

$$\int (bc_{,i} + cb_{,i}) \, dv = \int n_{,i} \, bc \, ds \tag{7.17}$$

If b and c represent large numbers of variable scalar quantities, they may be identified by the unidimensional sets $\underline{b}$ and $\underline{c}$ of the sizes (1xp) and (1xq) respectively. For any combination of single scalars, eqs. (7.17) reads

$$\int (b_\ell c_{m,i} + c_m b_{\ell,i}) \, dv = \int b_\ell n_{,i} c_m \, ds \tag{7.18}$$

If all quantities out of the sets $\underline{b}$ and $\underline{c}$ are considered, the expanded Green's theorem can be formulated with the use of sets as follows

$$\int (\underline{b}^t \underline{\partial}\ \underline{c} + \underline{c}^t \underline{\partial}^t \underline{b})\ dv = \int \underline{b}^t (\partial n)\ c\ ds \qquad (7.19)$$

where all single differential operators are now assembled in a rectangular operator matrix $\underline{\partial}$ of the size (pxq).

It is important to realize that $\underline{b}$ and $\underline{c}$ are sets and not matrices, since their coefficients are functions and not constant scalars. Replacing the sets $\underline{b}$, $\underline{\partial}$ and $\underline{c}$ by the sets $\underline{u}$, $\underline{D}$ and $\underline{\partial}$ of eqs. (7.6) to (7.8), the principle of conservation states that

$$\int (\underline{u}^t \underline{D}\ \underline{\sigma} + \underline{\sigma}^t \underline{D}^t \underline{u})\ dv = \int \underline{u}^t (\underline{D}n)\ \underline{\sigma}\ ds \qquad (7.20)$$

If Green's theorem is true for any sets of variable quantities as laid down in eq. (7.19), then it must also hold for eq. (7.20). Substituting the three governing equations (7.6) to (7.8) of the spatial elasticity problem into eq. (7.20), the general form of the virtual work principle is established

$$\int \underline{\varepsilon}^t \underline{\sigma}\ dv = \int \underline{u}^t \underline{X}\ dv + \int \underline{u}^t \underline{F}\ ds \qquad (7.21)$$

which apart from the logical order of the multiplied vectors is identical with eq. (7.16).

Considering a structural system under geometrical and mechanical boundary conditions, the principle of virtual work in the form (7.21) states that the displacement field is uniquely described, the forces are independent of the displacements, and the system remains motionless under the action of the forces.

In the equilibrium conditions in the system are restated by replacing the virtual stress system by the actual stresses, the principle of virtual displacements is formulated.

7.2.3. UNIT DISPLACEMENT THEOREM

Before expanding the principle of virtual work into the principle of minimum potential energy, it is intended to define the stiffness coefficients of a structure using the unit displacement theorem.

Considering an elastic structure in which all forces including the body forces are represented as one set of nodal forces, it is pertinent to investigate the effect that a single force acting at one point has on the deformation of another.

To proceed, the principle of virtual work (7.21), which expresses indirectly the equilibrium between the internal stresses, the body forces and the surface tractions in terms of the kinematical compatiblity conditions, is reduced to the case in which a single force X_i, say due to body pressure, is doing work along a virtual displacement u_i

$$u_i X_i = \int \varepsilon_i^t \sigma_j \, dv \tag{7.22}$$

The unit displacement theorem then states that for a unit displacement u_i at the location x_i the single force X_i at x_i can be interpreted as a stiffness coefficient such that the following defintion is rendered possible

$$1.k_{ij} = \int \varepsilon_i^t \sigma_j \, dv \tag{7.23}$$

where ε_i is a system of strains kinematically compatible with a unit displacement u_i at x_i, σ_j is the true stress system in the structure producing a unit displacement u_j at x_j and k_{ij} is the force required at x_i to produce a unit displacement u_j at x_j.

Considering an infinitesimal volume element, the stress component σ_j can be expressed by the local set of material stiffness coefficients $\underline{d}$ multiplied by the strain component ε_j. The unit displacement theorem then takes the form

$$1.k_{ij} = \int \varepsilon_i^t \underline{d} \varepsilon_j dv \tag{7.24}$$

Since ε_i and ε_j are sets of the size (1x1), they may be interchanged without altering the amount of virtual work done. To avoid ambiguity, it must, however, be assumed that both ε_i and ε_j are components of virtual strain system. Thus, it is concluded that

$$k_{ij} = k_{ji} \tag{7.25}$$

This is the Maxwell reciprocal theorem which states that the set of stiffness coefficients of an elastic structure is symmetric.

The advantage of the use of the displacement method in the stress analysis of elastic structures, in comparison with the force method, is that the overall set of stiffness coefficients of the structure, which later shall be called global stiffness matrix, can be found from the superposition of all coefficients k_{ij} without reference to how it is supported. The overall set of stiffness coefficients can be obtained as the basic set of the unsupported structure before the solution of the elasticity problem, since the strains represent virtual systems and the deformation is local for the unit displacement method as other displacements are suppressed.

7.2.4. PRINCIPLE OF MINIMUM POTENTIAL ENERGY

When the existence of a strain energy function is assured and the forces are assumed to be kept unchanged during the displacement variation, the principle of virtual work leads to the establishment of the principle of minimum potential energy, which is capable of taking into account the effects of thermal loads on the overall deformation.

Strain energy can be defined as the work done by the stresses along the conjugate strains which by virtue of ass. (7.1.2.5) are linearly dependent on them. It is encouraged where ever slowly increasing or decreasing loads induce linearly dependent deformations.

The principle of minimum potential energy with the unknown function being the displacement field may be stated as the vanishing of the first variation of the total potential energy. Contributions to the total potential energy are made by the internal strain energy, the thermal strain energy, the strain energy due to prestressing, the potential energy of the body forces and the potential energy of the external forces, respectively

$$I = \int \tfrac{1}{2}\underline{\varepsilon}^t\underline{\sigma}\, dv - \int \underline{\varepsilon}^t\underline{\sigma}_t\, dv - \int \underline{\varepsilon}^t\underline{\sigma}_p\, dv - \int \underline{u}^t\underline{X}\, dv - \int \underline{u}^t\underline{F}\, ds \qquad (7.26)$$

According to ass. (6.1.2.7), the thermal stresses $\underline{\sigma}_t$ are induced by thermal expansion under the conditions of zero strains for all unit volume element. Provided that all non-thermal loading conditions are absent, the internal strains $\underline{\varepsilon}$ ensure geometric compatibility between all unit volume elements of the thermally loaded structure, and their magnitudes will be known, once the structure has relaxed elastically under suppressed thermal conditions.

If each unit volume element were capable of expanding freely under a positive change in its temperature, the direct components of the unconfined thermal strain $\underline{\varepsilon}_t$ would be given by the product of the coefficient of thermal expansion and the temperature increment.

After the natural elastic relaxation of the continuum, the actual stresses thus result from multiplying the local set of material stiffness coefficient into the difference between the elastically balanced confined strains and the unconfined strains

$$\underline{\sigma}_t = \underline{d}(\underline{\varepsilon} - \alpha\underline{\theta}) \qquad (7.27)$$

The prestressing stresses $\underline{\sigma}_p$ would theoretically be achieved by the initial prestressing strains, if concrete were absolutely rigid. After the elastic relaxation of the stressed continuum, the equivalent initial forces would, however, undergo a loss due to the elastic contraction of the prestressing cables. If the continuum is merely subjected to prestress, the decrease in prestressing forces is governed by the internal strain field $\underline{\varepsilon}$ due to prestress.

In an iterative computation then, the effect of the correcting negative prestressing forces on the internal strains must be determined. If the internal strains have converged to a final set of $\underline{\varepsilon}$, the actual stresses are computed by multiplying the local set of material stiffness coefficients into the difference between the internal and the initial

prestressing strains

$$\underline{\sigma}_p = \underline{d}(\underline{\varepsilon} - \underline{\varepsilon}_o) \tag{7.28}$$

It must be realized that the present chapter deals with infinitesimals; in other words, the underbarred quatities represent rectangular sets of space-dependent functions and not matrices.

7.2.5. PRINCIPLE OF PROPAGATION OF HEAT

Concentrating on a unit volume element at any point of a homogeneous and isotropic continuum, Gauss' theorem states that any net change $a_{,i}$ of a continuous scalar variable a, which is continuous in its first partial derivatives, can only be brought about by a flux penetrating through the element surface

$$a_{,i}\, dv = n_{,i} ads \tag{7.29}$$

where $n_{,i}$ represents the direction cosines of the surface normal in the three directions.

If the flux a is recognized as the heat penetrating through the surface per unit time, Fourier's law may be applied. Assuming, in addition, that each unit volume element is losing heat at a rate proportional to its temperature, Fourier's law states that the total heat flux across any surface at a point depends linearly on the rates of change of temperature at that point

$$a = (q + o\theta) = - k\, grad\theta \tag{7.30}$$

where q is the heat generation in $Kcal/m^2day$, o is the outflow coefficient in $Kcal/m^2day^0C$ and k is the thermal conductivity in $Kcal/m.day^0C$. The negative sign is due to the fact that heat always propagates towards locations of lower temperature.

Substituting eq. (7.30) into eq. (7.29), the conservation of thermal energy is expressed

$$(-k\,\mathrm{grad}\theta)_{,i}\,dv = n_{,i}(q + o\theta)\,ds \tag{7.31}$$

Since it is obvious that only components normal to the surface contribute to the transport of thermal energy through the corresponding surfaces, eq. (7.31) may be rewritten as

$$(-k\,\mathrm{grad}\theta)_{,i} = (q + o\theta) \tag{7.32}$$

From hydrodynamics it is known that the continuity of mass flow demands

$$a_{,t} + \mathrm{div}\,(av) = 0 \tag{7.33}$$

Introducing the product ρc, which represents the material's specific heat per unit volume and degree centigrade, and replacing the product of the scalar a and the vector v by the right hand side of eq. (7.30), then eq. (7.33) may be interpreted as the continuity of thermal flow in a continuum

$$\rho c\theta_{,t} + (-k\,\mathrm{grad}\theta)_{,i} = q + o\theta \tag{7.34}$$

where ρ is the density in MN/m and c is the specific heat per unit mass in MN/m^3 and c is the specific heat per unit mass in $Kcal/MN^0C$.

With ass. (6.1.2.6), no heat transport takes place transversally to the surface normal, and thus Laplace's operators can reduce eqs. (7.34) to one general equation both for the three-dimensional and the axisymmetric cases

$$k\Delta\theta + q + o\theta = \rho c\theta_{,t} \tag{7.35}$$

For truly spatial temperature fields the operator follows def. (6.1.4.4) , whereas for axisymmetric fields def. (6.1.4.6) applies.

7.3. FUNCTIONALS IN THE ANALYSIS OF THERMOELASTIC CONTINUA

7.3.1. STRAIN ENERGY FUNCTIONAL FOR THREE-DIMENSIONAL CONTINUA

7.3.1.1. ADMISSIBLE FUNCTIONS

In the elastic and the thermoelastic analysis of continua a convenient functional to minimize is that of the total potential energy. Excluding the contributions due to conventional and prestressing forces which shall be used to described the mechanical and the geometric boundary conditions, respectively, this functional may be formulated in the tensor notation convention as follows

$$I = \int (\tfrac{1}{2}\varepsilon_{ij}\sigma_{ij} - \varepsilon_{ij}\sigma_{ij} - u_i X_i)\, dv \qquad (7.36)$$

Granting the difference from the set notation convention, the terms in functional (7.36) are readily identified with the first, the second and the fourth term of the total potential energy functional expounded in eq. (7.26).

Substituting eqs. (6.7), (6.8), (6.9) (6.20) and (6.21) into eq. (7.36), the class of admissible functions f is procured

$$f=\tfrac{1}{2}\begin{bmatrix} u_{i,i} \\ u_{i,j} + u_{j,i} \end{bmatrix}\begin{bmatrix} a(u_{i,i}+b(u_{j,j}+u_{k,k})) \\ a\frac{c}{d}(u_{i,j}+u_{j,i}) \end{bmatrix} - \begin{bmatrix} u_{i,i} \\ u_{i,j}+u_{j,i} \end{bmatrix}\begin{bmatrix} ae\alpha\theta \\ 0 \end{bmatrix} - u_i X_i \qquad (7.37)$$

From definition (7.11) it is already known that the space-dependence of the displacement functions compels f to be an infinitesimal.

7.3.1.2. EULER EQUATION

With the aim of proving that the functional (7.36) is suitable to describe a corresponding spatial elasticity problem and that its class of functions satisfies the Euler equation (7.12), the following derivatives are produced

$$\frac{\partial f}{\partial u_i} = - X_i$$

$$\frac{\partial f}{\partial u_{i,i})_{,i}} = a(u_{i,i} + b\ (u_{j,j} + u_{k,k}))_{,i} - ae\alpha\theta_{,i} \qquad (7.38)$$

$$\frac{\partial f}{\partial u_{j,i})_{,i}} = a\frac{c}{d}\ (u_{i,j} + u_{j,i})_{,i}$$

$$\frac{\partial f}{\partial u_{k,i})_{,i}} = -a\frac{c}{d}\ (u_{i,k} + u_{k,i})_{,i}$$

Substituting eqs. (7.38) into the Euler equation (7.12) and using the mathematical steps performed between eqs. (6.23) and (6.24), the following equation is obtained

$$-a\frac{c}{d}\ ((\Delta u_i + \frac{1}{c}\ \text{grad div}\ u_i + \frac{de}{c}\ \alpha\theta_{,i}) - X_i = 0$$

After substitution for the constants, a, b, c, d and e according to definitions (6.22) and subsequent cancellation, the Euler equation is found to lead to an expression, which is identical with the governing partial differential equation (6.24) of the small displacement theory applied to the spatial thermoelastic analysis

$$G(\Delta u_i + \frac{1}{1-2\mu}\ \text{grad div}\ u_i - \frac{2(1+\mu)}{1-2q)}\ \alpha\theta_{,i}) + X_i = 0 \qquad (7.39)$$

Since the Euler equation (7.12) satisfies identically the differential equation (6.24) which also takes the name natural boundary condition, it is proved that a displacement field exists which furnishes an absolute extreme value to the functional (7.36).

7.3.1.3. DIFFERENTIAL CALCULUS

Substituting an arbitrary admissible function $u_i + \beta\partial u_i$, consisting of a function plus a variation, into the functional (7.36), the necessary condition is expected to yield an expression that contains the displacement field u_i as an extremal, whether or not the corresponding value of the functional constitutes an absolute extremal.

In the process of deriving the first variation of the total potential energy functional (7.36), it is convenient

to postulate the existence of the following relations

$$\begin{aligned} \varepsilon_{ij} &= \underline{a}\,\underline{b}\,u_i \\ \sigma_{ij} &= \underline{d}\,\underline{a}\,\underline{b}\,u_i \\ \sigma_{tij} &= \underline{d}\,\alpha\theta \end{aligned} \tag{7.40}$$

where $\underline{a}$, $\underline{b}$ and $\underline{d}$ are rectangular sets of functions of some kind. With eqs. (7.40) the functional for an arbitrary admissible function thus becomes

$$\begin{aligned} I = \int \big(&\tfrac{1}{2}(u_i + \beta\partial u_i)\, \underline{b}^t\underline{a}^t\underline{d}\,\underline{a}\,\underline{b}\,(u_i + \beta\partial u_i) \\ &- (u_i + \beta\partial u_i)\, \underline{b}^t\underline{a}^t\underline{d}\alpha\theta - (u_i + \beta\partial u_i)\, X_i \big)\, dv \end{aligned} \tag{7.41}$$

From differential calculus, the first variation is equivalent to minimizing the total potential energy, permitting only the deformations to vary. Following the process of differentiation indicated in eq. (7.13), thus

$$\partial I = \partial u_i \int (\underline{b}^t\underline{a}^t\underline{d}\,\underline{a}\,\underline{b}\,u_i - \underline{b}^t\underline{a}^t\underline{d}\,\alpha\theta - X_i)\, dv = 0 \tag{7.42}$$

As eq. (7.42) must hold for all variations ∂u_i, including zero, it is concluded that the non-trivial solution of the first variation contains the extremal displacement functions u_i which also satisfy the natural boundary condition as stated by eq. (7.32). Thus the necessary condition is obeyed.

7.3.1.4. LIMITATIONS

The foregoing shows that the variational approach to spatial elasticity problems is mathematically rigorous, inasmuch as the class of admissible strain energy functions leads to displacement fields out of which the extremal (7.39) minimizes the functional (7.36). This displacement field, however, is still a function of position and hence subject to integration, with the result that the non-trivial solution of eq. (7.42) cannot be transformed into a set of uncoupled force-deformation equations.

Thus it must be realized that elasticity problems for three-dimensional continua cannot be solved for the unknown displacement functions by using the variational approach, unless the uncoupling of the equations is made possible by a convenient matrix analysis.

7.3.2. STRAIN ENERGY FUNCTIONAL FOR AXISYMMETRIC CONTINUA

7.3.2.1. ADMISSIBLE FUNCTIONS

Viewing a continuum of cylindrical geometry, which is subjected to torsional and axisymmetric deformations and exposed to axisymmetric temperature fields, the variational approach to its elastic and thermoelastic analysis proceeds again from the total potential energy functional (7.36). The stresses, strains, displacements and thermal gradients are now, however, functions of the cylindrical coordinates x_i as shown in figures (6.5) and (6.6), and thus the volume dV of an infinitesimal ring element is linked to the varying radius r. Consequently, the volume is understood as the product r.ds to enable the inclusion of the radius into the processes of differentiation.

Substituting eqs. (6.29) to (6.33) into eq. (7.36), the class of admissible functions following definition (7.11) is obtained in the form

$$f = \tfrac{1}{2} \begin{bmatrix} u_{i,i} \\ u_{j,j} \\ \frac{u_i}{r} + u_{k,k} \\ u_{i,j}+u_{j,i} \\ u_{k,j}+u_{j,k} \\ u_{i,k}+u_{k,i}-\frac{u_k}{r} \end{bmatrix} \begin{bmatrix} 2G(u_{i,i}+\frac{\mu}{c}\dot{\varepsilon}) \\ 2G(u_{j,j}+\frac{\mu}{c}\dot{\varepsilon}) \\ 2G(\frac{u_i}{r}+u_{k,k}+\frac{\mu}{c}\dot{\varepsilon}) \\ G(u_{i,j}+u_{j,i}) \\ G(u_{k,j}+u_{j,k}) \\ G(u_{i,k}+u_{k,i}-\frac{u_k}{r}) \end{bmatrix} r - \begin{bmatrix} u_{i,i} \\ u_{j,j} \\ \frac{u_i}{r}+u_{k,k} \end{bmatrix} \begin{bmatrix} 2G\alpha\theta \\ 2G\alpha\theta \\ 2G\alpha\theta \end{bmatrix} .r - \begin{bmatrix} u_i \\ u_j \\ u_k \end{bmatrix} \begin{bmatrix} X_i \\ X_j \\ X_k \end{bmatrix} .r \qquad (7.43)$$

In constrast to eq. (7.37), where the spatial concept encourages the use of one subscripted expression for each of the sets of the direct and the shear strain components, the coupling of the circumferential strain component here precludes the employment of the subscript summation convention.

7.3.2.2 EULER EQUATION

The suitability criterion for the functional of general axisymmetric elasticity problems is furnished anew by the satisfaction of the Euler equation (7.12), and thus the following partial derivatives are needed

$$\frac{\partial f}{\partial u_i} = 2G \left(\frac{u_i}{r} + u_{k,k} + \frac{\mu}{c}\varepsilon - \alpha\theta - X_i.r\right)$$

$$\frac{\partial f}{\partial u_j} = 2G \left(- X_j.r\right)$$

$$\frac{\partial f}{\partial u_k} = 2G \left(- X_k.r\right)$$

$$\left(\frac{\partial f}{\partial u_{i,i}}\right)_{,i} = 2G \left(u_{i,i} + ru_{i,ii} + \frac{\mu}{c}\varepsilon + \frac{r\mu}{c}\varepsilon_{,i} - \alpha\theta - r\alpha\theta_{,i}\right)$$

$$\left(\frac{\partial f}{\partial u_{j,j}}\right)_{,j} = 2G \left(r.u_{j,jj} + \frac{r\mu}{c}\varepsilon_{,j} - r\alpha\theta_{,j}\right)$$

$$\left(\frac{\partial f}{\partial u_{k,k}}\right)_{,k} = 2G \left(u_{i,k} + ru_{k,kk} + \frac{r\mu}{c}\varepsilon_{,k} - r\alpha\theta_{,k}\right) \qquad (7.44)$$

$$\left(\frac{\partial f}{\partial u_{j,i}}\right)_{,i} = G \left(r.u_{i,ji} + u_{i,j} + ru_{j,ii} + u_{j,i}\right)$$

$$\left(\frac{\partial f}{\partial u_{k,j}}\right)_{,j} = G \left(r.u_{k,jj} + r.u_{j,kj}\right)$$

$$\left(\frac{\partial f}{\partial u_{i,k}}\right)_{,k} = G \left(r.u_{i,kk} + r.u_{k,ik} - u_{k,k}\right)$$

$$\left(\frac{\partial f}{\partial u_{k,i}}\right)_{,i} = G \left(r.u_{i,ki} + u_{i,k} + r.u_{k,ii} + u_{k,i} - u_{k,i}\right)$$

$$\left(\frac{\partial f}{\partial u_{i,j}}\right)_{,j} = G(r.u_{i,jj} + r.u_{j,ij})$$

$$\left(\frac{\partial f}{\partial u_{j,k}}\right)_{,k} = G(r.u_{j,kk} + r.u_{k,jk})$$

The directions are denoted by the first subscript to the displacement functions and consequently the Euler equation can be established for each direction of the axisymmetric continuum by considering the relevant derivatives. Dividing all terms by the radius r, the expanded compatibility equations of section 6.3.4. are re-established.

Thus, following the mathematical steps performed between eqs. (6.33) and (6.34), the potential deformation equations (6.34) which constitute the natural boundary conditions for axisymmetric continua, subjected to multiple loading cases, are identically satisfied

$$\begin{aligned} G(\Delta u_i + \frac{3u_{k,k}}{r} - \frac{u_i}{r^2} + \frac{1}{c}\varepsilon_{,i} - 2\alpha\theta_{,i}) + X_i &= 0 \\ G(\Delta u_j + \qquad\qquad + \frac{1}{c}\varepsilon_{,j} - 2\alpha\theta_{,j}) + X_j &= 0 \qquad (7.45) \\ G(\Delta u_k + \frac{2u_{i,k}}{r} + \frac{u_{k,i}}{r} + \frac{1}{c}\varepsilon_{,k} - 2\alpha\theta_{,k}) + X_k &= 0 \end{aligned}$$

As a result, it can be stated that the identity of eqs.(6.34) and (7.45) proves the suitability of the strain energy functional (7.36) for the variational analysis of axisymmetric continua.

7.3.2.3. DIFFERENTIAL CALCULUS

Once it is conceded that the displacements u_i in eqs. (7.40) now describe fields of cylindrical geometry and that the sets $\underline{a}$, $\underline{b}$ and $\underline{d}$ are therefore of some different kind, it it apparent that eqs. (7.40) and the vanishing of the first variation (7.41) give rise to the following non-trivial solution

$$\int (\underline{b}^t \underline{a}^t \underline{d}\ \underline{a}\ \underline{b}\ u_i - \underline{b}^t \underline{a}^t \underline{d}\ \alpha\theta - X_i)\ rds = 0 \qquad (7.46)$$

Eq. (7.46) satisfies the necessary condition imposed onto the validity of the functional (7.36) in the axisymmetric

analysis and therefore could be used as the basic governing equation for the evaluation of continuous displacement fields in corresponding elastic continua.

7.3.2.4. LIMITATIONS

Unfortunately, the displacement field u_i, the sets of strain operator functions ab and the set of space-dependent stiffness coefficients d of eqs. (7.46) are highly interdependent, as already observed in eq. (7.42).

As far as the mathematical solubility is concerned, cylindrical geometry does not facilitate the analysis of corresponding elastic continua, and once again it is experienced that the variational approach in its analytic formulation does indicate new possibilities, but is incapable of overcoming the interdependence existing in the force-deformation equation.

7.3.3. HEAT CONDUCTION FUNCTIONAL FOR THREE-DIMENSIONAL CONTINUA

7.3.3.1. ADMISSIBLE FUNCTIONS

The functional equivalent to the partial differential equation (7.35) of the heat conduction within a three-dimensional continuum is given by the following integral

$$I = \int (\tfrac{1}{2}(k_i(\theta_{,i})^2 + k_j(\theta_{,j})^2 + k_k(\theta_{,k})^2) - (q + o\theta - \rho c\theta_{,t})\theta)\ dV \tag{7.47}$$

Using subscript summation convention, the class of admissible functions may therefore be written in a concise form as

$$f = \tfrac{1}{2} \sum_{i}^{3} k_i\ (\theta_{,i})^2 - (q + o\theta - \rho c\theta_{,t}) \tag{7.48}$$

where for wider applicability the conductivity coefficients are not yet assumed to be equal.

7.3.3.2. EULER EQUATION

Since the functional (7.47) has not been derived previously, it is particularly necessary to investigate whether its suitability criterion is satisfied. In the course of producing the Euler equation (7.12), the following derivatives of the class of admissible functions (7.48) are generated

$$\frac{\partial f}{\partial \theta} = - (q + o\theta - \rho c\theta_{,t}) \tag{7.49}$$

$$(\frac{\partial f}{\partial \theta_{,i}})_{,i} = k_i\theta_{,ii} \quad (\frac{\partial f}{\partial \theta_{,j}})_{,j} = k_j\theta_{,jj} \quad (\frac{\partial f}{\partial \theta_{,k}})_{,k} = k_k\theta_{,kk}$$

Keeping in mind that the terms of heat generation, heat storage and heat loss couple the effects of the temperature distribution into the three directions of the space, only one general Euler equations is available

$$k_i\theta_{,ii} + k_j\theta_{,jj} + k_k\theta_{,kk} + q + o\theta = \rho c\theta_{,t} \tag{7.50}$$

With the validity of ass. (6.1.2.8) eq. (7.50) may be conveniently reduced to

$$k\Delta\theta + q + o\theta = \rho c\theta_{,t} \tag{7.51}$$

where the operator is given by def. (6.1.4.4)

As eqs. (7.51) and (7.35) are identical, it is shown that the functional (7.47) furnishes an absolute extreme value to the temperature fields and is therefore suitable for the analysis of spatial heat conduction problems.

7.3.3.3. DIFFERENTIAL CALCULUS

Substituting an arbitrary admissible function which now is given by $\theta + \beta\partial\theta$ into the functional (7.47), the integral to be minimized reads

$$I = \int \left| \tfrac{1}{2} \sum_{i}^{3} (k_i(\theta + \beta\partial\theta)_{,i})^2 - (q + o\theta - \rho c\theta_{,t})(\theta + \beta\partial\theta) \right| dV \tag{7.52}$$

Employing the differential calculus, the first variation is equivalent to minimizing the heat conduction functional (7.52) under the preservation of the thermal energy, permitting only the temperature field to vary

$$\partial I = \int \sum_i^3 k_i (\theta_{,i} + O.\partial\theta_{,i})\partial(\theta_{,i} + O.\partial\theta_{,i}) - (q + o\theta - \rho c\theta_{,t})\partial(\theta + O.\partial\theta) dV = O \tag{7.53}$$

Substituting eqs. (7.49) into eq. (7.53), the following integral is formed

$$\int \Big| \sum_i^3 \left(\frac{\partial f}{\partial \theta_{,i}}\right) \partial\theta_{,i} + \frac{\partial f}{\partial \theta} \partial\theta \Big| dV = O \tag{7.54}$$

Eq. (7.54) may be transformed by integrating by parts. For this purpose the following differential operation is employed

$$\left(\partial\theta \frac{\partial f}{\partial \theta_{,i}}\right)_{,i} = (\partial\theta)_{,i} \frac{\partial f}{\partial \theta_{,i}} + \partial\theta \left(\frac{\partial f}{\partial \theta_{,i}}\right)_{,i}$$

After rearranging, thus

$$\partial\theta_{,i} \frac{\partial f}{\partial \theta_{,i}} = \left(\partial\theta \frac{\partial f}{\partial \theta_{,i}}\right)_{,i} - \partial\theta \left(\frac{\partial f}{\partial \theta_{,i}}\right)_{,i} \tag{7.55}$$

Substituting eqs. (7.55) into eq. (7.54), the first variation of the heat conduction functional takes the form

$$\int \Big| \sum_i^3 \left(\left(\partial\theta \frac{\partial f}{\partial \theta_{,i}}\right)_{,i} - \partial\theta \left(\frac{\partial f}{\partial \theta_{,i}}\right)_{,i} + \frac{\partial f}{\partial \theta} \partial\theta \right| dV = O \tag{7.56}$$

To proceed, it is necessary to employ the following theorem

$$\int_{x_a}^{x_b} (\Theta(x))_{,x} = \Theta(x) \Big|_{x_a}^{x_b} \qquad \text{---} \quad 7\text{-}57$$

where x_a and x_b designate the lower and the upper limit of the domain, respectively.

Subjecting the first term of eq. (7.56) to the rule of theorem (7.57), the following integro-differential equation is produced

$$\sum_{i}^{3} (\partial\theta(\frac{\partial f}{\partial \theta_{,i}})) \Big|_{x_{ai}}^{x_{bi}} - \partial\theta\int(\sum_{i}^{3}(\frac{\partial f}{\partial \theta_{,i}})_{,i} - \frac{\partial f}{\partial \theta}) \, dV = 0 \tag{7.58}$$

Fortunately, the calculus of variation as expounded in section 7.1.4. requires the admissible variation $\partial\theta$ to become zero along the spatial limits. Consequently, the first term of eq. (7.58) vanishes, with the result that the non-trivial solution of the first variation reduces to the simple form

$$\sum_{i}^{3} (\frac{\partial f}{\partial \theta_{,i}})_{,i} - \frac{\partial f}{\partial \theta} = 0 \tag{7.59}$$

Re-substituting for expressions (7.49) and assuming the existence of an isotropic coefficient of thermal conductivity, thus

$$k\Delta\theta + q + o\theta = \rho c\theta_{,t} \tag{7.60}$$

This is the elliptic partial differential equation in conformity with which the heat propagates through a spatial continuum. It is identical with eqs. (7.35) and (7.51) and therefore expresses the satisfaction of the natural boundary conditions.

7.3.3.4. SPECIAL CASES

The importance of the natural boundary conditions lies in the fact that, by adding or subtracting suitable terms to or from a functional, it is possible to alter the boundary conditions without violating the Euler equation.

Dropping those terms in the first of the derivatives (7.49) which represent the heat generation and the heat loss, the three-dimensional heat conduction problem reduces to that of the corresponding transient temperature distribution

$$k\Delta\theta = \rho c\theta_{,t} \tag{7.61}$$

If, finally, the time-dependent temperature distribution due to the heat retaining capacity of the material is eliminated, the first of the derivatives (7.49) becomes zero. Physically, this means that, by skipping the history

of the transient stages, the final steady state temperature distribution is arrived at

$$k\Delta\theta = 0 \tag{7.62}$$

Considering a constant coefficient k throughout the continuum, eq. (7.62) satisfies def. (6.1.4.4) identically.

7.3.3.5. LIMITATIONS

The necessary condition as stated by the Euler equation demands that the temperature θ in the heat loss term and the temperature gradient with respect to time $\theta_{,t}$ are invariant within a given time interval. Consequently, the heat conduction problem in its variational formulation can only be solved in an iterative process.

Furthermore, it must be realized that the temperature field in eq. (7.54) is space-dependent and thus subject to integration over the region. Even with the temperature and the temperature gradient in the instationary terms being invariant, the problem of heat conduction in a three-dimensional continuum remains insoluble, unless the uncoupling of the temperature function from the conductivity properties in eq. (7.53) or (7.54) is made possible by the adoption of a suitable matrix method.

7.3.4. HEAT CONDUCTION FUNCTIONAL FOR AXISYMMETRIC CONTINUA

7.3.4.1. ADMISSIBLE FUNCTIONS

Provided that Euler's equation and the natural boundary conditions are obeyed, the boundary value problem of the heat conduction is equivalent to a variational problem also for cylindrical geometry. Considering, therefore, an axisymmetric continuum, a convenient functional for the problem of investigating transient, non-axisymmetric temperature distributions due to heat propagation is

$$I = \int \left(r \sum_{i}^{3} (k_i \theta_{,i})^2 - 2r(q + o\dot{\theta} - \rho c \theta_{,t})\theta \right) ds \tag{7.63}$$

where in contrast to eq. (7.48) the subscript summation is now carried out over the three directions of the cylindrical coordinate system.

The class of admissible functions immediately becomes

$$f = r\sum_{i}^{3}(k_i\theta_{,i})^2 - 2r(q + o\theta - \rho c\theta_{,t}) \tag{7.64}$$

where, of course, the subscript i=1,2,3 are identical with the subcripts i,j,k of the unit basic triad in the cylindrical space.

7.3.4.2. EULER EQUATION

The partial derivatives required to establish the Euler equation (7.12) are readily found as

$$\begin{aligned}
\frac{\partial f}{\partial \theta} &= -2r(q + o\theta - \rho c\theta_{,t}) \\
(\frac{\partial f}{\partial \theta_{,i}})_{,i} &= 2rk_i\theta_{,ii} + 2k_i\theta_{,i} \\
(\frac{\partial f}{\partial \theta_{,i}})_{,j} &= 2rk_j\theta_{,jj} \\
(\frac{\partial f}{\partial \theta_{,k}})_{,k} &= 2rk_k\theta_{,kk}
\end{aligned} \tag{7.65}$$

Substitution of eqs. (7.65) into eq. (7.12) leads to the partial different equation

$$rk_i\theta_{,ii} + k_i\theta_{,i} + rk_j\theta_{,jj} + rk_k\theta_{,kk} + r(q + o\theta - \rho c\theta_{,t}) \tag{7.66}$$

Using ass. (6.1.2.6) and def. (6.1.4.5) eq. (7.66) identically satisfies the natural boundary conditions of the non-axisymmetric heat conduction problem in an axisymmetric continuum

$$k\Delta\theta + q + o\theta = \rho c\theta_{,t} \tag{7.67}$$

Thus the criterion for the suitability of the functional (7.63) is fulfilled.

7.3.4.3. DIFFERENTIAL CALCULUS

In proceeding to prove that under the conditions discussed in section 7.1.4. the first variation of the functional vanishes, an arbitrary admissible function of the kind $\theta + \beta\partial\theta$ is substituted into eq. (7.63)

$$I = \int (r\sum_{i}^{3} k_i(\theta_{,i} + \beta\partial\theta_{,i})^2 - 2r(q + o\theta - \rho c\theta_{,t})(\theta + \beta\partial\theta_{,i}))ds \qquad (7.68)$$

Analogous to eq. (7.53) the differential calculus now creates

$$I = \int (2\sum_{i}^{3} rk_i\theta_{,i}\partial\theta_{,i} - 2r(q + o\theta - \rho c\theta_{,t})\partial\theta)ds = 0 \qquad (7.69)$$

Using the derivatives (7.65), the first variation (7.69) may be transformed to

$$\int (\sum_{i}^{3} \frac{\partial f}{\partial\theta_{,i}} \partial\theta_{,i} + \frac{\partial f}{\partial\theta}\partial\theta)\, ds = 0 \qquad (7.70)$$

Since eq. (7.70) is the direct analogue to eq. (7.54) the mathematical steps performed between eqs. (7.54) and (7.60) may be repeated to yield

$$k\Delta\theta + q + o\theta = \rho c\theta_{,t} \qquad (7.71)$$

This is the governing elliptic partial differential equation of the heat propagation in an axisymmetric continuum and thus the necessary condition is satisfied.

7.3.4.4. SPECIAL CASES

If the problem of a transient, non-axisymmetric temperature field in an axisymmetric continuum is reduced to that of an axisymmetric field in the same body, the Laplace's operator does no longer comply with def. (6.1.4.5) but with def. (6.1.4.6).

Degenerating the problem of heat conduction to those of the transient and the steady state temperature distribution, respectively, eqs. (7.61) and (7.62) can in form be reproduced. The operators, of course, follow depending on the geometry of

the cylindrical temperature field now either def. (6.1.4.5) or (6.1.4.6).

7.3.4.5. LIMITATIONS

Since the variational approach to the analysis of temperature distributions in axisymmetric continua is incapable of uncoupling the temperature field from the conductivity properties, the corresponding thermal field problem remains insoluble, as closed mathematical solutions are available only for simple regular shapes.

7.4. CONCLUSIONS

Eqs. (7.42), (7.46), (7.51) and (7.71) contain the extremal displacement and temperature fields as inseparable functions of position. The situation expressed in these governing equation therefore would have constituted a genuine state of scientific collapse, if structural and thermal analyses were confined to analytic approaches.

The variational analysis does include the small displacement theory as a special case - and similarly the heat conduction theory - but it fails to abolish the limitations brought about by the impossibility of the displacement field to take prescribed values along the boundary.

Since the variational theory proves incapable of surmounting the difficulties already encountered in its implied special cases, methods in the design of continuous structures which are based on closed mathematical formulations have reached the ultimate state of development. New possibilities, though, are offered by the variational approach in conjunction with the implementation of appropriate matrix methods.

CHAPTER VIII

FINITE ELEMENT MATRIX ANALYSIS OF ELASTIC AXISYMMETRIC CONTINUA

8.1. INTRODUCTION

8.1.1. OBJECTIVE

The real contribution to the structural analysis made by the variational approach expounded in Chapter VII is that, by using finite element displacement techniques, the first variational of the strain energy functional is capable of being solved numerically.

Realizing the crucial importance of the overall structural stiffness matrix in the establishment of the global force-deformation equations in numerical form, the aim is to link the deformations at discrete nodal points of a coordinate system to the generalized global conjugate forces. The finite element matrix displacement method thus develops from an assemblage of finite elements to each of which a given strain distribution is prescribed in terms of generalized nodal displacements.

Consequently, the overall displacement field is represented by values pertaining to discrete nodal points of a chosen finite element mesh ; interpolation being the tool for the obtainment of further information within the elements. The applied forces are defined as corresponding to the nodal displacements and thus are concentrated at the nodal points. Although acting in the same sense, components of conjugate sets of forces and displacements are by origin totally unconnected.

Considering two discrete points of a continuous structure with one degree of freedom each, their mutual stiffness coefficient may be defined by the force required at one point to produce a unit displacement at the other. Accordingly, the stiffness matrix of an element contains a number of coefficients which is equal to the square of its degree of freedom, that is, of its number of independent displacement components. Owing to the validity of the reciprocal theorem, this matrix is symmetric for linearly elastic continua.

Superimposing all element stiffnesses in pattern prescribed by the numbering of the global nodal points, the global stiffness matrix is assembled. Once the set of simultaneous linear force-deformation equations is solved for the nodal displacements, resubstitution commences to evaluate the system's solution at all local points.

Considering a solid body of revolution, advantage can be taken of the axisymmetric state of stress and strain in its definition, as arrived at in Chapter VI. It reduces the structural analysis problem of the body to one of two degrees of freedom, thus requiring only a two-dimensional finite element mesh.

8.1.2. PROCESSIONAL STEPS

In the following the classical and the natural deformation modes concept in the finite element matrix displacement method for the axisymmetric stress analysis problem are developed. Before, however, going into the details of the two different global matrix formulations, it is intended to demonstrate that, although each deformation modes concept is of distinct nature, the processional steps, the algorithms and thus the required computer programming routines are similar to a large extent.

Irrespective of the type of geometry considered, with regard to the structure and its elements, two phases of the finite element analysis can be distinguished : the gathering of facts from the given and chosen physical, mechanical, geometrical and environmental conditions and the dissemination of information by resubstitution; the turning point is reached once the triangulation of the global stiffness matrix has arrived at the last linear equation, which then contains only one unknown displacement, viz. t h e solution of the system.

The general steps performed in any finite element structural analysis may be loosely described as follows :

(1) Subdivision of the structure into finite elements using nodal point meshes to obtain a geometrical idealization and a physical approximation

(2) Formulation of local displacements in terms of the unknown generalized nodal point displacements using interpolating functions to enable the description of the displacement field throughout the structure

(3) Formation of local strain-displacement relations to ensure the existence of strains that are kinematically compatible with the generalized displacements

(4) Constitution of local stress-strain relationships to achieve a true representation of the elements' varying physical properties

(5) Employment of the principle of minimum potential energy to guarantee statical equilibrium while kinematical compatibility is ensured

(6) Minimization of the strain energy functional with respect to the generalized displacements to define the local stiffness matrices and to prepare the ground for the establishment of the global force-deformation equations

(7) Introduction of connectivity matrices to identify local with global nodal points and to render feasible the superposition of the local stiffness matrices when synthesizing the global stiffness matrix as to link all forces and deformations

(8) Triangulation of the global stiffness matrix until the last equation with only one unknown displacement component is declared, to procure the solution of the structural problem

(9) Resubstitution of the solution and subsequent substitution of each newly acquired displacement solution, until all nodal point values of the overall displacement field are determined

(10) Resubstitution of the displacements into the local strain-displacement relations by inverting the connectivity matrices to obtain the strain distribution within each element and hence throughout the structure

(11) Resubstitution of the strains into the local stress-strain relationships to evaluate the stress components and the

angle of the major principle stress component at any point of the structure

(12) Assessment of the numerical solutions by first interpolating the displacement, strain and stress fields at points of a superimposed evenly gridded mesh and by subsequently displaying them as either contour fields or isometric surfaces

8.2. THE CLASSICAL DEFORMATION MODES CONCEPT

8.2.1. THE TRIAX 3 ELEMENT

The TRIAX 3 element is commonly known as the triangular sectioned ring element that may be generated by rotating a simple triangular membrane element with three nodal points about the relevant axis of revolution. Its cross-sectional geometry and unit displacement components are shown in figure (8.1). In special cases, the angle of rotation included between its two faces can be arbitrary, as long as the state of stress and strain are correspondingly defined.

The element has six degrees of freedom and thus assumes linear interpolating functions for the displacements, so as to enable the expression of the displacement components in terms of the nodal deformation anywhere within the element. Since the strain vector involves first derivatives of the displacements, the local strain and stress fields are of constant values.

8.2.2. CLASSICAL DEFORMATION MODES

The classical way of measuring strain, is to introduce the cartesian strain vector, which involves differentiations of the displacements with respect to the directions of the cartesian coordinate system. For axisymmetric geometry, it leads to three direct stresses and a shearing contribution that couples the axial with the radial component.

Considering axisymmetric elastic continua under axisymmetric loading, the cartesian strain vector is defined by eqs. (6.29) and eq. (6.29a).

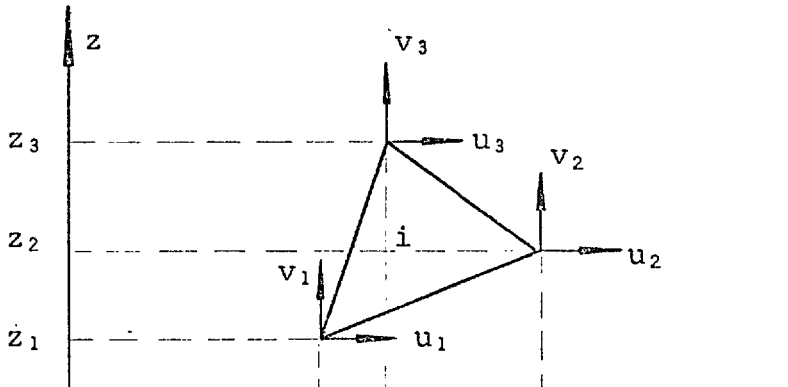


Fig. 8.1. Cross-sectional geometry and unit displacement components for the TRIAX 3 element

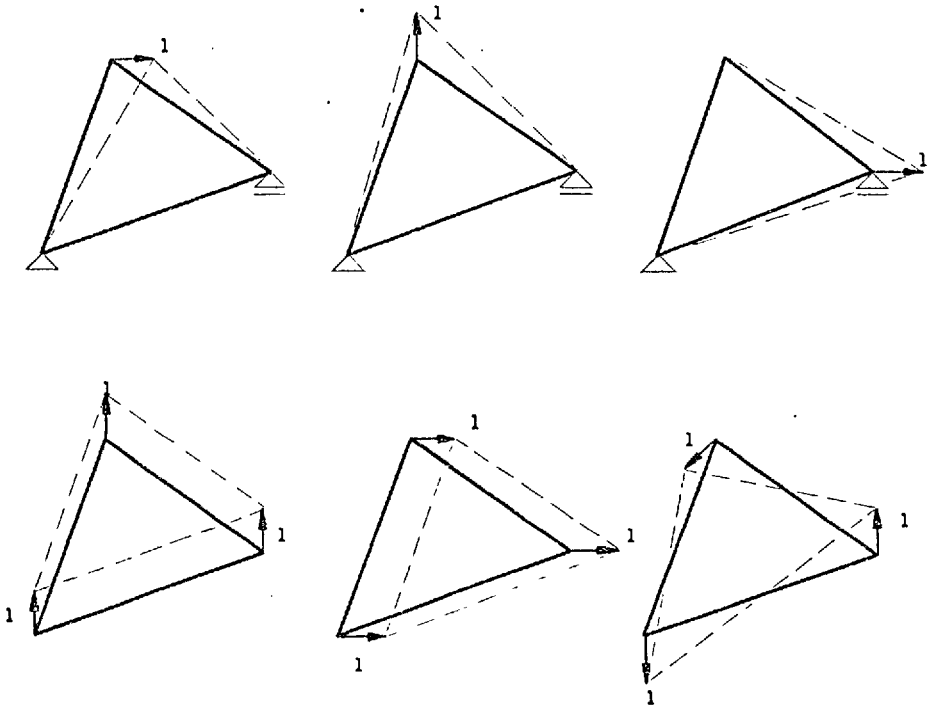


Fig. 8.2. Mode shapes for the elastic and rigid body displacements of the TRIAX 3 element

The simple triangular-sectioned ring element with six unknown displacement components has three rigid body motions. It thus requires the design of three classical deformation modes; the only condition satisfied by each is the mode forces are self-equilibrating, in order not to do any work on the rigid body displacements and the other modes, and they are of a magnitude which produces a unit amount of virtual work. The mode shapes and the conjugate sets of forces are shown in figure (8.2), where the upper row illustrate the deformation modes and the lower the rigid body motions.

8.2.3. GEOMETRICAL AND ANALYTICAL ADVANTAGES

Whatever is the geometry, the subdivision of a solid continuum into an assemblage of triangular-sectioned elements has the great advantage that the shape of these elements fits easily into any topological configuration and that for adequate representation of what is happening locally within the structure corresponding geometrical adjustment is possible.

If a finer idealization in a region of steep gradients of stress or strain fields is required, the elements can either be drawn smaller in the original mesh, or additional elements can be produced by subsequent division of local elements. If the gradients are expected to be less severe, fewer elements will suffice. Rectangular- and trapezoidal elements can go smaller too, but their size is controlled by the smallest element and the introduction of additional elements is not possible.

Analytically and computationally, the main advantages of the classical deformation modes concept lie in the simplicity and the clarity of the implemented method of approach.

8.2.4. STIFFNESS MATRIX FOR THE TRIAX 3 ELEMENT

After an axisymmetric solid continuum is subdivided into a finite number of discrete triangular-sectioned ring elements, two interpolating linear displacement functions are assumed within each element

$$v_r(r,z) = q_1 + (r - r_1)q_2 + (Z - Z_1)q_3$$

$$v_z(r,z) = q_4 + (r - r_1)q_5 + (Z - Z_1)q_6 \qquad (8.1)$$

The six parameters q correspond to the six unknown displacement components of the TRIAX 3 element to be evaluated. As ratios of the radii at the various nodes of an element tend to unity for axisymmetric geometries of large diameters, the analysis is more accurate if the assumed polynomials are functions of the local positional differences $(r-r_1)$ and $(z-z_1)$.

Alternatively, functions (8.1) can take the matrix form

$$v\ (r,z) = \underline{M}\ \underline{Q}^i \qquad (8.2)$$

where $\underline{M}$ is a (6x6) operator and $\underline{Q}^i$ is the local (6x1) parameter vector.

The expanded forms of all operators and matrices occurring in the present chapter are listed in Appendix A4; thus $\underline{M}$ and $\underline{Q}^i$ are given by eqs. (A4.1) and (A4.2), respectively.

In applying the finite element method, the approximate displacement functions (8.2) are evaluated at the nodal points $j = 1,2,3$ of each element $i = 1,2,...n$. It should be noted that in the structural analysis of an axisymmetric elastic continuum using ring elements a nodal displacement, strain or stress value represents a combined effect of the deformation or mechanical action instantly existing along the whole circumference of the circle forming the element node.

Substituting the evaluated inversion of eq. (8.2) into eq. (8.2) again, there is

$$\underline{Q}^i = (\underline{M}^i)^{-1}\ \underline{u}^i \qquad (8.3)$$

where $\underline{M}^i$ is a matrix of constant coefficients and thus distinct from the operator $\underline{M}$. $\underline{M}^i$ is given by eq. (A4.3) and $\underline{u}^i$ by eq. (A4.4).

Introducing $\underline{B}^i$ as $(\underline{M}^i)^{-1}$, the local variable displacement field becomes

$$v(r,z) = \underline{M}\ \underline{B}^i\underline{u}^i \qquad (8.4)$$

where $\underline{B}^i$ is a (6x6) matrix expanded in eq. (A4.5).

In order to relate the local displacement components to the generalized displacements of the assembled structure, connectivity matrices of the following kind are interposed.

$$\underline{u}^i = \underline{C}^i \underline{u} \tag{8.5}$$

where $\underline{C}^i$ is a (6xk) Boolean coincidence matrix and $\underline{u}$ is the global displacement vector of the size (kx1); k being the total number of the overall displacement components.

Substituting eq. (8.5) into eq. (8.4) thus

$$v(r,z) = \underline{M}\ \underline{B}^i \underline{C}^i \underline{u} \tag{8.6}$$

In the case of axisymmetric deformation, four components of strain must be considered. Proceeding from eqs. (6.29), (6.29a) and (8.2), the strain vector may be defined by

$$\varepsilon(r,z) = \underline{d\ M}\ \underline{Q}^i \tag{8.7}$$

where $\underline{d\ M}$ is a (4x6) operator involving operations on the displacement functions according to the definitions of the four strain components ; its collocation is shown in eq.(A4.6)

Analogous to eq. (8.6), thus

$$\varepsilon(r,z) = \underline{d\ M}\ \underline{B}^i \underline{C}^i \underline{u} \tag{8.8}$$

The hoop strain varies with the radius, while the other components are constant within each TRIAX 3 element, since first derivatives of linear displacement functions are involved. If the local operator $\underline{d\ M}$ is evaluated at the centroid of the element, a matrix $\underline{A}^i$ of constant coefficients is formed. For a prescribed invariant loading case, the strain vector then comprises element-wise constant components accordingly, eq. (8.8) becomes

$$\underline{\varepsilon}^i = \underline{A}^i \underline{B}^i \underline{C}^i \underline{u} \tag{8.9}$$

The (4x6) matrix $\underline{A}^i$ and the (4x6) matrix product $\underline{A}^i \underline{B}^i$ are defined by eqs. (A4.7) and (A4.8), while the

formulation of some coefficients of the latter are simplified in eqs. (A4.9) and (A8.10).

With the absence of torsion, the circumferential displacement component and all subsequent differentiations vanish; the internal strain components in terms of the stresses are thus constituted by the first four of eqs. (6.33), provided that the third is reduced by $u_{k,k}$ and no thermally induced strains exist. The complemental definition to eq. (8.9) reads

$$\underline{\varepsilon}^i = \underline{F}^i \underline{\sigma}^i \tag{8.10}$$

where $\underline{F}^i$ is the (4x4) material flexibility matrix, the coefficients of which are arranged in eq. (A.11).

The locally applicable elastic law is obtained by inverting eq. (8.10)

$$\underline{\sigma}^i = \underline{D}^i \underline{\varepsilon}^i \tag{8.11}$$

where $\underline{D}^i$ is the (4x4) elasticity or, better, the material stiffness matrix which is identical with the inverse of the material flexibility matrix and set up in eq. (A4.12).

Substituting first eq. (8.11) and then eq. (8.9) into the first term of the total potential energy functional (7.26), thus

$$\Delta I^i = \tfrac{1}{2}\underline{u}^t \int (\underline{A}^i \underline{B}^i \underline{C}^i)^t \underline{D}^i \underline{A}^i \underline{B}^i \underline{C}^i \mathrm{rds}.\underline{u} \tag{8.12}$$

where for the purpose of admissible matrix multiplication the first set in the symmetric matrix expression must appear in its transposed form, as indicated by the superscript t.

Applying the first variation to the partial functional (8.12) following eqs. (7.41) and (7.42), the element stiffness matrix emerges as a local multiplier to the generalized displacement vector

$$\underline{K}^i.\underline{u} = \int (\underline{A}^i \underline{B}^i \underline{C}^i)^t \underline{D}^i \underline{A}^i \underline{B}^i \underline{C}^i \mathrm{rds}.\underline{u} \tag{8.13}$$

In contrast to eq. (7.46), where the local stiffness constitutes a set of variable stiffness coefficients, the (6x6) element stiffness matrix now accommodates numerical values which

are mathematically uncoupled from the conjugate displacement components. The expressions for the stiffness coefficients are carefully derived in eqs. (A.13) to (A4.15).

8.2.5. LOAD VECTORS FOR THE TRIAX 3 ELEMENT

Proceeding from the total potential energy functional (7.26), it is realized that its first term is responsible for the construction of the stiffness matrix, whereas the following four terms latently contain load vectors.

Considering thermally induced stresses, the second term of eq. (7.26) must be expanded. Concerning this, the set of variable material stiffness coefficients $\underline{d}$ in the third of eqs. (7.40) is replaced by the local material stiffness matrix $\underline{D}^i$ of eq. (8.11) to yield the stress-strain relationship

$$\underline{\sigma}_t^{\,i} = \underline{D}^i \underline{\varepsilon}_t^{\,i} \tag{8.14}$$

where the first three, the direct components of the (4x1) thermal strain vector are given by $_{\alpha}\theta^i$ and the shearing contribution is zero; θ^i represents the temperature value instantly existing at the centroid of the element.

With eq. (8.9), the contribution from the local thermal expansion to the total potential energy functional (7.26) thus becomes

$$\Delta I = \int (\underline{A}^i \underline{B}^i \underline{C}^i)^t \underline{D}^i \underline{\varepsilon}_t^{\,i} \; rds.\underline{u} \tag{8.15}$$

Employing the variational calculus with the generalized displacement field $\underline{u}$ being the varied function, the (6x1) thermal load vector for an individual element appears as the non-trivial solution

$$\underline{P}_t^i = \int (\underline{A}^i \underline{B}^i \underline{C}^i)^t \underline{D}^i \underline{\varepsilon}_t^{\,i} \; rds \tag{8.16}$$

As discussed in section 7.2.4., the initial elastic shortening of the prestressing tendons causes a loss to occur in the prestressing forces, implying the necessity for a repeated analysis, if the third term of the functional (7.26)

is considered. Accordingly, a successive iteration is performed ; the imposition of the local prestressing strains during each of the computational steps manifests itself in the (6x1) force vector

$$\underline{P}_p^i = \int (\underline{A}^i \underline{B}^i \underline{C}^i)^t \, \underline{D}^i \underline{\varepsilon}_p^i r ds \qquad (8.17)$$

where $\underline{\varepsilon}_p^i$ is the (4x1) centroidal strain vector of the element having the instant radial, axial and circumferential components ε_{pr}, ε_{pz}, ε_{pt} and a zero shearing contribution.

Imagining straight and circular ungrouted tendons for either planar and the tangential direction, respectively, corrective terms must amend the corresponding diagonal coefficients of the stiffness matrices of the elements adjacent to the anchorage points. The magnitudes of these amounts to $E_s F_s/l$ and $2 E_s F_s/r_m$, where l measures the length of the vertical and radial tendons, $2\pi r_m$ describes the length of a hoop tendon and E_s and F_s constitute the modulus of elasticity and the relevant cross-sectional areas of the tendons.

If the continuum possesses a vertical axis of revolution, also the action of body pressure due to gravity can be accounted for. One of the advantageous approximation of stress resultants directly to the nodal points, where they act on the conjugate displacement components. The integration over the varying displacement field, as expressed by eq. (8.6), is thus circumvented. Instead, the displacement vector (8.5) and a prescribed body force vector are substituted into the fourth term of the functional (7.26).

Assuming the existence of a constant density throughout the element, each of the vertical nodal force components due to self-weight are defined as one third of the body pressure resultant. After variation thus

$$\underline{P}_x^i = \int 1/3 \, \underline{C}^{it} \underline{X}^i \rho r ds \qquad (8.18)$$

where $\underline{X}^i$ is a (6x1) vector that has zero entries for the radial components in the first three locations and unit entries for the axial ones in the fourth to the sixth location.

Similarly, external nodal forces due to prescribed surface stresses can be considered. The concentrated nodal force components are expressed in terms of the distributed surface loads by introducing a local surface normal vector, of which the coefficients are direction cosines of the stress resultant. If loads are uniformly distributed along one element side, equal contributions go to each of the neighbouring surface nodes. Analogous to eq. (8.18), thus

$$\underline{P}_e^i = \int_S \tfrac{1}{2}\underline{C}^{it}\underline{N}^i\sigma_s \, ds \qquad (8.19)$$

where $\underline{N}^i$ is a (6x1) vector which selects the element surface nodes and allocates the relevant direction cosines to them; it has a zero entry for the internal node. S is the area of the element's circumferential strip which is exposed to the surface traction.

8.2.6. CLASSICAL FORCE-DEFORMATION EQUATIONS

In Chapter VII the coupled force-deformation equations of the elastically deformed continuum are arrived at by deduction ; although still insoluble then, they are symbolically defined by the non-trivial solution of the functional's first variation.

In the preceding sections8.2.4. and 8.2.5., contrarily, it shows to be convenient to proceed inductively, as the preparation of the ground for programming the element stiffness and the various element load vectors into computer language favours a separate construction of each matrix expression.

It is obvious that the first term of the functional (7.26), as the primitive function of the stiffness matrix, becomes physically meaningful only in conjunction with the subsequent term, which represent the primitive functions of the load vectors. Consequently, it is intended to return to the holistic approach by superimposing the contributions from all individual TRIAX 3 elements to the total potential energy functional (7.26); due to the functional's numerical nature, its first variation then yields a set of uncoupled linear force-deformation equations.

The approximate volume of a triangular-sectioned ring element is given by $2\Pi A^i r_m^i$, where A^i is its cross-sectional area and r_m^i the centroidal radius. Composing then the functional's first variation by first adding the terms (8.13) and (8.16) to (8.19) and by subseqently summing over the total number of finite elements and equating to zero, the axisymmetric elastic analysis in its classical finite element form is established

$$\sum_{i=1}^{n} (2\Pi A^i r_m^i (\underline{A}^i\underline{B}^i\underline{C}^i)^t \underline{D}^i \underline{A}^i\underline{B}^i\underline{C}^i) . \underline{u} =$$

$$\sum_{i=1}^{n} (2\Pi A^i r_m^i ((\underline{A}^i\underline{B}^i\underline{C}^i)^t \underline{D}^i \underline{\varepsilon}_t^i + (\underline{A}^i\underline{B}^i\underline{C}^i)^t \underline{D}^i \underline{\varepsilon}_p^i + \underline{C}^{it}\underline{X}^i\rho/3 + \underline{C}^{it}\underline{N}^i\sigma_s/2) \tag{8.20}$$

Considering unit displacements $\underline{u}$, the terms in eq. (8.20) may be identified as the global stiffness matrix and the global vectors for the thermal loads, the prestress, the gravity loads and the external forces, respectively. Thus, eq. (8.20) may take the global matrix form

$$\underline{K} \cdot \underline{u} = \underline{P}_t + \underline{P}_p + \underline{P}_x + \underline{P}_e \tag{8.21}$$

where $\underline{K}$ initially is a (kxk) matrix and all vectors are of the size (kxl).

8.3. THE NATURAL DEFORMATION MODES CONCEPT

8.3.1. THE TRIAX 6 ELEMENT

The TRIAX 6 element is usually understood as the triangular-sectional ring element, which may be generated by rotating a triangular membrane element with six nodal points fully about the relevant axis of revolution; geometrically, it evolves from the TRIAX 3 element by the introduction of three further nodes at the midpoints of the triangle's sides. The cross-sectional subdivision and the allocation of the unit cartesian displacement components is shown in figure (8.3).

The axisymmetric state of stress may be expressed by the superposition of a two dimensional state of stress in an axial cross-sectional and a one-dimensional one in the tangential direction. All stress components are invariant

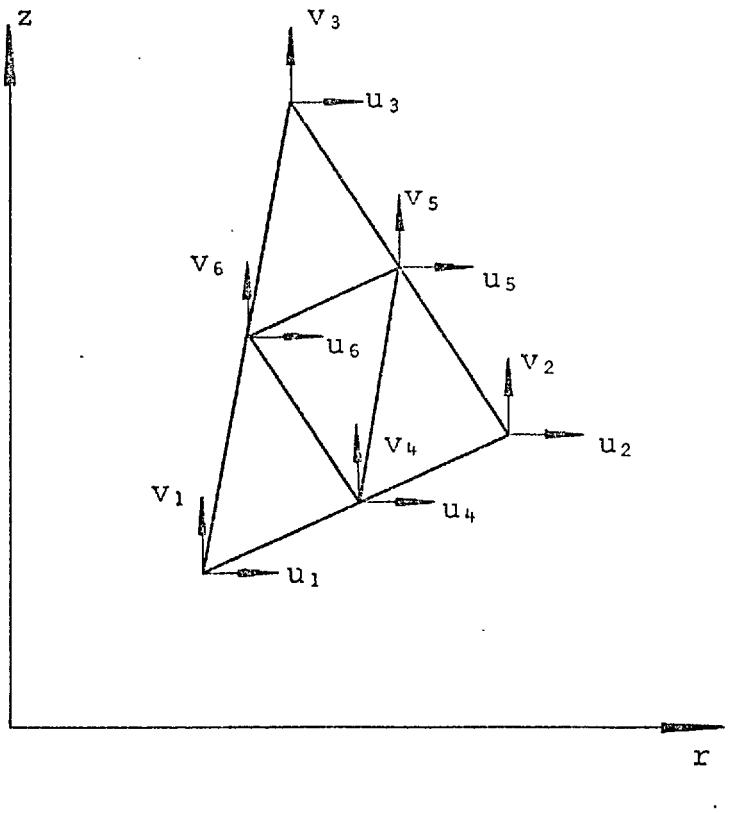


Fig. 8.3. Cross-sectional subdivision and cartesian displacement components for the TRIAX 6 element

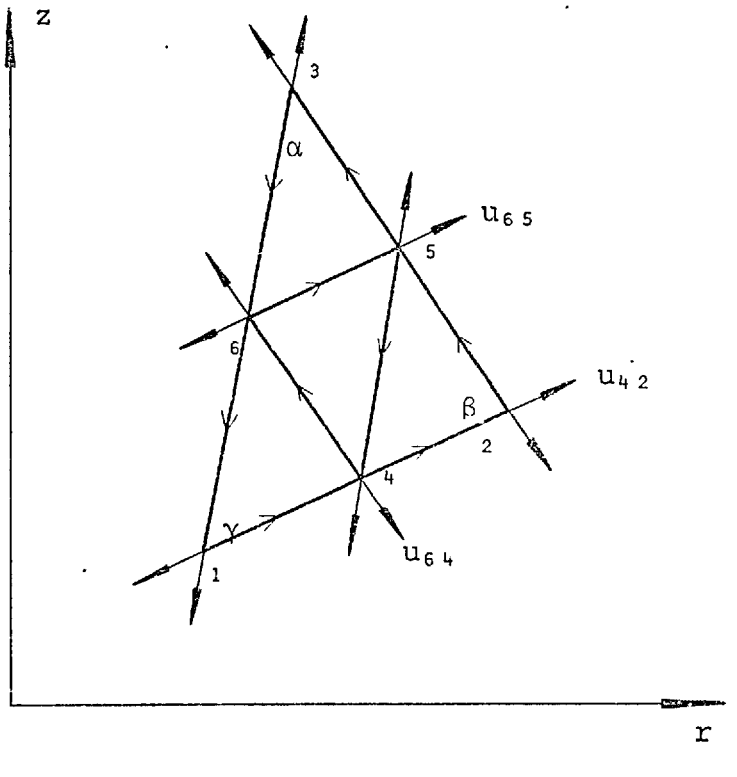


Fig. 8.4. Cross-sectional subdivision and natural displacement components for the TRIAX 6 element

with the angle of rotation and so are the strains. The invariance implies that no tangential stresses are acting on the interfaces between adjoining elements, hence the uncoupling of cross-sectional and tangential effects is possible.

The potentiality is crucial in the construction of the local stiffness matrix, as it favours the derivation of its coefficients in a partitioned form.

8.3.2. NATURAL DEFORMATION MODES

Striding to minimize the size of the system matrix and hence the number of required storage locations, which quickly inflate with the total number of nodal points, a measure for strains in harmony with the geometry of the triangle is introduced. Natural strains are optimally defined when measured parallel to the sides; thus the natural deformations are equivalent to the elongations of the sides. The adjective 'natural' is derived from the fact that the deformations develop in the triangle's basic directions.

The natural strains lead to symmetric expressions excluding shearing contributions; but, from statically indeterminate analysis, their implementation is still governed by the criterion that individual sets of self-equilibrating forces must be prevented from doing virtual work on more than one natural deformation mode.

The natural stiffness matrix, which ignores rigid body motions, thus links in a concise manner the natural force components and elongations, parallel to the element's sides. The natural strains are related to the classical cartesian strain definitions by Mohr's strain circle transformation formulae; the existence of this convertibility is decisive in the transformation of local natural strains into global cartesian ones and manifests itself in the embodiment of the (9x9) natural stiffness matrix into the (12x12) cartesian stiffness matrix.

The shortcomings of the TRIAX 3 element, essentially due to the assumption of locally constant stress and strain

fields, are overcome by adopting linear approximations to the strain distribution. The kinematical compatibility requirements are still satisfied along each side of the element's triangular cross-section, since the corresponding parabolic displacement field is uniquely described by the displacement values pertaining to the three nodal points of a side.

8.3.3. GEOMETRICAL AND ANALYTICAL ADVANTAGES

Although any finite element matrix displacement method must rely on interpolating displacement functions, one approximation may be nearer to the exact solution than another. Despite the fact that one cannot state beforehand which is the most suitable approximation, it appears logical that a second order polynomial, due directly to its higher degree of freedom, offers a better fit to the displacement field with varying gradients, than a linear one.

Geometrically and computationally, the main advantage of the natural deformation modes concept is that, by implementing TRIAX 6 elements, a finite element grid optimization is achieved. Owing to the adoption of quadratic displacement functions, a tremendous reduction in nodal points can be enjoyed, leading to a deflation of computer input data and a cut in computing cost; the reference criterion being an accuracy equal to that obtained by the classical modes analysis.

Since there is no way whatsoever of checking the stiffness matrix by physical insight, the natural modes concept has an analytic advantage, in that it starts off with circumventing the difficulty of differentiating non-linear polynomials by forming immediately explicit expressions for the strains.

8.3.4. STIFFNESS MATRIX FOR THE TRIAX 6 ELEMENT

Compared with the classical approach, the implementation of the natural deformation modes concept in the axisymmetric elastic analysis is, by one order of difficulty, more laborious. Accordingly, to convey the general idea of the concept, it is prudent to derive the cartesian stiffness matrix for the TRIAX 6 element first deductively, using suppositional steps.

The cartesian stiffness matrix emerges from the retransformation of the natural stiffness matrix into the orthogonal system, which initially enables the natural material stiffness matrix to be expressed in terms of classical definitions. Once the general formulation of the cartesian stiffness matrix is established, its construction can be reproduced in detail; in this way, clearer and more pronounced intermediate objectives can be pursued.

Upon stating that analogous matrices, though different in size and value, are arrived at when formulating the classical and the natural deformation modes concepts, it is plausible that the symbolic names of corresponding matrices should, for the sake of reference, be chosen identically.

For the purpose of relating the natural strains which develop in the cross-sectional plane of the element to the global cylindrical displacement components, a matrix expression similar to that of eq. (8.9) is postulated.

$$\underline{\varepsilon}^{i}_{NN} = \underline{A}^{i}\underline{B}^{i}\underline{O}^{i}\underline{C}^{i}\underline{u} \qquad (8.22)$$

where the matrix product $\underline{A}^{i}\underline{B}^{i}$ represents the (9x9) natural strain operator matrix and $\underline{C}^{i}$ is the local (12xk) connectivity matrix, which due to the element's 12 degrees of freedom is now larger than its analogue encountered in eq. (8.5).

The (9x9) matrix $\underline{A}^{i}$ determines the in-plane deformation at any position within the triangular field, arising from conjugate unit extensions of the lines and may therefore be called topology matrix. The (9x9) matrix $\underline{B}^{i}$ contains the reciprocals of the lengths of the sides and thus is termed reciprocity matrix. The coefficients of $\underline{A}^{i}$ and $\underline{B}^{i}$ are set up in eqs. (8.59) and (8.44) respectively. In contrast to the classical strain vector (8.9), the natural modes concept additionally requires the introduction of the (9x9) mode transformation matrix $\underline{O}^{i}$, which is discussed in eq. (8.64).

The derivation of the tangential strain, which varies with the position in the triangular field, does not involve any transformations of classical deformation modes into natural ones. The corresponding matrix expression is immediately

accomplished in the orthogonal system as

$$\underline{\varepsilon}^{i}_{TT} = \frac{1}{r}\,\underline{M}^{i}\underline{C}^{i}\underline{u} \tag{8.23}$$

where $\underline{M}^{i}$ is a (1x12) topology vector of non-dimensional triangular coordinates, describing the radial deformations within the triangular field due to conjugate unit displacements at the nodes; the vector is expanded in eq. (8.66).

Introducing the partitioned strain operator matrix $\underline{J}^{i}$, the total strain tensor may be described by

$$\underline{\varepsilon}^{i}_{N} = \underline{J}^{i}\underline{u} \tag{8.24}$$

where

$$\underline{J}^{i} = \{\underline{A}^{i}\underline{B}^{i}\underline{O}^{i}\underline{C}^{i}\ \frac{1}{r}\,\underline{M}^{i}\underline{C}^{i}\}$$

Proceeding from the (4x4) orthogonal material stiffness matrix $\underline{D}^{i}$ of eq. (8.11), the relationship between the natural stress and strain components can be deduced as

$$\underline{\sigma}^{i}_{N} = (\underline{G}^{i}\underline{H}^{i})^{t}\underline{D}^{i}\underline{G}^{i}\underline{H}^{i}\ \underline{\varepsilon}^{i}_{N} \tag{8.25}$$

where the (4x4) matrices $\underline{G}^{i}$ and $\underline{H}^{i}$ are responsible for the transformation of orthogonal stress and strain definitions into natural ones ; $\underline{G}^{i}$ and $\underline{H}^{i}$ are derived in eqs. (8.36) and (8.34) respectively.

From eq. (8.25), the natural material stiffness matrix is ascertainable as

$$\underline{K}^{i}_{N} = (\underline{G}^{i}\underline{H}^{i})^{t}\underline{D}^{i}\underline{G}^{i}\underline{H}^{i} \tag{8.26}$$

Its detailed construction is discussed in eqs. (8.37) and (8.38).

As already emphasized in section 8.3.1., the formation of the element stiffness matrix, based on the natural deformation modes, is only realizable, if it is preceded by the partitioning of the contributing matrices. Consequently, the

natural material stiffness matrix (8.26) must appear in the form

$$\underline{K}_N^i = \begin{bmatrix} \underline{K}_{NN} & \underline{K}_{NT} \\ \underline{K}_{TN} & \underline{K}_{TT} \end{bmatrix} \tag{8.27}$$

where $\underline{K}_{NN}$ is the (3x3) in-plane stiffness, $\underline{K}_{NT}$ and $\underline{K}_{TN}^t$ are the (3x1) coupling stiffnesses and the scalar value K_{TT} represents the circumferential contribution.

Substituting first eq. (8.25) and then eq. (8.24) into the first term of the total potential energy functional (7.26) and subsequently producing the first variation with respect to the global displacements, the element stiffness matrix emerges as a (12x12) multiplier to the generalized displacement vector $\underline{u}$.

$$\underline{K}^i.\underline{u} = \int_{s^i} \{ \underline{A}^i\underline{B}^i\underline{O}^i\underline{C}^i \; \frac{1}{r}\underline{M}^i\underline{C}^i \}(\underline{G}^i\underline{H}^i)^t\underline{D}^i\underline{G}^i\underline{H}^i\{\underline{A}^i\underline{B}^i\underline{O}^i\underline{C}^i \; \frac{1}{r}\underline{M}^i\underline{C}^i\} r ds.\underline{u} \tag{8.28}$$

With the partitioned strain vector (8.24) and the partitioned material stiffness matrix (8.27), the element stiffness matrix in eq. (8.28) is hence obtainable as the superposition of four (12x12) matrices.

$$\underline{K}^i = \underline{K}_{AA}^i + \underline{K}_{AB}^i + \underline{K}_{BA}^i + \underline{K}_{BB}^i \tag{8.29}$$

The first term of eq. (8.29) characterizes the cartesian in-plane stiffness

$$\underline{K}_{AA}^i = (\underline{O}^i\underline{C}^i)^t \, 2\pi \int (\underline{A}^i\underline{B}^i)^t \underline{K}_{NN}\underline{A}^i\underline{B}^i r ds \; (\underline{O}^i\underline{C}^i) \tag{8.30}$$

where the expression under the integral represents the (9x9) natural stiffness matrix for the curvilinearly tapered triangular membrane element with six nodal points and a unit angle of rotation, TRIM 6. The integral expression and the whole equation (8.30) are transposed into numerical form in eqs. (8.63) and (8.65) respectively.

The second and the third term of eq. (8.29) constitute the coupling stiffnesses that withstand shear actions

$$\underline{K}^{i}_{AB} = \underline{K}^{it}_{AB} = (\underline{O}^{i}\underline{C}^{i})^{t}\, 2\Pi \int (\underline{A}^{i}\underline{B}^{i})^{t}\underline{K}_{NT}\underline{M}^{i}\underline{C}^{i} ds \qquad (8.31)$$

of which the numerical conformation is expounded in eq. (8.76)

The fourth term of eq. (8.29), finally symbolizes the hoop stiffness, which resists actions in the circumferential tangential direction

$$\underline{K}^{i}_{BB} = 2\Pi \int (\underline{M}^{i}\underline{C}^{i})^{t}\underline{K}_{TT}(\underline{M}^{i}\underline{C}^{i})\frac{1}{r}\, ds \qquad (8.32)$$

The all-matrix form of eq. (8.32) is set up in eq. (8.72)

8.3.5. DERIVATION OF STIFFNESS SUBMATRICES

8.3.5.1. NATURAL MATERIAL STIFFNESS MATRIX

Looking at figures (8.5) and (8.6) with the intention of finding conjugate sets of stresses and strains which in their definition comply with the principle of virtual work, it is realized that corresponding and conjugate mode shapes are not identical. Clearly, the natural component stress σ_{ic} gives rise to stresses not only parallel to the side l_i but also parallel to the sides l_j and l_k, since a corresponding strain σ_{ic} deforms all sides. If, however, the same σ_{ic} acts on the mode shape of the total natural strain ε_{it}, which leaves the sides l_j and l_k unstrained, the first out of three necessary individual self-equilibrating sets of stresses and strains is designed. The remaining two are defined correspondingly.

Hereafter, only conjugate sets are considered; for the sake of brevity, therefore, the types of natural components are no longer specified. Expanding the natural stress and strain vectors of the TRIAX element by the tangential component, which follows the orthogonal definition, the partitioned nature of these is recognized

$$\underline{\sigma}_{N} = \{\ \sigma_i \quad \sigma_j \quad \sigma_k \quad \sigma_t\ \}$$

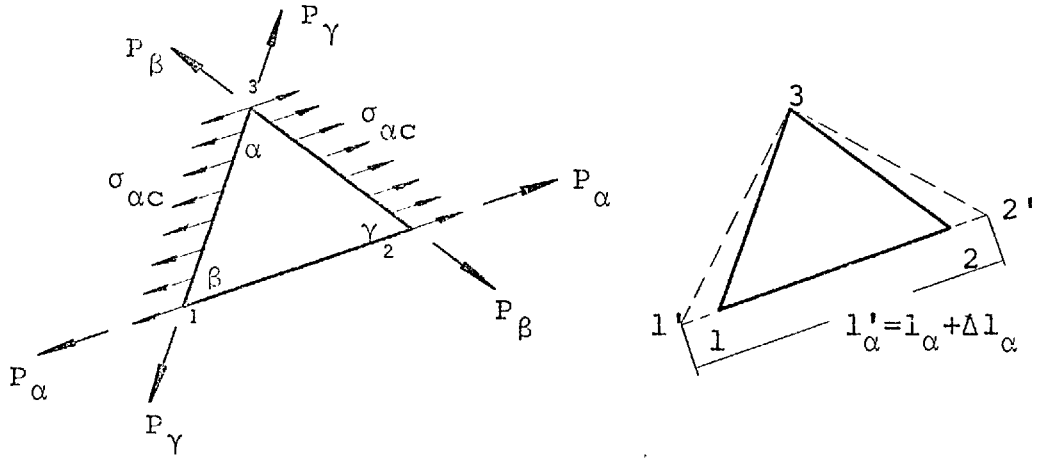


Fig. 8.5. Natural component stress and natural component strain for the TRIM 3 element

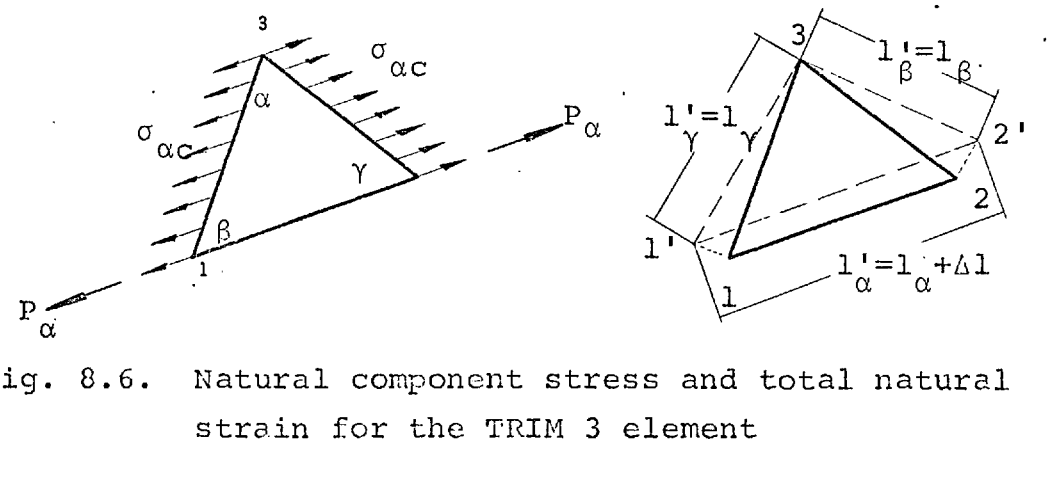


Fig. 8.6. Natural component stress and total natural strain for the TRIM 3 element

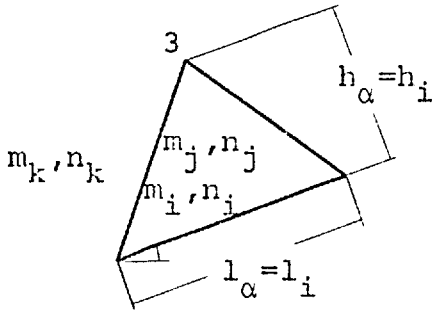


Fig. 8.7. Direction cosines for the TRIM 3 element

$$\underline{\varepsilon}_N = \{\varepsilon_i \quad \varepsilon_j \quad \varepsilon_k \quad \varepsilon_t\} \tag{8.33}$$

With the absence of shearing contributions, double subscription is inapplicable here. Since, furthermore, all matrix expressions in section 8.3.5. refer to an individual element, the superscript i is ignored.

The elastic law follows either the orthogonal definition (8.11) or the natural definition (8.25) ; the transition from the first to the latter is enabled by the introduction of the vector transformations

$$\begin{aligned} \underline{\sigma} &= \underline{H}\,\underline{\sigma}_N \\ \underline{\varepsilon} &= \underline{H}^t\underline{\varepsilon} \end{aligned} \tag{8.34}$$

where $\underline{H}$ is a (4x4) transformation matrix of direction cosines, as shown in eq. (A4.16).

To verify the coefficients of eq. (A4.16), the direction cosines m_i, n_i, i = 1,2,3 of a generating triangular membrane element are entered into figure (8.7). Using Mohr's transformation formulae, thus

$$\begin{aligned} m_i^4 + n_i^4 + 2m_i^2n_i^2 &= (m_i^2 + n_i^2)^2 = 1 \\ m_i^2m_j^2 + n_i^2n_j^2 + 2m_im_jn_in_j &= (m_im_j + n_in_j)^2 = \cos^2\gamma \end{aligned} \tag{8.35}$$

with eqs. (8.35), the existence of the following equivalence can be confirmed

$$\underline{H}^t\underline{H} = \underline{G}^{-1} \tag{8.36}$$

where $\underline{G}^{-1}$ is a (4x4) matrix assembled in eq. (A4.17).

Substituting eqs. (8.34) into eq. (8.11), the relationship between the natural strains and stresses is established

$$\underline{\varepsilon}_N = \underline{H}^t\underline{D}^{-1}\underline{H}\,\underline{\sigma}_N \tag{8.37}$$

By definition, the natural material flexibility matrix, which

is identical with the inverse of the natural material stiffness matrix, arises from eq. (8.37) as

$$\underline{K}_N^{-1} = \underline{H}^t \underline{D}^{-1} \underline{H} \tag{8.38}$$

After solving eq. (8.36) for $\underline{H}$ and $\underline{H}^t$, the corresponding expressions are substituted into eq. (8.38), which may be inverted to yield the natural stiffness matrix (8.26).

8.3.5.2. NATURAL STIFFNESS MATRIX FOR THE TRIM 3 ELEMENT

As indicated in eqs. (8.29) to(8.32), the stiffness matrix of the TRIAX 6 element is conveniently derived in a partitioned form. Aiming to construct the in-plane stiffness of such an element, first a triangular membrane element with three nodal points, TRIM 3, is analysed.

Here, the natural deformation modes are simply the elongations of its sides. Consequently, its numerical strain-deformation relation is obtainable as

$$\underline{\varepsilon}_N = \underline{B}_{(3)} \underline{u}_N \tag{8.39}$$

where $\underline{B}_{(3)}$ is the (3x3) diagonal strain operator matrix, which after suppression of its zero entries is contracted to

$$\underline{B}_{(3)} = \left[\ell_i \quad \ell_j \quad \ell_k\right]^{-1} \tag{8.40}$$

Substituting first the relevant partition of eq. (8.27) and then eq. (8.11) into the first term of the functional (7.26) and subsequently deriving the first variation with respect to the natural displacements, the integral expression for the material stiffness matrix of the TRIM 3 element, is completed

$$\underline{K}_{N(3)} \cdot \underline{u}_N = \int_{s^i} \underline{B}_{(3)} \underline{K}_{NN} \underline{B}_{(3)}\, t\, ds \cdot \underline{u}_N \tag{8.41}$$

where $\underline{K}_{NN}$ coincides with the upper left (3x3) partition of eq. (8.28).

Integrating over the volume of the membrane element, the stiffness matrix is determined numerically as

$$\underline{K}_{N(3)} = A.t\ \underline{B}^{t}_{(3)}\underline{K}_{NN}\underline{B}_{(3)} \qquad (8.42)$$

where A is the planar area and t is the thickness.

8.3.5.3. NATURAL STIFFNESS MATRIX FOR THE TRIM 6 ELEMENT

Considering a triangular membrane element with additional nodes at the midpoints of the sides, TRIM 6, the existence of more parameters enables the introduction of linear strain fields. Suppressing the three rigid body motions, which are governed by the equilibrium equations of the statical determinate analysis, nine independent natural deformation modes must be designed, as the element has 12 degrees of freedom.

The natural displacement configuration are designed as the extensions of each line in turn - the other lines having zero extensions - and thus the cumbersome determination of strains by differentiation can be successfully avoided. Parallel to each side three lines exist; consequently, the natural displacement vector of eq. (8.39) is expanded to become a (9x1) vector that accommodates three (3x1) subvectors

$$\underline{u}_N = \{u_{14}u_{42}\ u_{65}\ u_{25}\ u_{53}u_{46}\ u_{36}\ u_{61}\ u_{54}\} \qquad (8.43)$$

where

$$\underline{u}_i = \{\ u_{14}\ u_{42}\ u_{65}\ \}$$

$$\underline{u}_j = \{\ u_{25}\ u_{53}\ u_{46}\ \}$$

$$\underline{u}_k = \{\ u_{36}\ u_{61}\ u_{54}\ \}$$

The subscript notation is eq. (8.43) originates from the numbering of points laid down in figure (8.3). The natural deformation mode $\underline{u}_i$ is depicted in figure (8.8) ; similarly, the remaining two modes can be designed.

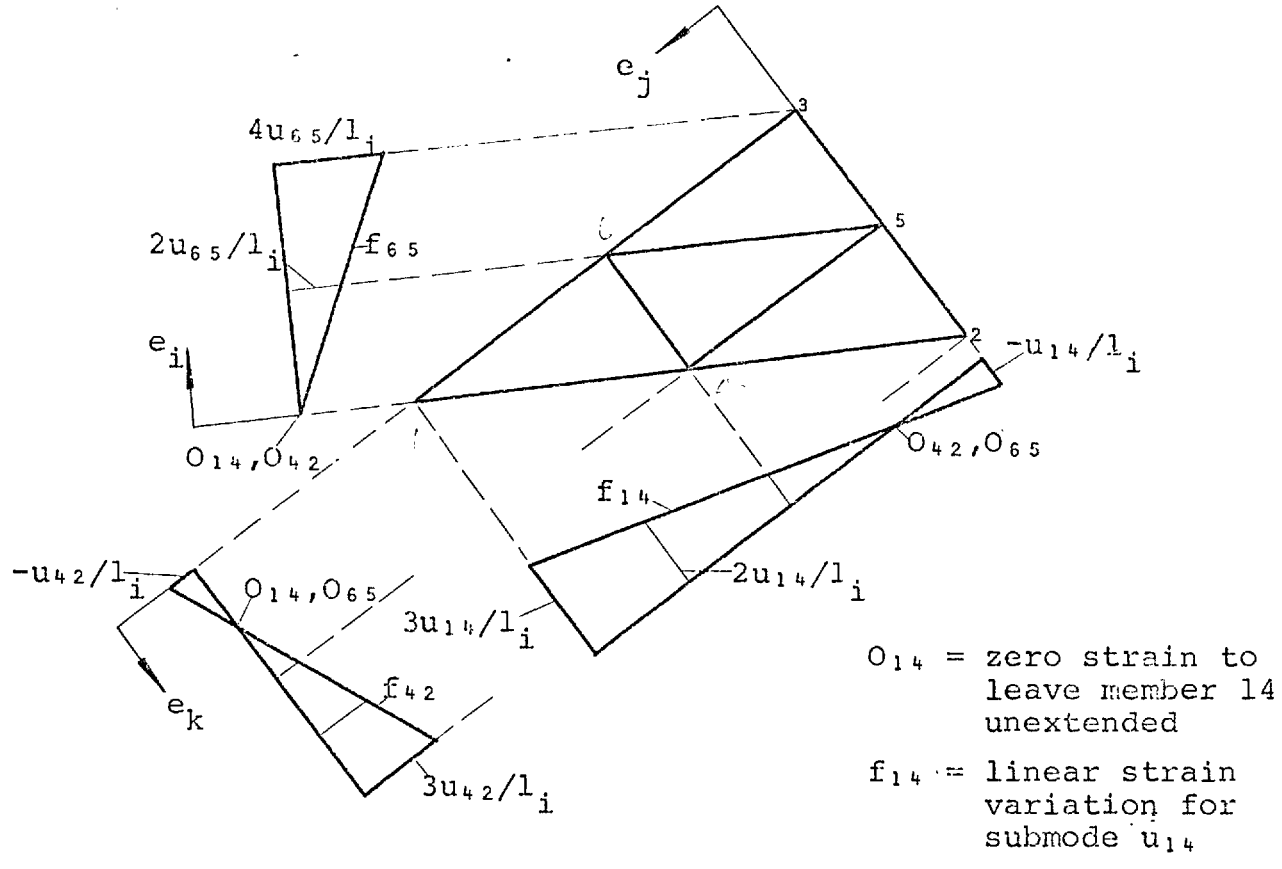


Fig. 8.8. Natural deformation mode $\underline{u}_i$ for the TRIM 6 element

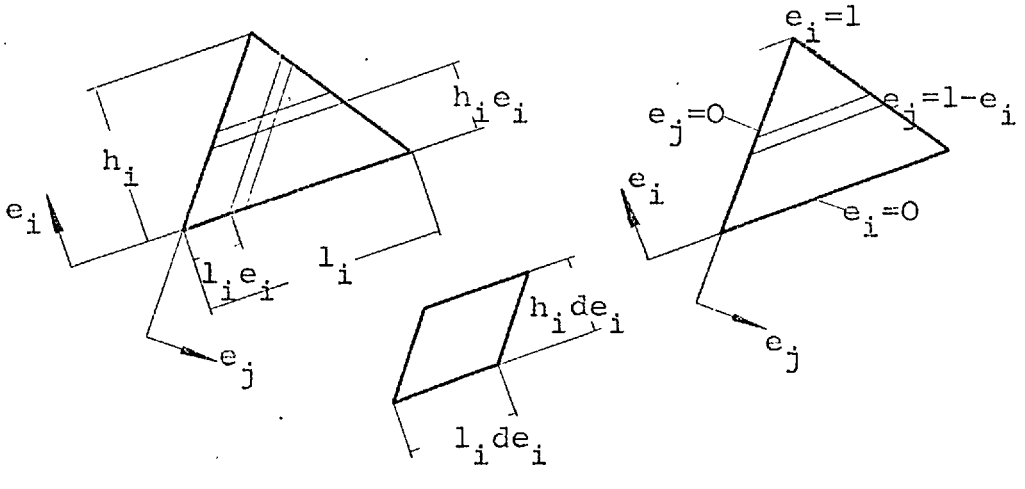


Fig. 8.9. Integration over TRIM 6 element using non-dimensional coordinates

With the expansion of the displacement vector, also the natural strain operator matrix $\underline{B}_{(3)}$ augments its coefficients. Due to the linear variation of strains, $\underline{B}_{(3)}$ is not only expanded to become the (9x9) reciprocity matrix $\underline{B}$ entered into eq. (8.22), it is also premultiplied by a (9x9) topology matrix $\underline{A}_{(6)}$. As a result, the strain operator matrix is now symbolized by

$$\underline{A}_{(6)}\underline{B} = \lceil \underline{a}_i \underline{a}_j \underline{a}_k \rfloor \lceil \ell_i \underline{I}_3 \ \ell_j \underline{I}_3 \ \ell_k \underline{I}_3 \rfloor^{-1} \tag{8.44}$$

where

$$\underline{a}_i = \left[(-1 + 4e_2) \ (-1 + 4e_3) \ 4e_1 \right]\underline{I}_3$$

$$\underline{a}_j = \left[(-1 + 4e_3) \ (-1 + 4e_1) \ 4e_2 \right]\underline{I}_3$$

$$\underline{a}_k = \left[(-1 + 4e_1) \ (-1 + 4e_2) \ 4e_3 \right]\underline{I}_3$$

Replacing eq. (8.40) by eq. (8.44), the integral multiplier to the natural displacements in eq. (8.41) is now identical with the natural stiffness matrix of the TRIM 6 element

$$\underline{K}_{N(6)} = \int \lceil \underline{a}_i \underline{a}_j \underline{a}_k \rfloor \ \underline{B}^t K_{NN} \underline{B} \ \lceil \underline{a}_i \underline{a}_j \underline{a}_k \rfloor \ t \ ds \tag{8.45}$$

Expanding eq. (8.45), thus

$$\underline{K}_{N(6)} = \underline{B}^t \int \begin{bmatrix} K_{11}\underline{a}_i^t\underline{a}_i & K_{12}\underline{a}_i^t\underline{a}_j & K_{13}\underline{a}_i^t\underline{a}_k \\ K_{21}\underline{a}_j^t\underline{a}_i & K_{22}\underline{a}_j^t\underline{a}_j & K_{23}\underline{a}_j^t\underline{a}_k \\ K_{31}\underline{a}_k^t\underline{a}_i & K_{32}\underline{a}_k^t\underline{a}_j & K_{33}\underline{a}_k^t\underline{a}_k \end{bmatrix} \text{tds}.\underline{B} \tag{8.46}$$

where $K_{11} = K_{NN_{11}}$ etc.

The solution of the individual integrals (8.46) requires some special attention. To define the location of a point within a triangular field, either two of its three non-dimensional coordinates are sufficient ; the third is automatically determined by the relation

$$e_i + e_j + e_k = 1 \tag{8.47}$$

Realizing the nature of the coefficients in eq. (8.44), the solution of eq. (8.46) involves integrals of the following kind

$$I = \int e_i^m e_j^n \, ds \tag{8.48}$$

The definition of an infinitesimal area is obtainable from figure (8.9) as

$$ds = 2A \, de_i \, de_j \tag{8.49}$$

Thus eq. (8.48) takes the form

$$\int e_i^m e_j^n \, ds = 2A \int e_i^m e_j^n de_i de_j \tag{8.50}$$

After the performance of some integral operations, which are specified in eqs. (A4.18), the following equivalence is arrived at

$$\int e_i^m e_j^n ds = \frac{2A \, m! n!}{(m+n+2)!} \tag{8.51}$$

Regarding the first coefficient of eq. (8.46), it may be presented in the long hand writing

$$K'_{N(6)11} = \underline{B}^t K_{11} \int \begin{bmatrix} (-1 + 4e_2) \\ (-1 + 4e_3) \\ 4e_1 \end{bmatrix} \begin{bmatrix} (-1 + 4e_2) & (-1 + 4e_3) & 4e_1 \end{bmatrix} t ds . \underline{B} \tag{8.52}$$

The multiplication of the vector components in eq. (8.52) involves three possible types of expressions (8.51)

$$\begin{aligned} 4 \int e_i ds &= 4 . \frac{2A}{3.2} = \frac{4}{3} A \\ 16 \int e_i e_j ds &= 16 . \frac{2A}{4.3.2} = \frac{4}{3} A \\ 16 \int e_i^2 ds &= 16 . \frac{4A}{4.3.2} = \frac{8}{3} A \end{aligned} \tag{8.53}$$

Applying eqs. (8.53) to eq. (8.52), the integration over the existing products of sums produces

$$\int (-1 + 4e_i)(-1 + 4e_j)\, ds = \begin{cases} A(1 - \frac{4}{3} - \frac{4}{3} + \frac{8}{3}) = A & \text{if } i=j \\ A(1 - \frac{4}{3} - \frac{4}{3} + \frac{4}{3}) = \frac{A}{3} & \text{if } i\neq j \end{cases}$$

$$\int (-1 + 4e_i)\, 4e_j\, ds = \begin{cases} A(-\frac{4}{3} + \frac{8}{3}) = \frac{4}{3}A & \text{if } i=j \\ A(-\frac{4}{3} + \frac{4}{3}) = 0 & \text{if } i\neq j \end{cases} \qquad (8.54)$$

In consequence, the coefficients under the integral (8.46) may be expressed in numeric form using

$$\begin{aligned} \int \underline{a}_i^t \underline{a}_i ds &= \int \underline{a}_j^t \underline{a}_j ds = \int \underline{a}_k^t \underline{a}_k ds = \frac{A}{3}\underline{b}_1^t \\ \int \underline{a}_i^t \underline{a}_j ds &= \int \underline{a}_j^t \underline{a}_k ds = \int \underline{a}_k^t \underline{a}_i ds = \frac{A}{3}\underline{b}_2 \\ \int a_i^t a_j ds &= \int a_k^t a_j ds = \int a_j^t a_i ds = \frac{A}{3}\underline{b}_3 \end{aligned} \qquad (8.55)$$

where $\underline{b}_1$ and $\underline{b}_2$ are (3x3) submatrices assembled in eqs. (A4.19).

Substituting eqs. (8.55) into eq. (8.46), the (9x9) natural stiffness matrix of the TRIM 6 element is procured

$$\underline{K}_{N(6)} = \frac{A}{3}\, t\, \underline{B}^t \cdot \int \begin{bmatrix} k_{11}\underline{b}_1 & k_{12}\underline{b}_2 & k_{13}\underline{b}_2^t \\ k_{21}\underline{b}_2^t & k_{22}\underline{b}_1 & k_{23}\underline{b}_2 \\ k_{31}\underline{b}_2 & k_{32}\underline{b}_2^t & k_{33}\underline{b}_1 \end{bmatrix} .B \qquad (8.56)$$

where $K_{11} = K_{NN_{11}}$ etc. are coefficients of the (3x3) partition of the material stiffness matrix (8.27).

8.3.5.4. NATURAL IN-PLANE STIFFNESS FOR THE TRIAX 6 ELEMENT

Analysing a tapered triangular element, which is generated by rotating a TRIM 6 element about the relevant axis, such that the end cross-sections include a unit angle $\emptyset$, the natural in-plane stiffness matrix of the TRIAX 6 element can be expounded.

The thickness at the corner points of such a curvilinearly tapered element is determined by

$$t_i = \emptyset\, r_i \tag{8.57}$$

where r_i, i=1,2,3 are the radial distances of the vertices from the axis of revolution.

Combining eqs. (8.47) and (8.57), the varying thickness within the element boundaries may be expressed by

$$t = \emptyset\, (r_i e_i + r_j e_j + r_k e_k) \tag{8.58}$$

Due to the presence of taper, the coefficients of the topology matrix $\underline{A}_{(6)}$ in eq. (8.44) become more complex; the natural in-plane strain vector (8.44) now reads

$$\underline{\varepsilon}_N = \underline{A}\ \underline{B}\ \underline{u}_N \tag{8.59}$$

where with fig. (8.10)

$$\underline{a}_i = \left[(3e_1 - e_2 - e_3)(-e_1 + 3e_2 - e_3)\ 4e_3\right] \underline{I}_3$$

$$\underline{a}_j = \left[(-e_1 + 3e_2 - e_3)(-e_1 - e_2 + 3e_3) 4e_1\right] \underline{I}_3$$

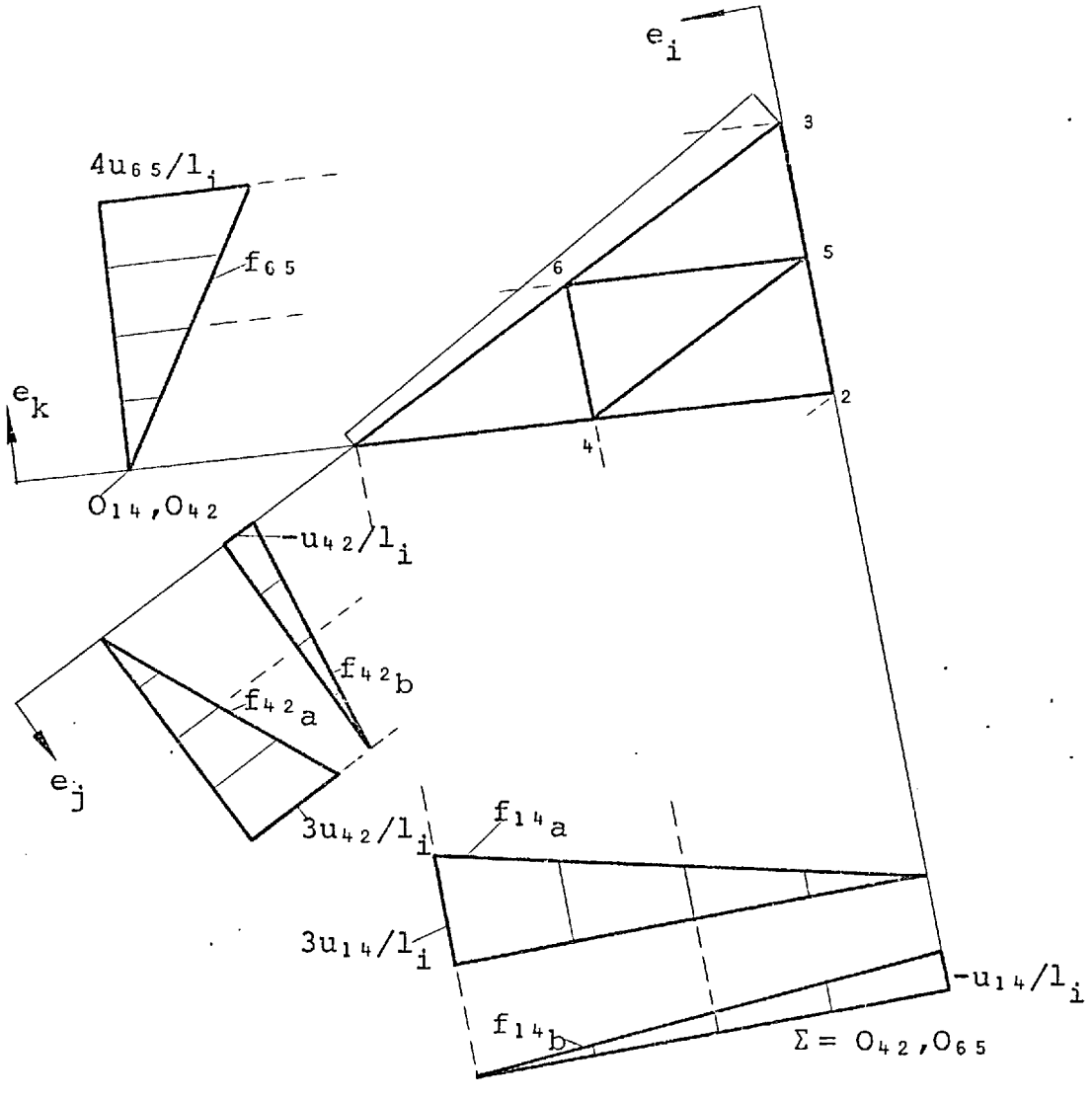
$$\underline{a}_k = \left[(-e_1 - e_2 + 3e_3)(3e_1 - e_2 - e_3)\ 4e_2\right] \underline{I}_3$$

Substituting eqs. (8.58) and (8.59) into eq. (8.45), the natural in-plane stiffness matrix of the TRIAX 6 element is obtained in its integral form

$$\underline{K}_N = \underline{B}^t \int (r_i \lceil \underline{a}_i\underline{a}_j\underline{a}_k \rfloor \underline{K}_{NN} e_i \lceil \underline{a}_i\underline{a}_j\underline{a}_k \rfloor + r_j \lceil a_i a_j a_k \rfloor K_{NN}\ e_j \lceil a_i a_j a_k \rfloor$$

$$+ r_k \lceil a_i a_j a_k \rfloor K_{NN} \lceil a_i a_j a_k \rfloor \quad) 2\Pi ds.\underline{B} \tag{8.60}$$

If integration is carried out over the domain of the integral (8.60), clearly, products of three non-dimensional coordinates are involved. As a special case of eq. (8.51), Argyris ([7]) states the existence of the relation



$f_{14} = f_{14}a + f_{14}b$

$f_{42} = f_{42}a + f_{42}b$

O_{42} = zero strain to leave member 42 unextended

f_{42} = linear strain variation for submode u_{42}

Fig. 8.10. Natural deformation mode $\underline{u}_i$ for the TRIAX 6 element

$$\int e_i e_j e_k \, ds = \begin{cases} \frac{A}{60} & \text{if } i \neq j \neq k \\ \frac{A}{30} & \text{if } i = j \neq k \\ \frac{A}{10} & \text{if } i = j = k \end{cases} \qquad (8.61)$$

Piece-wise integration of the treble products in eq. (8.60) gives rise to expressions which correspond in form to eqs. (8.55)

$$\begin{aligned}
\int \underline{a}_i^t \underline{a}_i e_k ds &= \int \underline{a}_j^t \underline{a}_j e_i ds = \int \underline{a}_k^t \underline{a}_k e_j ds = A.\underline{c}_{11} \\
\int \underline{a}_i^t \underline{a}_j e_k ds &= \int \underline{a}_j^t \underline{a}_k e_i ds = \int \underline{a}_k^t \underline{a}_i e_j ds = A.\underline{c}_{12} \\
\int \underline{a}_k^t \underline{a}_i e_k ds &= \int \underline{a}_i^t \underline{a}_j e_i ds = \int \underline{a}_j^t \underline{a}_k e_j ds = A.\underline{c}_{13} \\
\int \underline{a}_j^t \underline{a}_j e_k ds &= \int \underline{a}_k^t \underline{a}_k e_i ds = \int \underline{a}_i^t \underline{a}_i e_j ds = A.\underline{c}_{22} \\
\int \underline{a}_j^t \underline{a}_k e_k ds &= \int \underline{a}_k^t \underline{a}_i e_i ds = \int \underline{a}_i^t \underline{a}_j e_j ds = A.\underline{c}_{23} \\
\int \underline{a}_k^t \underline{a}_k e_k ds &= \int \underline{a}_i^t \underline{a}_i e_i ds = \int \underline{a}_j^t \underline{a}_j e_j ds = A.\underline{c}_{33}
\end{aligned} \qquad (8.62)$$

where the (3x3) submatrices $\underline{c}$ are numeric arrays composed in eqs. (A4.20). The first coeficient of $\underline{c}_{11}$, for instance, can be produced with eqs. (8.59) and (8.61) as

$$\int (3e_1 - e_2 - e_3)(3e_1 - e_2 - e_3) \, ds =$$

$$\left(\frac{9}{30} - \frac{3}{60} - \frac{3}{30} - \frac{3}{60} + \frac{1}{30} + \frac{1}{30} - \frac{3}{30} + \frac{1}{30} + \frac{1}{10} \right) A = \frac{3}{15} A$$

Substitution of eqs. (8.62) into eq. (8.60) results in the conformation of the natural in-plane stiffness matrix for the curvilinearly tapered TRIM 6 element ; to obtain the natural in-plane stiffness matrix for the TRIAX 6 element, the angle of rotation is replaced by 2Π

$$\underline{K}_N = 2\Pi A \, \underline{B}^t \{ r_3 \underline{A}^t \underline{K}_{NN} e_3 \underline{A} + r_1 \underline{A}^t \underline{K}_{NN} e_1 \underline{A} + r_2 \underline{A}^t \underline{K}_{NN} e_2 \underline{A} \} \underline{B} \qquad (8.63)$$

where the matrix products within the brackets are identical with the matrix collocation (A4.21)

8.3.5.5. CARTESIAN IN-PLANE STIFFNESS FOR THE TRIAX 6 ELEMENT

In the process of identifying the natural deformation modes, viz. the elongations of the lines, with the global cylindrical displacement components, the matrix product $\underline{O}\ \underline{C}$, as first encountered in eq. (8.22), is introduced.

The mode transformation matrix $\underline{O}$ is in itself a product of matrices of which the first (9x18) matrix contains the direction cosines of the nine lines

$$\underline{O} = \left[\underline{O}_i\ \underline{O}_i\ \underline{O}_i\ \underline{O}_j\ \underline{O}_j\ \underline{O}_j\ \underline{O}_k\ \underline{O}_k\ \underline{O}_k\right] \tag{8.64}$$

where

$$\underline{O}_i = \frac{1}{\ell_i}\left[(r_b - r_a)\ (z_b - z_a)\right]$$

The subscripts a and b designate the first and the second node of the line; the order being determined by the arrows in figure (8.4). The second (18x12) matrix of $\underline{O}$ is a difference matrix which selects in turn the two nodes (r_a, z_a) and (r_b, z_b) associated with each line. To show how the coefficients of eq. (8.64) link the elongations of the lines to the cylindrical displacement components, the matrix $\underline{O}$ is symbolically arranged in eq. (A4.22).

Expressing the natural displacements $\underline{u}_N$ in eq. (8.59) in terms of the global orthogonal displacements, the in-plane strain vector (8.22) is arrived at. Thus, pre- and postmultiplication of eq. (8.63) with the matrix product $\underline{O}\ \underline{C}$ leads to the establishment of the cartesian in-plane stiffness matrix for the TRIAX 6 element

$$\underline{K}_{AA} = 2\Pi\ (\underline{B}\ \underline{O}\ \underline{C})^t \{r_3 \underline{A}^t \underline{K}_{NN} e_3 \underline{A} + r_1 \underline{A}^t \underline{K}_{NN} e_1 \underline{A} + r_2 \underline{A}^t \underline{K}_{NN} e_2 \underline{A}\} \cdot \underline{B}\ \underline{O}\ \underline{C} \tag{8.65}$$

which represents the numeric form of eq. (8.30).

8.3.5.6. CARTESIAN HOOP STIFFNESS FOR THE TRIAX 6 ELEMENT

To calculate the stiffness in the circumferential direction of the ring shaped TRIAX 6 element, it must be realized that the (1x12) topology vector in eq. (8.23) is determined by

$$\underline{M} = [(-e_1 + 2e_1^2)\ 0\ 4e_1e_2\ \ 0\ (-e_2 + 2e_2^2)\ 0$$

$$4e_2e_3\ 0\ (-e_3 + 2e_3^2)\ 0\ 4e_3e_1\ 0\ ] \qquad (8.66)$$

where e_i, i = 1,2,3 are the non-dimensional coordinates of the triangle.

Substituting eq. (8.66) into the integral expression (8.32), integrals of the following types must be solved

$$I_{1,2} = \int \frac{1}{r}\, e_1^m e_2^n de_1 de_2 \quad = \quad (1^m, 2^n)$$

$$I_{2,3} = \int \frac{1}{r}\, e_2^m e_3^n de_2 de_3 \quad = \quad (2^m, 3^n) \qquad (8.67)$$

$$I_{3,1} = \int \frac{1}{r}\, e_3^m e_1^n de_3 de_1 \quad = \quad (3^m, 1^n)$$

Substituting first the radius as defined in eq. (8.58) and then eq. (8.47) into eqs. (8.67), the integrals become

$$I = \int_0^1 \int_0^{1-e_1} \frac{e_1^m e_2^n de_2 de_1}{(r_1-r_3)e_1+(r_2-r_3)e_2+r_3} \qquad (8.68)$$

For convenience, the following equivalences are introduced

$$a = (r_1 - r_3) \qquad b = (r_2 - r_3) \qquad c = r_3$$

$$e_1 = \tfrac{1}{2}(1 + e) \qquad de_1 = \tfrac{1}{2}\, de \qquad (8.69)$$

$$e_2 = \tfrac{1}{4}(1 - e)(1-f) \qquad de_2 = \tfrac{1}{4}(1-e)df$$

With eqs. (8.69), the general integral (8.68) may be rewritten as

$$I = \frac{1}{2(m+n)} \int_0^1 \int_0^{1-e_1} \frac{\tfrac{1}{2}(1+e)^m \left(\frac{1-e}{2}\right)^{n+1} \tfrac{1}{2}(1+f)^n}{\frac{a}{2}(1-e)+\frac{b}{4}(1-e)(1+f)+c} \qquad (8.70)$$

Applying the numeric Gaussian method for double integration as expounded by Berezin and Zidkov ([26]) , the integral (8.70) becomes

$$I = \frac{1}{2(m+n)} \sum_{i=1}^{P} \frac{c_i}{2} (1+e_i)^m (1-e_i)^{n+1} \sum_{j=1}^{P} \frac{c_j}{2} \cdot \frac{(1+f_j)^n}{\frac{a}{2}(1+e_i)+\frac{b}{4}(1-e_i)(1+f_j)+c} \qquad (8.71)$$

where for p = 7, c_i and $e_i = f_i$ take the values given in eqs. (A4.23).

Expanding the integral (8.71), the integral form of the hoop stiffness (8.32) may be transformed to the matrix expression

$$\underline{K}_{BB} \doteq 2\Pi A \, K_{TT} \, \underline{C}^t \underline{T} \, \underline{C} \qquad (8.72)$$

where $\underline{T}$ is a (12x12) matrix of which the coefficients are integrals of the types (8.67), to be evaluated according to eq. (8.71). The matrix $\underline{T}$ is assembled in eq. (A4.24).

8.3.5.7. CARTESIAN COUPLING STIFFNESSES FOR THE TRIAX 6 ELEMENT

With the aim of separating the numeric terms in eq. (8.31) from the variable ones, first the multiplication of the (3x1) material stiffness matrix in shear $\underline{K}_{TT}$ and the (9x9) reciprocity matrix $\underline{B}$ of eq. (8.44) is carried out; the matrix multiplication is made admissible by expanding $\underline{K}_{NT}$ to a (9x9) matrix of the diagonal form

$$\underline{K}_{NT(ex)} = \begin{bmatrix} K_{NT1}\underline{I}_3 & K_{NT2}\underline{I}_3 & K_{NT3}\underline{I}_3 \end{bmatrix} \qquad (8.73)$$

Thus the coupling stiffness $\underline{K}_{AB}$ in eq. (8.31) becomes

$$\underline{K}_{AB} = (\underline{K}_{NT(ex)} \, \underline{B} \, \underline{O} \, \underline{C})^t \, 2\Pi \int \underline{A} \, \underline{M} \, ds \qquad (8.74)$$

Substituting for $\underline{A}$ and $\underline{M}$ according to eqs. (8.59) and (8.66) respectively, integrals of the following kind must be solved

$$I = \int \begin{bmatrix} (3e_1 - e_2 - e_3) \\ (e_1 + 3e_2 - e_3) \\ 4e_3 \end{bmatrix} \begin{bmatrix} (-e_1 + 2e_1^2) & 0 & 4e_1e_2 & \text{etc.} \end{bmatrix} \tag{8.75}$$

Employing the formulae (8.53) and (8.61), a (9x12) matrix $\underline{S}$ is formed, of which the coefficients are given in eq. (A5.25). The first coefficient, for instance, is obtained in the following way

$$\int (3e_1 - e_2 - e_3)(-e_1 + 2e_1^2)ds = (-\frac{3}{6} + \frac{1}{12} + \frac{1}{12} + \frac{6}{10} - \frac{2}{30} - \frac{2}{30}) = \frac{2}{15}A$$

Substituting the matrix $\underline{S}$ into eq. (8.74), the coefficients of the cartesian coupling stiffness matrix can be calculated from

$$\underline{K}_{AB} = 2\Pi A \, (\underline{K}_{NT(ex)} \; \underline{B} \; \underline{O} \; \underline{C})^t \underline{S} \tag{8.76}$$

Finally, to construct the total cartesian stiffness matrix for the TRIAX 6 element as defined in eq. (8.29), the contributions from eqs. (8.65) and (8.72) and twice the contribution from eq. (8.76) must be superimposed.

8.3.6. NATURAL FORCE-DEFORMATION EQUATIONS

Using eqs. (8.28), the set of force-deformation equations underlying the natural modes analysis becomes

$$\sum_i^n \int_{S^i} \{\underline{A}^i \underline{B}^i \underline{O}^i \underline{C}^i \; \frac{1}{r} \; \underline{M}^i \underline{C}^i\} \, (\underline{G}^i \underline{H}^i)^t \underline{D}^i \underline{G}^i \underline{H}^i \cdot \{\underline{A}^i \underline{B}^i \underline{O}^i \underline{C}^i \; \frac{1}{r} \; \underline{M}^i \underline{C}^i\} \, rds \cdot \underline{u} = \underline{F} \tag{8.77}$$

where the global force vector $\underline{F}$ represents the superposition of the contributions from the thermal strains, the body pressure and the external forces, as defined in form by the four terms on the right hand side of eq. (8.20); $\underline{u}$ is the global displacement vector.

Employing eqs. (8.29) to (8.32) eq. (8.77) takes the final global matrix form

$$\underline{K} \cdot \underline{u} = \underline{F} \qquad (8.78)$$

where $\underline{K}$ is the (kxk) global stiffness matrix constructed from the superposition of n local contributions $\underline{K}^i$; k and n being the total numbers of nodes and elements, respectively.

8.4. CONCLUSIONS

In the process of recapitulating the progress of structural analysis in Chapters VI to VIII, the existence of a final state of the relevant analytic theories is discovered. Since the elliptic property encountered in the elastic behaviour leads to differential or integral equations which contain the field variable as insoluble space-dependent function, the development of finite element methods in structural analysis was overdue ~~for a long time.~~

The novalty brought by the finite element method manifests itself in the regression of space-dependent problems to merely topological ones. As regards structural analysis, the breakthrough lies in the transformation of element-wise space-dependent displacement functions to matrix expressions for scalar displacement values at discrete topological points.

During the solution procedure of the linear simultaneous force-deformation equations which are set up for grid points of suitably chosen finite element meshes, the nodal points lose their physical identity. The stiffness coefficients the displacement and the force components only satisfy topological criteria during the system analysis, i.e. their allocation to numeric arrays meets matrix and programming requirements only.

The first limitation of the analytic approach, the space-dendence or, in other words, the coupling between displacements and stiffness coefficients, is surmounted by the solution of node-oriented force-deformation matrix equations, which contain the stiffness coefficients, the displacement and the force components as scalars of three unconnected arrays.

The second limitation of the analytic approach, the impossibility of the field variables to take prescribed values

along the boundary, is overcome by substituting the node-wise approximated boundary conditions directly into the corresponding storage locations of the structure's global displacement and force vectors.

CHAPTER IX

COMPUTER AIDED ELASTIC ANALYSIS OF AXISYMMETRIC CONCRETE CONTINUA

9.1. PURPOSE

Owing to the nature of the theory of thermoviscoelasticity, as expounded in Chapter X, the successful creep analysis of concrete continua relies on the correct investigation into their initial elastic behaviour. Prior to the development of computer programs for viscoelastic and thermoviscoelastic analyses, it is pertinent therefore, to check the reliability of those program sections that yield the elastic solutions.

Both the classical and the natural deformation modes concepts of the finite element method, as derived in Chapter VIII, are applied to verify the elastic stresses occurring in a typical axisymmetric prestressed concrete pressure vessel due to internal gas pressure. Since no experiments on model pressure vessels were carried out, the two sets of approximate solutions are meant to check each other.

All programs were run on the CDC 6400 of the Imperial College Computer Centre.

9.2. COMPUTER PROGRAMS

9.2.1. FORTRAN SOURCE DECKS

The source programs I and II designed by the author in FORTRAN language for the analysis of elastic axisymmetric continua, using TRIAX 3 and TRIAX 6 elements respectively, consist of about 2000 cards each and are structurally very complex. Thus the detailed description of their logic falls beyond the scope of this work. For reference, however, the listing of Programs I and II was published in ([44]).

Apart from internal gas pressure, for which the global stress components activated in a typical vessel are graphically displayed as fields in figs. (9.7) to (9.24), the loading cases accepted by Programs I and II may constitute gravitational loads, conventional external forces, prestress, settlement of

supports, and thermal loads due to either stationary or transient temperature distributions.

9.2.2. DATA PROCESSING

Naturally, the computer print-outs contain the numeric results in any quantity desired. Irrespective of the degree of order and clarity in the layout of the results, this easily leads to an excess of information which engineers who are not familiar with computer programming and the finite element school of thought will fail to handle.

In addition to the creation of well-documented and computationally efficient computer programs, with well-conceived notions of the function of each subroutine and programs fragment, the author thus sees the original contribution to the numerical analysis of complex axisymmetric structures in the development of high-powered calcomp plotting-routines for the graphical processing of output data.

The routines which were created for the purpose of surmounting the above mentioned difficulties existing at the interface between systems analysis by computer programming and the analyst's task of assessing and utilizing the results, are called MESH, FEMESH, CONTRS, SURPLT and SURFIT. Their brief description is found in section 9.4.

9.3. CASE STUDY

9.3.1. VESSEL DESIGN

It has become increasingly attractive to use prestressed concrete for the construction of pressure vessels for gas-cooled reactors, the main reason being the required increase in their dimension.

Large nuclear power stations of high generating capacity produce electric energy relatively more cheaply than smaller ones. Higher capacity, however, means higher temperature of the graphite moderator which absorbs the kinetic energy released by fission fragments. For better heat transfer therefore, the gas coolant must circulate under higher pressure, higher temperature and in larger volumes.

Also, for reasons of economy and safety, it is desirable to enclose the whole radioactive primary circuit of gas cooling in the pressure vessel. As a result, thick-walled prestressed concrete pressure vessels of large diameters must be designed to sustain the induced mechanical and thermal stresses and to provide biological shielding against radioactive radiation.

In a case study, the elastic response of a typical continuum of this kind to internal gas pressure is analysed by employing the classical and the natural deformation modes concepts of the finite element method using Programs I and II.

9.3.2. VESSEL GEOMETRY

The geometry of the axisymmetric reactor pressure vessel, which is also considered symmetric with respect to its equatorial plane, is prescribed by the radius of the inner sphere r = 14.65 m, the maximum cylindrical radius R = 18.00 m and the semi-height h = 18.72 m. The physical properties are given by the modulus of elasticity of E = 40 KN/mm and the ratio of transverse contraction μ = 0.16.

Since the hoop stiffness in the natural deformation modes concept, as formulated in eq. (8.32), includes the integration over the term $\frac{1}{r}$, an instability in the determination of displacements is unavoidable as the radius tends to zero. As a measure against this mathematical limitation, the existence of a cut-out is imagined for the analysis using TRIAX 6 elements.

Though, after optimization, a cut-out of the radius r_c = 2.50 m was considered appropriate, the loss in surface area suffered by the inner sphere is still less than 3% and thus the geometry of the vessel is not falsified appreciably. In return to this slight modification of the vessel's configuration however, the error in the axial displacements near the axis of revolution is reduced from 130 to 40% ; the reference values being those obtained from the finite element analysis using TRIAX 3 elements. The optimization of the vessels geometry was discussed in detail in the author's presentation of the paper ([46]).

9.4. GRAPHICAL DISPLAY OF RESULTS

9.4.1. SILHOUETTES OF CONTINUUM

The upper half of the geometrical configuration of the pressure vessel and its equatorial plane presented in fig. (9.1) which is automatically drawn off-line from magnetic tape utilizing the author's surface plotting routine SURPLT. Due to the symmetry assumed with respect to the equatorial plane, the consideration of the upper half of the continuum is sufficient for the structural analysis, provided that zero displacement and a zero rate of change of displacements and temperatures across the equatorial plane is specified.

Also, fig. (9.1) is meant to expose the limitations encountered when drawing curved lines into or over rectangular grids. A better approximation than the one shown is only accomplished by the use of finer meshes, thus, at the expense of a rapid increase in computing time. It is hoped therefore that the approximate reproduction of curves by polygons is appreciated.

To stimulate the realization that ring-shaped finite elements for the axisymmetric analysis may be represented by their cross-sectional configuration in a longitudinal centroidal plane, without actually degenerating to planar elements, fig. (9.2) shows the silhouette of a centroidal plane, in which the triangular-sectioned TRIAX 3 and TRIAX 6 elements may appear.

Secondly, fig. (9.2) discloses that the routine SURPLT, which is described in section 9.4.4, is incapable of drawing truly vertical lines, as only one surface point can be allocated to each intersection of the rectangular grid.

9.4.2. FINITE ELEMENT MESHES

With the silhouette of the concrete continuum in mind, the discretization of the structure into finite elements may be embarked upon. Owing to the inherent symmetry of the continuum with respect to its axis of revolution and its equatorial plane, the tracing out of cross-sectional lines of finite elements in the first quadrant is quite sufficient.

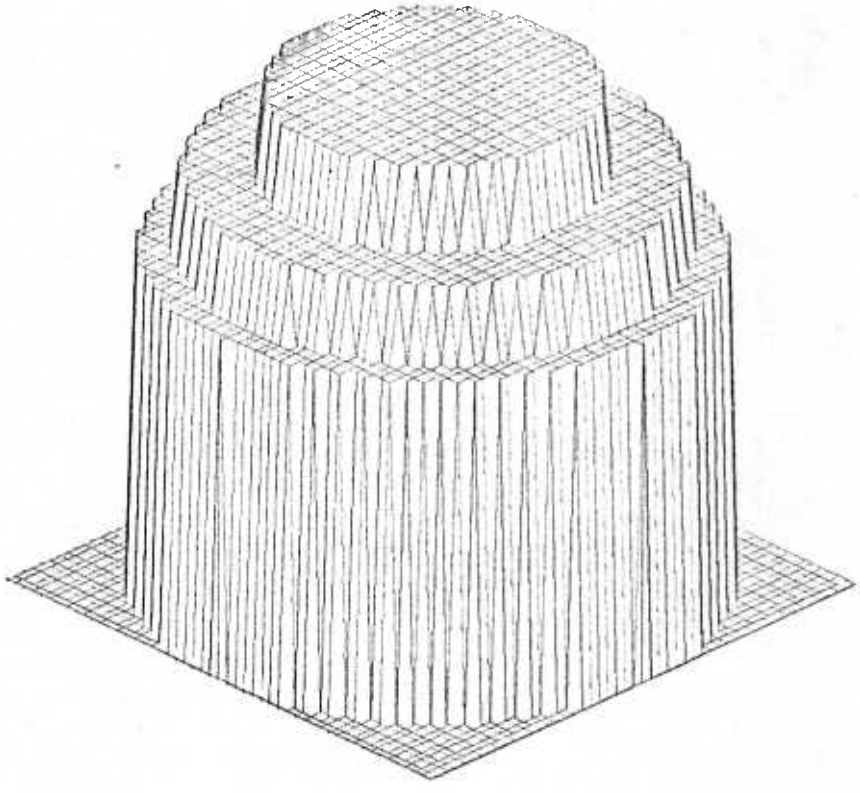


Fig. (9.1) Silhouette of upper half of concrete pressure vessel R = 18.00 m h = 18.72 m

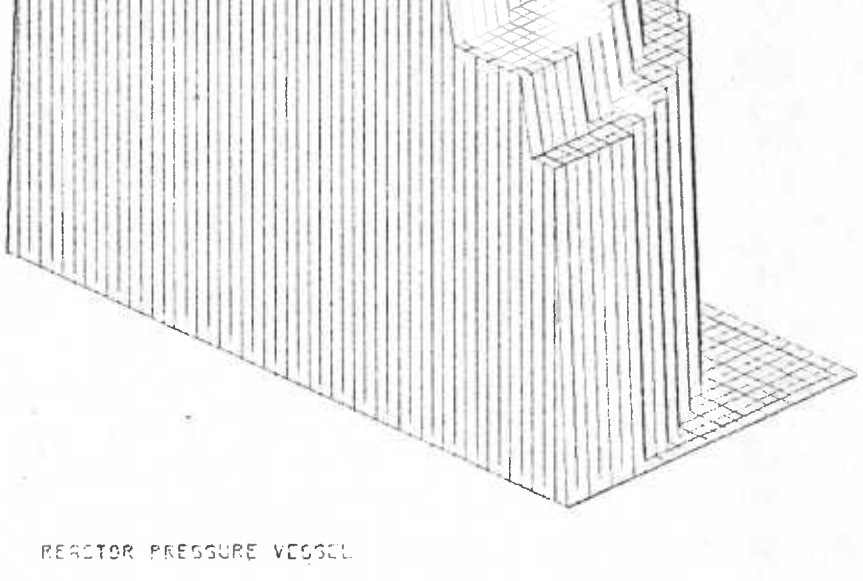


Fig. (9.2) Silhouette of longitudinal cross-section of concrete pressure vessel

R = 18.00 m h = 18.72 m

Figs. (9.3) and (9.5) display the topological meshes for the axisymmetric analysis using TRIAX 3 and TRIAX 6 elements respectively. The meshes shown are generated by utilizing the author's plotting routine FEMESH, which here also identifies the finite elements and the created nodal points by individual series of integer numbers starting with one.

As may be seen, the classical modes analysis uses 287 TRIAX 3 elements associated with 172 nodes, while the natural modes analysis does with 25 TRIAX 6 elements and 22 major nodal points. The high ratio of nearly 12 which is arrived at by comparing the number of elements used in the two different approaches should be borne in mind when assessing the quality of the finite element solutions in the following sections.

The finite element meshes of figs. (9.3) and (9.5) are reproduced in figs. (9.4) and (9.6) respectively, this time in order to convey the geometrical information by assigning numerical values in cm to the radial and axial coordinates of the nodal points.

9.4.3. CONTOURS OF STRESS FIELDS

A subroutine called CONTRS which generates a plot was developed by the author to draw temperature, displacement, strain and stress fields into the topological configuration of the cross-sections of the vessel investigated. It is based on a path finding technique and assigns an identifying value to each contour that hits the boundary.

The plotting, as for all calcomp routined developed, is done off-line from magnetic tape and is performed by a digital incremental plotter, consisting of a revolving drum and a pen mechanism which moves at right angles to the motion of the drum.

The routine only accepts input data allocated to points of evenly gridded rectangular meshes; manually and automatically generated finite element meshes, however, are almost always irregular due to oddly shaped geometries or for reasons of convergence. This contradiction between ideal and existing

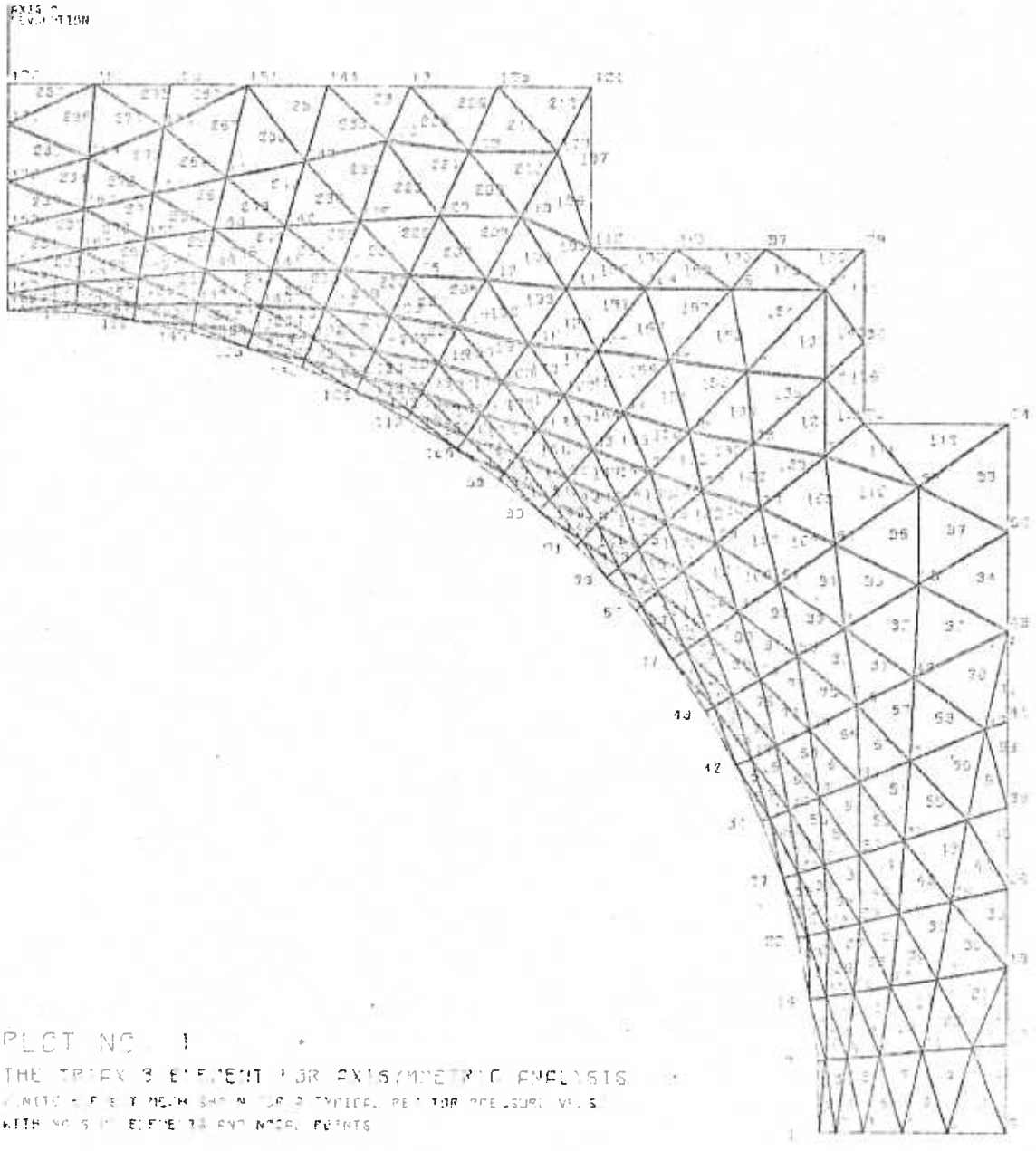


Fig. (9.3) Topological mesh for axisymmetric analysis using TRIAX 3 elements Scale 1:125

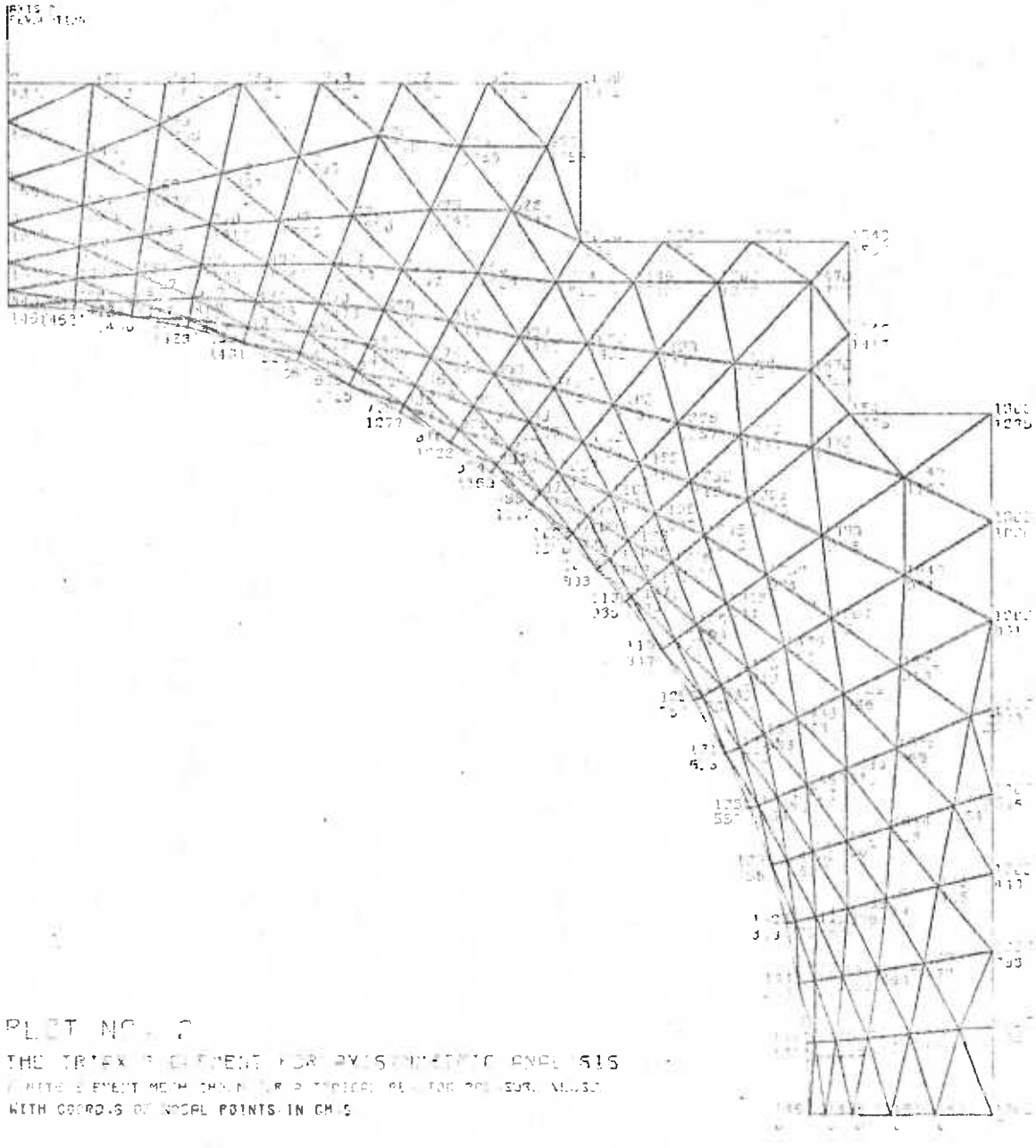


Fig. (9.4) Geometrical mesh for axisymmetric analysis using TRIAX 3 elements Scale 1:125

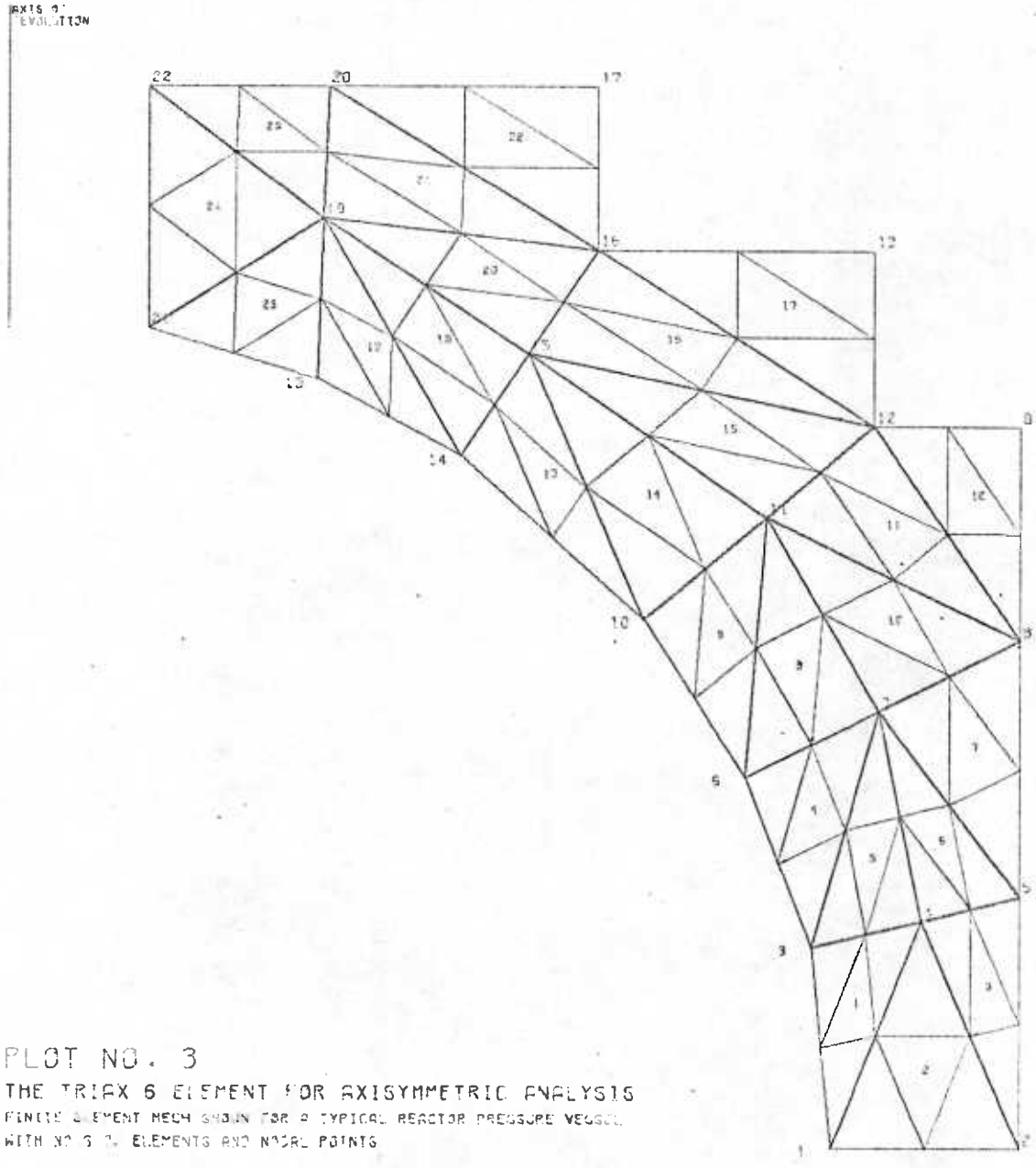


Fig. (9.5) Topological mesh for axisymmetric analysis using TRIAX 6 elements Scale 1:125

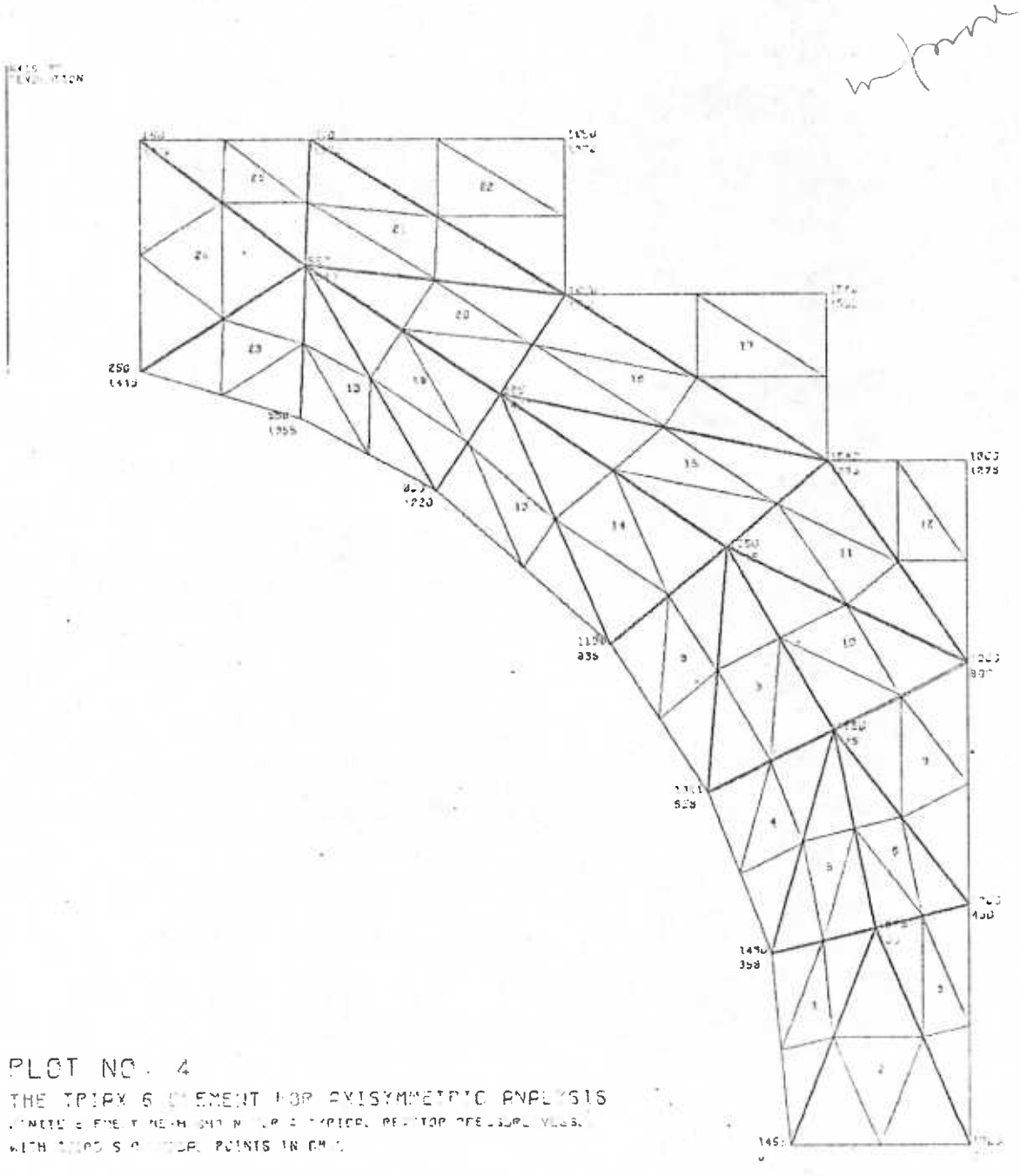


Fig. (9.6) Geometrical mesh for axisymmetric analysis using TRIAX 6 elements Scale 1:125

meshes is overcome by the introduction of interpolating surface functions for the fields to be drawn and by their subsequent evaluation at the grid points employing the author's routine MESH.

In figs. (9.7) to (9.18), the radial, axial, shear, hoop and principle stress fields developing in the concrete pressure vessel as an elastic response of the structure to the presence of internal gas pressure are represented by contours which are generated by virtue of the combined implementation of the routines MESH and CONTRS. The contour values are multiples of 5 N/mm^2 and positive or negative to indicate the existence of either tensile or compressive stresses.

9.4.4. SURFACES OF STRESS FIELDS

Engineering feeling is the most important asset in the initial estimation of the potential structural behaviour especially of complex continua such as prestressed concrete pressure vessels, where decisions on the vessel shape, the wall thickness, the quantity and location of prestress, etc. must be made at the same time.

Owing to the availability of digital computers of increasing storage and speed and the rapid development of finite element computer techniques, however, the engineer has largely grown away from viewing structural problems phenomenologically. In addition, the general physical insight into what is happening mechanically in the structure is easily lost due to the tremendous volumes of locally applicable, numerical output data obtained from computer-aided finite element analyses.

Since computer programming relieves the engineer from the burden of carrying out structural analyses in the labourious long-hand writing, it has thus become even more important to cultivate his intuitive quality, in order to enable him to assess confidently the applicability of the results and hence the safety of the structure.

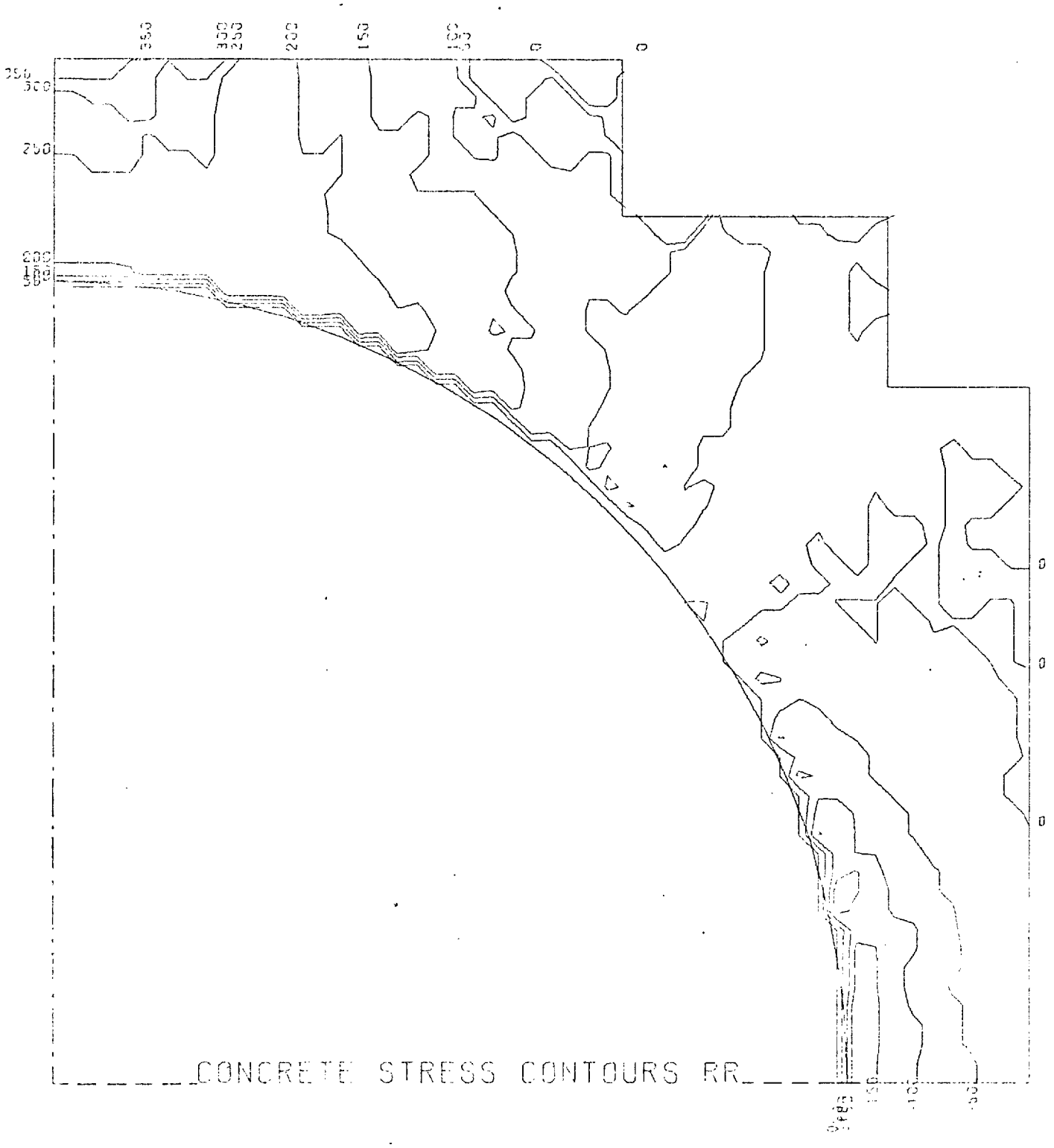


Fig. (9.7) Contours of elastic radial stresses due to internal gas pressure of 2 N/mm^2 using TRIAX 3 elements (in 0.1N/mm^2 or kp/cm^2)



Fig. (9.8) Contours of elastic radial stresses due to internal gas pressure of 2 N/mm^2 using TRIAX 6 elements (in 0.1 N/mm^2 or kp/cm^2)

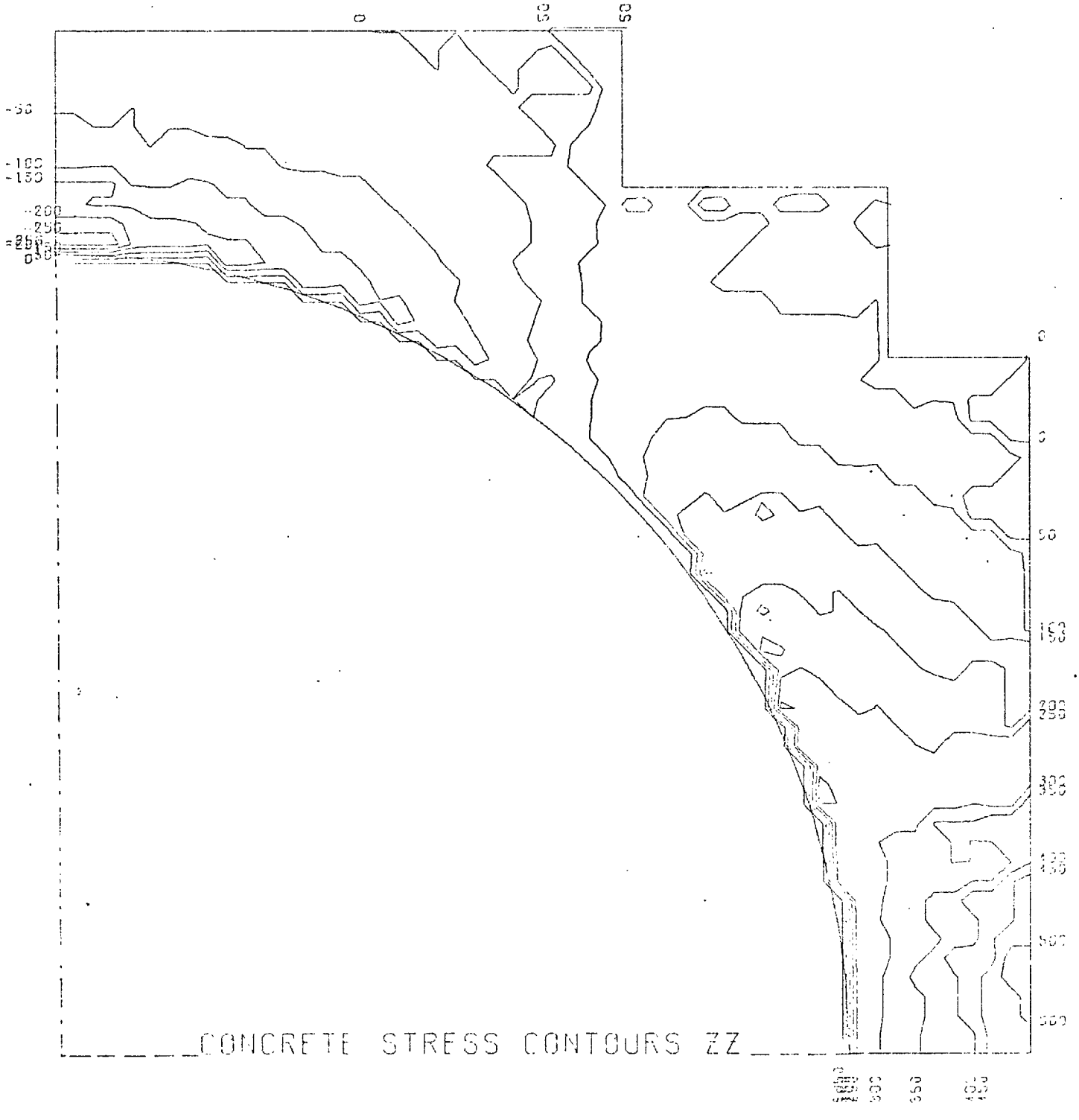


Fig. (9.9) Contours of elastic axial stresses due to internal gas pressure of 2 N/mm^2 using TRIAX 3 elements (in 0.1 N/mm^2 or kp/cm^2)

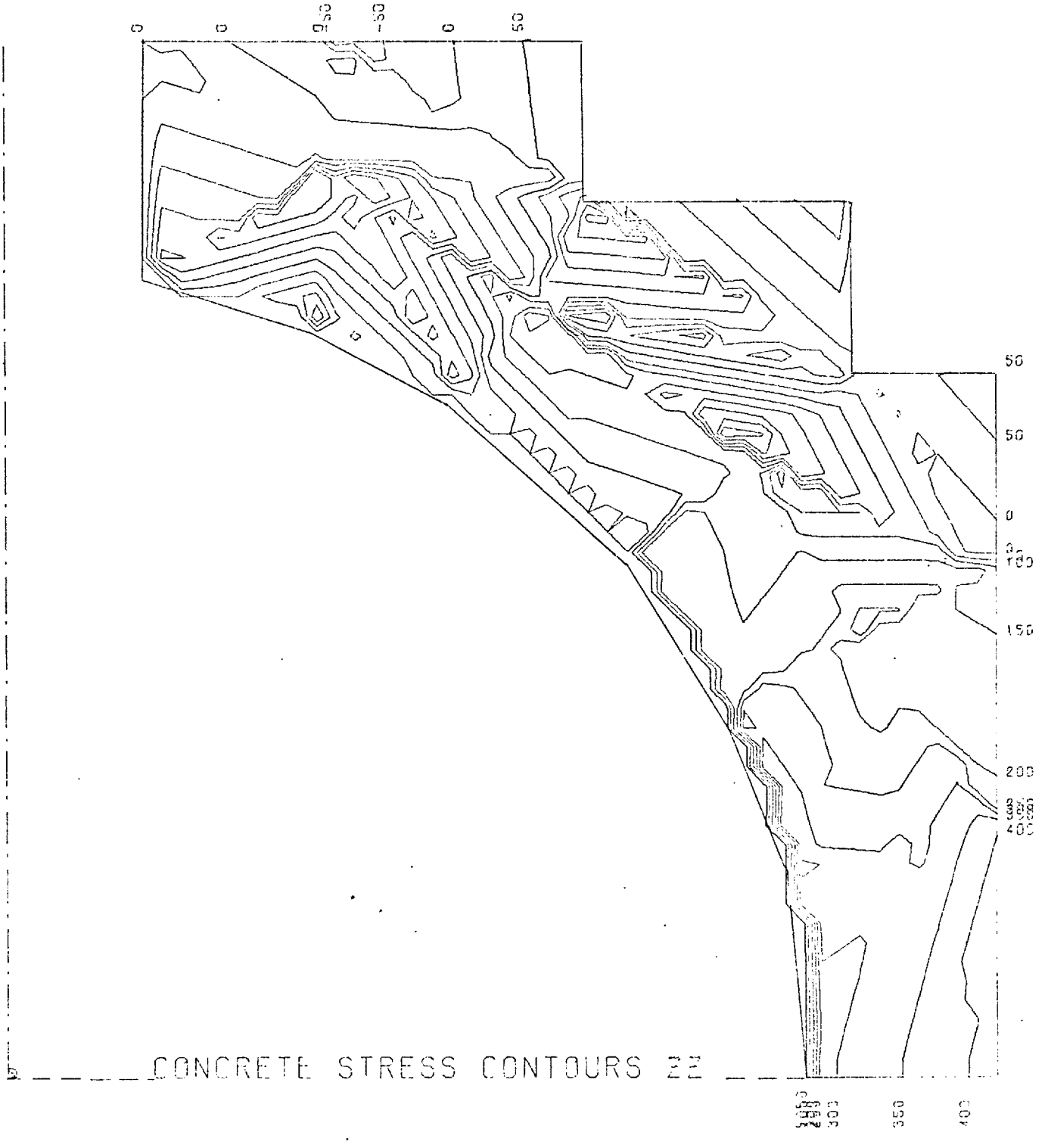


Fig. (9.10) Contours of elastic axial stresses due to internal gass pressure of 2 N/mm^2 using TRIAX 6 elements (in 0.1 n/mm^2 or kp/cm^2)

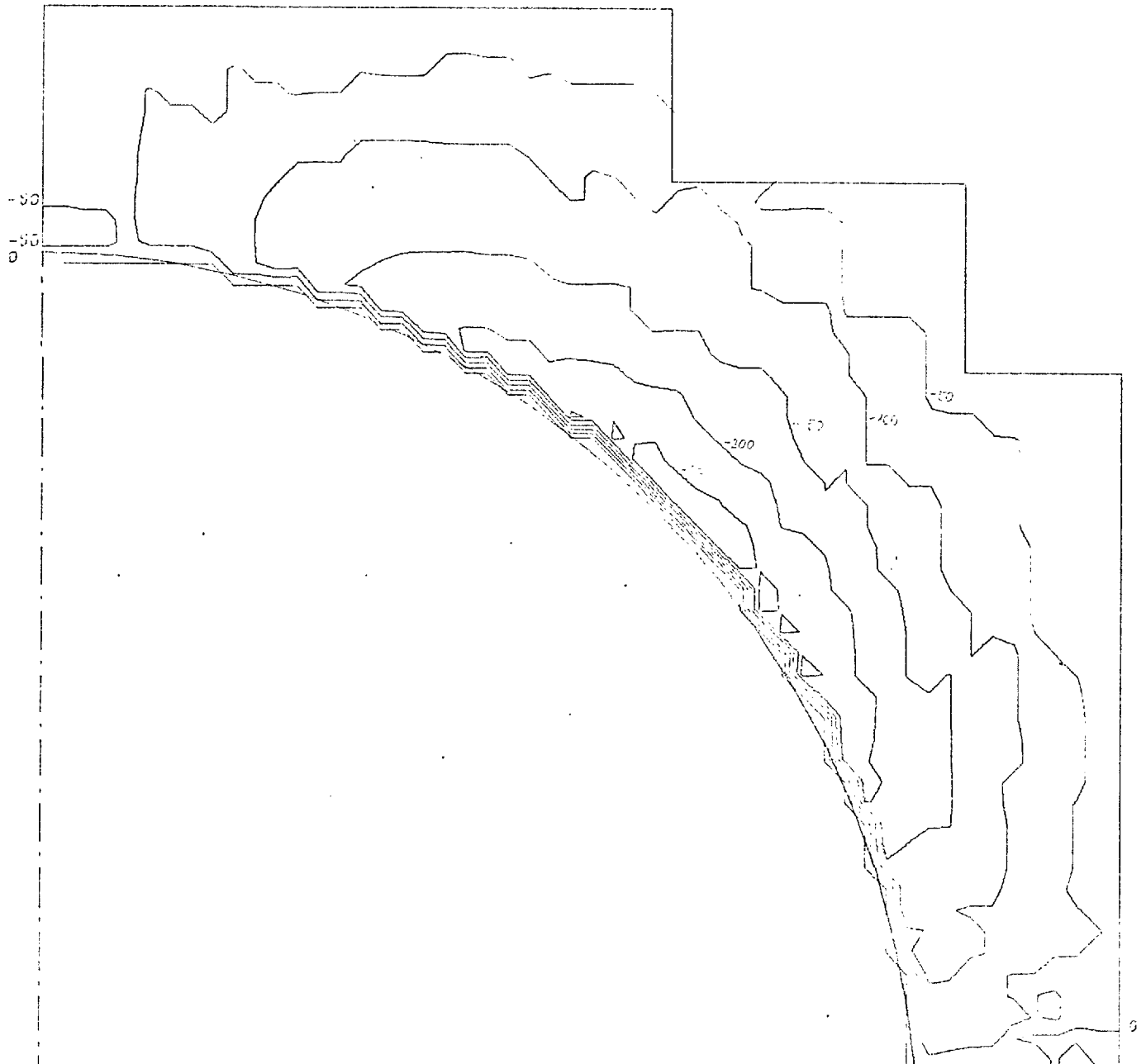


Fig. (9.11) Contours of elastic shear stresses due to internal gas pressure of 2 N/mm^2 using TRIAX 3 element (in 0.1 N/mm^2 or kp/cm^2)

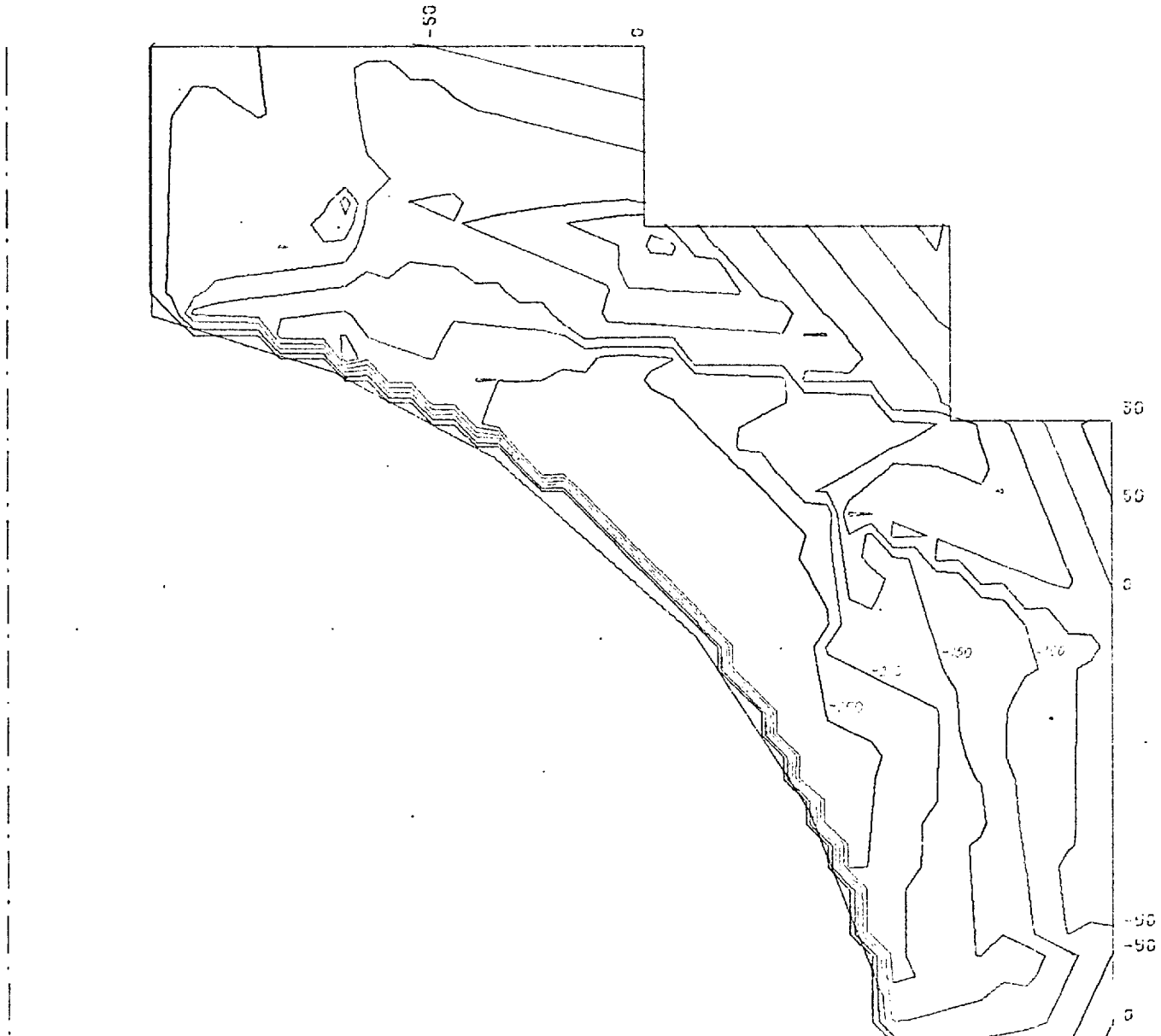


Fig. (9.12) Contours of elastic shear stresses due to internal gas pressure of 2 N/mm^2 using TRIAX 6 elements (in 0.1 N/mm^2 or kp/cm^2)

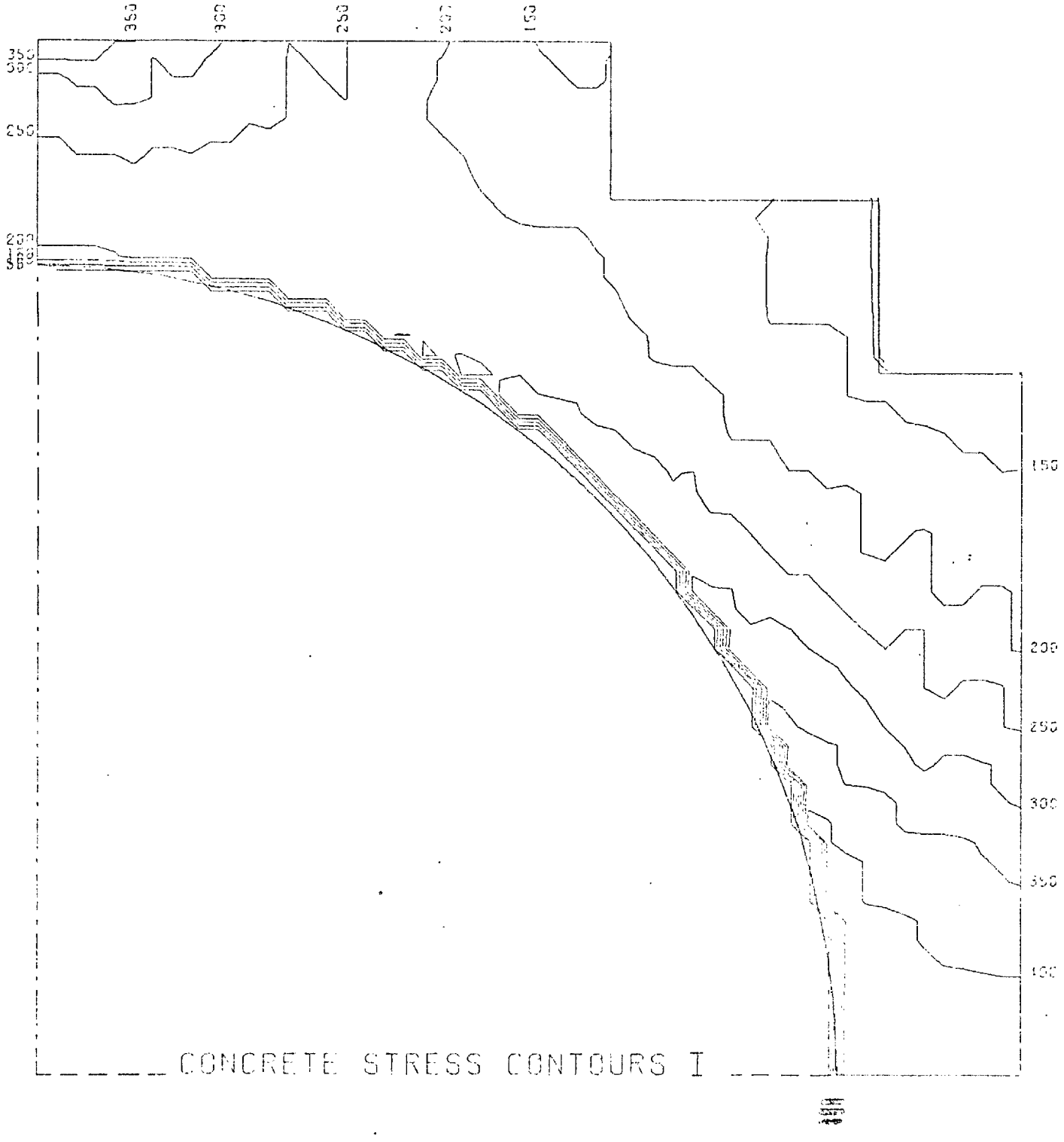


Fig. (9.13) Contours of elastic hoop stresses due to internal gas pressure of 2 N/mm^2 using TRIAX 3 elements (in 0.1 N/mm^2 or kp/cm^2)

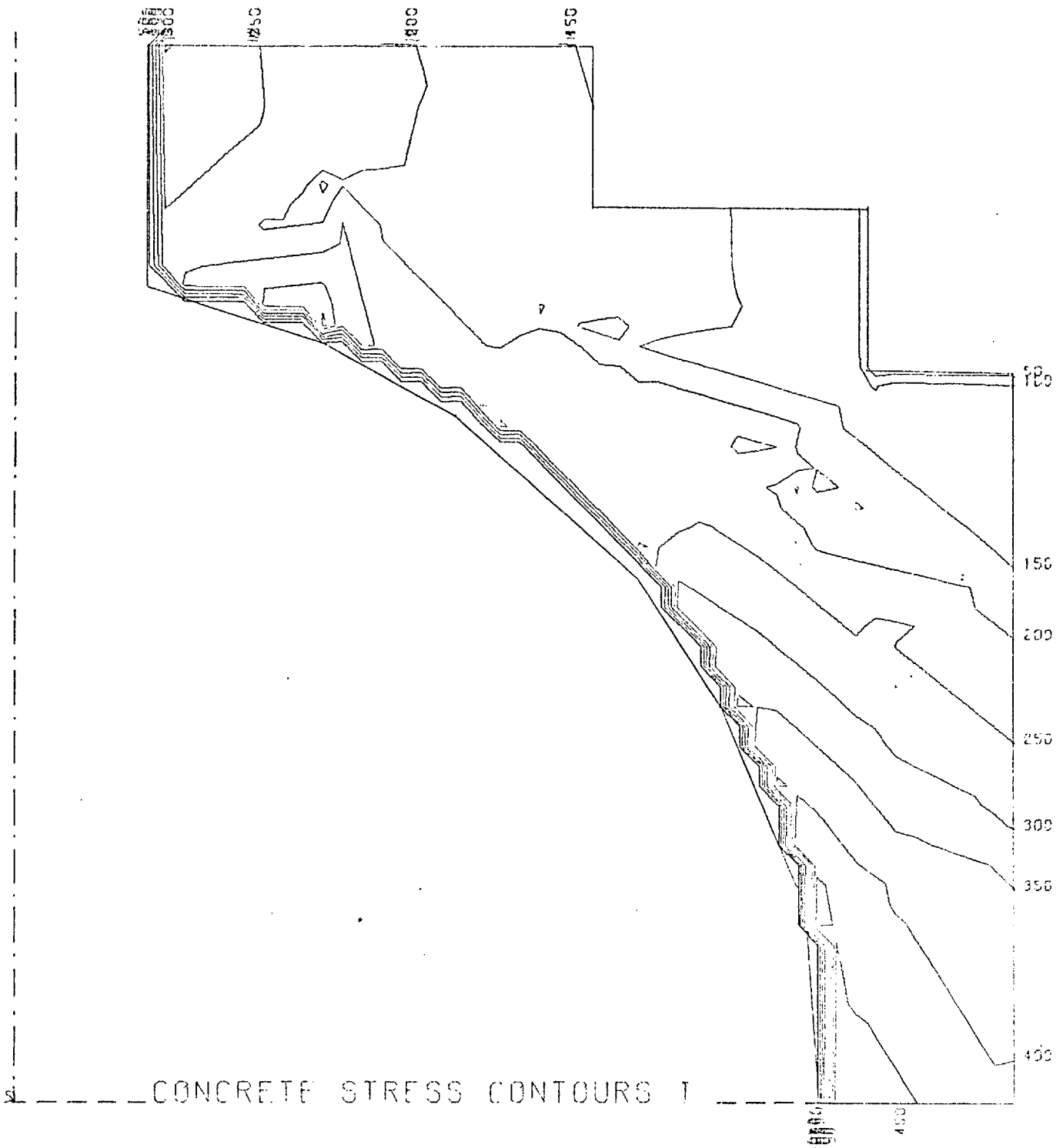


Fig. (9.14) Contours of elastic hoop stresses due to internal gas pressure of 2 N/mm^2 using TRIAX 6 elements (in 0.1 N/mm^2 or kp/cm^2)

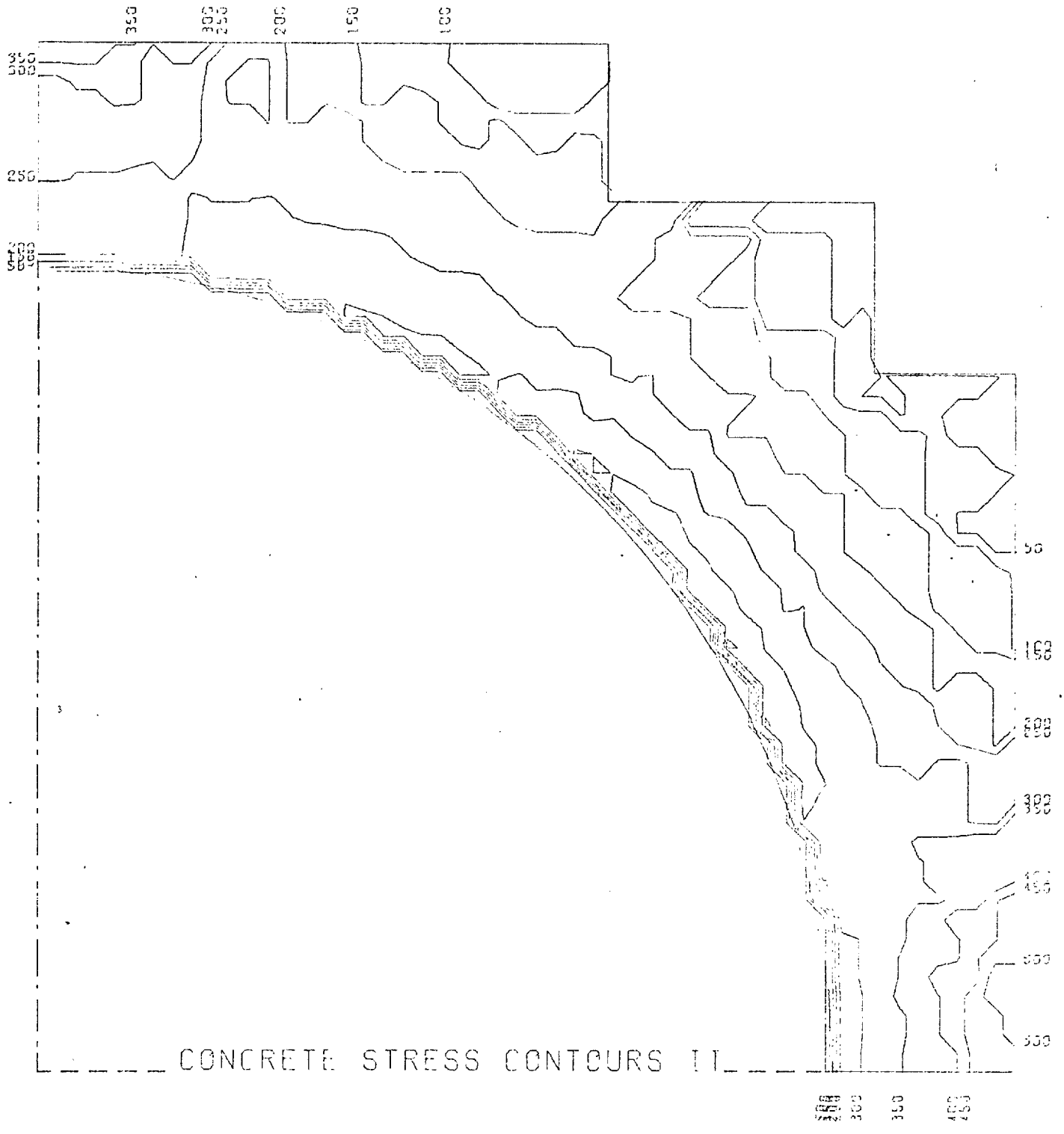


Fig. (9.15) Contours of elastic major principle stresses due to internal gas pressure of 2 N/mm^2 using TRIAX 3 elements (in 0.1 N/mm^2 or kp/cm^2)

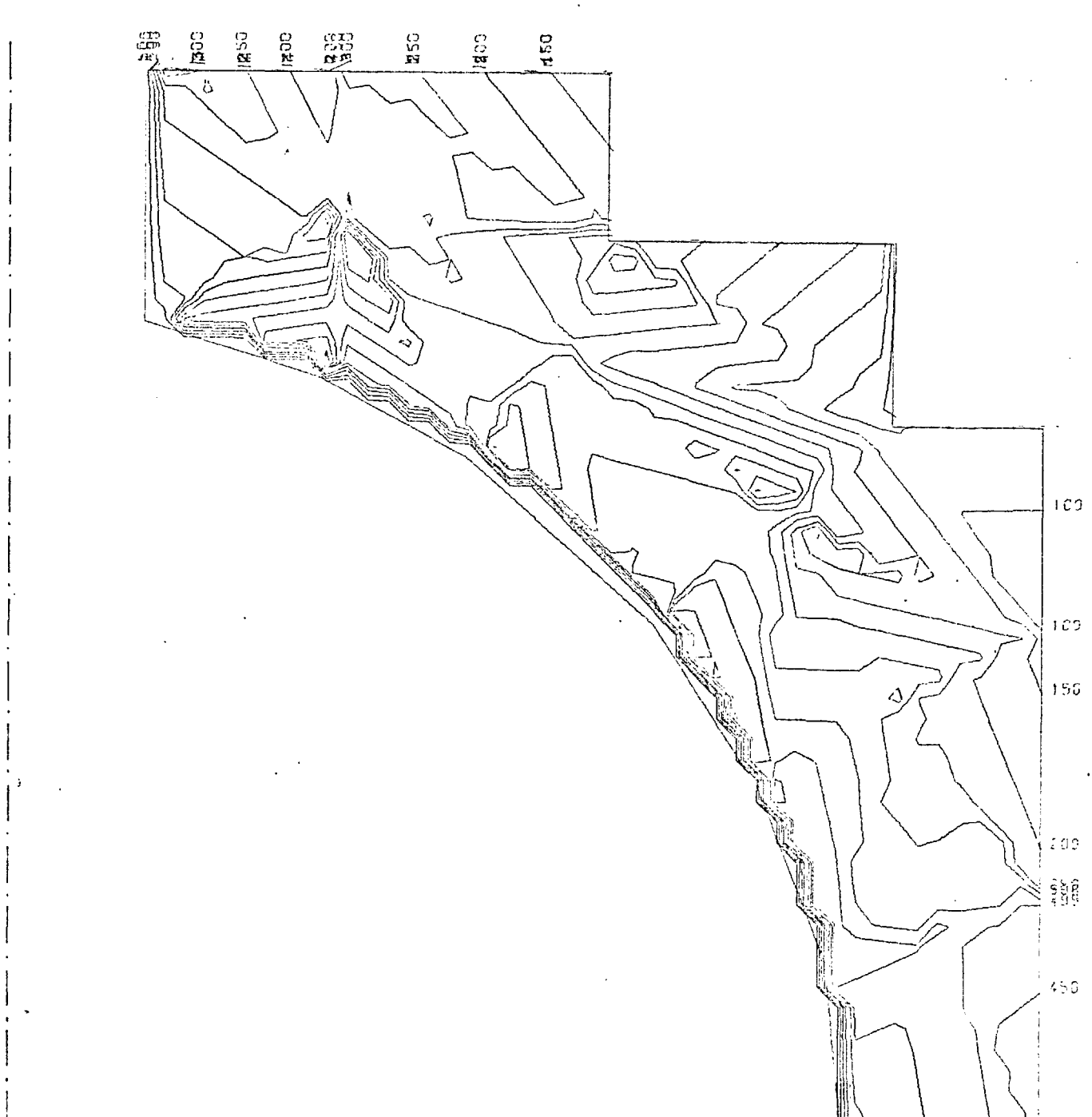


Fig. (9.16) Contours of elastic major principle stresses due to internal gas pressure of 2 N/mm^2 using TRIAX 6 elements (in 0.1 N/mm^2 or kp/cm^2)

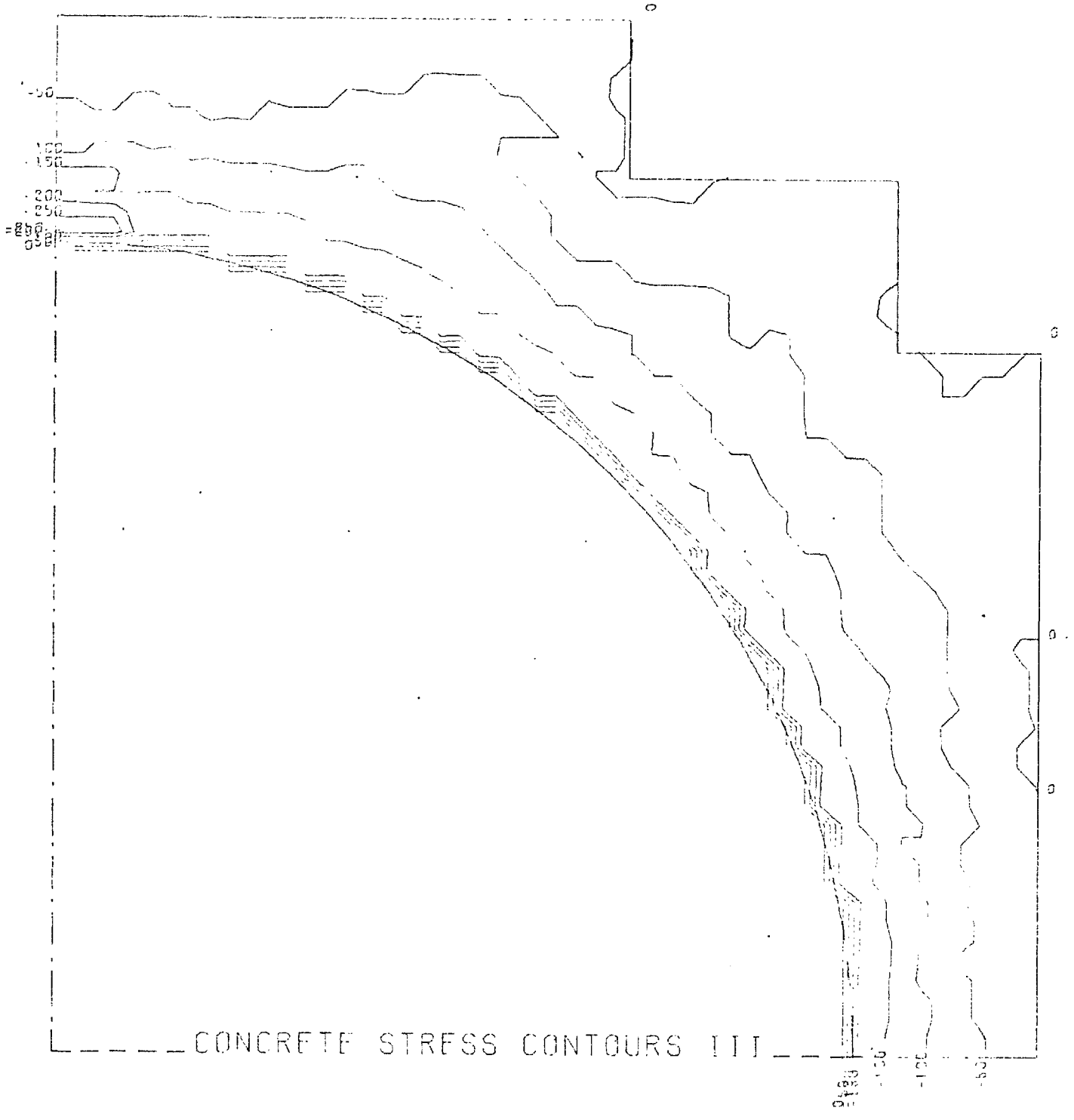


Fig. (9.17) Contours of elastic minor principle stresses due to internal gas pressure of 2 N/mm^2 using TRIAX 3 elements (in 0.1 N/mm^2 or kp/cm^2)

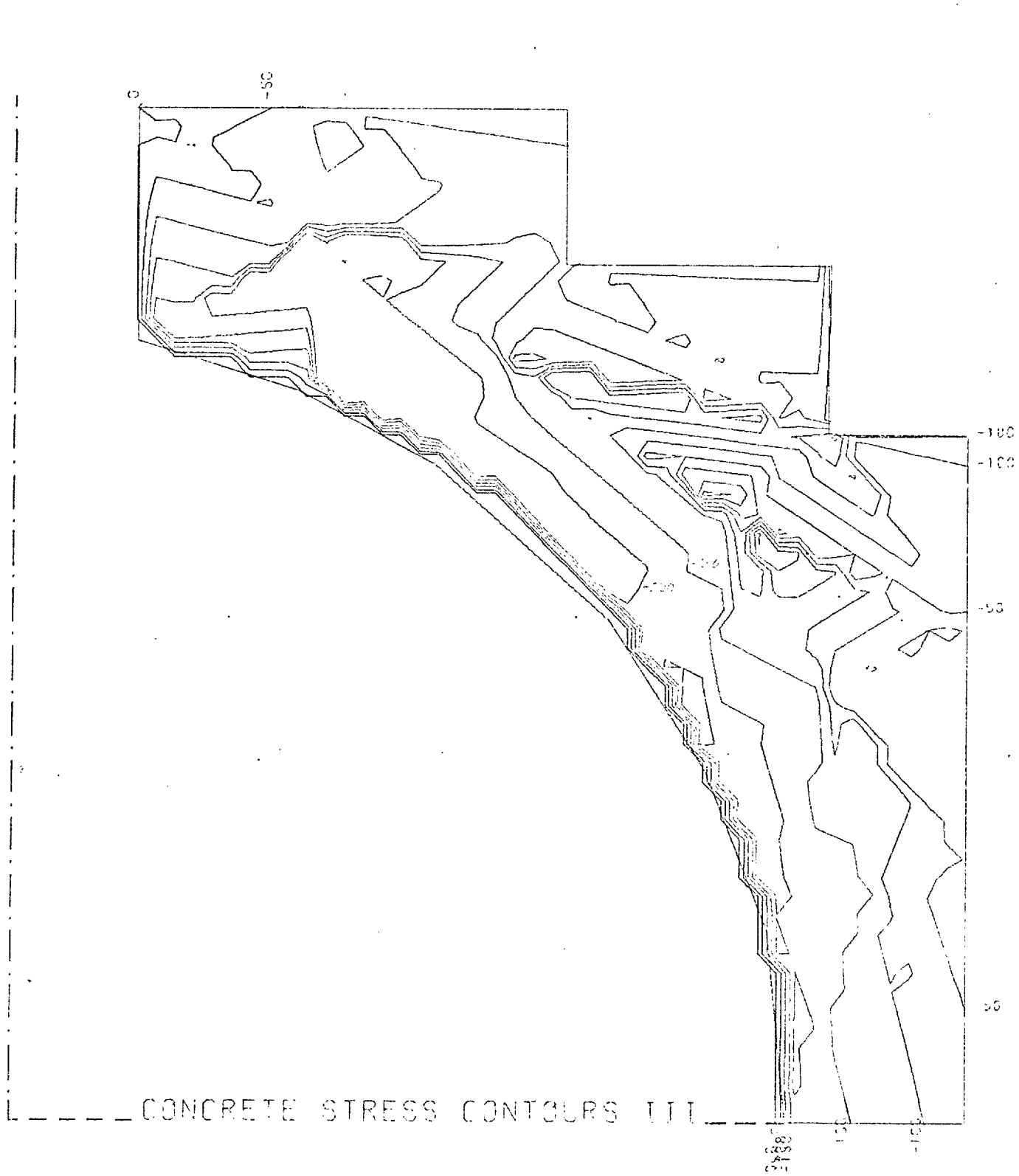


Fig. (9.18) Contours of elastic minor principle stresses due to internal gas pressure of 2 N/mm^2 using TRIAX 6 elements (in 0.1 N/mm^2 or kp/cm^2)

To foster this endeavour, the author has originated the routine SURPLT which graphically displays sets of evenly gridded data as isometric surfaces. Depending on the general slopes of the field functions to be illustrated, SURPLT allows the isometric surfaces to be viewed from six different points. These are the four corners of the rectangular grid and the two corners formed cutting the surfaces vertically along one of the two topological centre lines.

Thus the visual assessment of the results is made possible without being distracted by numerical values, inferring that the geometrical and structural optimization process for the continuum may be accelerated by the adoption of a semi-analytic, semi-visual procedure. The process of alternately rejecting results and improving the concept is continued to the designer's satisfaction. Having finally approved of a particular design, stress fields and displacement configuration may be displayed by calling the routine SURPLT and evaluated numerically by implementing the routine CONTRS.

Figs. (9.19) to (9.30) show the radial, axial, shear, hoop and principle stress fields arising in the concrete pressure vessel due to the loading case investigated. The figures depict alternately the solutions yielded by the classical and the natural deformation modes concept of the finite element method. The minimum and maximum values of the stress surfaces, followed by the numbers of the corresponding elements in brackets, are given in the captions of the figures. Because of the linear variation of stress occurring in the TRIAX 6 elements, for the natural modes analysis also the number of the relevant major node is entered in the brackets.

9.4.5.FUNCTIONS OF STRESS FIELDS

Another way of making convincing representation of the results obtained from finite element analyses is to describe cartesian surface polynomials, which enable temperature, displacement, strain and stress fields to be reproduced graphically by plotting the functional relation existing between a few computed coefficients. The mathematical

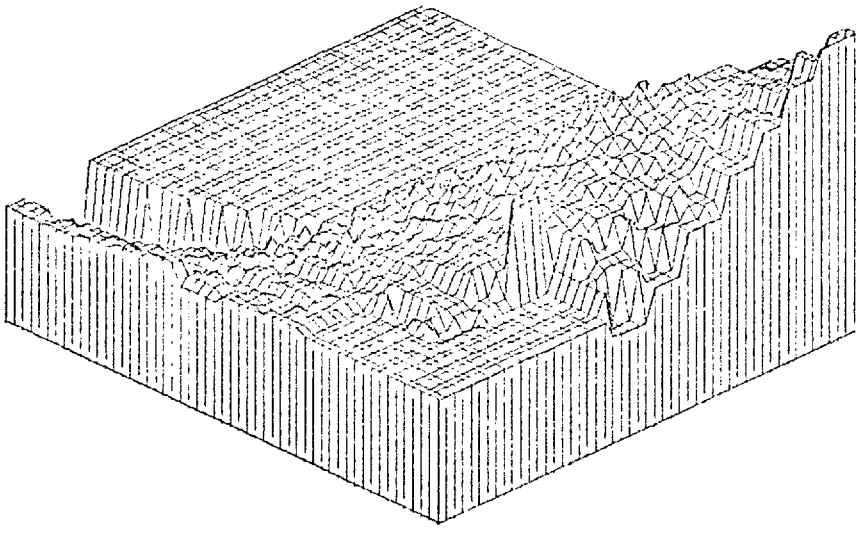


Fig. (9.19) Surface of elastic radial stresses due to internal gas pressure of 2 N/mm^2 using TRIAX 3 elements
σ_{min} = - 1.9 N/mm^2 (1) σ_{max} = 3.5 N/mm^2 (287)

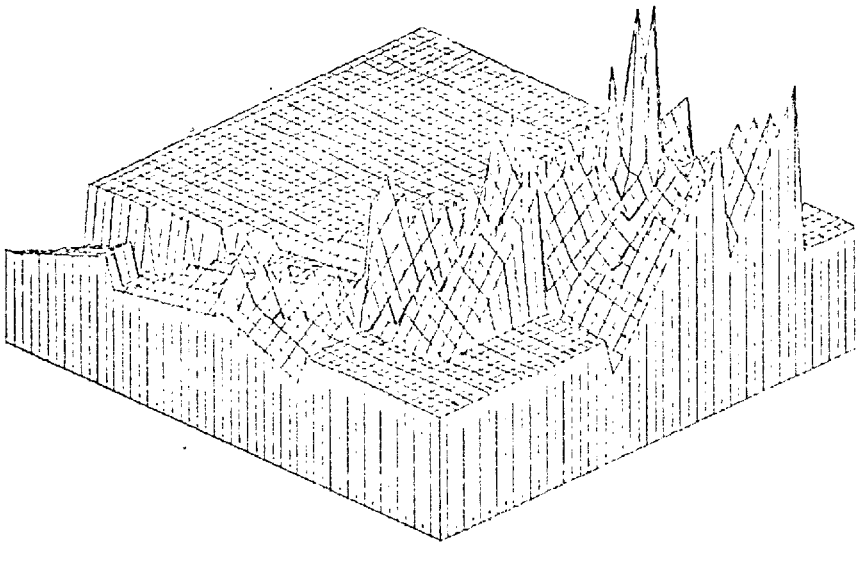
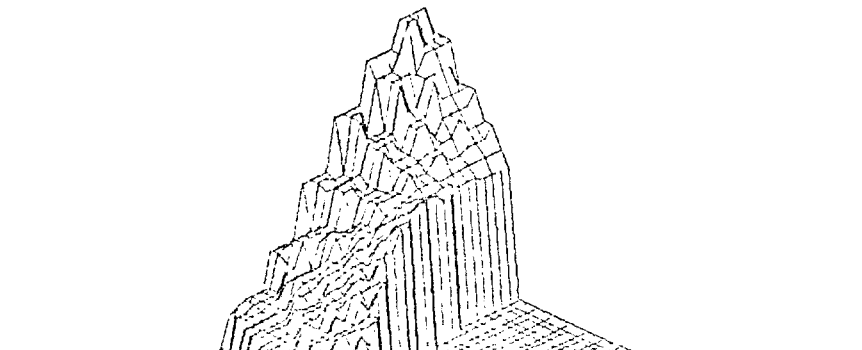
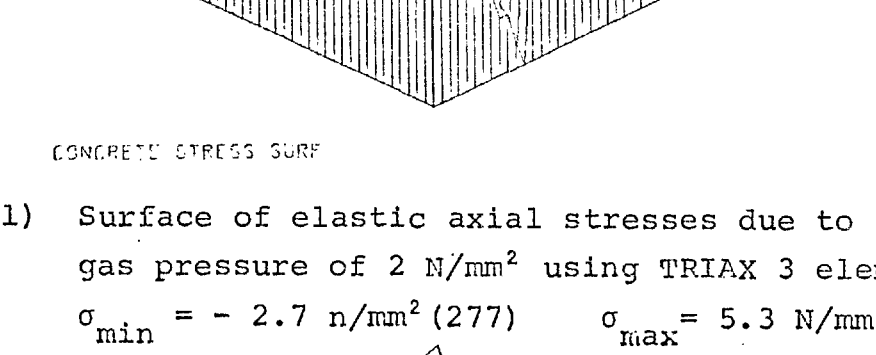


Fig. (9.20) Surface of elastic radial stresses due to internal gas pressure of 2 N/mm^2 using TRIAX 6 elements
σ_{min} = - 2.1 N/mm^2 (1,1) σ_{min} = 3.5 N/mm^2 (25,3)



CONCRETE STRESS SURF

Fig. (9.21) Surface of elastic axial stresses due to internal gas pressure of 2 N/mm^2 using TRIAX 3 elements
σ_{min} = - 2.7 n/mm^2 (277) σ_{max} = 5.3 N/mm^2 (11)



CONCRETE STRESS SURF

Fig. (9.22) Surface of elastic axial stresses due to internal gas pressure of 2 N/mm^2 using TRIAX 6 elements
σ_{min} = - 3.5 N/mm^2 (20,3) σ_{max} = 5.0 N/mm^2 (3,1)

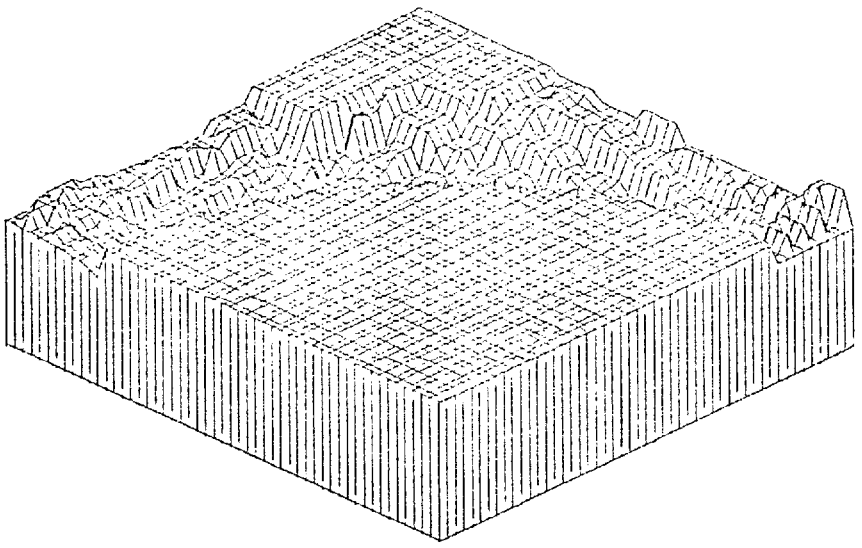


Fig. (9.23) Surface of elastic shear stresses due to internal gas pressure of 2 N/mm^2 using TRIAX 3 elements
σ_{min} = - 2.9 N/mm^2 (99) σ_{max} = 0.2 N/mm^2 (11)

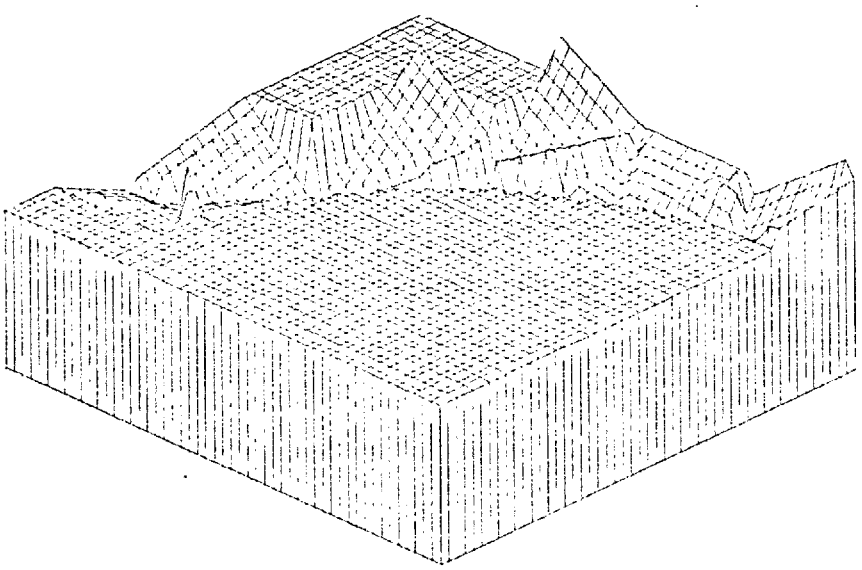


Fig. (9.24) Surface of elastic shear stresses due to internal gas pressure of 2 N/mm^2 using TRIAX 6 elements
σ_{min} = - 3.7 N/mm^2 (13,3) σ_{max} = 1.2 N/mm^2 (3,1)

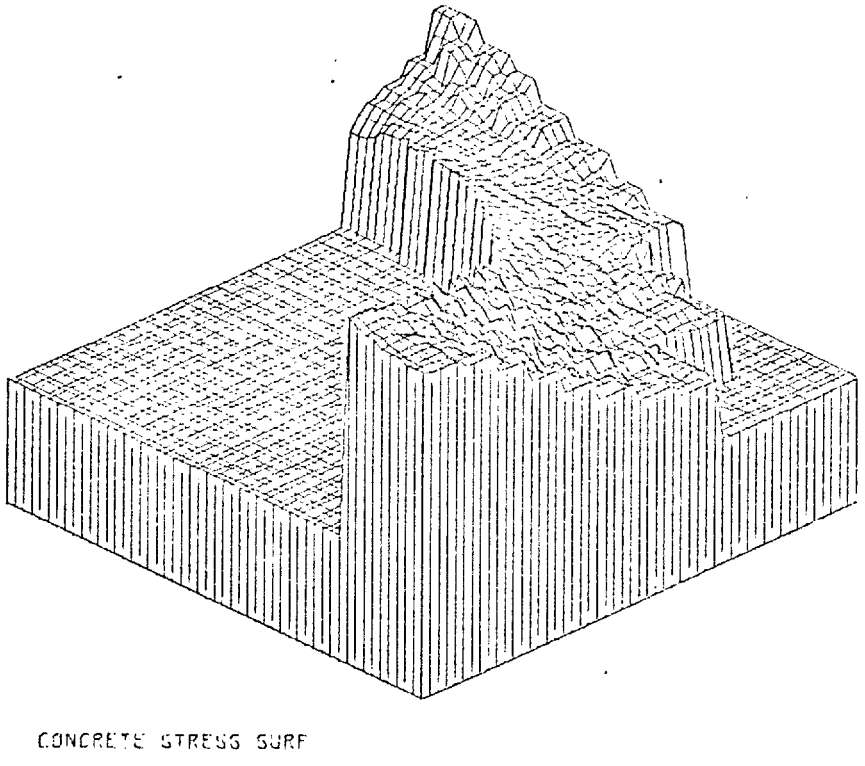


Fig. (9.25) Surface of elastic hoop stresses due to internal gas pressure of 2 N/mm^2 using TRIAX 3 elements
σ_{min} = 1.2 N/mm^2 (98) σ_{max} = 4.4 N/mm^2 (1)

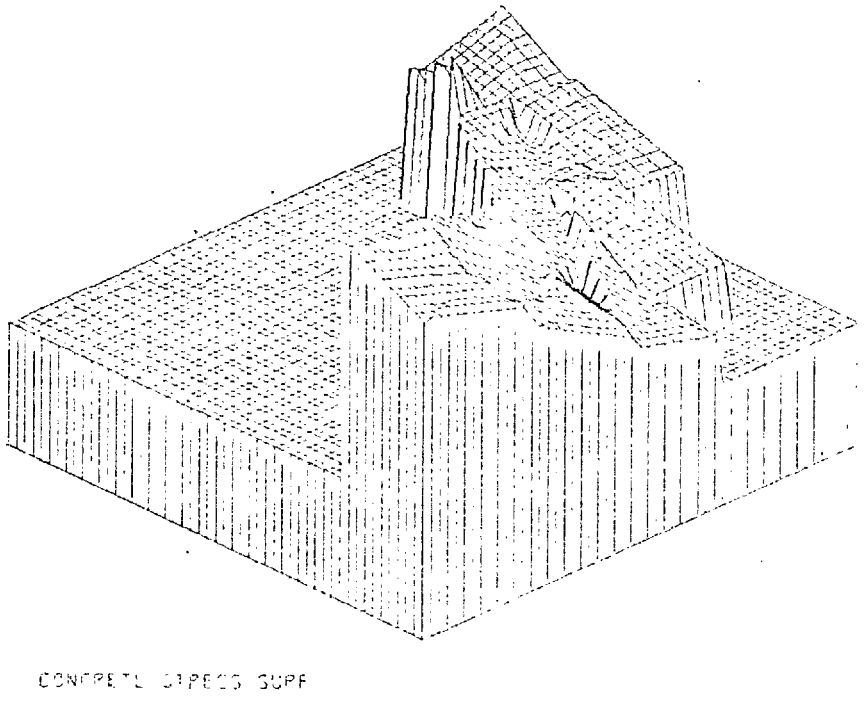


Fig. (9.26) Surface of elastic hoop stresses due to internal gas pressure of 2 N/mm^2 using TRIAX 6 elements
σ_{min} = 0.9 N/mm^2 (15,2) σ_{max} = 4.8 N/mm^2 (2,1)

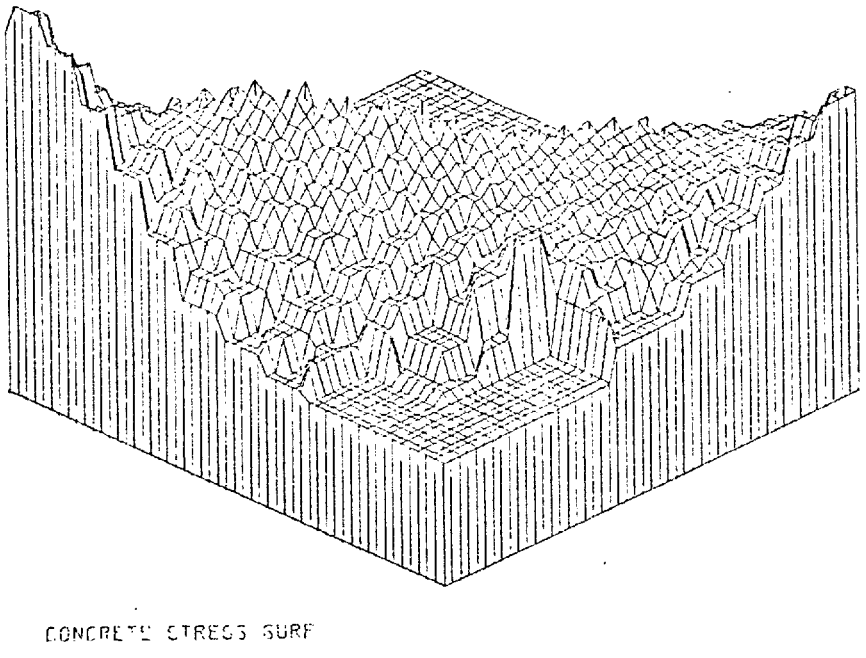


Fig. (9.27) Surface of elastic major principle stresses due to internal gas pressure of 2 N/mm^2 using TRIAX 3 elements σ_{min}=0.1 N/mm^2 (155) σ_{max}=5.4 N/mm^2 (11)

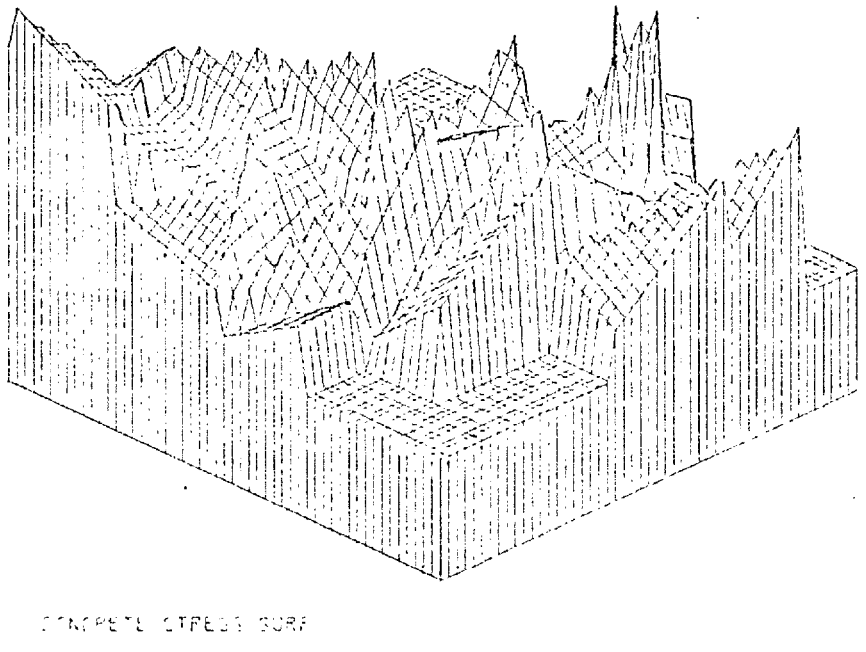


Fig. (9.28) Surface of elastic major principle stresses due to internal gas pressure of 2 N/mm^2 using TRIAX 6 elements σ_{min} = - 0.1 N/mm^2 (23,2) σ_{max} = 5.4 N/mm^2 (15,1)

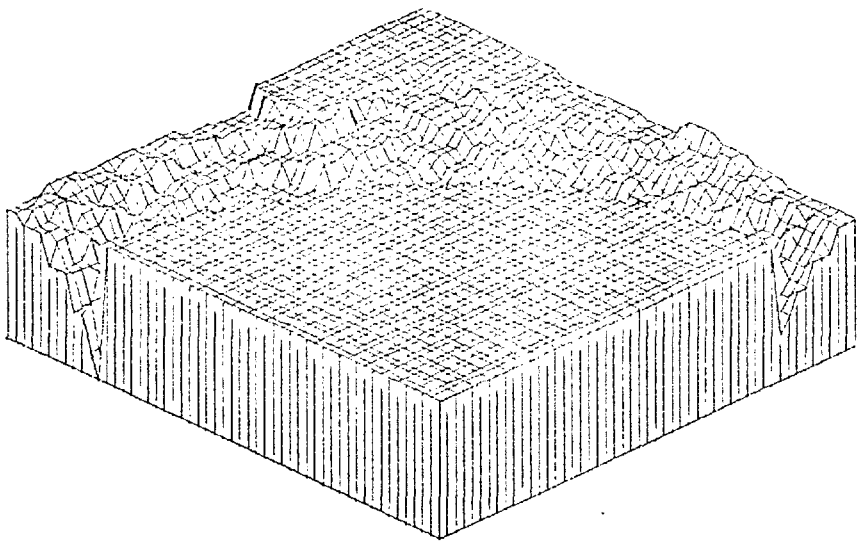


Fig. (9.29) Surface of elastic minor principle stresses due to internal gas pressure of 2 N/mm^2 using TRIAX 3 elements σ_{min} = - 2.0 N/mm^2 (142) σ_{max} = 0.1 N/mm^2 (183)

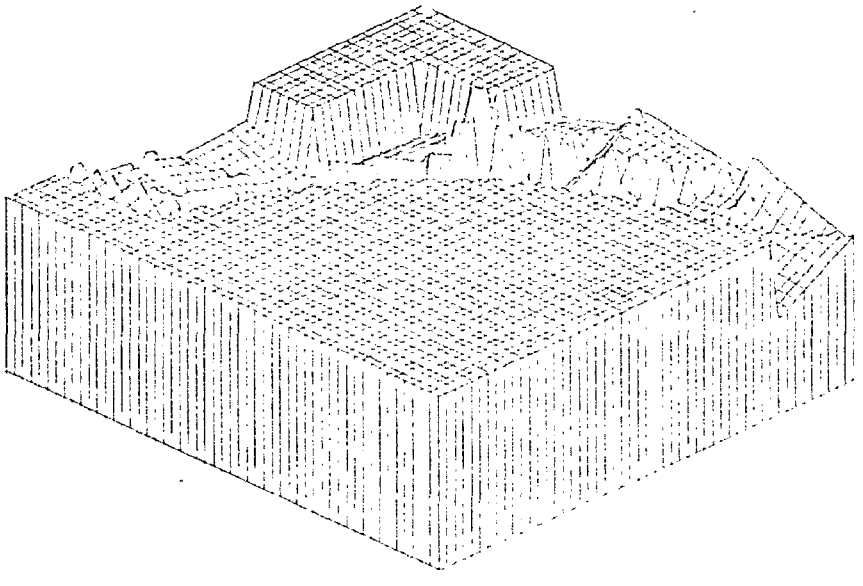


Fig. (9.30) Surface of elastic minor principle stresses due to internal gas pressure of 2 N/mm^2 using TRIAX 6 elements σ_{min} = - 3.6 N/mm^2 (19,1) σ_{max}=0.3 N/mm^2 (24.2

formulation of such a polynomial is given in eq. (11.1).

Thus a plotting routine SURFIT was developed to fit a surface to a rectangular set of output data by minimizing the sum of squares of deviations between calculated and original data points. SURFIT copes with polynomials of a power less or equal to six. Meshes of input data are prepared either manually by allocating the corresponding orthogonal rectangular coordinates to each known surface point or automatically by transforming the finite element solution by virtue of the routine MESH to rectangular sets of numerical values.

Requesting, say, a quartic polynomial, fifteen coefficients are computed and stored to enable the field response to be determined for any coordinate pair. An example for the fitting of a quartic polynomial to the surface of the axial concrete stresses, already determined and displayed in figs. (9.9) and (9.21), is produced in fig. (9.31) by the combined implementation of the routines SURFIT and SURPLT.

The origin of the polynomial is placed in the centre of the mesh and thus the fit is very good in its vicinity. However, due to the inherent mathematical limitations of the minimization technique employed, the fit becomes poor at points furthest away from the centre. Since the deviation from the original data values does not fall below 25% for these points irrespective of the order of the polynomial, the idea of fitting surfaces to finite element solutions using SURFIT is no longer pursued.

Furthermore, it can be argued that the potential of finite element solutions to adapt to local disturbances should not be wasted by the superposition of peak-smoothing polynomials. Their usefulness and easy availability for isometric display and the general visual assessment of results, however, is undisputed.

9.5. SUITABILITY CRITERIA

The applicability of a finite element solution obtained from an axisymmetric analysis is immediately verified by checking whether the shear stresses in an axial plane vanish

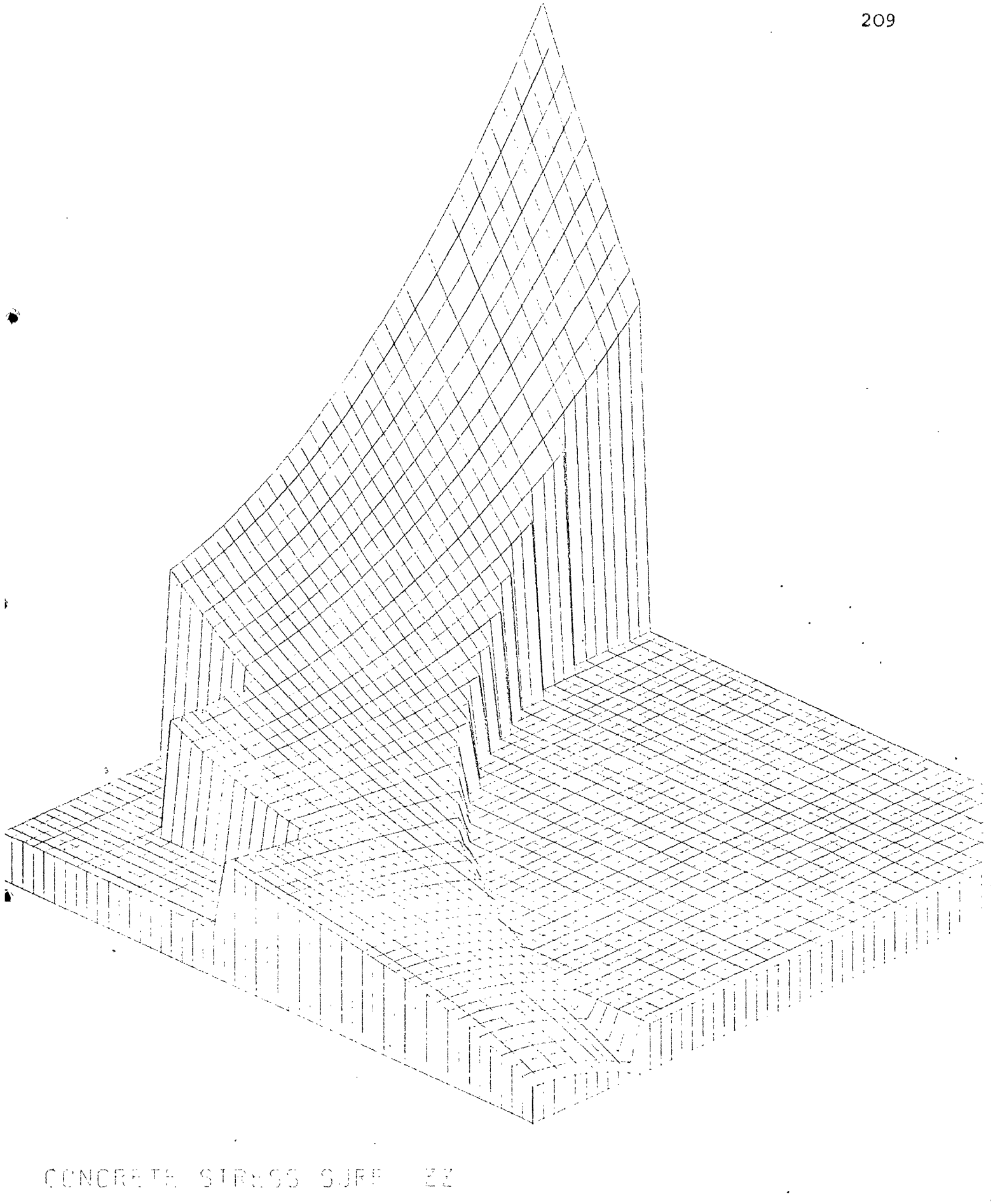


Fig. (9.31) Surface polynomial for elastic axial stresses displayed in figs. (9.9) and (9.21)

when approaching the axis of revolution or the equatorial plane, as symmetry with respect to these geometrical location imposes the equivalence of normal and principle stresses.

As regards the present example, this criterion is satisfied, since the stress contours drawn in the plots hit the lines of symmetry vertically; i.e. the angle formed between normal and principle stress resultants becomes zero.

The inaccuracy in the integration over the term $\frac{1}{r}$ for radii approaching zero is the most serious mathematical limitation suffered by both methods to a varying degree. Since the TRIAX 3 element considers the locally space-invariant radius of its centroid, the classical approach is affected slightly only where two nodes of an element rest on the axis of revolution. Thus it can be stated that the classical modes analysis is crude but unconditionally stable; it can cope with a radius tending to zero.

Imposing similar conditions onto the natural modes analysis would create instability - hence the postulation of the cut-out. Though mathematically and structurally the natural modes concept is more sophisticated, as the underlying theory and the computer programming is more involved, satisfactory solutions results only for ideally subdivided, idealized continua. Such structures require a void in the vicinity of their axis of revolution and elements which are nearly equilateral.

The structurally unjustified peaks observed in the stress surfaces for element No. 18, for instance, are due directly to the poor shape of the element. Also, for steep general gradients in the stress surfaces, considerable jumps are encountered along the interelement lines.

For a mutual check of validity, nevertheless, the natural modes solutions are satisfactory. The largest radial displacement encountered in the equatorial plane for the loading case investigated is $u_r = 1.73$ mm as opposed to $u_r = 1.62$ mm obtained from the classical analysis. The largest axial displacements near the axis of revolution are $u_z = 1.85$ mm and

u_z = 1.21 mm, respectively.

9.6. OUTLOOK

Regarding finite element methods, the solution of problems can be enjoyed which would be impracticable to solve in the long tradition. Furthermore, by transition from the classical to the natural deformation modes concept, under the observation of the above mentioned criteria considerable improvements can be made concerning computer efficiency and accuracy.

In fact, if it is desired to include the parabolic property of time-like processes - as shown for transient thermoviscoelastic effects in Chapter X and XI - the next step in the structural analysis is synthesized by the alternate implementation if iterative finite element and marching finite difference techniques. Since these field are capable of being expressed in terms of a system matrix, a field variable and a load vector of some kind, their solution is brought about by coding a sequence of time-dependent sets of linear simultaneous equations into computer language.

CHAPTER X

FINITE DIFFERENCE ANALYSIS OF THERMOVISCOELASTIC AXISYMMETRIC CONTINUA

10.1. INTRODUCTION

10.1.1. PROBLEM

The general transient thermoviscoelastic problem, in which the material is ageing and creeping viscoelastically and the temperature field changes with time, may be stated by two mixed partial differential equations. For the structural behaviour there is

$$\frac{G(T,\tau,t)}{2(1+\mu)}\left(\Delta u_i(t) + \frac{1}{1-2\mu}\,\text{grad div}\, u_i(t) - \frac{2(1+\mu)}{1-2\mu}\alpha_o\theta_{,i}(t)\right)+X_i = 0 \tag{10.0a}$$

with $G(T,\tau,0)$ is the initial modulus of thermoelasticity at the reference age.

The heat conduction is governed by

$$k\Delta\theta(t) + o\theta(t) + q(t) = \rho c\theta_{,t}(t) \tag{10.0b}$$

Clearly, eqs. (7.39) and (7.62) of the general thermoelastic behaviour and the steady state temperature distribution are time-independent, special cases of eqs. (10.0a) and (10.0b).

10.1.2. SUITABILITY CRITERION

The criterion, whether to use a finite element method or a finite difference scheme as the analytical tool for the solution of second order systems, is imposed by the relevant governing partial differential equation. These take their names from the shape of the conical sections which the boundaries of the disturbances describe when propagating from a perturbation point ([45]).

The elliptic partial differential equations (7.39) and (7.62) represent boundary value problems with specified mechanical, geometrical and thermal conditions at all spatial limits. As shown in eqs. (8.20), (8.77) and (10.10), boundary value problems are conveniently solved by the implementation of finite element methods.

The time-like processes expressed in eqs. (10.0a) and (10.0b) are parabolic and hence represent initial value problems with conditions specified only at the smallest value of the time variable but not at the largest. Thus, finite difference techniques must be employed.

10.1.3. TIME-LIKE PROCESSES

Processes with time-like character, such as transient temperature distribution, the creep-relaxation interaction and the development of viscoelastic deformations,do not lend themselves to finite element techniques, since they do not satisfy the necessary conditions as stated by Euler's equation of the calculus of variation.

The characteristic common to all time-like processes is that a current disturbance does not bear any retroactive effect on the conditions that existed at any time instant elapsed. Considering the physical problems mentioned above, the corresponding disturbances may appear as local temperature increases, stress increments and imposed displacements, respectively.

The uncoupling of these problems in the time variable is accomplished by using finite difference techniques, whereas the solution in the space coordinates is arrived at by the employment of finite element methods, with the time-dependent variables treated step-wise as invariants. For reasons of accuracy, exhibited in Chapter IX, the classical concept of the finite element analysis will be used.

10.2. TRANSIENT TEMPERATURE DISTRIBUTION

10.2.1. FINITE ELEMENT TEMPERATURE FORMULATION

Naturally, time-dependent or stationary temperature distributions existing in concrete continua must be determined prior to any further analysis on their thermoelastic or thermoviscoelastic behaviour.

To show the striking similarities between the finite element forms of the temperature distribution and the elastic stress analysis problem, names of matrices in section 8.2.4. will be maintained, if assumptions and operations are analogous in both cases. It must of course be realized that the corresponding matrices are different in size and value, for they pertain to different physical problems.

Analogous to eq. (8.1), the temperature within a TRIAX 3 element can be approximated by

$$\theta(r,z) = q_1 + (r - r_1)\, q_2 + (z - z_1)\, q_3 \qquad (10.1)$$

where $\theta(r,z)$ is understood as the difference between the current and the initial or previous temperature value, at any location in the element.

The finite element matrix formulation of the local temperature function is thus given by the analogue of eq. (8.6)

$$\theta(r,z) = \underline{M}\, \underline{B}^i \underline{C}^i \underline{T} \qquad (10.2)$$

where $\underline{M}$ is the (1x3) operator (A5.1), $\underline{B}^i$ is the (3x3) matrix (A5.3), $\underline{C}^i$ is the (3xk) local connectivity matrix and $\underline{T}$ is the (1xk) global temperature vector; k being the total number of overall temperature values ; i.e. nodal points.

Evaluation of eq. (10.2) at the local nodal points leads to the establishment of the elemental temperature vector

$$\underline{T}^i = \underline{M}^i \underline{B}^i \underline{C}^i \underline{T} \qquad (10.3)$$

where $\underline{M}^i$ is the (3x3) matrix (A5.2).

Omitting the arguments for brevity, the thermal

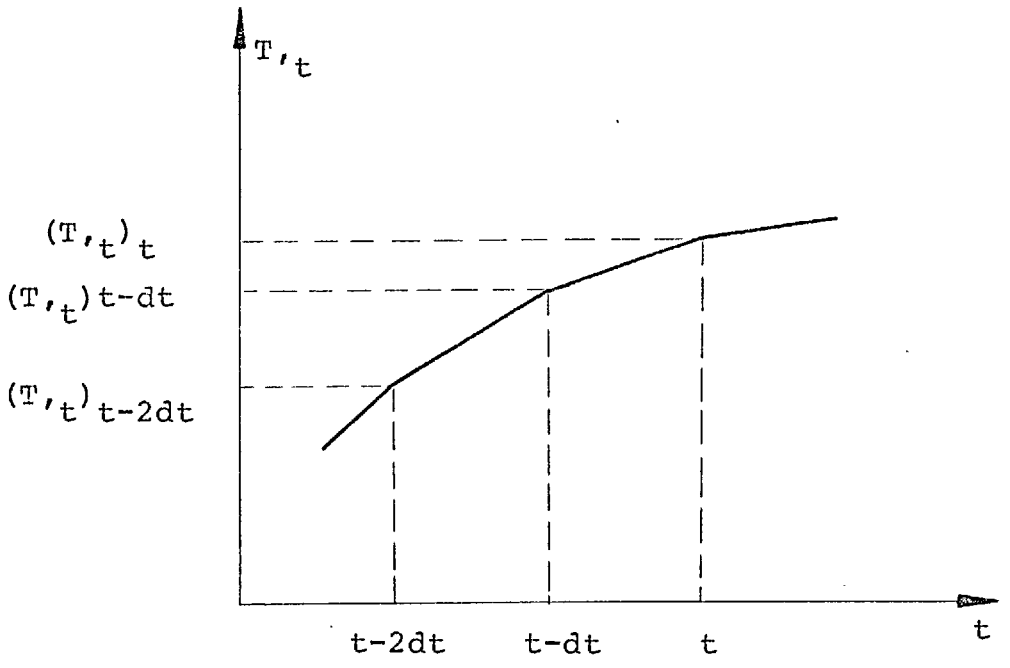


Fig. 10.1. Finite difference approximation to time-dependent thermal gradients

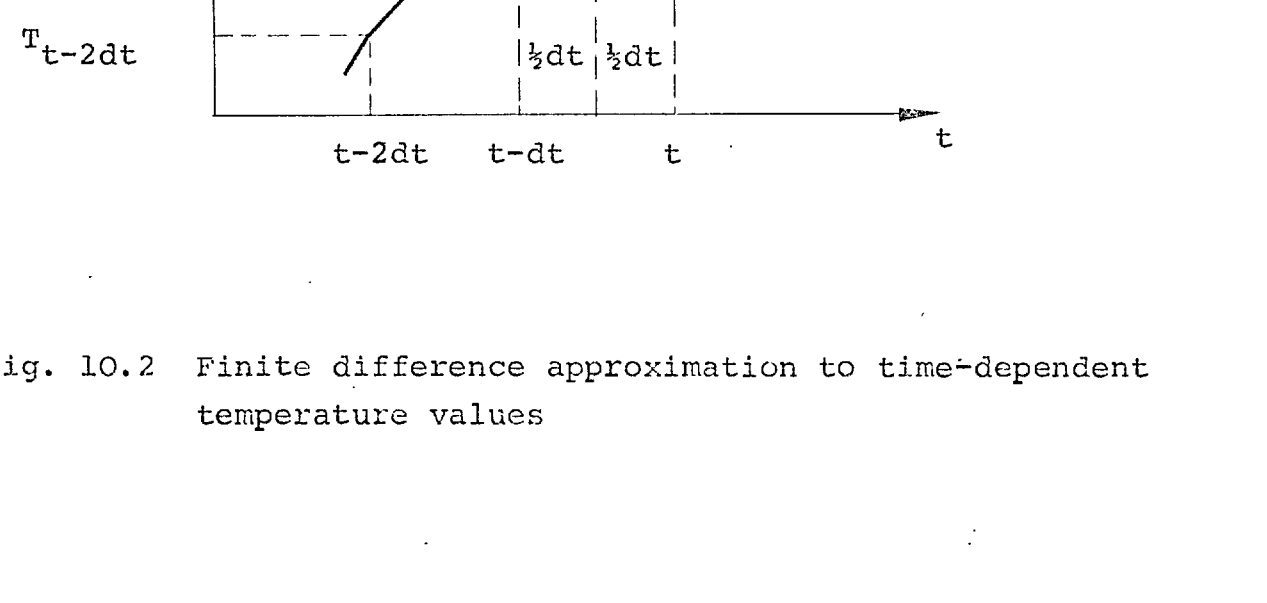


Fig. 10.2 Finite difference approximation to time-dependent temperature values

gradients take the form

$$\begin{aligned} \theta,r &= \underline{M},_r \underline{B}^i \underline{C}^i \underline{T} \\ \theta,z &= \underline{M},_z \underline{B}^i \underline{C}^i \underline{T} \end{aligned} \tag{10.4}$$

Since the differentiated operators contain constant coefficients only, they may be given the matrix names $\underline{A}_r^i$ and $\underline{A}_z^i$ respectively

$$\begin{aligned} \theta,r &= \underline{A}_r^i \underline{B}^i \underline{C}\ \underline{T} \\ \theta,z &= \underline{A}_z^i \underline{B}^i \underline{C}^i \underline{T} \end{aligned} \tag{10.5}$$

where $\underline{A}_r^i$ and $\underline{A}_z^i$ are the (1x3) matrices (A5.4).

Differentiation of eqs. (10.3) and (10.5) with respect to in turn all nodal temperature values T_j, j = 1,2,3 merely affects the global temperature vector. Thus,

$$\begin{aligned} (\underline{M}^i \underline{B}^i \underline{C}^i \underline{T}),_{T_{1,2,3}} &= \underline{M}^i \underline{B}^i \underline{C}^i \underline{E} \\ (\underline{A}_r^i \underline{B}^i \underline{C}^i \underline{T}),_{T_{1,2,3}} &= \underline{A}_r^i \underline{B}^i \underline{C}^i \underline{E} \\ (\underline{A}_z^i \underline{B}^i \underline{C}^i \underline{T}),_{T_{1,2,3}} &= \underline{A}_z^i \underline{B}^i \underline{C}^i \underline{E} \end{aligned} \tag{10.6}$$

where $\underline{E}$ is the (1xk) global unit vector. Reference is made to def. (A5.5) and (A5.6).

10.2.2. TEMPERATURE DISTRIBUTION EQUATIONS

For axisymmetric temperature distributions, only the directions r and z need to be considered. The contribution from an individual element to the first variation of the heat conduction functional (7.63) thus becomes

$$I,_{T_{1,2,3}} = \int 2r\{k_r \theta,_r (\theta,_r),_{T_{1,2,3}} + k_z \theta,_z (\theta,_z),_{T_{1,2,3}} - (q - o\theta - \rho c \theta,_t)\ \theta,_{T_{1,2,3}}\}\ ds \tag{10.7}$$

To proceed, eq. (10.7) is evaluated at the three associated nodes in turn. If the temperature value in the outflow term and the time-dependent thermal gradient are treated as invariants, then substitution of eqs. (10.3), (10.5) and

(10.6) into eq. (10.7) yield the local contribution to the functional's first variation in matrix form. Superimposing all contributions and subsequently equating to zero, the governing matrix equation of the axisymmetric heat conduction problem in its classical finite element form is established

$$\sum_{i=1}^{n} A^i r_m^i \left(k_r (\underline{A}_r^i \underline{B}^i \underline{C}^i)^t \underline{I}^i \underline{A}_r^i \underline{B}^i \underline{C}^i + k_z (\underline{A}_z^i \underline{B}^i \underline{C}^i)^t \underline{I}^i \underline{A}_z^i \underline{B}^i \underline{C}^i\right) \underline{T}$$

$$= \sum_{i=1}^{n} (\underline{M}^i \underline{B}^i \underline{C}^i)^t \underline{I}^i (q - o\theta' - \rho c \theta'_t) \qquad (10.8)$$

where $\underline{I}^i$ is a (3x3) identity matrix. The local thermal conductivity matrix $\underline{k}^i$ and the local thermal load vector $\underline{F}^i$ are set up in eqs. (A5.7) to (A5.9).

Considering unit temperature values $\underline{T}$, the terms in eq. (10.8) may be identified with the global thermal conductivity matrix $\underline{K}$ and the global thermal load vector $\underline{F}$, respectively.

Thus, eq. (10.8) takes the global matrix form

$$\underline{K}\,\underline{T} = \underline{F} \qquad (10.9)$$

In the case of stationary temperature distributions, a thermal load vector, which instigates the temperature field to change, does not exist. Consequently,

$$\underline{K}\,\underline{T} = \underline{O} \qquad (10.10)$$

10.2.3. FINITE DIFFERENCE SCHEME

To allow for time dependence, eq. (10.9) of the transient temperature distribution must be rewritten in such a way that it permits the thermal gradients to vary. This is arrived at by separating in the thermal load vector $\underline{F}$ the effects of the heat generation and the time-dependent distribution

$$\underline{F} = \underline{F}_q - \underline{P}\,\underline{T}'_t \qquad (10.11)$$

Substituting eq. (10.11) into eq. (10.9), thus

$$\underline{K}\,\underline{T} + \underline{P}\,\underline{T}_{,t} - \underline{F}_q = \underline{0} \qquad (10.12)$$

Subdividing the history of the heat conduction process into time intervals of constant duration and assuming that within these intervals of time dt the nodal thermal gradients vary linearly with time, the temperature values at a particular instant t can be expressed in terms of those found at the previous instant t-dt and the gradients averaged over the interval which has just elapsed

$$\underline{T}_t = \underline{T}_{t-dt} + \{(\underline{T}_t)_{,t} + (\underline{T}_{t-dt})_{,t}\} \tfrac{1}{2}dt \qquad (10.13)$$

Solving for the current thermal gradients, thus

$$(\underline{T}_t)_{,t} = -(\underline{T}_{t-dt})_{,t} + (\underline{T}_t - \underline{T}_{t-dt})\frac{2}{dt} \qquad (10.14)$$

Substitution of eq. (10.14) into eq. (10.12) and separation of the current nodal temperature values from the known values and gradients of the previous step, leads to the formulation of the following recursion formula

$$(\underline{K} + \frac{2}{dt}\underline{P})\,\underline{T}_t = \underline{P}\{\frac{2}{dt}\underline{T}_{t-dt} + (\underline{T}_{t-dt})_{,t}\} + \underline{F}_{qt} \qquad (10.15)$$

After the initial values of the temperature field have been computed by a finite element analysis, the initial thermal gradients can be obtained by evaluating eq. (10.12) at time zero. For any time instant other than zero, the thermal gradients are arrived at by substituting eq. (10.13) into eq. (10.12).

The finite difference marching technique predicts the new values and gradients by extrapolation along parabolas, which require the function and its derivative evaluated at the last two time steps. Reference is made to figures (10.1) and (10.2). The second recursion formula is thus conveniently expressed at time t-dt.

$$(\underline{K}\frac{dt}{2} + \underline{P})(\underline{T}_{t-dt})_{,t} = -\underline{K}\,\underline{T}_{t-2dt} - \frac{dt}{2}\underline{K}(\underline{T}_{t-2dt})_{,t} + \underline{F}_{qt-dt} \qquad (10.16)$$

Once the heat waves start to propagate, the alternate evaluation of eqs. (10.15) and (10.16) for the temperature values and gradients, provides a solution at any time instant required.

10.3. CREEP-RELAXATION DUALITY

10.3.1. SUPERPOSITION HYPOTHESIS

Considering concrete continua, the superposition hypothesis assumes that the whole process of concrete creep, including the ageing effect, is linear inasmuch as the strains, occurring at any time after the instantaneous application of a stress increment at any age of concrete, are independent of the effects of any loading initiated either earlier or later than that age.

It includes the assumptions that linear constitutive equations exist for constant, variable and different age, which from figure (5.8) can be considered true for temperature up to 140°C and stress/ cold strength ratios up to 0.66. Thus the independent deformations resulting from each stress increment or decrement are capable of being superimposed to yield the solution of the strain history at any time ([60],[76]).

If the concrete is considered undisturbed prior to its age at loading and the stresses vary linearly with time, the isothermal stress-strain relationship may be represented by a hereditary integral of the form

$$\sigma(t) = \int_{\tau}^{t} G(T,\tau,\beta)\ (\varepsilon(\beta))_{,\beta}\ d\beta \qquad (10.17)$$

where $\underline{\sigma}(t)$ and $\underline{\varepsilon}(t)$ are the time-dependent stress and strain fields and $G(T,\tau,t)$ is the temperature, age and time-dependent relaxation response function which is linear in the deformations. β is dummy time and age parameter.

10.3.2. ELEMENTAL CONSTITUTIVE RELATIONSHIPS

Properly described stress-strain relationships are the precondition for a satisfactory solution of any stress analysis problem. Presenting the functional of the thermal

creep analysis in the finite element matrix displacement form, the phenomena of ageing and the thermoviscoelasticity are conveniently reproduced by relaxation surface functions pertaining to various temperature levels.

Considering an element i and allowing for temperature dependence, the local constitutive relationship in matrix form is established by rewriting eq. (10.17)

$$\underline{\sigma}^i(t) = \underline{D}^i \int_{\tau}^{t} G(T,\tau,\beta)\,(\underline{\varepsilon}^i(\beta) - \alpha_o \underline{\theta}^i(\beta))_{,\beta}\, d\beta \qquad (10.18)$$

where $\underline{\sigma}^i(t)$ and $\underline{\varepsilon}^i(t)$ are the local stress and strain vector(s) (8.10) and (8.11), $\underline{D}^i$ is the normalized material stiffness matrix A4.12, having a unit modulus of elasticity. α_o is the coefficient of linear thermal expansion at the base temperature and $\underline{\theta}^i(t)$ is the local pseudo-temperature vector of the value $\alpha_0^{-1} \int_{T_o}^{T(t)} \alpha(\beta)\, d\beta$.

If the age at loading is replaced by the lower time limit zero, partial integration of eq. (10.18) leads to the more convenient local isothermal viscoelastic constitutive equation. Treating the contributions from conservative forces and thermal loads separately, thus

$$\underline{\sigma}^i(t) = \underline{D}^i\{G(T,\tau,t)\underline{\varepsilon}^i(t) - \int_{o}^{t} (G(T,\tau,\beta))_{,\beta}\underline{\varepsilon}^i(\beta)\, d\beta\} \qquad (10.19)$$

$$\underline{\sigma}_t^i(t) = \underline{D}^i\{-G(T,\tau,t)\alpha_0\underline{\theta}^i(t) + \int_{o}^{t} (G(T,\tau,\beta))_{,\beta}\alpha_0\underline{\theta}^i(\beta)d\beta\} \qquad (10.20)$$

where the initial relaxation response $G(T,\tau,0)$ is the modulus of thermoelasticity at the reference age. Details are given in figure (5.9).

10.3.3. RELAXATION SURFACE FUNCTIONS

Uniaxial isothermal relaxation functions and a time-independent Poisson's ratio are sufficient to reproduce the material behaviour in eq. (10.18). Difficulties, however, arise in the experimental determination of the relaxation responses. Thus the relaxation functions must be deduced analytically from the thermal creep functions which are based on the results entered in figures (5.1) to (5.5).

The mathematical link between the creep and relaxation phenomena is established by the following integral equation ([90]).

$$H(t-\tau) = \int_{\tau}^{t} J(T,\beta,t)\,(G(T,\tau,\beta))_{,\beta}\, d\beta \qquad (10.21)$$

where $H(t-\tau)$ is the normalized Heavyside step function and $J(T,\tau,t)$ is the isothermal creep surface function. The initial response $J(T,\tau,0)$ is the thermoelastic strain.

Taking the lower time limit as zero and subsequently integrating over the time domain, eq. (10.21) becomes

$$t = \int_{o}^{t} (T,\tau,t)\,G(T,\tau,\beta)\, d\beta \qquad (10.22)$$

The numerical solution of this first order Volterra-integral equation requires the creep and relaxation surface functions normalized to their initial thermoelastic values. The normalized functions are given readily by $\phi(t)=J(T,\tau,t)/J(T,\tau,0)$ and $\psi(t) = G(T,\tau,t)/G(T,\tau,0)$ respectively.

10.3.4. FIRST ORDER INTEGRAL EQUATION

For invariable age and isothermal conditions, eq. (10.22) may be transformed to

$$\begin{aligned} t &= \int_{o}^{t} \phi(\beta)\psi(t-\beta)\,d\beta \\ &= \int_{o}^{t} \phi(t-\beta)\psi(\beta)\,d\beta \end{aligned} \qquad (10.23)$$

In proceeding to solve eq. (10.23) numerically, the following integral is introduced

$$f(t) = \int_{o}^{t} \phi(\beta)\,d\beta \qquad (10.24)$$

Subdividing the time scale into intervals of constant duration by the values t_i, $i = 1,2,3, \ldots n, (n+1)$, with $t_1 = 0$ and $t_{n+1} = t$, the trapezoidal rule for integration may be employed

$$f(t_{n+1}) = f(t_n) + \tfrac{1}{2}\{\phi(t_{n+1}) + \phi(t_n)\}(t_{n+1})-t_n) \qquad (10.25)$$

Treating the gradual changes in the creep and

relaxation responses as a series of small increments, summation can be applied. Eq. (10.23) thus becomes

$$t_{n+1} = \sum_{i=1}^{n} \int_{t_i}^{t_{i+1}} \phi(t_{n+1}-\beta)\psi(\beta)\, d\beta \qquad (10.26)$$

Noting from eq. (10.24) that $\phi(t) = f'(t)$, expression (10.26) may be transformed to

$$t_{n+1} = \sum_{i=1}^{n} \tfrac{1}{2}\{\psi(t_{i+1})+\psi(t_i)\} \int_{t_i}^{t_{i+1}} f'(t_{n+1}-\beta)d\beta \qquad (10.27)$$

The corresponding finite difference approximation reads

$$t_{n+1} = \tfrac{1}{2}\psi(t_{n+1})f(t_{n+1}-t_n)+\tfrac{1}{2}\psi(t_n)f(t_{n+1}-t_n)$$
$$-\tfrac{1}{2}\sum_{i=1}^{n-1}\{\psi(t_{i+1})+\psi(t_i)\}\{f(t_{n+1}-t_{i+1})-f(t_{n+1}-t_i)\} \qquad (10.28)$$

With the creep responses known from experiments and theoretically reproduced by fitting appropriate exponential functions, the creep-relaxation conversion problem can be formulated by a set of linear algebraic equations, which are solved for the required relaxation values using the following finite difference approximation

$$\psi(t_{n+1}) = \frac{2t_{n+1}}{f(t_{n+1}-t_n)} - \psi(t_n)$$
$$+ \frac{\sum_{i=1}^{n-1}\{\psi(t_{i+1})+\psi(t_i)\}\{f(t_{n+1}-t_{i+1})-f(t_{n+1}-t_i)\}}{f(t_{n+1}-t_n)} \qquad (10.29)$$

A computer program CRELAX (150 cards) was originated by the author to perform the creep-relaxation conversion and to plot both the original creep functions and the resulting relaxation functions.

10.4. CONVOLUTION INTEGRAL OF STRAIN HISTORY

10.4.1. QUASI-STATIC ENERGY PRINCIPLE

In the case of thermoviscoelastic stress analysis

problems, the principle of minimum potential energy may be written in its quasi-static form, which considers the work done by the internal stress components along the conjugate strains that are linearly dependent on them, during the slow motion of the system between time zero and any later instant.

Considering axisymmetric geometry, substitution of eqs. (10.19), (10.20) and (8.9) into eq. (7.26) and superposition of all contributions leads to the finite element matrix form of the overall quasi-static functional. After variation, thus

$$\begin{aligned}
\underline{0} = \sum_{i=1}^{n} & G(T,\tau,t) \int_{V^i} (\underline{A}^i\underline{B}^i\underline{C}^i)^t \underline{D}^i \underline{A}^i\underline{B}^i\underline{C}^i dV.\underline{u} \\
& - \int_0^t (G(T,\tau,\beta))_{,\beta} \int_{V^i} (\underline{A}^i\underline{B}^i\underline{C}^i)^t \underline{D}^i \underline{A}^i\underline{B}^i\underline{C}^i dV.\underline{u}\, d\beta \\
& - G(T,\tau,t)\alpha_0\, \underline{\Theta}^i(t) \int_{V^i} (\underline{A}^i\underline{B}^i\underline{C}^i)^t \underline{D}^i \underline{I}^i dV \\
& + \int_0^t (G(T,\tau,\beta))_{,\beta}\alpha_0\underline{\Theta}^i(\beta) \int_{V^i} (\underline{A}^i\underline{B}^i\underline{C}^i)^t \underline{D}^i \underline{I}^i dV d\beta \\
& - \int_{V^i} (\underline{A}^i\underline{B}^i\underline{C}^i)^t \underline{D}^i \underline{\varepsilon}_p^i(t) dV - \int_{V^i} (\underline{M}^i\underline{B}^i\underline{C}^i)^t \underline{X}^i dV \\
& - \int_{S^i} (\underline{M}^i\underline{B}^i\underline{C}^i)^t \underline{N}^i \underline{\sigma}_s(t)\, ds
\end{aligned} \tag{10.30}$$

For unit displacements $\underline{u}$, the terms in eq. (10.30) may be identified with the time-dependent stiffness matrix $\underline{K}$, the history-dependent stiffness matrix, the time-dependent thermal load vector $\underline{R}$, the history-dependent load vector, the prestress vector $\underline{F}_p$, the body force vector $\underline{F}_x$ and the external force vector $\underline{F}_e$, respectively.

In global matrix form, the governing equation of the transient thermoviscoelastic stress analysis problem thus reads

$$\begin{aligned}
& \underline{K}(T,\tau,t)\underline{u}(t) - \int_0^t (\underline{K}(T,\tau,\beta))_{,\beta}\underline{u}(\beta)\, d\beta \\
& = \underline{F}_p + \underline{F}_x + \underline{F}_e + \underline{R}(T,\tau,t) - \int_0^t (\underline{R}(T,\tau,\beta))_{,\beta} d\beta
\end{aligned} \tag{10.31}$$

However, eq. (10.31) is incapable of being represented by a set of simultaneous linear-deformation equations, for the history-dependent stiffness coefficients and displacement components are still coupled in the time variable.

10.4.2. THERMOVISCOELASTIC LOAD-DEFORMATION EQUATIONS

Turing attention to the transient, purely thermoviscoelastic stress analysis probelm eq. (10.31) is reduced by the loading vectors $\underline{F}_p$, $\underline{F}_x$ and $\underline{F}_e$. In attempting to solve the governing matrix equation, matrices of known coefficients are separated from variable functions. For a time instant t_{n+1}, thus

$$G(T,\tau,t_{n+1})\ \underline{K}'\underline{u}(t_{n+1}) - \int_0^{t_{n+1}} (G(T,\tau,\beta)),_\beta \underline{K}'\underline{u}(\beta)d\beta =$$

$$G(T,\tau,t_{n+1})\ \underline{R}'\underline{\theta}(t_{n+1}) - \int_0^{t_{n+1}} (G(T,\tau,\beta)),_\beta \underline{R}'\underline{\theta}(\beta)d\beta \qquad (10.32)$$

where $\underline{K}'$ is the (kxk) residual stiffness matrix and $\underline{R}'$ is the (kxl) residual thermal load vector; k is the number of global displacements.

Before the convolution-integral equation (10.32) can be solved in the space coordinates by the finite element methods discussed in Chapter VIII, it must be uncoupled in the time variable.

10.4.3. SECOND ORDER INTEGRAL EQUATION

In the treatment of coupled linear Volterra-integral equations, the difficulty to surmount is the transformation of a history-dependent integral expression to a series of time-dependent scalar values. These are understood as weighting factors that embody and value a process, which is dependent on the entire unfolded evolution of a natural phenomenon, since the perturbation was initiated.

The numerical procedure carried out to solve the memorizing convolution integral in eq. (10.32) turn out to be rather similar to that discussed in section 10.3.4. Volterra-integral equations of the second kind, however, contain a

separate current value term appearing in addition to the integral. For a typical time instant t_{n+1} of the subdivided time scale, the normalized, non-dimensional version of the integral expression may be written in the form

$$y(t_{n+1}) = f(t_{n+1}) - \sum_{i=o}^{n} \int_{t_i}^{t_{i+1}} y(\beta)\,(f(t_{n+1}-\beta))_{,\beta}\,d\beta \qquad (10.33)$$

The finite difference expression for the time-dependent weighting factors differs from eq. (10.28) in that it contains a time-dependent and a history-dependent term

$$y(t_{n+1}) = f(t_{n+1}) - \sum_{i=o}^{n} \tfrac{1}{2}\{y(t_{i+1})+y(t_i)\}\{f(t_{n+1}-t_{i+1}) - f(t_{n+1}-t_i)\} \qquad (10.34)$$

For $n = 0$, i.e. $t_{n+1} = t_1$, the initial value is directly given by $y(0) = 1$. Thus, at time zero when a disturbance is introduced, a hereditary process does not yet exist; which is obvious. Taking $n = 1,2,3,\ldots$, eq. (10.34) gives rise to expressions for the determination of weighting factors at successive steps

$$\begin{aligned} y(t_{n+1}) = {} & f(t_{n+1}) - \tfrac{1}{2}\, y(t_{n+1})\{f(0)-f(t_{n+1}-t_n)\} \\ & - \tfrac{1}{2}\, y(t_n)\{f(0) - f(t_{n+1}-t_n)\} \\ & - \tfrac{1}{2} \sum_{i=1}^{n+1} \{y(t_{i+1}) + y(t_i)\}\{f(t_{n+1}-t_{i+1}) - f(t_{n+1}-t_i)\} \end{aligned} \qquad (10.35)$$

Solving for the current weighting factor $y(t_{n+1})$, the governing finite difference equation for the numerical solution in the time variable becomes

$$y(t_{n+1}) = \frac{f(t_{n+1}) - \tfrac{1}{2}y(t_n)\{f(0)-f(t_{n+1}-t_n)\}}{1 + \tfrac{1}{2}\{f(0) - f(t_{n+1} - t_n)\}} - \frac{\tfrac{1}{2}\sum_{i=1}^{n-1}\{y(t_{i+1})+y(t_i)\}\{f(t_{n+1}-t_{i+1})-f(t_{n+1}-t_i)\}}{1 + \tfrac{1}{2}\{f(0) - f(t_{n+1}-t_n)\}} \qquad (10.36)$$

where f is the function of the investigated natural phenomenon.

10.4.4. RELAXATION WEIGHTING FACTORS

At a time instant t_n, the strain history of the thermally loaded concrete structure of locally varying temparature and age, can be analysed in the space coordinate by momentarily eliminating the ageing effect, using a set of isothermal relaxation weighting factors. As the relaxation phenomenon continuously unrolls itself, the establishment of a new set of weighting factors, reflecting the ageing effects at time t_{n+1}, requires the reconstruction anew of the entire preceding strain history.

Considering the relaxation weighting factors as operators acting on the global displacement and pseudo-temperature vectors, eq. (10.33) takes the form

$$\underline{W}(t_{n+1}) = \underline{f}(T,\tau,t_{n+1}) - \sum_{i=o}^{n} \int_{t_i}^{t_{i+1}} \underline{W}(\beta)\,(\underline{f}(T,\tau,t_{n+1}-\beta))_{,\beta}\,d\beta \qquad (10.37)$$

The set of continuous functions is given by the normalized relaxation responses of the concrete material at the corresponding nodal points

$$\underline{f}\,(T,\tau,t_{n+1}-\beta) = \frac{G(T,\tau,\beta)}{G(T,\tau,O)} \cdot \underline{E} \qquad (10.38)$$

where $\underline{E}$ is a (1xk) global unit vector.

The time-dependent sets of weighting factors $\underline{W}(t_{n+1})$ indicate that the finite difference procedure (10.33) to (10.36) is to be carried out for each nodal point of the chosen finite element mesh.

Substituting eqs. (10.37) and (10.38) into eq. (10.32), the step-wise uncoupled load-deformation matrix equation of the transient thermoviscoelastic stress analysis problem is established

$$G(T,\tau,O)\ \underline{W}^{t}(t_{n+1})\underline{K}'\underline{W}(t_{n+1})G(T,\tau,O)\ \underline{u}\ (t_{n+1})$$

$$= G(T,\tau,O)\ \underline{W}^{t}(t_{n+1})\ \underline{R}'\underline{\Theta}(t_{n+1}) \qquad (10.39)$$

CHAPTER XI

THERMOVISCOELASTIC ANALYSIS OF AXISYMMETRIC CONCRETE CONTINUA USING RELAXATION WEIGHTING FACTORS

11.1. OBJECTIVE

The incorporation of thermoviscoelastic strains into the structural behaviour of concrete continua is mathematically rigorous. Thus the first concern in the present chapter is to reconcile the functional description of the 33 creep curves with the experimental data given in Chapter V and to show to what extent the regression of thermal creep strains to linear thermoviscoelastic strains is justified.

Secondly, the procedure for the generation of thermal relaxation weighting factors from the fitted thermal creep functions is explained and carried out by usage of the computer program CRELAX. The weighting factors enable the embodiment of the whole strain history preceding the time instant for which the solution of the time-dependent structural problem is requested. For a concrete of the given mix and age, these factors are produced as a set of temperature and time-dependent scalars, ready to be read on as input data for computer-aided ambient or thermal stress analyses.

The concept of weighting stiffness coefficients using relaxation factors is first demonstrated in a small example.

Then, to illustrate the general applicability of thermal relaxation weighting factors, a complex case study is carried out. The computer program THERMO AXICON computes the transient temperature distributions and the time-dependent thermal stresses developing in the axisymmetric concrete pressure vessel described in Chapter IX. The transient thermoviscoelastic behaviour of the vessel is analysed by implementing a combined finite element and finite difference method of approach in conjunction with the proposed set of factors.

11.2. SHAPE OPTIMIZATION OF CREEP PROFILES

11.2.1. CARTESIAN POLYNOMIALS

The plotting routine SURFIT introduced in Chapter IX may be used to fit a surface to a rectangular set of experimental creep data by minimizing the sum of squares of deviations between calculated and original data points. If the variables constitute the temperature T and the time t, with the age τ and the stress/ cold strength ratio s being invariants, any cartesian polynomial for normalized creep surfaces develops from

$$\phi(T,t) = a_0 + a_1 T + a_2 t + a_3 T^2 + a_4 T t... \qquad (11.1)$$

The limitations obstructing the satisfactory surface fitting based on cartesian polynomials are caused by the fact that the variation of deviations of calculated values from recorded ones takes place in the direction of the third coordinate and not, as desirable, normal to the locally varying profile. Even by weighting the importance of the initially recorded values, the steep initial gradients of creep strain strain curves cannot be reproduced adequately.

After a discussion on creep surface functions during the presentation of the author's paper ([45]), the employment of cartesian polynomials for this purpose was abandoned.

11.2.2. PARAMETRIC POLYNOMIALS

Under usage of the computer program PARFIT ([48]), also parametric polynomials were employed to described surface functions fitted to corresponding sets of creep data. The local minimization is based on the constrained Fletcher-Reeves method in which not only the creep surface but also its variables appear as functions of two non-dimensional parameters u and v ([36,37]).

Fitting an age and time-dependent creep surface, with the temperature being invariant, the parametric polynomials develop from

$$\tau(u,v) = a_0 + a_1u + a_2v + a_3u^2 + a_4uv + \ldots$$

$$t(u,v) = b_0 + b_1u + b_2v + b_3u^2 + b_4uv + \ldots \qquad (11.2)$$

$$\phi(u,v) = c_0 + c_1u + c_2v + c_3u^2 + c_4uv + \ldots$$

Considering the local surface normal, the parameter u follows the configuration of the relevant surface contour, while the parameter v indicates the direction of the steepest local descent. Since the variation of deviations between computed and recorded values occurs in the direction of the locally varying surface normal, the fit improves drastically.

An example is shown for a creep surface at ambient temperature in fig. (11.a). Although requesting quartic parametric polynomials which require the computation of three times 25 coefficients, fluctuations about the ordinate cannot be avoided.

Comparing parametric and cartesian polynomials, the evaluation of the former is considerably more involved. Also, the back-transformation of the parametric functions (11.2) to real functions creates difficulties; it is only realizable in a cumbersome numeric procedure.

The foregoing thus suggests not to pursue the implementation of parametric polynomials in thermal creep analyses; they are optimally exploited only when used as an end. In fact, PARFIT was originally designed to make possible the graphical display of topological contours of ship vessels.

11.2.3. NON-LINEAR PARAMETERS

One of the most extensively used techniques in function fitting is the estimation of non-linear parameters using least squares methods in conjunction with differential correction techniques. Realizing that the relation between the developing creep strains and the time variable represents a natural process at least for low temperatures and low stress/ cold strength ratios, the isothermal, normalized creep response may be reproduced by the simple exponential expression

$$\phi(t) = a_1 - a_2e^{-a_3t} \qquad (a_1 - a_2 = 1) \qquad (11.3)$$

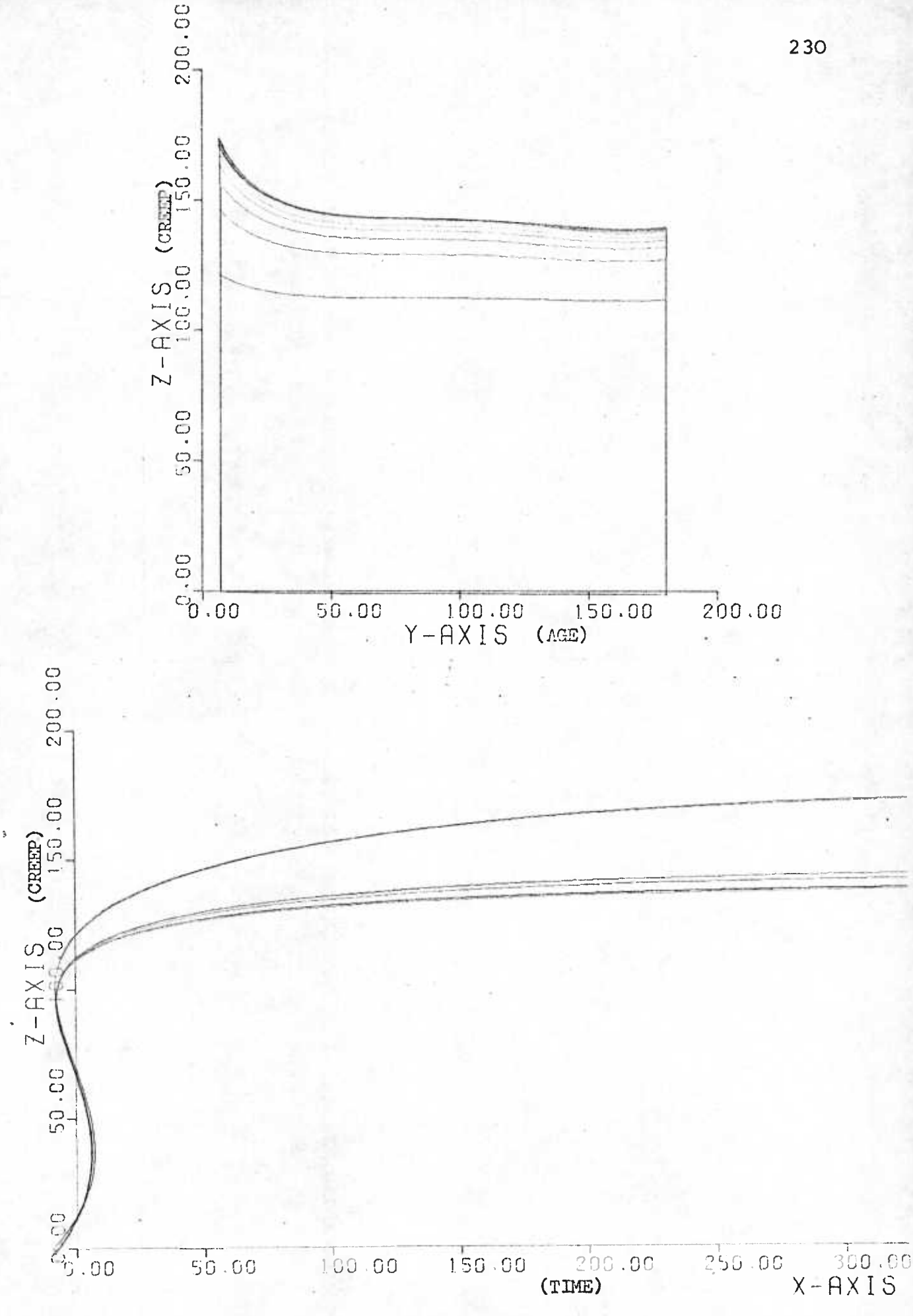


Fig. 11.a. Normalized age and time-dependent creep surface fitted by parametric polynomials

When the application of the differential correction technique is built in to a successive approximation scheme, whereby one iteration is one cycle of such an approximation process, the j-th iteration of eq. (11.3) reads

$$\phi(i) = f(t(i), a_1^j, a_2^j, a_3^j) = a_1^j - a_2^j e^{-a_3^j t(i)} \qquad (11.4)$$

where $t(i)$, $i = 1,2,\ldots m$ is a series of time instants at specific intervals ([53]).

If estimates of the parameters exist, their values for the following iteration can be improved using least squares. Upon stating that the residual $R(i)$ represents the difference between the computed function value $\phi(i)$ and the normalized recorded strain response $r(i)$ associated with it, the j-th set of residuals becomes

$$R^j(i) = \phi^j(i) - r(i) \qquad (11.5)$$

In order to obtain improved values for the parameters eq. (11.4) is first expanded about the estimates using a Taylor series expansion of the form

$$\phi^{j+1}(i) = \phi^j(i) + \frac{\partial \phi^j(i)}{\partial a^i{}_k} \; 1_k^{j+1} (k = 1,2,3) \qquad (11.6)$$

where $$1_k^{j+1} = a_k^{j+1} - a_k^j \qquad (11.7)$$

Evaluating eq. (11.6) at all time steps $t(i)$ and subtracting the corresponding recorded values from both sides, the link between the current and the predicted residuals is established. The functional to minimize is

$$\sum_{i=1}^{m} (R^{j+1}(i))^2 = \sum_{i=1}^{m} \left(R^j(i) + \sum_{k=1}^{3} \frac{\partial \phi^i(i)}{\partial a^j{}_k} 1_k^{j+1}\right)^2 \qquad (11.8)$$

Since the vanishing of the first variation of the functional (11.8) must hold for all variations (11.7), the non-trivial solution in matrix form is given by

$$(R^j + \underline{S}^{jt} \underline{L}^{j+1}) \; \underline{S}^{jt} = \underline{O} \qquad (11.9)$$

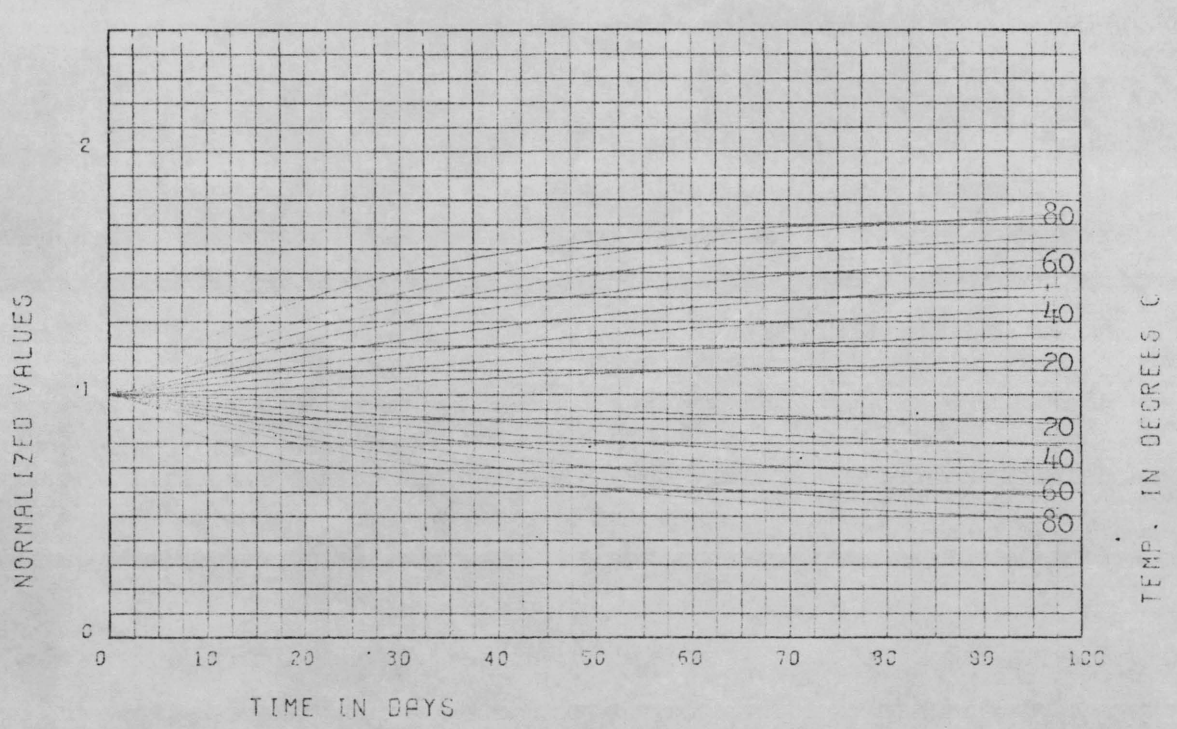


FIG.11.b. NORMALIZED ISOTHERMAL CREEP & RELAXATION FUNCTIONS

where R^j is the sum of the current residual, $\underline{S}^j$ is the gradient vector and $\underline{L}^{j+1}$ is the vector of the extremal differential corrections.

Any standard matrix inversion technique can be implemented to solve eq. (11.9) for the differential corrections, if it is rewritten in the form

$$\underline{S}^j \underline{S}^{jt} \underline{L}^{j+1} = - R^j \underline{S}^j \qquad (11.10)$$

The precaution that must be ovserved in employing the differential correction technique is that the initial empirical estimates of the parameters are sufficiently close to the actual values in order to guarantee convergence.

A subroutine ESTIM (150 cards) was originated to find the parameters of such simple exponential functions. However, it was observed that the fitted creep curves exhibited much shallower initial gradients than the profiles drawn from experiments. This led to the underestimation of the effect of the creep phenomenon on the behaviour of thermoviscoelastically deforming structures.

An example of the relatively poor shape of creep and relaxation functions fitted by ESTIM is given in fig. (11.b). Although the results could be considered sufficient as a first approximation, the estimation of non-linear parameters was abandoned as being too unambitious an approach.

11.2.4. CREEP RATE PROFILES

From the test results recorded in Chapter V, the author observed that, in plotting the creep rate against time in a double-logarithmic scale, a linear function of negative slope may be fitted to the scatter of data pairs from each test. An example is shown in fig. (11.1) for a stress/cold strength ratio of $s = 0.4$ and a temperature of $T = 300^0 C$.

The mathematical procedure for the evaluation of such a fitted creep rate approximation is straightforward. With the parameters $a(s,T)$ and $b(s,T)$ determined, the linear relation between creep increment and time in the mentioned scale can be established. Suppressing for the present the

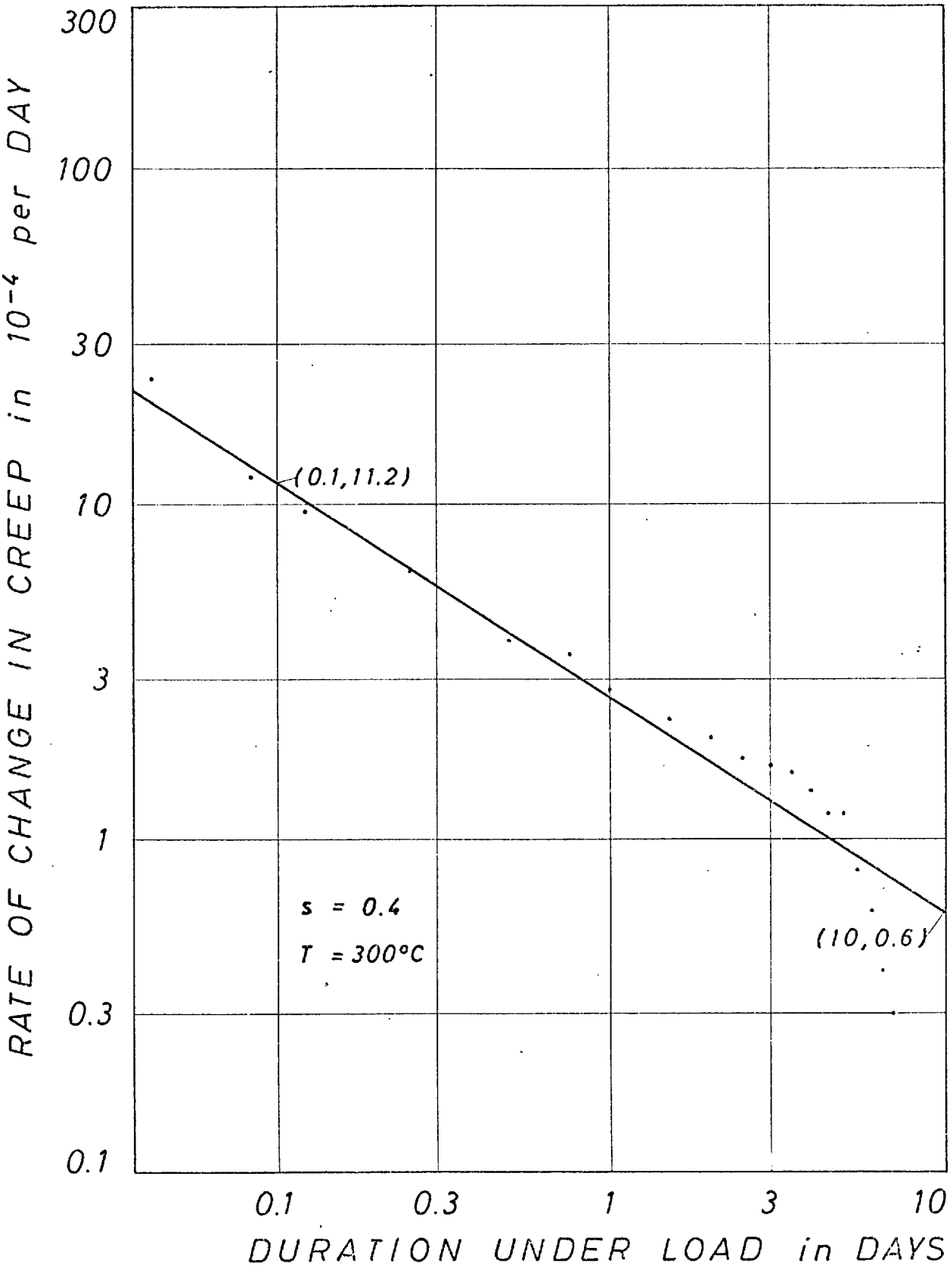


FIG. 11.1. RATE OF CHANGE IN CREEP IN LOG - LOG SCALE

load and temperature-dependence of the parameters in order to attain mathematical clarity, the fitted function reads

$$\log \varepsilon_{,t} = a + b \log t \tag{11.11}$$

With $\log x = 0.43429 \ln x$, the conversion to the natural logarithmic form yields

$$\ln \varepsilon_{,t} = 2.3025 \; a + b \ln t \tag{11.12}$$

Solving explicitly for the real creep increment, thus

$$\varepsilon_{,t} = \exp (2.3025 \; a + b \ln t) \tag{11.13}$$

Employing $e^{\ln t} = t$, the integration of eq. (11.13) procures

$$\begin{aligned} \varepsilon(t) &= \varepsilon(0) + e^{2.3025\, a} \int e^{b \ln t} \, dt \\ &= \varepsilon(0) + e^{2.3025\, a} \int t^{b} \, dt \\ &= \varepsilon(0) + \frac{e^{2.3025\, a}}{b+1} \, t^{b+1} \end{aligned} \tag{11.14}$$

For various stress/ cold strength ratios and temperatures the initial values $\varepsilon(0)$ are known from experiments, whereas the optimization of the numerical values for the parameters $a(s,T)$ and $b(s,T)$ is performed in a semi-visual, semi-analytical way. A family of straight lines is drawn into the double-logarithmic diagrams such that they fall within the zones populated with entries taken from experiments. In this way, each line is sufficiently represented by two coordinate pairs.

Applying the laws for subtracting and adding logarithmic values, the slope $b(s,T)$ of the linear approximation is defined by

$$b = \frac{\log \frac{\varepsilon_{,t_1}}{\varepsilon_{,t_2}}}{\log \frac{t_1}{t_2}}$$

whereas the intersecting point $a(s,T)$ on the ordinate is given by

$$a = \frac{1}{2} \left(\log (\varepsilon_{,t_1} \cdot \varepsilon_{,t_2}) - b \log (t_1 \cdot t_2) \right) \tag{11.16}$$

Out of each family of straight lines, the optimal is found, once the corresponding coordinate pairs produce such values for the parameters a(s,T) and b(s,T) that the real creep curve is fitted satisfactorily by formula (11.14). The criterion adopted for the best fit is the coinciding of calculated values for at least three points of the manually drawn mean profile.

11.3. NUMERIC REGRESSION OF CREEP DATA

11.3.1. ANALYSIS OF THERMAL CREEP STRAINS

Plotting the values for the intersecting point a(s,T) and the slope b(s,T), which together describe the linear approximations of the creep rate in the double logaritmic scale, against the test temperature T, the following linear relations are found

$$\begin{aligned} a(0.2\ ,T) &= -0.50 + 0.0026\ T \\ a(0.4\ ,T) &= -0.15 + 0.0024\ T \\ a(0.66,T) &= -0.05 + 0.0021\ T \end{aligned} \qquad (11.17)$$

$$\begin{aligned} b(0.2\ ) &= -0.60 \\ b(0.4\ ) &= -0.65 \\ b(0.66) &= -0.72 \end{aligned} \qquad (11.18)$$

Examining eqs. (11.17) and (11.18), for which graphs are shown in fig. (11.2), a further regression to generality is possible. Treating the stress/ cold strength ratio as a variable, the intersecting point becomes a field parameter

$$a(s,T) = c(s) + d(s)T \qquad (11.19)$$

where $c(s) = \log s + 0.2$

and $d(s) = 0.0028 - 0.001\ s$

In contrast, the slope is sufficiently represented by the temperature-independent function

$$b(s) = -0.55-0.25\ s \qquad (11.20)$$

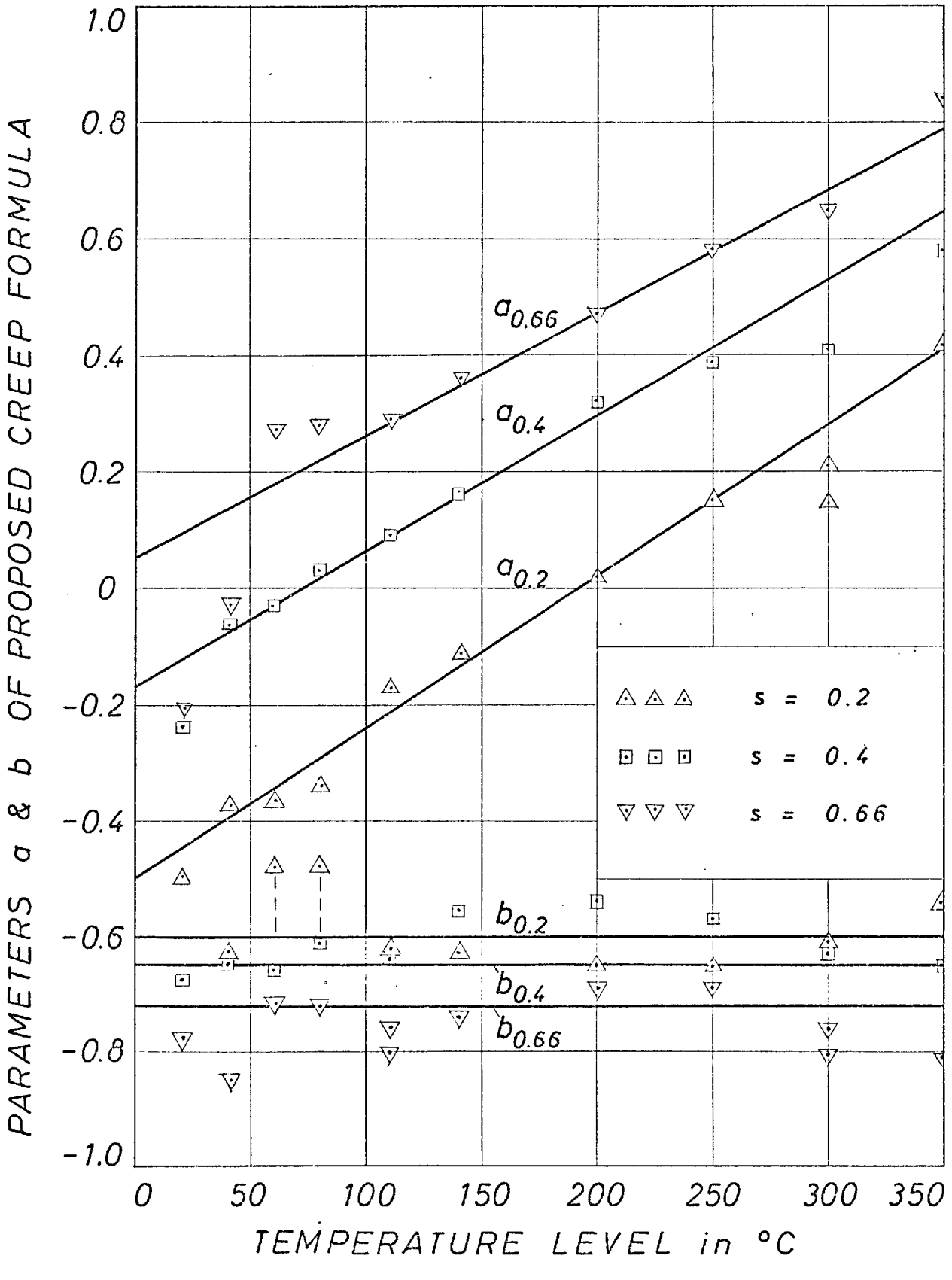


FIG. 11.2. TEMPERATURE-DEPENDENT PARAMETERS OF PROPOSED CREEP FORMULA

The diagrams for the parameters b(s), c(s) and d(s) are illustrated in fig. (11.3). The field parameter a(s,T) appears as an exponent in the exponential term of formula (11.14), which must vanish as the stress tends to zero, because regardless of the temperature, zero loads by definition do not activate creep strains. With the exponential function converging to zero for minus infinity, thus a logarithmic approximation to the parameter c(s) follows logically.

Taking the initial thermoelasto-plastic strains from fig. (5.9), the prediction of the creep responses for individual combinations of stress and temperature may be accomplished by evaluating the field equation

$$\varepsilon(s,T,t) = \varepsilon(s,T,0) + \frac{e^{2.3025\ a(s,T)}}{b(s)+1}\, t^{b(s)+1} \qquad (11.21)$$

where $\varepsilon(s,T,0)$ follows formula (5.1) for $T \leq 200^0C$ and formula (5.2) for $T \geq 200^0C$. The duration under load is substituted in days, while the strain values from eq. (11.21) are given in 10^{-4}, i.e. 100 μ.

The only precaution to be observed when employing formula (11.21) is that eq. (5.7) for the ultimate endurable temperature is satisfied. No creep curve, for instance, should be predicted for the coordinate pair $(0.8, 300^0C)$ as it is located in the domain of failure-procuring conditions. Concrete subjected to such conditions has no history.

11.3.2. ANALYSIS OF THERMOVISCOELASTIC STRAINS

As demonstrated in Chapter X, a mathematimatically rigorous incorporation of the effects of thermal creep into matrix analyses of structures is only possible, if the superposition hypothesis holds, i.e. if the total creep strains are linear in the stress variable.

Convincing illustration of the overlay of normalized creep strains which develop under conditions milder than $(0.66, 300^0C)$ is given in figs. (5.11) and (5.12). Within this range, the phenomenological notion of thermal creep thus may be simplified to the mathematical concept of thermoviscoelasticity.

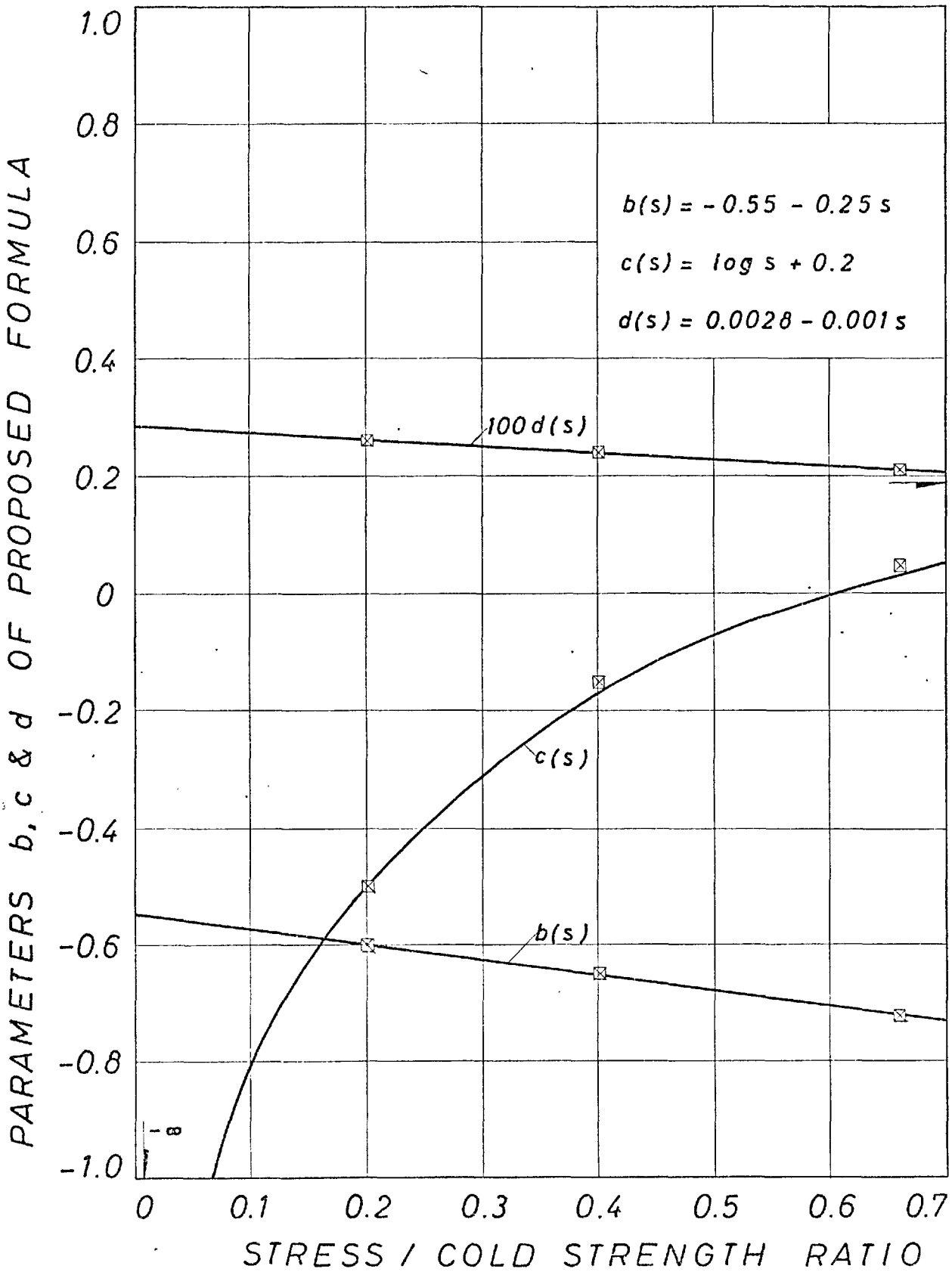


FIG. 11.3. STRESS-DEPENDENT PARAMETERS OF PROPOSED CREEP FORMULA

Using, as stipulated in Chapter V, the stress/ cold strength ratio of s = 0.2 as a base, formula (11.21) may be replaced by another which is limited to the computation of thermoviscoelastic strains

$$\varepsilon(s,T,t) = \frac{s}{0.2}\,\varepsilon(0.2,T,0) + \frac{e^{2.3025\ a(0.2,T)}}{b(0.2)+1}\,t^{b(0.2)+1} \tag{11.22}$$

To make eq. (11.22) generally applicable, material constants must be considered. To commence, the thermoelastic strains recorded in fig. (5.15) are expressed in terms of the modulus of elasticity for ambient temperature by rewriting eq. (5.1) in the form

$$\varepsilon(0.2,T,0) = \frac{\sigma_{0.2}}{E(20^0C)}\,f(T) \tag{11.23}$$

where dependent on the temperature range, the non-dimensional tri-linear function reads

$$\begin{aligned} f(T) &= (1.0 + 0.00833\ (T - 30)) \quad (30 \leq T \leq 60) \\ f(T) &= (1.25 - 0.00250\ (T - 60)) \quad (60 \leq T \leq 110) \\ f(T) &= (1.125 + 0.00349\ (T - 110)) \quad (110 \leq T \leq 300) \end{aligned} \tag{11.24}$$

Expressing the applied stress in terms of the strength of concrete, there is

$$\sigma = s\,c'_{yu} \tag{11.25}$$

Substituting eqs. (11.23) to (11.25) and the inversion of eq. (11.25) into eq. (11.22), the author's formula for the ascertainment of stress, temperature and time-dependent strains occurring in virgin concrete is arrived at

$$\varepsilon(s,T,t) = s\,\frac{c'_{yu(20^0C)}}{E(20^0C)}\,f(T) + \frac{e^{2.3025\ a(0.2,T)}}{b(0.2)+1}\,t^{b(0.2)+1} \tag{11.26}$$

where f(T) follows eqs. (11.24), a(0.2) is given by the first of eqs. (11.17) and b(0.2) = - 0.60 from the third of eqs. (11.18). The time is substituted in days and the strains are obtained in 100 μ.

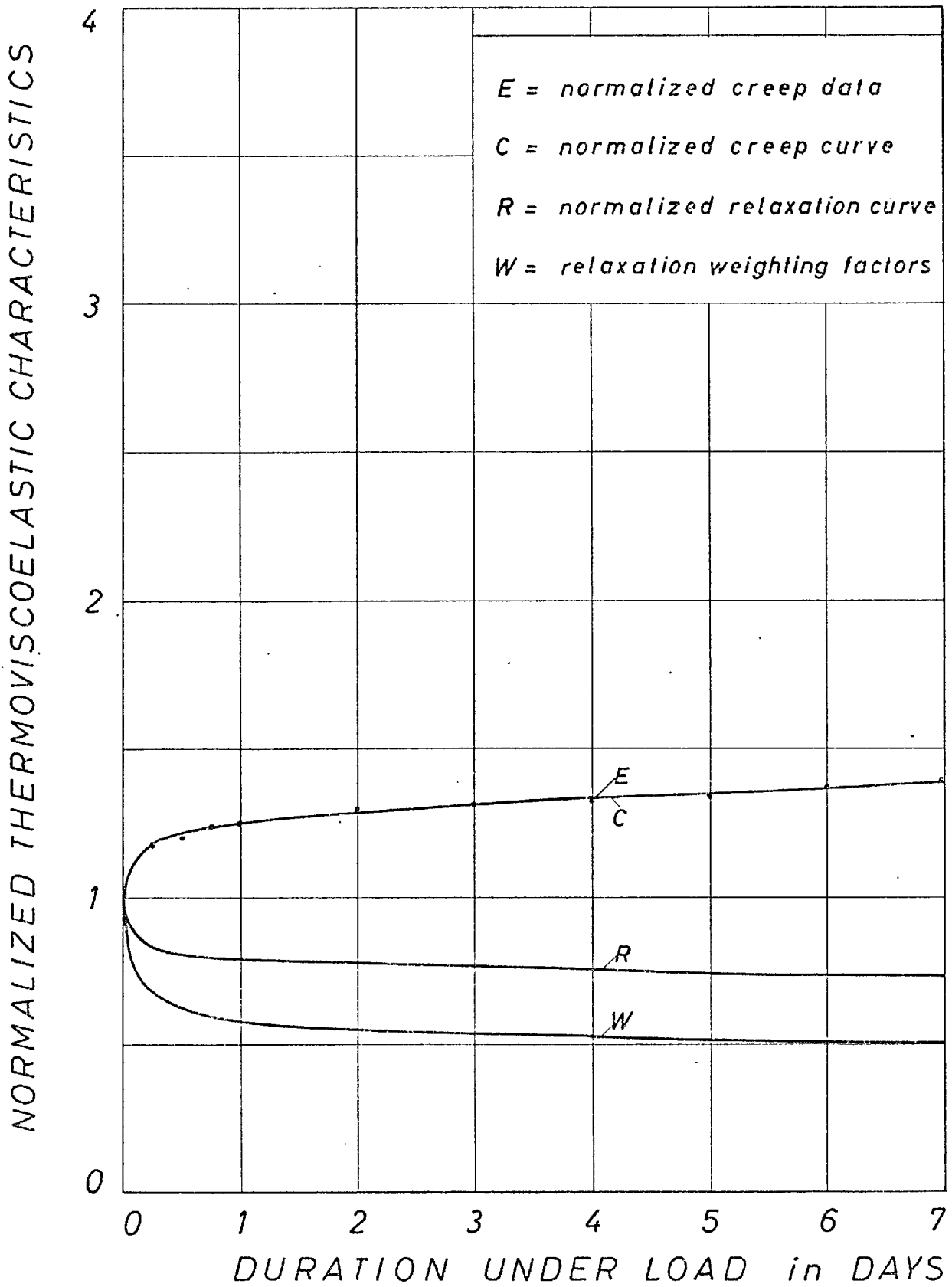


FIG. 11.4. THERMOVISCOELASTIC CHARACTERISTICS OF CONCRETE AT 20°C

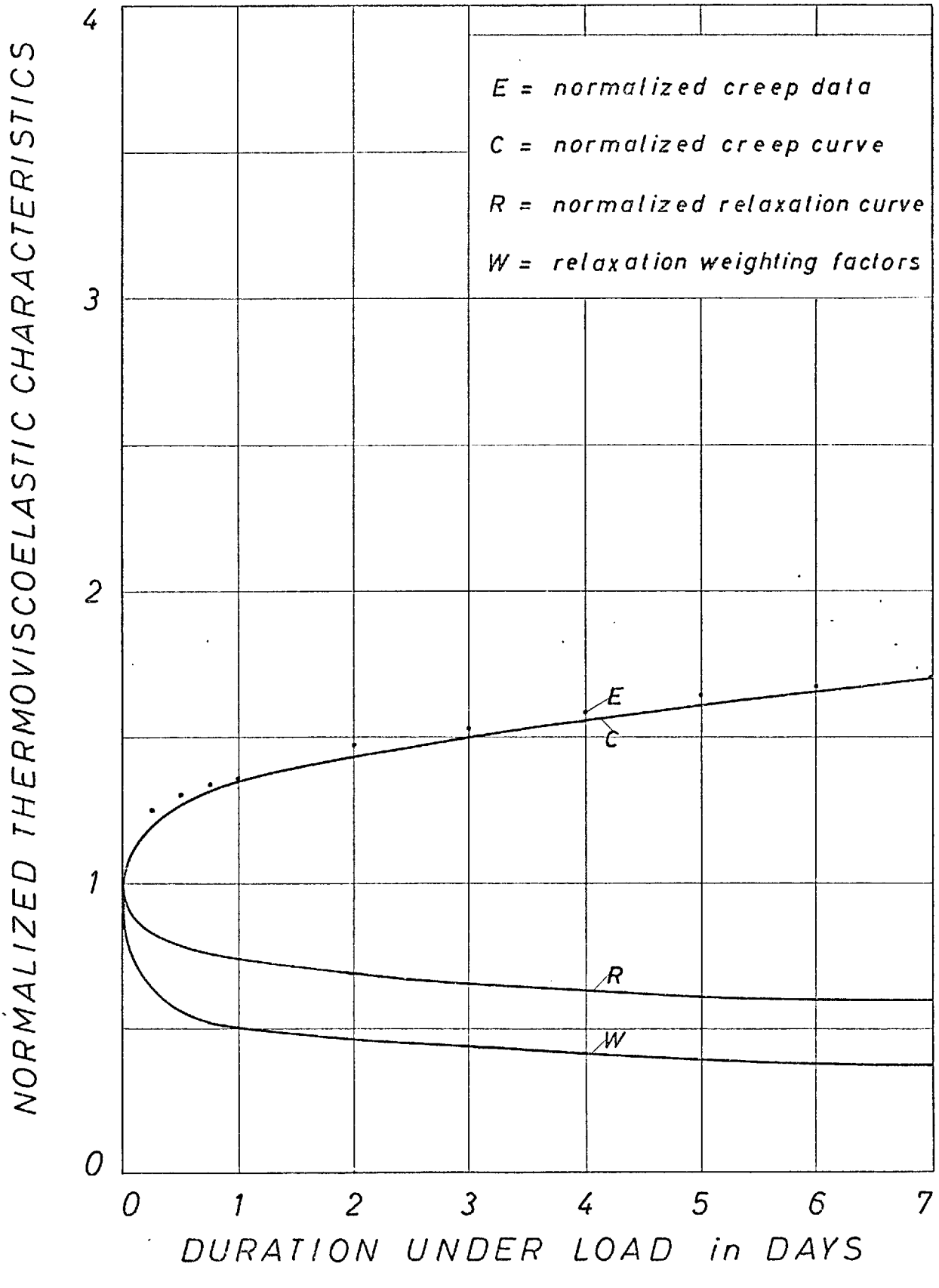


FIG. 11.5. THERMOVISCOELASTIC CHARACTERISTICS OF CONCRETE AT 40°C

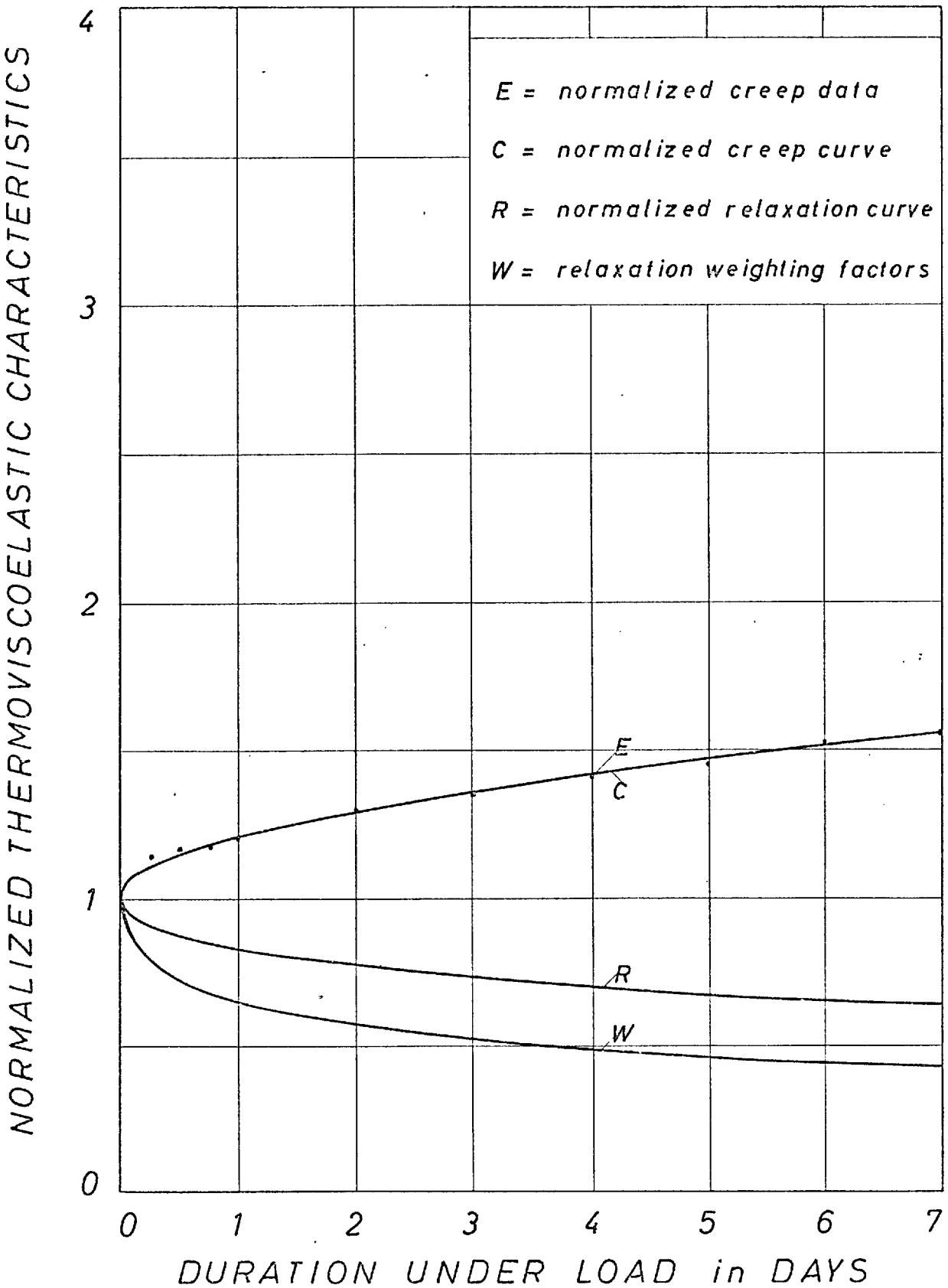


FIG. 11.6. THERMOVISCOELASTIC CHARACTERISTICS OF CONCRETE AT 60°C

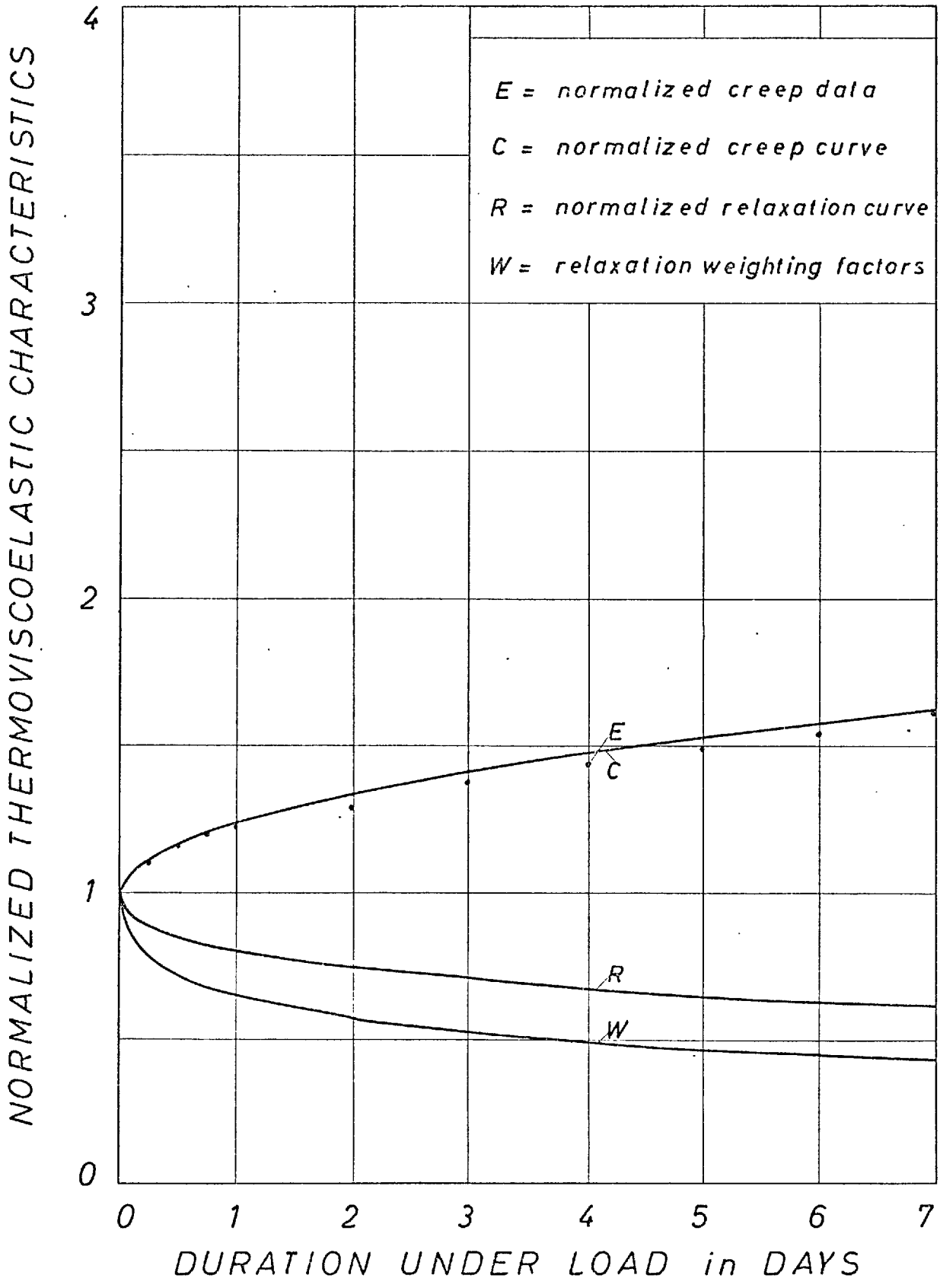


FIG. 11.7. THERMOVISCOELASTIC CHARACTERISTICS OF CONCRETE AT 80°C

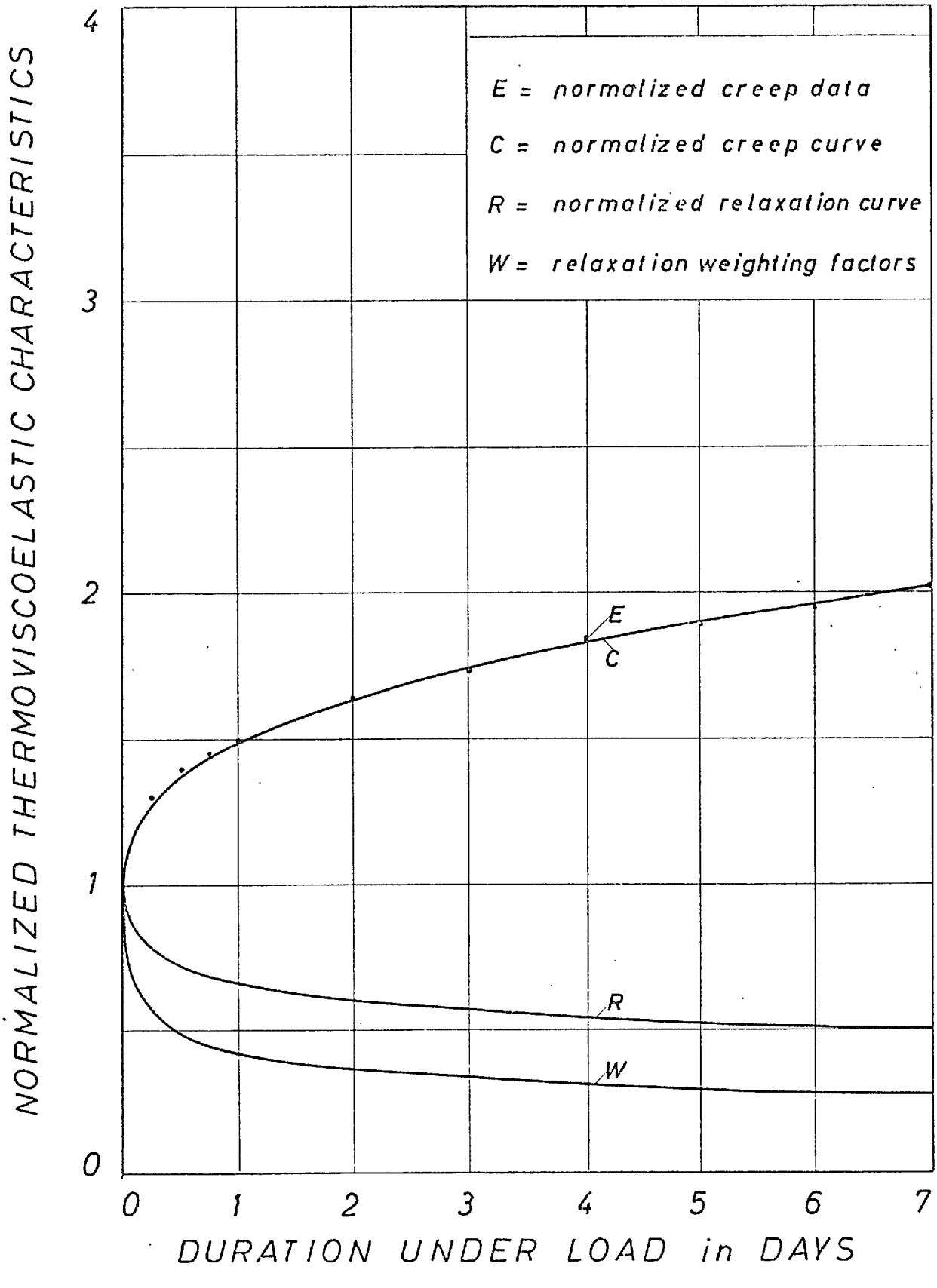


FIG. 11.8. THERMOVISCOELASTIC CHARACTERISTICS OF CONCRETE AT 110°C

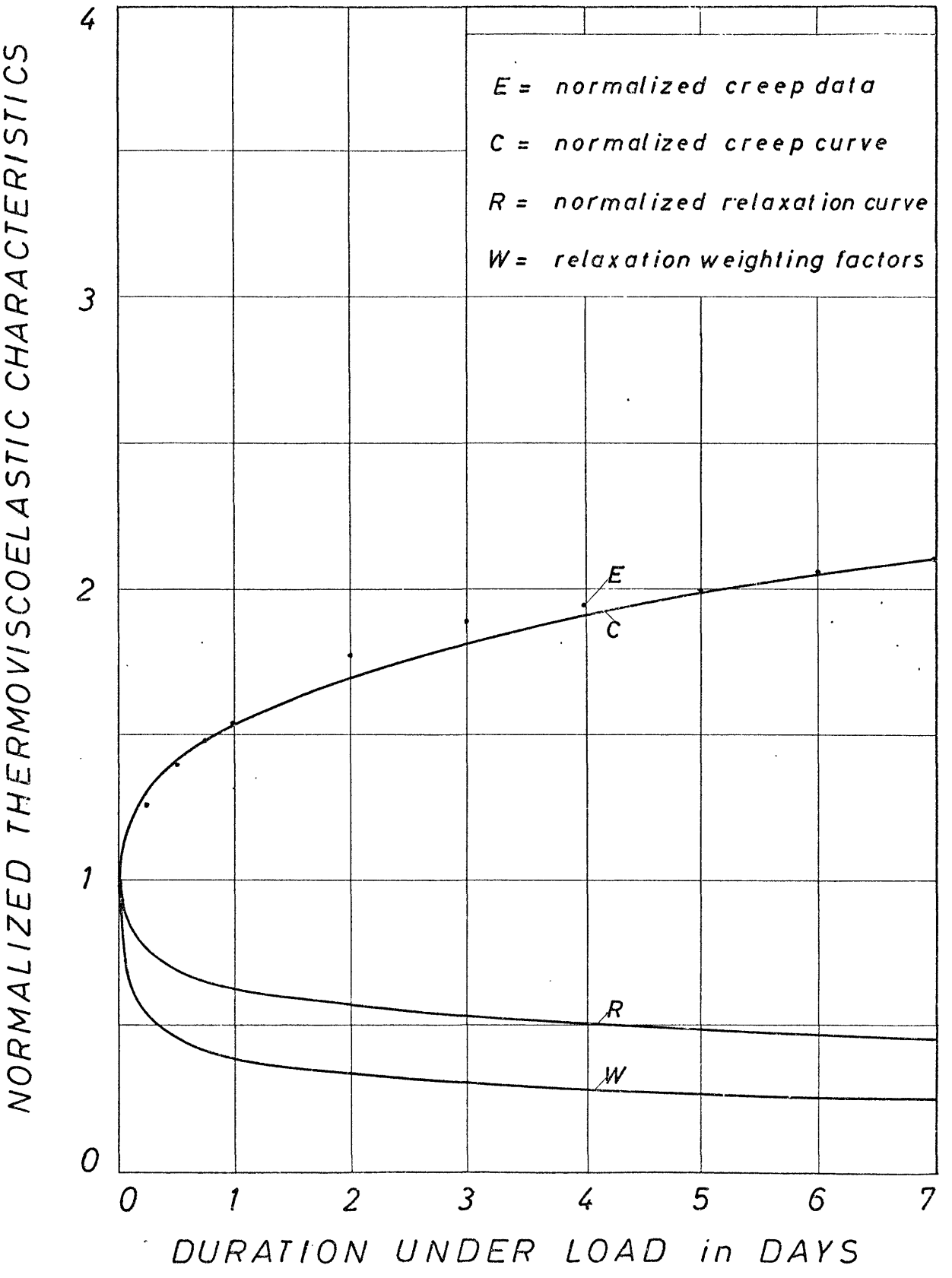


FIG. 11.9. THERMOVISCOELASTIC CHARACTERISTICS OF CONCRETE AT 140°C

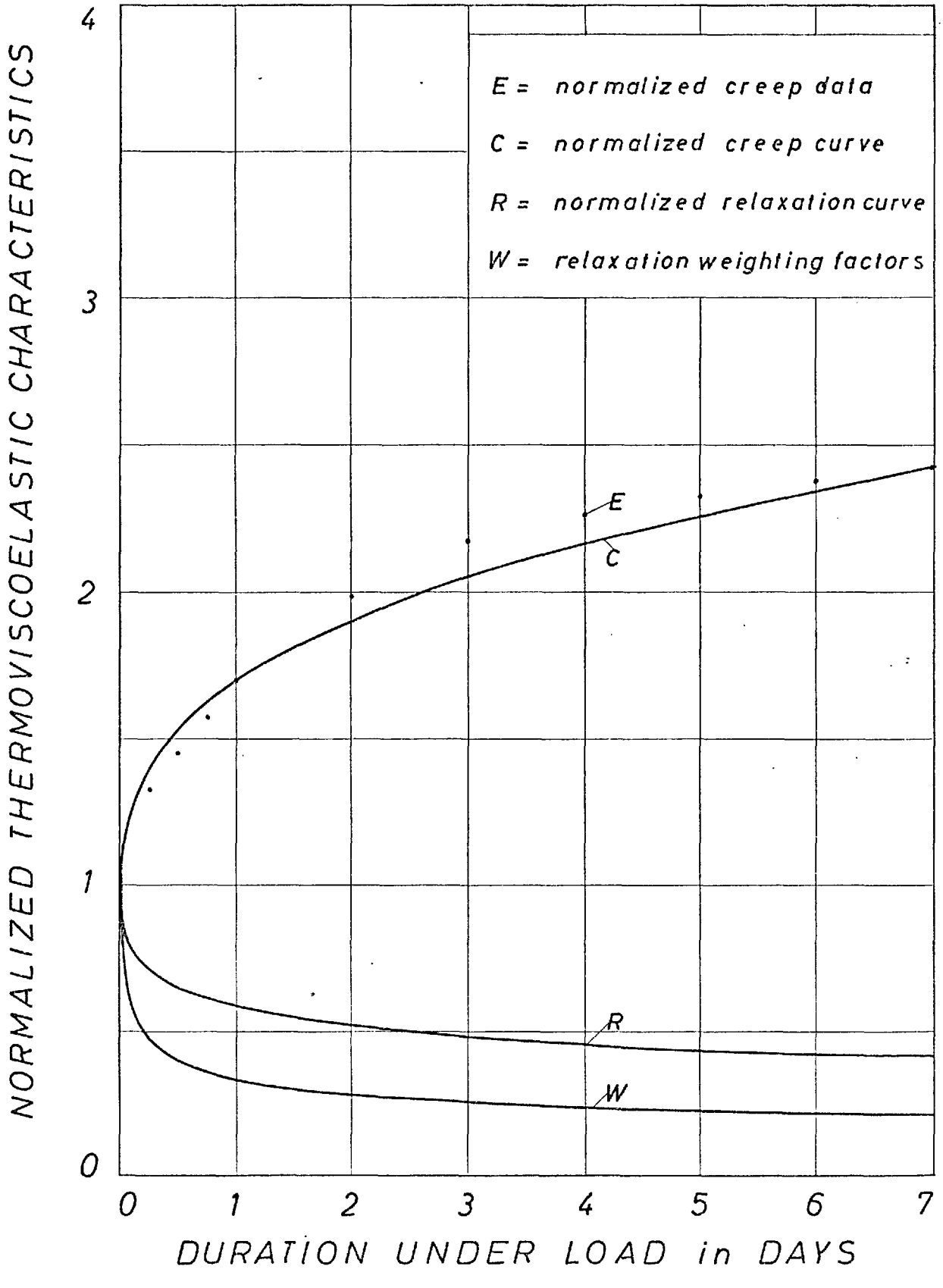


FIG. 11.10. THERMOVISCOELASTIC CHARACTERISTICS OF CONCRETE AT 200°C

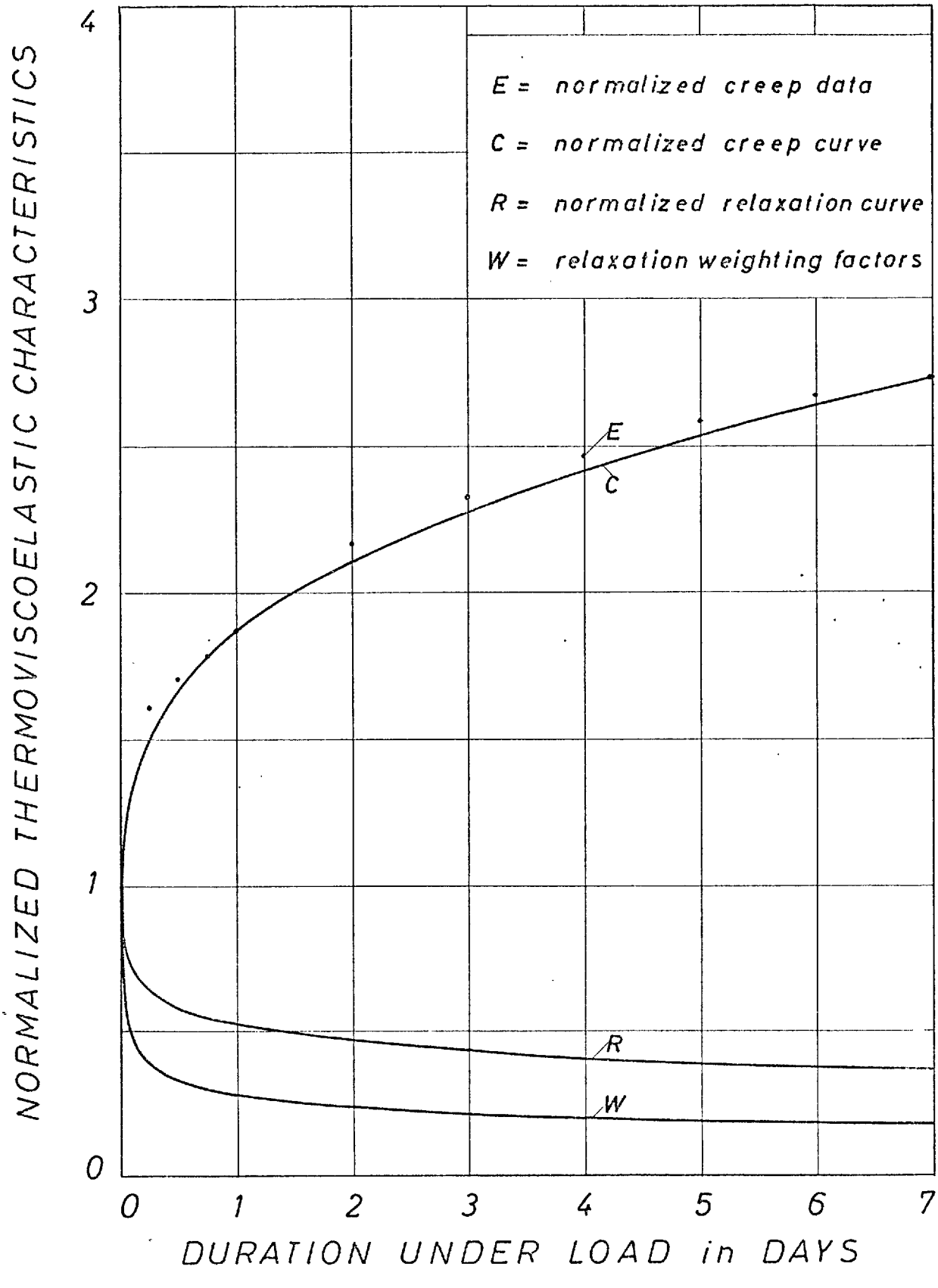


FIG. 11.11. THERMOVISCOELASTIC CHARACTERISTICS OF CONCRETE AT 250°C

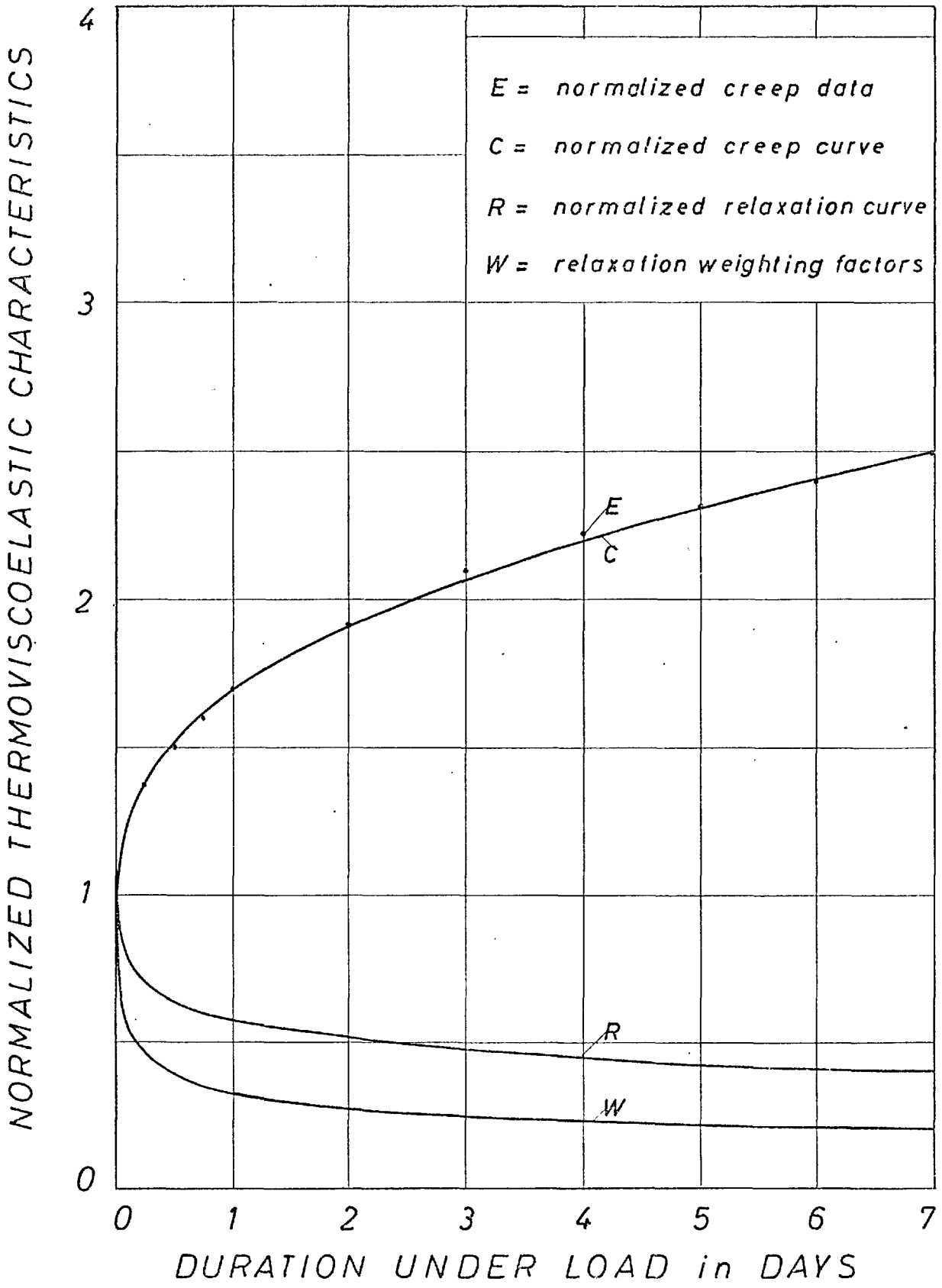


FIG. 11.12. THERMOVISCOELASTIC CHARACTERISTICS OF CONCRETE AT 300°C

11.4. THERMAL RELAXATION WEIGHTING FACTORS

11.4.1. GENERATION OF WEIGHTING FACTORS

Creep and relaxation functions must be available in a form normalized to unity as to make them compatible to the solution procedure for the history-dependent integrals (10.22) and (10.33). Any time-dependent strain response must be devided by the value recorded at time zero.

A computer program CRELAX designed by the author surmounts the difficult task of converting original thermal creep curves to time-dependent thermal relaxation weighting factors, which in the linear thermoviscoelastic analysis are employed as multipliers to the coefficients of the structure's global stiffness matrix. First the program transforms the creep curves as reproduced by formula (11.26) to sequences of relaxation responses on the basis of the creep-relaxation duality as expressed in eq. (10.23). Then it regresses the latter to time-dependent relaxation weighting factors by evaluating the history-dependent arithmetic expression (10.29).

For illustration, in figs. (11.4) to (11.12), the normalized, linear thermoviscoelastic strain curves, experimentally obtained for test temperatures between 20 and 300^0 C, are compared with those generated by evaluation of the author's formula (11.26). Also, the corresponding normalized thermal relaxation functions and the pertaining relaxation weighting factors are displayed.

Since for design purposes only the thermal relaxation weighting factors are of interest, these are entered independently in a semi-logarithmic scale in fig. (11.13). It should be said that each profile is really a sequence of discrete time-dependent scalars and does not represent a continuous function, since each scalar value is obtained by a separate integral (10.36).

The figs. (11.4) to (11.13) are considered self-explanatory. However, it is important to realize that the initial gradients of the relaxation curves - and thus the drop in value of the initial weighting factors - are much steeper than those of the creep curves. Rephrased, the phenomenon

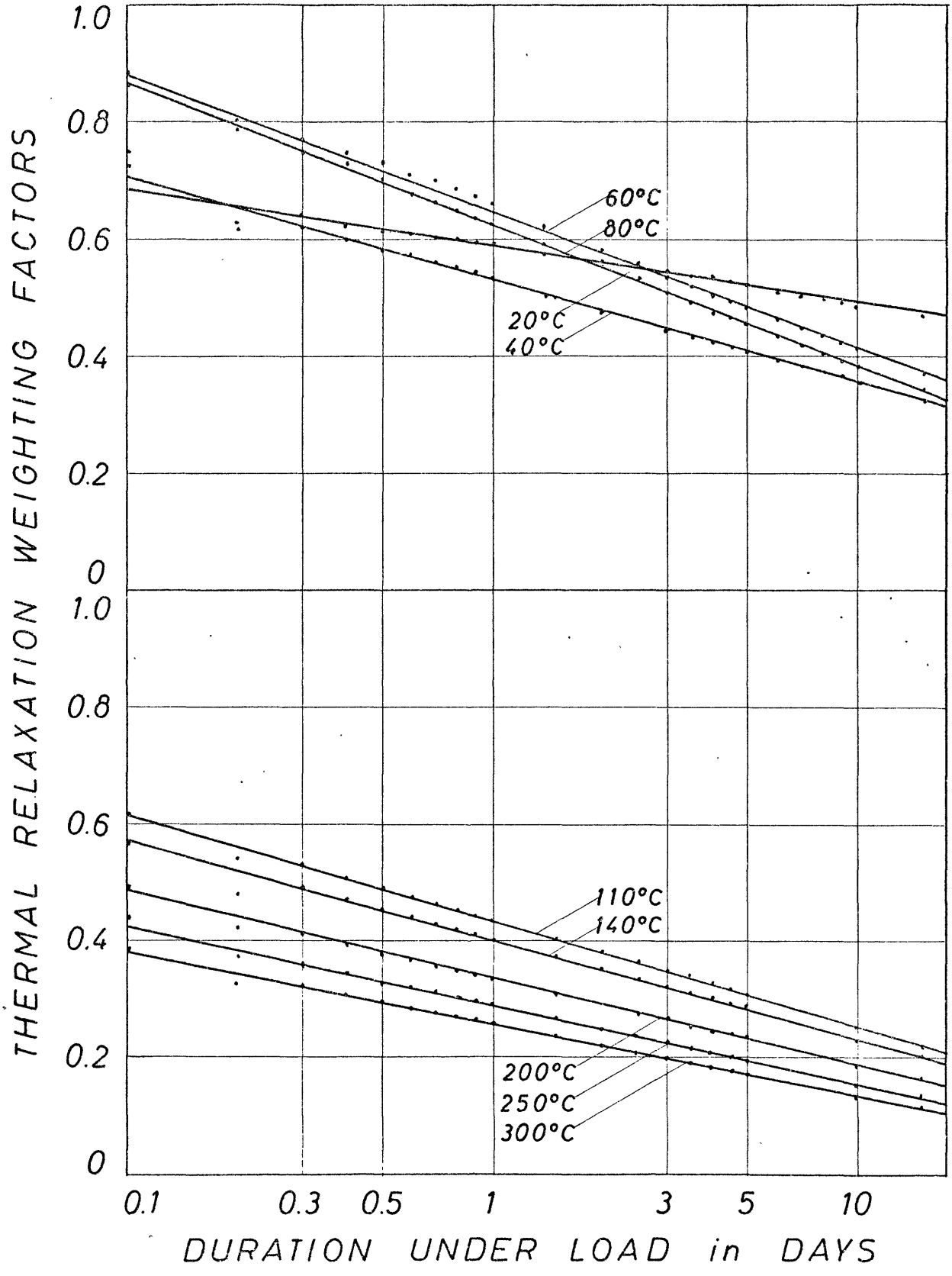


FIG. 11.13. THERMAL RELAXATION WEIGHTING FACTORS IN SEMI-LOG SCALE

of relaxation in a structure is activated at a much faster rate than the phenomenon of creep.

This observation is very satisfying, as it corroborates that the proposed stiffness approach to structural thermoviso-elastic analysis using relaxation weighting factors is more efficient than the flexibility method of approach.

To preserve the positive definiteness of the stiffness matrix of the structure to be analysed, neither the relaxation functions nor the pertaining relaxation weighting factors are permitted to take negative values. As shown in figs. (11.4) to (11.12), this holds regardless of the prevailing temperature. It follows that the profiles in fig. (11.13) may converge to but never intersect the abscissa.

If CRELAX produces negative values, the underlying finite differences time step is too large. The step length chosen for processing the data of the present research is $\Delta t = 0.1$ days for temperature up to 200 C and $\Delta t = 0.05$ for others. A list of the author's thermal relaxation weighting factors is given in table A6.4 of Appendix VI.

11.4.2. EMPLOYMENT OF WEIGHTING FACTORS

The principle of employing thermal relaxation weighting factors is discussed in detail in Chapter X. However, to verify the applicability of the factors, in the following a comparison between recorded and predicted strains is given.

The strains developing in the concrete cylinders are measured between two collars which are positioned 26 mm away from the end faces. Reference is made to fig. (3.12). Thus the stress distribution may be assumed to be uniform across any imagined horizontal plane between the collars. This condition enables the stiffness matrix of the vertically loaded specimens to be reduced to a single scalar stiffness coefficient.

With only one displacement component u to be considered, the inter-dependence of system points, as explained by Maxwell's reciprocity principle (7.25) for matrix analyses, is inapplicable. Consequently, the weighting factor premultiplied to the stiffness coefficient and the force component in the single

force-deformation equation may be cancelled.

Also, the stress acting in the direction of the only displacement component is fixed, inferring that the history-dependent term of integral (10.33) vanishes. With the stress being prescribed and time-independent, the history-dependent thermal relaxation weighting factors degenerates to simple time-dependent thermal relaxation responses. Hence eq. (10.39) reduces to

$$m(T)\ E(20^0C)\ \frac{A}{l}\ r(A,t)\ u(s,T,t) = F(s) \qquad (11.27)$$

where $l = 127$ mm is the distance between the collars.

With figs. (5.1) to (5.5) and (11.4) to (11.12) showing strain developments, eq. (11.27) is suitably solved for the strains. From the author's observation reported in Chapter V, the coordinate pair $(s,T) = (0.66, 300^0C)$ marks the boundary of the linear thermoviscoelastic domain of concrete. Employed in eq. (11.27), it enables an estimation of the largest error to be encountered in the proposed thermo-viscoelastic analysis of concrete structures. The selected time instant is seven days.

According to eq. (5.5) and table 5.2, the reference modulus of elasticity is $E(20^0C) = 28.1$ KN/mm^2 and the associated temperature-dependent reduction factor is $m(300^0C) = 0.62$. The applied force amounts to $F(0.66) = 77.2$ KN and the circular cross-sectional area to $A = 2822$ mm^2. The thermal relaxation response, finally, may be read from curve R in fig. (11.12) as $r(300^0C, 7\ \text{days}) = 0.39$. Substitution into the inverse of eq. (11.27) yields

$$(0.66, 300^0C, 7\ \text{days}) = 77.2/(28.1 \cdot 0.62 \cdot 2822 \cdot 0.39) = 4020\ \mu \qquad (11.28)$$

The experimental value, as recorded in fig. (5.5), is 4600 μ. The largest error to be expected in the thermo-viscoelastic analysis using the author's formula (11.26) thus works out at $(46 - 40.2)/46 = 12.6$ %. For a composite material like concrete this error may be considered acceptable.

11.5. COMPUTER PROGRAM**THERMO AXICON**

11.5.1. GENERAL

The main features of the computer program THERMO AXICON (Transient thermoviscoelastic analysis of axisymmetric concrete continua) written to solve numerically the problem set out in this thesis is described. The program was developed by the author on the FUN compiler of the Imperial College CDC 6400 computer. It should also work on other compilers of these machines.

A list of the source deck of the program is not included in this thesis, as the program can readily be obtained in the Civil Engineering Departmental program library. However, the underlying flow chart which gives insight into the logic of the program is listed in Appendix II. It contains the sequence of the subroutines called and states their function with respect to the governing matrix equations to be solved.

11.5.2. TRANSIENT TEMPERATURE DISTRIBUTIONS

The first part of the computer program THERMO AXICON determines the temperature values existing at the nodal points of the relevant finite element mesh at any time instant required. The underlying theory is expounded in Chapter X.

As an example, transient temperature fields propagating through the concrete pressure vessel described in Chapter IX are solved for various time instants. The initial thermal boundary conditions imposed are the following : temperature of the body and on the outer surface $T = 20^0C$, step change in temperature on the inner surface to $T = 90^0C$.

Since the governing matrix equations are given prior to the listing of the flow chart in Appendix II, no reference is made to them here.

The physical and thermal properties of the concrete involved are the ~~specific~~ density $\rho = 2500$ kg/m^3, the heat generation $q = 0$ Kcal/m^3 day, the specific heat $c = 0.23$ Kcal/^{0}C kg and the thermal conductivities $k_r = k_z = 60$ Kcal/^{0}C m day (1 Btu = 0.252 Kcal).

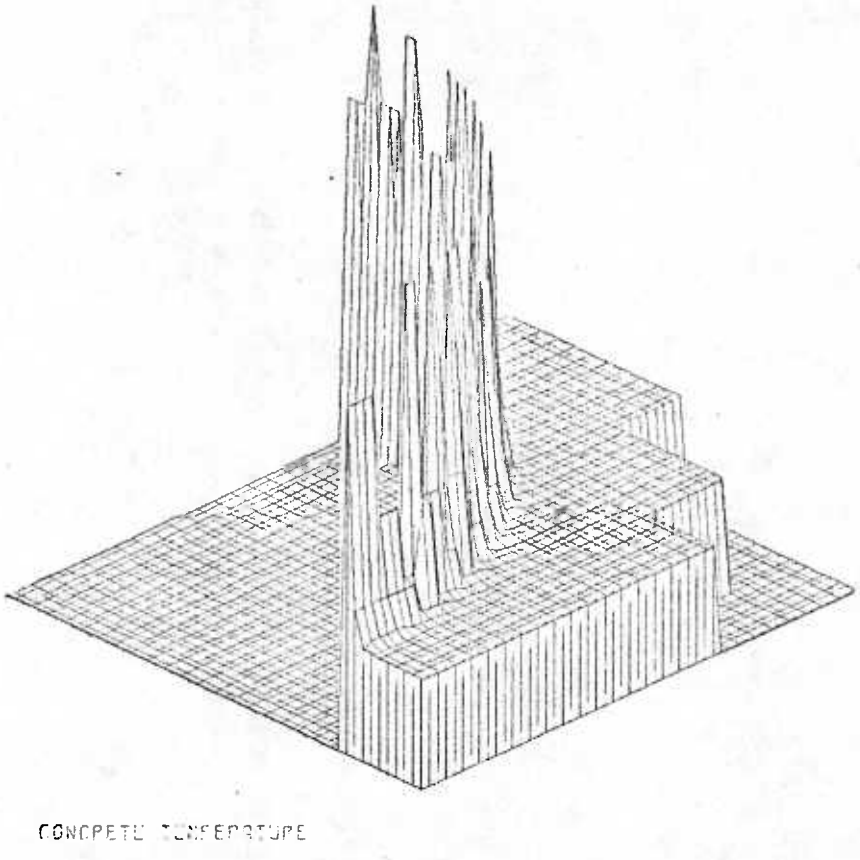


Fig. 11.14. Temperature distribution after 1 day, inner surface 90°C, outer surface 20°C

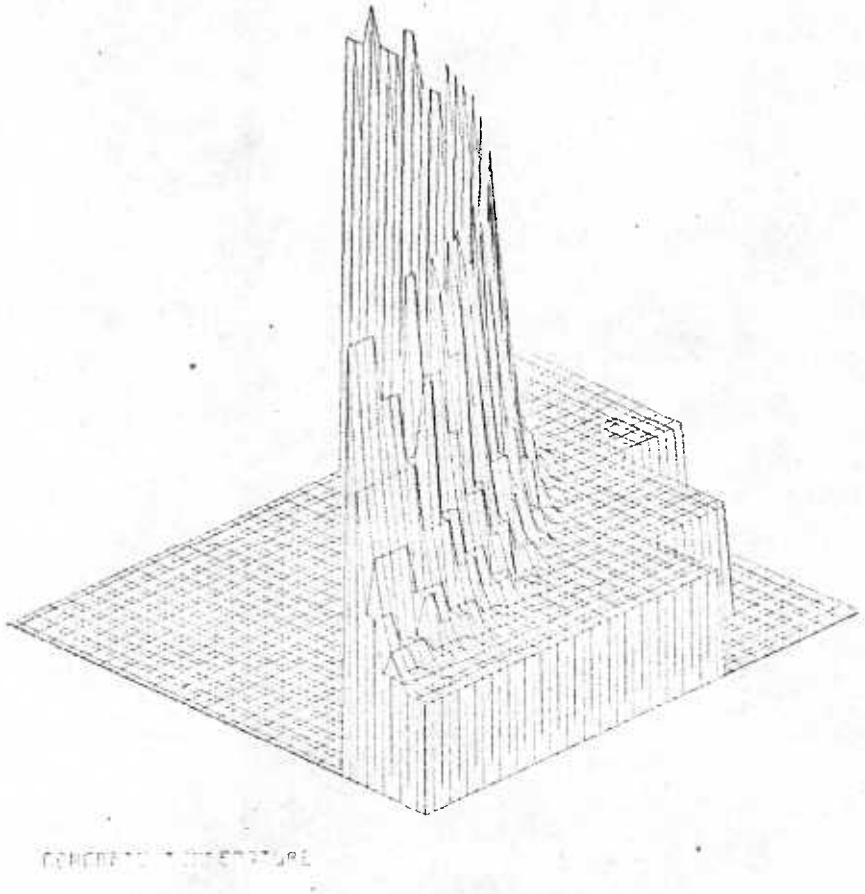


Fig. 11.15. Temperature distribution after 10 days, inner surface 90°C, outer surface 20°C

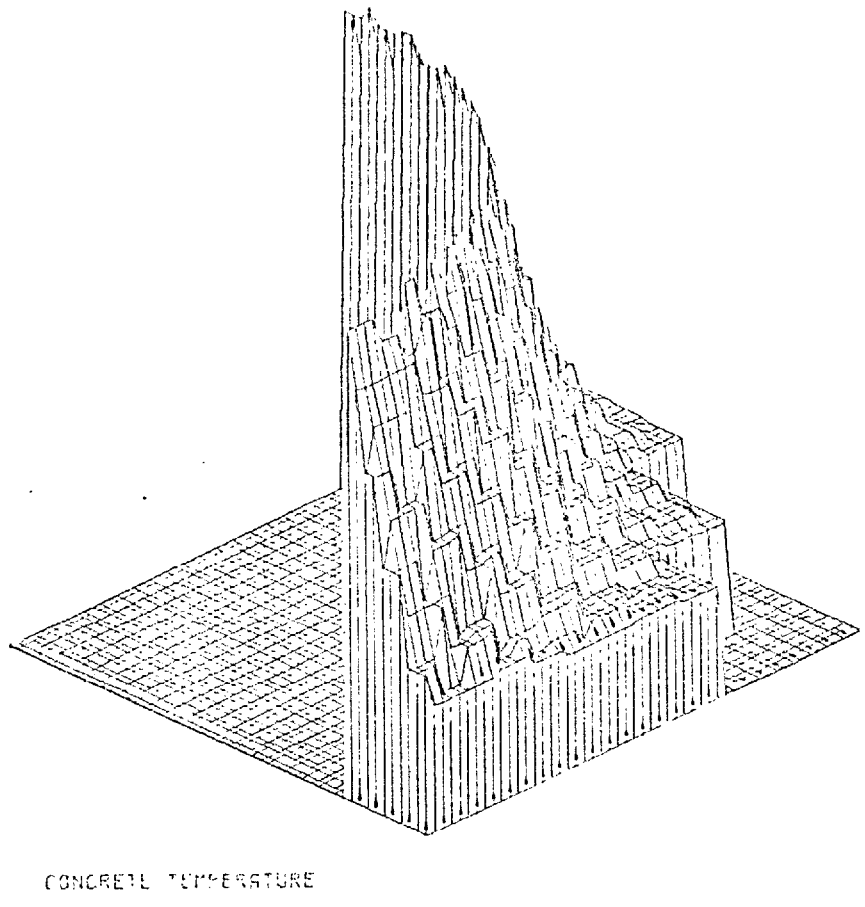


Fig. 11.16. Temperature distribution after 100 days, inner surface 90°C, outer surface 20°C

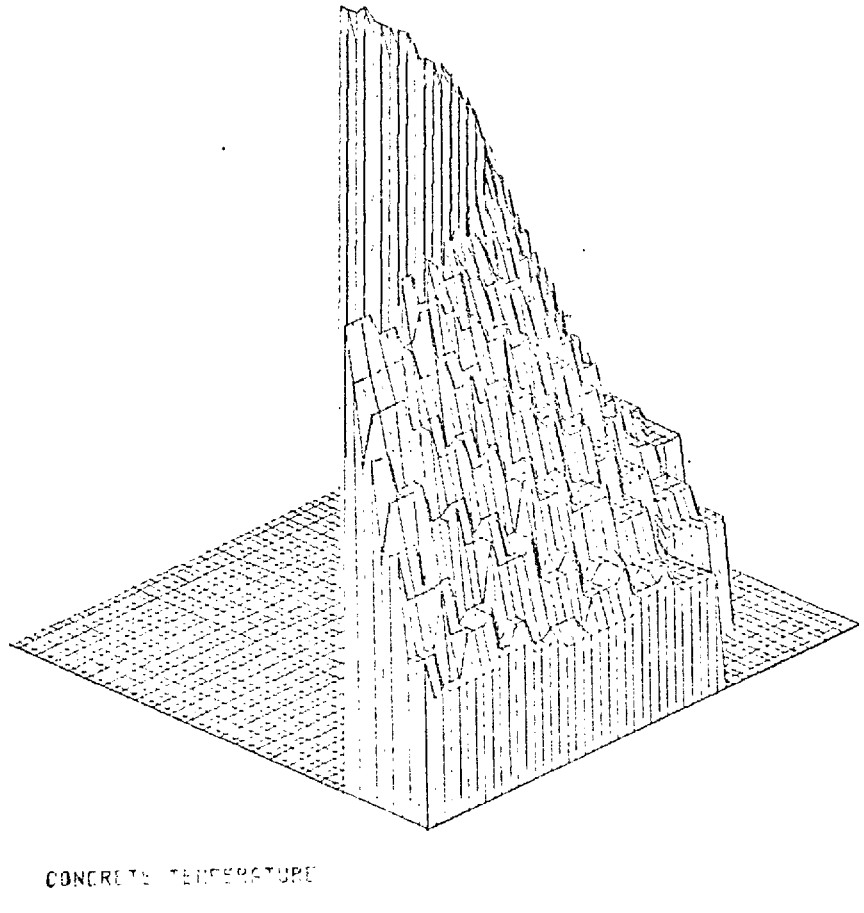


Fig. 11.17. Temperature distribution at infinity, inner surface 90°C, outer surface 20°C

The initial, transient and stationary cross-sectional temperature distributions that appear at 1 day, 10 days 100 days and infinity after the instantaneous application of the above mentioned step change in temperature, are drawn in figs. (11.14) to (11.17), respectively. The figures are produced by the combined usage of the author's routines MESH and SURPLT.

Since only two out of three nodal points of each element adjacent to the inner sphere lie on the actual surface and the analysis of thermally induced stresses is based on temperatures averaged over the individual elements, it is observed that the ridge of the temperature field in fig. (11.14) has not yet reached the value 90°C. Otherwise, figs. (11.14) to (11.17) may be considered self-explanatory.

11.5.3. TRANSIENT THERMOVISCOELASTIC STRESS FIELDS

The circumferential stress fields which build up as a thermoviscoelastic response of the axisymmetric concrete vessel due to temperature fields displayed in figs. (11.14) to (11.17) are illustrated in figs. (11.18) to (11.21).

To emphasize the difference between the effects of steady state and transient temperature distributions on the mechanical behaviour of the structure, figs. (11.20) and (11.21) must be compared.

11.6. CONCLUSIONS

The major conclusions are that due to the thermoviscoelastic nature of the concrete material, stress fields may locally change the sign, as indicated by the ridge of the tensile stresses along the upper part of the inner surface in fig. (11.20), i.e. after 100 days of thermal creep.

Thus the approximation of transient temperature fields by step-wise steady state temperature distributions which gives rise to quasi-thermoelastic stress fields is completely unjustified. By the time the transient temperature distribution has reached, if at all, a steady state, the strain history has already altered the material characteristics.

With the employment of thermal relaxation weighting

factors, any strain history may be reproduced rigorously and realistically.

Comparing the results of the present chapter with those obtained in Chapter IX, thermally induced stresses are by one order of magnitude higher than those due to mechanical action on the structure.

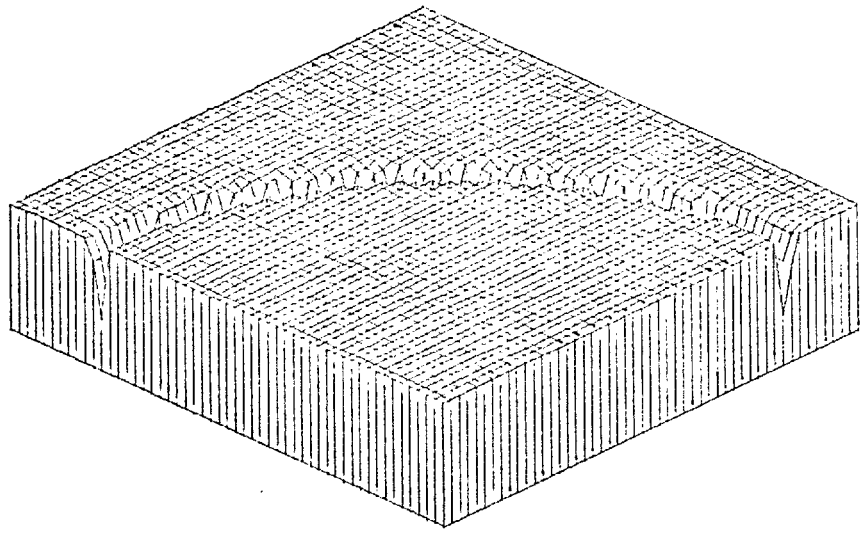


Fig. (11.18) Transient thermoviscoelastic circumferential stresses after 1 day

σ_{min} = - 22 N/mm^2(264) σ_{max} = 1 N/mm^2(3)

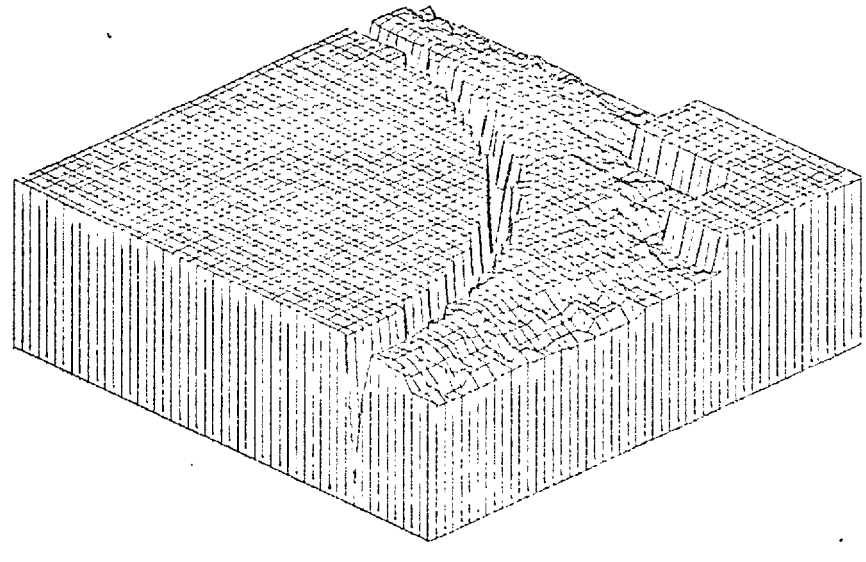


Fig. (11.19) Transient thermoviscoelastic circumferential stresses after 10 days

σ_{min}= - 44 N/mm^2(276) σ_{max} = 6.5 N/mm^2(287)

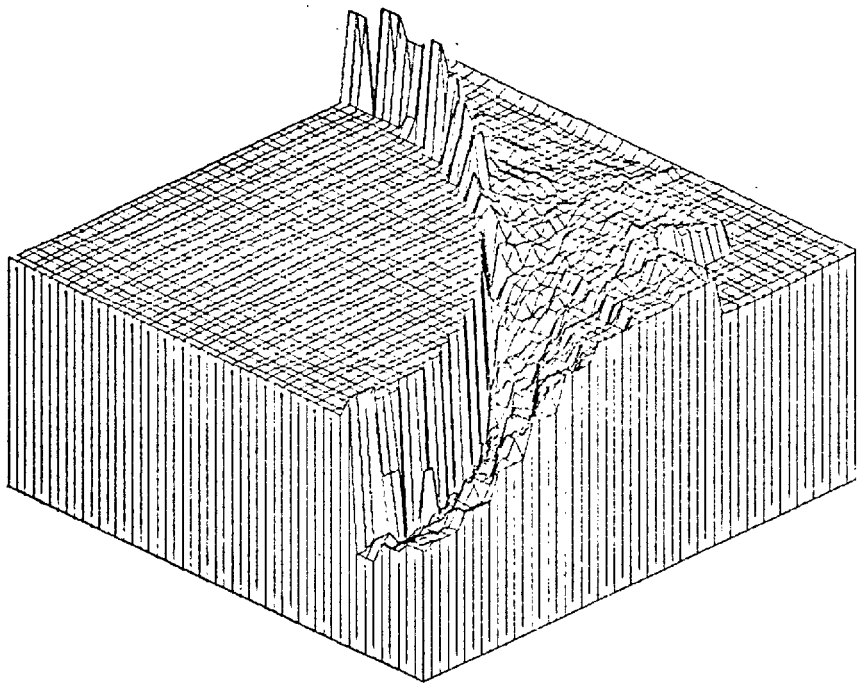


Fig. (11.20) Transient thermoviscoelastic circumferential stresses after 100 days

σ_{min} = 151 N/mm² (1) σ_{max} = 136 N/mm² (264)

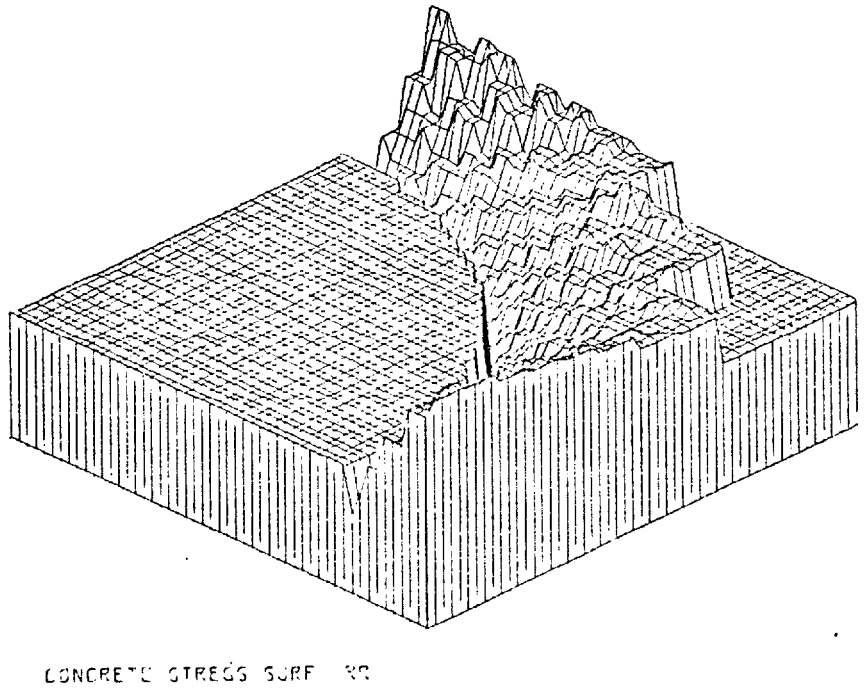


Fig. (11.21) Steady state thermoelastic circumferential stresses

σ_{min} = - 22 N/mm² (276) σ_{max} = 21 N/mm² (287)

CHAPTER XII

CONCLUSIONS AND RECOMMENDATIONS FOR FUTURE RESEARCH

12.1. CONCLUSIONS

In recapitulating the work presented in the individual chapters, the following general conclusions are arrived at.

12.1.1. CHAPTER I

(1) The original contribution is seen in embarking on the formulation of the difficult and neglected problems of thermal creep in the analysis of concrete continua and in motivating the quest for matrix methods as a tool in its solution procedure.

(2) The concern about the behaviour of concrete under elevated and high temperature is explained.

(3) The insolubility of the mixed elliptic and parabolic continuity and compatibility equations in the heat conduction and the stress analysis problem is stated.

(4) The necessity for techniques to separate conductivity and stiffness coefficients from the temperature and the displacement field in space and time is recognized.

(5) The need for methods to allow the temperature and displacement fields to take prescribed time-dependent values along the physical boundaries is emphasized.

(6) The search for mathematically rigorous concepts to account for the change of conductivity coefficients with temperature and the stiffness coefficients with time is motivated.

12.1.2. CHAPTER II

(1) The original contribution is seen in recognizing the dialectic nature, i.e. the dynamically balanced, simultaneous occurrence of the creep and relaxation phenomena.

(2) The dual approach to structural analysis is set forth, permitting concepts based on the variation of either

strains under prescribed stress system or stresses under prescribed strain systems.

(3) The theoretical convertibility of creep curves into relaxation responses is pointed out.

(4) The definition for thermal creep and relaxation as convenient for structural analysis are given.

(5) The definition of linear thermoviscoelastic strains is formulated as convenient for mathematically practicable analysis.

(6) The concept of the superposition hypothesis and its profound importance in linear elastic and thermoelastic analyses is outlined.

(7) The approximation to be made for structures creeping under the influence of transient temperature fields is explained.

(8) The impossibility of exploiting creep tests conducted under transient thermal conditions for rigorous analyses is disclosed.

(9) The restriction of the number of variables in the constitutive equations to temperature, age, time and stress/ cold strength ratio is justified.

(10) The contradiction between the experimentally practicable investigation into the thermal creep problem and the fact that matrix methods favour the incorporation of the relaxation phenomenon is set up.

(11) The decision to employ matrix displacement methods in conjunction with thermal relaxation characteristics deduced from creep data is made.

(12) The feature imposed onto the design of the proposed creep testing machine and the model for the mathematical reproduction of the thermoviscoelastic problem are listed.

12.1.3. CHAPTER III

(1) The original contribution is seen in the design and construction of creep testing machines for the

experimental investigation into the thermal creep and /or thermoviscoelastic strain problem.

(2) The testing machines are described and photographs for their visual assessment are presented. Plates 1 to 5.

(3) Twelve small size design drawings which include the specification of the machine parts are completed. Figs. (3.1) to (3.12).

(4) The criteria imposed onto the design of the testing machines are listed.

(5) The major proving tests on the applicability of the testing machines are reported.

12.1.4. CHAPTER IV

(1) The original contribution is seen in carrying out tests on the mix, the drying shrinkage, the moisture loss and the cold strength of concrete specimens which enable the reduction in the number of variables influencing the subsequent creep tests.

(2) Investigations into the phenomenon of drying shrinkage show that for ages greater than six months its effect on the maturity of concrete becomes negligible. Fig. (4.1).

(3) The relative reduction in weight due to moisture loss is discovered to have a possibly direct affinity to the drying shrinkage. Figs. (5.2) to (4.4).

(4) The relative reduction in weight appears to be a linear function of the specimens' surface-volume ratio. Table 4.2.

(5) The rough estimation of shrinkage strains from tests on moisture loss is found to be possible.

(6) The Gaussian distribution curve is reproduced for the cold strength of concrete. Fig. (4.5).

(7) The increase in concrete strength after four months is found to have little bearing on the results of relevant calculations. Figs. (4.6) to (4.10).

(8) The time-dependent ratio of cylinder strength to cube strength is determined. Fig. (4.11).

(9) The ratio of the 28-day strength of the approximated final strength is ascertained both for cylinder and cube specimens.

12.1.5. CHAPTER V

(1) The original contribution is seen in the performance of thermal creep tests on concrete specimens and the fitting of formulae to some of its temperature and/or stress-dependent characteristics.

(2) The quest for data on thermal creep compliance is set fourth.

(3) The creep curves obtained are drawn. Figs. (5.1) to (5.5).

(4) Linearity in the stress-dependence of the initial thermal strains is observed for temperature up to 200^0C. Fig. (5.6)

(5) A formula of tri-linear nature is proposed for the determination of thermoelastic strains. Eq. (5.1). Fig. (5.15).

(6) Values for the ultimate initial and ultimate creep strains are arrived at. Eqs. (5.3), (5.4). Figs. (5.6), (5.7).

(7) The bandwidth between the domains of safe and failure-procuring test conditions is drawn. Fig. (5.13).

(8) A formula is proposed for the reduction of the modulus of thermoelasticity with temperature. Eq. (5.5). Table 5.1.

(9) A formula of tri-linear nature is proposed for the temperature-dependence of the ultimate stress/ cold strength ratio. Eq. (5.6). Fig. (5.10).

(10) A formula of tri-linear nature is proposed the dependence of the ultimate test temperature on the stress/ cold strength ratio. Eq. (5.7).

(11) A formula is proposed for the stress and temperature

dependence of the modulus of quasi-thermoelasto-plasticity. Eq. (5.8). Table 5.2. Fig. (5.9).

(12) A formula is proposed for the temperature-dependence of the ultimate cylinder strength. Eq. (5.10). Fig. (5.10).

(13) The applicability of the superposition hypothesis to the overlay of thermal creep strains is proven. Figs. (5.11), (5.12).

(14) Information is given on thermally induced shrinkage strains. Fig. (5.16).

12.1.6. CHAPTER VI

(1) The original contribution is seen in formulating the established small displacement theory of linear elasticity and thermoelasticity as applied to three-dimensional and axisymmetric continua such that the possiblities and limitations of the infinitesimal approach to structural analysis are disclosed.

(2) The assumptions, under which the theory is developed, are stated and the implications these bear on the detailed derivation are discussed. Ass. (6.1.2.i).

(3) The equations of force equilibrium, the strain-deformation relations, the consitutive relationships and the compatibility requirements for the three-dimensional analysis are arrived at. Eqs. (6.5), (6.10), (6.10), (6.24).

(4) The corresponding expressions are derived for the axisymmetric analysis. Eqs. (6.28), (6.32), (6.33), (6.34).

(5) The compatibility equations are found to satisfy the sufficient conditions, proving the applicability of the small displacement theory.

(6) Mathematically, an infinite number of solutions is found to exist for any structural analysis, unless boundary conditions are imposed.

(7) Physically, the disturbances due to the action of forces, prestressing strains or imposed displacements

are found to be incapable of being described in a closed form.

(8) Philosophically, the compatibility equations are found to be general and particular at the same time, disclosing that the development of the small displacement theory has arrived at the ultimate concept of its analytic approach.

(9) The necessity for the reconstruction of the structural theory from new fundamentals is concluded.

12.1.7. CHAPTER VII

(1) The original contribution is seen in employing energy principles and variational methods such that the elliptic compatibility equations of the small displacement theory are re-established from new fundamentals, and new possiblities for solution procedures are arrived at.

(2) The assumptions are stated under which the energy principles lead to the variational theory of linear elasticity and themoelasticity, and the inferred implications are discussed. Ass. (7.1.2.i).

(3) Set theory is introduced for the equations of internal equilibrium of forces, the equations of force equilibrium at the boundary and the strain-deformation relations. Eqs. (7.6) to (7.10).

(4) The calculus of variation is introduced. Eq. (7.13).

(5) The principle of conservation based on Green's theorem is derived. Eq. (7.15).

(6) The principle of virtual work based on the principle of virtual work is deduced. Eq. (7.25).

(7) The unit displacement theorem based on the principle of virtual work is deduced. Eq. (7.25).

(8) The principle of minimum potential energy based on the principle of virtual work and the unit displacement theorem is established. Eq. (7.26).

(9) The principle of propagation of heat based on Gauss'

theorem and the continuity of heat flow is arrived at. Eq. (7.35).

(10) The strain energy functional in conjunction with the calculus of variation and Euler's suitability criterion is found to re-establish. The compatibility equations of the small displacement theory. Eqs. (7.39), (7.45).

(11) The governing equations of the variational approach to spatial elasticity problems are attained. Eqs. (7.42), (7.46).

(12) The heat conduction functional in conjunction with the calculus of variation and Euler's suitability criterion is found to re-establish the continuity equations of the heat transport theory. Eqs. (7.51), (7.60), (7.67), (7.71).

(13) The continuity and compatibility equations of the heat conduction and the thermoelastic problems are found to be insoluble despite their variational formulation.

(14) The variational approach is found to be incapable of abolishing the limitations brought about by the impossibility for the temperature and displacement fields to take prescribed values along the boundary.

(15) The variational approach proves incapable of uncoupling the temperature and the displacement fields from the conductivity and the stiffness coefficients.

(16) The variational approach is found to offer new possiblities in conjunction with the implementation of appropriate matrix methods as the continuity and compatibility equations are replaced by equivalent integral expressions. Eqs. (7.36),(7.43), (7.47), (7.63).

12.1.8. CHAPTER VIII

(1) The original contribution is seen in establishing the force-deformation equations of elastically and thermo-elastically deforming axisymmetric continua in the classical and the natural deformation modes concepts of the finite element method.

(2) The crucial importance of the global stiffness matrix

in the force-deformation equations of a loaded structure is discussed.

(3) The processional steps, the algorithms and the required computer programming routines are found to be similar to some extent for both modes concepts.

(4) The TRIAX 3 element is described. 8.2.1.

(5) The classical deformation modes are defined. 8.2.2.

(6) The geometrical and analytical advantages of the classical modes concept are pointed out. 8.2.3.

(7) The stiffness matrix for the TRIAX 3 element is set up. Eq. (8.13).

(8) The load vectors for the TRIAX 3 element are defined. Eqs. (8.16) to (8.19).

(9) The classical force-deformation equations are established. Eqs. (8.20), (8.21).

(10) The TRIAX 6 element is described. 8.3.1.

(11) The natural deformation modes are defined. 8.3.2.

(12) The geometrical and analytical advantages of the natural modes concept are pointed out. 8.3.3.

(13) The stiffness matrix for the TRIAX 6 element is set up. Eqs. (8.28) to (8.32).

(14) The derivation of the stiffness submatrices is performed. Eqs. (8.38),(8.42),(8.56),(8.63),(8.65),(8.72),(8.76).

(15) The natural force-deformation equations are established. Eqs. (8.77), (8.78).

(16) The novalty of the finite element method is found to manifest itself in the regression of space-dependent problems to mere topological ones.

(17) As regards structural analysis, the breakthrough is found to lie in the transformation of element-wise space-dependent displacement functions to matrix expressions for scalar displacement values at discrete topological points.

(18) The coupling between displacements and stiffness

coefficients is surmounted by the solution of node-oriented force-deformation matrix equations which contain the stiffness coefficients, the displacements and the force components as scalars of three unconnected arrays.

(19) The impossibility of the field variables to take prescribed values along the boundary is overcome by substituting the node-wise approximated boundary conditions directly into the corresponding storage locations of the structure's global displacement or force vector.

12.1.9. CHAPTER IX

(1) The original contribution is seen in the development of two finite element computer programs, Program I and II, for the elastic and thermoelastic analysis of axisymmetric concrete continua.

(2) Programs I and II which are based on the classical and natural deformation modes concepts repsectively, are found to verify their applicability mutually.

(3) The loading cases accepted by Programs I and II may constitute gravitational loads, external forces, prestress settlement of supports, and thermal loads due to either steady state or transient temperature distributions.

(4) The applicability of Program I and II to the design of a prestressed concrete reactor pressure vessel is verified; a case study is carried out.

(5) High-powered calcomp plotting routines for the graphical processing of finite element output data are introduced.

(6) The routine SURPLT is proposed to display surfaces of stress fields etc. Figs. (9.1),(9.2),(9.19) to (9.30).

(7) The routine MESH is proposed for grid transformations.

(8) The routine FEMESH is proposed to draw finite element meshes automatically. Figs. (9.3) to (9.6).

(9) The routine CONTRS is proposed to draw contours of stress fields etc. Figs. (9.7) to (9.18).

(10) The routine SURFIT is proposed to described smooth

surfaces of stress fields etc. Fig. (9.31).

(11) The classical deformation modes concept is found to be crude but unconditionally stable.

(12) The natural deformation modes concept is found to be mathematically and structurally sophisticated, but sensitive to non-ideal finite element meshes.

(13) With the structural problem solved in the space variables using finite element methods, the uncoupling of the temperature and displacement fields from the conductivity and stiffness coefficients in the time variable using finite difference techniques may be embarked upon.

12.1.10. CHAPTER X

(1) The original contribution is seen in accomplishing the uncoupling of the field variables in time from the characteristics of the structure by applying finite difference techniques to the problems of heat conduction, creep-relaxation interaction and thermoviscoelasticity.

(2) The mixed elliptic and parabolic partial differential equations which constitute combined boundary and initial value problems are stated. Eqs. (10.0a),(10.0b).

(3) The disturbances in time-like processes are found to have no retroactive effect on the conditions that existed at any time instant elapsed.

(4) The parabolic time-like processes are found to lend themselves to finite difference marching techniques.

(5) The finite element temperature formulation for axisymmetric heat flows is derived. Eq. (10.6).

(6) The governing matrix equation of the axisymmetric heat conduction problem in its classical finite element form is established. Eqs. (10.8) to (10.10).

(7) A finite difference scheme is proposed for the local change of temperature with time, assuming that the approximating temperature functions are step-wise

parabolas. Eqs. (10.15), (10.16).

(8) A finite difference technique is proposed for the creep-relaxation conversion, using the superpositoin hypothesis, local thermal constitutive equations and the normalized Heavyside step function. Eqs. (10.17), (10.19),(10.20),(10.21),(10.29).

(9) A finite difference technique is proposed for the solution of the convolution integral of the strain history, using the quasi-static strain energy principle and the thermviscoelastic load-deformation equations. Eqs. (10.31),(10.32),(10.36).

(10) The load-deformation equations of the transient thermoviscoelastic stress analysis problem is established in global matrix form. Eq. (10.39).

12.1.11. CHAPTER XI

(1) The original contribution is seen in the incorporation of concrete for thermoviscoelastic strains into the structural analysis of concrete continua and in reconciling the proposed functional description of isothermal creep curves with the experimental data obtained.

(2) Techniques based on cartesian polynomials, parametric polynomials and simple exponential functions in conjunction with least squares methods are proposed to fit recorded thermal creep data; the fit is found to be approximate only. Eqs. (11.1),(11.2),(11.10). Figs. (11.a), (11.b).

(3) The quasi-linearity of the creep rate-time relation in the double logarithmic scale is recognized. Fig.(11.1).

(4) A mathematical equation is proposed to fit thermal creep curves. Eqs. (11.14) to (11.16).

(5) Experimentally substantiated expressions are proposed for the temperature and stress-dependence of the pertaining parameters. Eqs. (11.19), (11.20). Figs. (11.2), (11.3).

(6) A formula is proposed for the development of thermal

creep strains. Eq. (11.21).

(7) A formula is proposed for the development of thermo-viscoelastic strains. Eq. (11.22).

(8) A formula of tri-linear nature is proposed for the temperature-dependence of initial strains. Eqs. (11.23), (11.24).

(9) The author's general formula for the determining of linear thermoelastic strains occurring in virgin concrete is arrived at. Eq. (11.26), Figs. (11.4) to (11.12).

(10) Using the proposed subprogram CRELAX, normalized thermal creep curves are first transformed to thermal relaxation curves; subsequently, the author's thermal relaxation weighting factors are arrived at. Figs.(11.4) to (11.12).

(11) For design purposes, the thermal relaxation weighting factors are presented in a semi-logarithmic scale and in a table. Fig. (11.13). Table A6.4.

(12) The proposed stiffness approach to the thermoviscoelastic structural analysis using the proposed thermal relaxation weighting factors is found to be rigorous and appropriate.

(13) The weighting factors are verified by comparison between recorded and predicted creep strains. Eq. (11.28).

(14) The computer program THERMO AXICON written to solve the problem set out in this thesis is described.

(15) Transient temperature distributions are computed and illustrated in a case study. Figs. (11.14) to (11.17).

(16) Stress fields arising due to the presence of steady state and transient thermal fields are computed and compared. Figs. (11.18) to (11.22).

12.2. RECOMMENDATIONS FOR FUTURE RESEARCH

Restricting attention to the problem set out in this thesis, the following recommendations are made for future research.

12.2.1. EXPERIMENTS

(1) Using the testing machines proposed, test series should be carried out on thermal creep of concrete under transient temperature regimes to study the influence that the preheating period of one day had on the numerical values of the creep data obtained in this work.

(2) Since an infinite number of creep curves is possible to form for transient thermal conditions, a standard rate of heating should be adhered to, in order to render the results comparable.

(3) Following the procedure described, further test on isothermal creep compliance should be conducted with the intention of making parameter studies on the influence of the mix and age of concrete.

(4) Test series should be carried out to study the temperature dependence of the coefficient of thermal expansion, the specific heat, the thermal conductivity and the thermal diffusivity of concrete.

(5) Test series should be conducted for thermal creep compliance of concrete under tension.

(6) Test series should be performed to investigate the effect of the size of test specimens on the development of thermal creep strains in concrete.

(7) Testing machines for experiments on multiaxial thermal creep should be designed to enable the investigation into the stress and temperature dependence of the Poisson's ratio in concrete.

12.2.2. THEORY

(1) Formulae should be fitted to the above mentioned characteristics.

(2) Since due to the necessity of step-wise invariant conditions in matrix methods, creep curves obtained for transient temperatures do not lend themselves to rigorous analyses unless each of them is approximated by a set of isothermal creep curves, relevant theories not based on the superposition hypothesis appear doubtful.

(3) The applicability of the proposed computer programs should be verified by comparison with test results from model analyses of prestressed concrete pressure vessels or other axisymmetric continua.

(4) The computer programs should be used to analyse other loading cases.

(5) The computer programs should be extended to account for the possible propagation of cracks.

(6) The computer programs should be extended to cope with complex, three-dimensional structural problems.

(7) Thermal relaxation weighting factors should be determined also for other ages and mixes of concrete.

APPENDIX I

LIST OF REFERENCES

1. Argyris, H.J., The Tapered TRIM 6 Element for the Matrix Displacement Method, J. Roy. Aeron. Soc., Nov. 1966.

2. Argyris, J.H., "Continua and discontinua", Proc. Conf. on Matrix Methods of Structural Analysis, WPAB, AFFDL-TR-66-80, 1966.

3. Argyris, J.H. and Kamel, H. Boolean Matrices as a Stanard Facility in a Matrix Code. Research Report to The Boeing Company. Airplane Division, December 1964 (to be published externally).

4. Argyris, J.H., Kamel, H., Pretsch, H., Sorensen, M. and Schmid, G. Automatic System for Kinematic Analysis (ASKA) Research Report to The Boeing Company, Airplane Division, February 1965 (to be published externally).

5. Argyris, J.H. Triangular Elements with Linearly Varying Strain for the Matrix Displacement Method, Research Report to The Boeing Company Airplane Division, August 1964.

6. Argyris, J.H. Energy Theorems and Structural Analysis Butterworths, London, 1960.

7. Argyris, J.H. The TRIAX 6 Element for Axisymmetric Analysis by the Matrix Displacement Method, Part I Foundations. Journal of the Royal Aeronautical Society Vol. 70, December 1966.

8. Argyris, J.H., Lecture notes on "Numerical methods", Imp. Coll. London 1969.

9. Arthanari, S. Influence of Temperature and Biaxial Stress on Creep in Concrete. Ph.D., Thesis U. London,1966.

10. Arthanari, S. and Yu, C.W., "Creep of Concrete Under Uniaxial and Biaxial Stresses at Elevated Temperatures, "Magazine of Concrete Research, Cement and Concrete Association, Vol. 19, No. 60, September 1967, pp 149-156.

11. Ali, J., and Kesler, C.E., "Creep in Concrete with and without Exchange of Moisture with the Environment," Univ. of Illinois, Dept. Theor. Appl. Mech., Report No. 641, Urbana, December 1963.

12. Abrams, M.S., and Orals, D.L., "Concrete Drying Methods and Their Effect on Fire Resistance," in "Moisture of Materials in Relation to Fire Tests", STP No. 385, 1965, 52-73, publ. by Amer. Soc. for Testing Materials (PCA Bulletin 181).

13. Ali, L. and Kesler, C.E., "Mechanism of Creep in Concrete," Symposium on Creep of Concrete, Houston, Special Publication No. 9, pp 35-63, 1964, American Concrete Institute.

14. Bazant, Z.P., "Electric Analogues for Creep of Concrete Structures," Conf. on Exper. Methods of Investigating Stress and Strain in Structures, Techn. Univ. Prague, Building Res. Inst., 5-8 October 1965, 797-809.

15. Bazant, Z.P., "Mathematische Ermittlung der Rhealogishen Eigenschaften von Glassfaserverstärkten," Proc., Erste Internationale Tagung über GFP und Epoxydharze, Berlin, Institut für Kunststoffe, Deutsche Akademie der Wissenschaften, 23-27 September 1965, Paper E3/1.

16. Bazant, Z.P., "Phenomenological Theories for Creep of Concrete Based on Rheological Models," Acta Technica CSAV (Prague), 1966, No.1, 82-109.

17. Bazant, Z.P., "Langzeitige Durchbiegungen von Spannbetonbrücken unter Verkehrslasten," Beton und Stahlbetonbau, 1968, No.12 282-285.

18. Bazant, Z.P., "A Model for Creep and Shrinkage of Concrete Based on Thermodynamics of Adsorption," Internal Research Report, No. 68/1, Dept. of Civil Engineering, University of Toronto, Toronto, November 1968.

19. Bazant, A.P., "Thermodynamic Theory of Concrete Deformation at Variable Humidity and Temperature," Report to Oak Ridge National Laboratory, Union Carbide Corporation, Nuclear Division, No. SESM 69-11, Department of Civil Engineering, University of California, Berkeley, July 1969.

20. Bogner, F.K., Fox, R.L., and Schmit, L.A., "Finite Deflection Analysis Using Flats and Cylindrical Shell Discrete Elements", AIAA/ASME 8th Structures. Structural Dynamics and Materials Conference (1967).

21. Bresler, B., and Selna, L., "Analysis of Time Dependent Behaviour of Reinforced Concrete Structures," in "Symposium on Creep," Amer. Concrete Inst., Publ. SP-9, Detroit, 1964, 115-128.

22. Browne, R.D. "Properties of Concrete in Reactor Vessels," Conf. on Prestressed Concrete Reactor Pressure Vessels, Institution of Civil Engineers, Paper C13, London, March 1967.

23. Browne, R.D. and Blundell, R., "The Influence of Loading Age and Temperature on the Long Term Creep Behaviour of Concrete in a Sealed, Moisture Stable, State, "RILEM Colloquium on Physical and Chemical Causes of Creep and Shrinkage of Concrete, Munich, Apr. 1968; also Materials and Structures (RILEM), vol. 2, No.8 March 1969,pp 133-144.

24. Berg, P.W., "Calculus of variation", Handb. Eng. Mech., McGraw Hill, 1962.

25. Boltzmann, L., Ann. Phys., Ergänzungsband 7, 1876.

26. Berezin, I.S. and Zhidkov, N.P., Computing Methods vol. 1, Pergamon Press, London, 1965.

27. Carmichael, G.D.T., "The Application of Three Dimensional Finite Elements to the Analysis of Podded Boiler Type Prestressed Concrete Pressure Vessels", Nucl. Engl Degn., (1971).

28. Collatz, L., "The Numerical Treatment of Differential Equations." Springer, Berlin, 1960, p. 271.

29. Clough, R.W., "The Finite Element Method in Structural Mechanics", Ch.7. Stress Analysis, edited by O.C.Zienkiewicz and G.S. Hollister, Wiley, New York, 1965.

30. Clough, R.W., Rashid, Y.R., "Finite Element Analysis of Axi-Symmetric Solids", ASCE, Engg. Mech. Div. Journal, vol. 91, No. EM 1, pp 71-85, February, 1965.

31. Coleman, B.D., "Thermodynamics of Materials with Memory,"

Archives for Rational Mechanics and Analysis, vol.17, pp. 1-46, (1964).

32. Cruz, C.R., "Elastic Properties of Concrete at High Temperatures," Journal of the Portland Cement Assoc. Res. and Dev. Lab., vol. 8, January 1966, No. 1, 37-45 (PCA Bulletin 191)(with reference 3).

33. Dischinger, F., Untersuchung über die Knicksicherheit, die elastische Verformung und das Kriechem des Betons bei Bogenbrücken. Bauingenieur 1937, Heft 33/34, S. 487/520 und Bauingenieur 1939, Heft 5/6, S.53/63.

34. Davis, R.E., Davis, H.E., and Hamilton, J.S., "Plastic Flow of Concrete under Sustained Stress," Proc., Amer. Soc. for Testing Materials, vo. 37, 1934, 354-386.

35. Eringen, A.C., "Nonlinear Theory of Continuous Media," McGraw-Hill, New York, 1962 (Chpt. 5,8, 10).

36. Fletcher, R., and Powell, M.J.D., "A Rapidly Convergent Descent Method for Minimization", The Computer Journal 6, 163 (1963).

37. Fletcher, R., and Reeves, C.M., "Function Minimization by Conjugate Gradients". The Computer Journal 7, 149 (1964).

38. Flügge, W., "Viscoelasticity," Ginn/Blaisdell, Waltham, Mass. - Toronto - London, 1967.

39. Freudenthal, A.M., and Roll, F., "Creep and Creep Recovery of Concrete under High Compressive Stress," J. Amer. Concrete Inst., No. 12, June 1958, 1111-1142.

40. Freyssinet, E., "The Deformation of Concrete," Magazine of Concrete Research (London), December 1951, 49-56.

41. Gross, H., "Statische Berechnung einer Schraegseil-fussgaengerbruecke mit zentralem Pylon aus Spannbeton," Diplomarbeit, Techn. Uni. Berlin, 1968.

42. Gross, H., "Creep Analysis of a Prestressed Concrete Channel-Bridge", D.I.C. Dissertation, Dept. of Civil Engineering, Imperial College, London, 1969.

43. Gross, H., "A Testing Machine for Thermal Creep of

Concrete", Res.Rep. CSTR71/6, Dept. of Civil Engineering Imperial College, London, September 1971.

44. Gross, H., "Classical and Natural Deformation Modes Concepts in the Finite Element Analysis", Res. Rep., CSTR71/7, Dep. of Civil Engineering, Imperial College, London, September, 1971.

45. Gross, H., "Thermoviscoelastic Axisymmetric Stress Analysis by Finite Element and Finite Difference Computer Techniques", 1st Int. Conf. on SMiRT, Berlin, September 1971.

46. Gross, H., "Classical and Natural Conduction and Deformation Modes Concepts for Axisymmetric Variational Problems", Int. Conf. on Variational Methods in Engineering, Southampton, September 1972, Pap. X9.

47. Gross, H., "On High-Temperature Creep of Concrete", to be published, 2nd Int. Conf. on SMiRT, Berlin, September 1973.

48. Grossman, M., "The Application of a Computer to the Mathematical Definition of Ship Hull Forms", Ph.D. Thesis, London University, 1972.

49. Gamble, B.R. A Constitutive Relationship for Maturing Concrete. Paper 10. Symposium Design of Concrete Structures for Creep, Shrinkage and Temperature Changes. Madrid 1970.

50. Glücklich, J., Ishai, O., "Creep Mechanism in Cement Mortar," Jour., Amer. Concrete Inst., vol. 59, 1962, 923-948.

51. Greenbaum, G.A., "Creep Analysis of Axisymmetric Bodies", Ph.D.dissertation, University of California, Los Angelos, 1966.

52. Guyon, Y., Construtions En Béton Précontraint. Band 1, Seite 40, Paris: Editions Eyrolles 1966.

53. Hald, A., "Statistical theory with engineering applications", Wiley, N.Y. 1952.

54. Hannant, D.J., "Strain behaviour of concrete up to 95°C under compressive stresses", Conf. on PCPV, Inst. Civ. Eng., London 1967.

55. Hansen, T.C., "Creep and Stress Relaxation of Concrete, A Theoretical and Experimental Investigation,"Proceedings NR 31, Swedish Cement and Concrete Research Institute of Technology, Stockholm, 1960.

56. Hansen, T.C., and Mattock, A.H., "Influence of Size and Shape of Member on the Shrinkage and Creep and Concrete," J. ACI, 63, 267-290, 1966.

57. Hanson, J.A., "Effects of Curing and Drying Environments on Splitting and Tensile Strength of Concrete," Jour., Amer. Concrete Inst., vol. 65, July 1968, 5351543 (PCA Bulletin D141).

58. L'Hermite, R., "Les Déformations du Béton,"Cahier de la Recherche No. 12 I.T.B.T.P. et A.F.R.E.M.C., Paris, Eyrolles, 1961.

59. L'Hermite, R.G., and Mamillan, M., "Further Results of Shrinkage and Creep Tests," Intern. Conf. on the Structure of Concrete, Paper H2, 1965, Imperial College, London, publ. by Cement and Concrete Assoc.

60. McHenry, D., "A New Aspect of Creep in Concrete and its Application to Design," Proc. ASTM, vol. 43, 1943, 1069-1089 (with discussion by H. Laedreman).

61. Hickey, K.B. "Creep, Strength, and Elasticity of Concrete at Elevated Temperatures," Report No. C-1257, December 1967, Bureau of Reclamation, Washington, D.C.

62. Hrennikof, A., "Shrinkage, Swelling and Creep in Cement," Proc. ASCE, J. of Eng. Mech. Div.,EM3, July 1959, 111-135.

63. Hopkins, I.L. and Hamming, R.W.,"On creep and relaxation", J. Appl. Phys., vol. 28, No. 8, August 1957.

64. Hilsdorf, H., "Versuchstechnische Problems beim Studium der Verformungseigenschaften des Betons," Materialpruefung 5/1963, Nr. 11, Munich.

65. Kesler, C.E., Ali, J., "Rheology of Concrete - A Review," Univ. of Illinois, Dept. Theor. Appl. Mech., Report No. 636, Urbaba, 1963.

66. Kimishima, H., and Kitashara, Y., "Creep and Creep Recovery of Mass Concrete," Techn. Report C-64001, September 1964, Central Res. Inst. of Electric Power Industry, Tokyo.

67. Krishnamorthy, S., "Thermal Creep Behaviour of Concrete Portal Frames", Ph.D. Thesis, London University, 1969.

68. Launay, P. Charpenet G. and Vouillon, C., Prestressed Concrete Pressure Vessels : Two Dimensional Thermo-elasticity Computer Program", Nuclear Engineering and Design (pp 443-459) North-Holland Publishing Company, Amsterdam (1968).

69. Lee, E.H. and Rogers, T.G., "Solution of viscoelastic stress analysis problems using measured creep or relaxation function" J. Appl. Mech., Am. Soc. Mech. Eng. Trans., Ser. E, 1963, 30.

70. Leonhardt, F. Spannbeton für die Praxis, 2.Auflage. Berlin: W. Erst u. Sohn 1962.

71 Marechal, J.C., "Causes physiques et chimiques du fluage et du retrait du béton," RILEM Colloquium on the Physical and Chemical Causes of Creep and Shrinkage of Concrete, Munich, Apr. 1968 ; also Materials and Structures (RILEM), vol. 2, No. 8, Mar. 1969, pp 111-116.

72. Mukaddam, M.A. and Bresler B. Behaviour of Concrete Under Variable Temperature and Loaded. A.C.I. Seminar Conc. for Nuclear Reactors Berlin 1970.

73. Muki, R., and Sternberg, E., "On Transient Thermal Stresses in Viscoelastic Materials with Temperature-Dependent Properties", J. of Appl. Mech., June 1961.

74. Nasser, K.W. and Neville, A.M. "Creep of Old Concrete at Normal and Elevated Temperature," J. ACI. V. 64, February 1967, 97-103.

75. Neville, A.M., "Properties of Concrete," J. Wiley, New York, 1963.

76. Neville, A.M., "Theories of Creep in Concerete," Proceedings, American Concrete Institute, vol. 52, 1956, pp47-60.

77. Oden, J.T., Finite Elements of Nonlinear Continua, McGraw Hill Book Co., New York (1971).

78. Oden, J.T., Armstrong, W.H., "Analysis of Nonlinear Dynamic Coupled Thermoviscoelasticity Problems by the Finite Element Method," Journal of Computers and Structures (to appear).

79. Oden, J.T., Aguirre-Ramirez, G., "Formulation of General Discrete Models of Thermomechanical Behaviour of Materials with Memory," International Journal of Solids and Structures, vol. 5, No. 10, pp. 1077-1093 (1969).

80. Oden, J.T., Poe, J., "On the Numerical Solution of a Class of Problems in Dynamic Coupled Thermoelasticity," Proceedings, 5th SECTAM, Developments in Theoretical and Applied Mechanics, Ed. by D. Frederick, Pergamon Press, Oxford (1970).

81. Oden, J.T., "Finite Formulation of Problems of Finite Deformation and Irreversible Thermodynamics of Nonlinear Continua - A Survey and Extension of Recent Developments," Recent Advances in Matrix Methods of Structural Analysis and Design, Ed. by R.H. Gallagher, Y. Yamada, and J.T. Oden, University of Alabama Press, University, Alabama, pp. 693-724 (1971).

82. Oden, J.T., Key, J.E., "Numerical Analysis of Finite Axisymmetric Deformation of Incompressible Elastic Solids of Revolution," International Journal of Solids and Structures, vol. 6, pp. 497-518 (1970).

83. Oden, J.T., "Note on an Approximate Method for Computing Nonconservative Forces on Finitely Deformed Finite Elements," AIAA Journal, vol. 8, No. 11, pp. 2088-2090 (1970).

84. Oden, J.T. Key, J.E., "Analysis of Finite Deformation of Elastic Solids by the Finite Element Method," IUTAM Syposium High Speed Computing of Elastic Structures, Liege, Belgium (1970).

85. Pian, T.H.H., Tong, P., "Basis of Finite Elements Methods for Solids Continua", International Journal for Numerical Methods in Engineering, vol. I, pp 3-28 (1969).

86. Pian, T.H.H., "Derivation of Element Stiffness Matrices by Assumed Stress Distributions", AIAA Journal, vol. 2, pp 1333-1336 (1964).

87. Powers, T.C., "Mechanism of Shrinkage and Reversible Creep of Hardened Cement Paste," International Conf. on the Structure of Concrete, London, September 1965, Paper GI, Imperial College, publ. by Cement and Concrete Assoc.

88. Powers, T.C., "The Nature of Concrete," in "Significance of Tests and Properties of Concrete-Making Materials," ASTM, STP No. 169-A, 61-62, 1966 (P.C.A. Bulletin No.196).

89. Pucher, A., Lehrbuch des Stablbetonbaus, 3. Auflage, S. 22, Wien: Springer-Verlag.

90. Rashid, Y.R. and Rockenhauser, W., "Pressure vessel analysis by finite element techniques', Conf. on PCPV, Inst., Civ. Eng., London 1967.

91. Ross, A.D., Creep of Concrete Under Variable Stress A.C.I. 29th March, 1968.

92. Ross, A.D. Illston, J.M. and England, G.L., "Short- and Long-Term Deformations of Concrete as Influenced by its Physical Structure and State," Intern. Conf. on the Structure of Concrete, Paper H1, 1965, Imperial College, London, publ. by Cement and Concrete Assoc.

93. Ross, A.D., and England, G.L., "Reinforced Concrete under Thermal Gradients", Mag. of Concr. Res., vol. 14, No. 40, 1962.

94. Reiner, M. Rheologie, Handbuch der Physik. Bd. vl. Elastizitat und Plastizitat. Berlin, Springer 1958.

95. Rüsch, H. u. Kupfer, H.:Bemessung von Spannbetonbauteilen. Abschnitt 7, Spannungsnachweis unter Gebrauchslast. Im Beton-Kalender 1967, I. Teil, S. 487. Berlin/München: W. Ernst u. Sohn.

96. Serafim, J.L. and Guerreiro, M.Q., "Influence of Temperature on the Creep of Mass Concrete," RILEM Colloquium on the Influence of Time Upon Strength and Deformation of Concrete, Munich, November 1968.

97. Da Silveira, A.F. and Florentino, C.A., "Influence of Temperature on the Creep of Mass Concrete," American Concrete Institute Symposium on the Effect of Temperature on Concrete, Memphis, November 1968.

98. Sullivan, P.J.E. The Structural Behaviour of Concrete at Elevated Temperature. Ph.D. Thesis. London University, 1970.

99. Sullivan, P.J.E. Time-Temperature extrapolation Techniques as applied to concrete creep strains. Int. Conf. Struct. Mech. Reacter Technology Berlin 1971.

100. Sullivan, P.J.E. and Butcher, E.G. The Calculation of the Effect of a Fire on a building structure. Paper for the Convention Europeenne des Associations de la Construction Metallique, March, 1971.

101. Sutherland, W.H., "A Finite Element Computer Code (Axicrp) For Creep Analysis", BNWL-1142, Battelle Memorial Institute, October, 1969.

102. Timoshenko, "Theory of Plates and Shells, Mc Graw-Hill,1959.

103. Theuer, A.U., "Effect of Temperature on the Stress-Deformation on Concrete," Journal of Research (U.S. Nat. Bureau of Standards), RP970, vol. 18, February 1937, No. 2, 195-204.

104. Thorne, C.P., "Concrete Properties Relevant to Reactor Shield Behaviour," Proceedings, American Concrete Institute, vol. 57, 1961, pp 1491-1508.

105. Trost, H. Spannungs-Dehnungsgesetz eines viskoelastischen Festkörpers wie Beton und Folgerungen für Stabtragwerke aus Stahlbeton und Spannbeton. beton 1966, S.233.

106. Trost, H., "Auswirkungen des Superpositionsprinzips auf Kriech und Spannbeton", Beton u. Stahlbetonbau, Heft 10 u. 11/ 1967, Berlin.

107. Trost, H., "Zwechmaessige Ermittlung der Durchbiegung von Stahlbetontraegern" Beton u. Stahlbetonbau, Heft 6/1969, Berlin.

108. Wagner, O., "Das Kriechen unbewehrten Betons," Deutscher Ausschuss für Stahlbeton, H., 131, W. Ernst and Sohn,Berlin 1958.

109. Wallo, E.M. and Kesler, C.F., "Prediction of Creep in Structural Concrete," Bulletin 498, 1968, Engineering Experiment Station, University of Illinois, Urbana, Ill.

110. Washizu, K., "Variational methods in elasticity and plasticity", Pergamon Press, 1968.

111. Wilson, E.L., "Structural Analysis of Axisymmetric Solids", AIAA Journal, pp 2269-74, January 1965.

112. Wilson, E.L. and Nickell, R.E., "Application of the Finite Element Method to Heat Conduction Analysis," Nuclear Engineering and Design 4 (1966), 276-286 (North Holland Publ. Co., Amsterdam).

113. York, G.P. et al. Experimental Determination of Poissons Ratio for Creep. A.C.I. Seminar Conc. for Nuclear Reactors. Berlin 1970.

114. Zerna, W. u. Trost, H. Rheologische Beschreibungen des Werkstoffes Beton, B.u.St. 1967, Heft 7. S. 165.

115. Zienkiewicz, O.C., Watson, M., Cheung, Y.K., "Stress Analysis by the Finite Element Method - Thermal effects", paper No. 35, Proceedings of the Conference on Prestressed Concrete Pressure Vessels, March 1967, London.

116. Zienkiewicz, O.C. and Cheung, Y.K., "The finite element method in structural and continuum mechanics", 1st edn., Mc Graw Hill, London, 1967.

International Conferences attended in conjunction with the present work

i Int. Conf. on Prestressed Concrete Pressure Vessels, Inst. of Civ. Eng., London, March 1967.

ii Symposium on Siting and Safety, Inst. of Civ. Eng., London, March 1969.

iii Int. Conf. on Structures, Solid Mechanics and Engineering, Univ. of Southampton, April 1969.

iv 1st Int. Conf. on Structural Mechanics in Reactor Technology Kingresshalle Berlin, September 1971.

v Int. Conf. on Variational Methods in Engineering, Univ. of Southampton, September 1972.

APPENDIX II

FLOW DIAGRAM OF THE COMPUTER PROGRAM ** THERMO AXICON**

Development of stresses in axisymmetric concrete reactor pressure vessels due to heat conduction using finite element method, finite difference techniques and isothermal relaxation weighting factors

Gov equ 1 : $\underline{W} = \text{fct}(T,\tau,t)$ cf. eq. (10.36)

Gov equ 2 : $\underline{G}\ \underline{DTDT} = -\underline{H}\ \underline{T} - \underline{FQ}$ cf. eq. (10.12)

$\underline{G}\ \underline{DTDT} = \underline{BB}$

Gov equ 3 : $(\frac{AT}{2}\underline{H} + \underline{G})\underline{DTDT} = -\underline{H}\ \underline{TU} - \frac{AT}{2}\underline{H}\ \underline{DTUDT} + \underline{FQ}$

$\underline{GH}\ \underline{DTDT} = -\underline{FO} - \frac{AT}{2}\underline{AA} + \underline{FQ} = \underline{BB}$ cf. eq. (10.16)

Gov equ 4 : $(\underline{H} + \frac{2}{AT}\underline{G})\underline{T} = \underline{G}\ (\frac{2}{AT}\underline{TO} + \underline{DTDT}) + \underline{FQ}$

$\underline{HG}\ \underline{T} = \underline{G}\ \underline{BBB} + \underline{FQ} = \underline{CC}$ cf. eq. (10.15)

Gov equ 5 : $\underline{W}^t\underline{K}\ \underline{W}\ \underline{u} = \underline{W}^t\underline{R}\ \underline{\Theta}$ cf. eq. (10.39)

Gov equ 6 : $\underline{K}\ \underline{T} = \underline{Q}$ cf. eq. (10.10)

Basic dimensions

KMAX	=	tot no of nod pts
NMAX	=	tot no of TRIAX 3 elmts
MBAND	=	bandwdth for nod pts
KK	=	KMAX*MBAND
JMAX	=	tot no of displ comps
JBAND	=	bandwdth for nod displ comps
JJ	=	JMAX*JBAND
AT	=	1 day, but other unit time-step poss

Temperature fields and fields of thermal gradients

T = temp distr at current day

TO = temp distr at last day

TU = temp distr at last day but one

DTDT = temp grads at last day

DTUDT = temp grads at last day but one

THERMO AXICON

READ IN DATA consts, dims, coords, connectivity matrs
for loc + glob pts, displs

Thermal creep and relaxation functions

CALL CRELAX to determ isotherm relax weight factors

Transient temperature distribution

CLEAR STORE to obtain zero information for some matrs

DO 30 I = 1, NMAX

CALL DUMMY to relate loc nod pt nos to glob ones

CALL CONDO to constr coeffs of loc therm conductivity matr

CALL THERM to constr coeffs of loc therm distribution matr

CALL GLOBAL to assemble glob therm condty matr H

30 CALL GLOBAL to assemble glob therm distr matr G

CALL HEATIN to find heat generatn vec FQ

DO 1001 N = 1, no of cycles

DO 40 K = 1, KK

CONSTR system matr GH to solve for therm grads (Gov equ 3)

```
40 CONSTR        system matr HG to solve for curr temp vals
                 (Gov equ 4)
   COUNT         days(AGE) since init therm condn occurred
   NO  IF(N.EQ.1)
          YES
   CALL MAMULT   to multiply glob condty matr H with TO at time
                 zero
   GO TO 42
   CALL MAMULT   to multiply H with temp vals TU
   CALL MAMULT   to multiply H with temp grads DTUDT
42 DO   50       I = 1, KMAX
   NO  IF(N.EQ.1)
          YES
   CONSTR        coeffs of system vect BB (Gov equ 2)
   GO TO 50
   CONSTR        coeffs of system vect BB (Gov equ 3)
50 CONTINUE
   NO  IF(N.EQ.1)
          YES
   CALL TRANS    to transfer known prods G*DTDT for giv bound
                 vals of therm grads at last day into BB
                 (Gov equ 2)
   CALL SOLVE    to solve lin simul eqs to find temp grads
                 at zero
   GO TO 45
   CALL TRANS    ****at last day
   CALL SOLVE    ****at last day
45 DO   60       K  =  1, KMAX
   60 CONSTR     coeffs of system vect BBB for curr day,
                 BBB stored in AA
```

```
      CALL MAMULT   to multiply G with BBB for curr day, BBB
                    stored in AA
      DO   70       K  =  1, KMAX
70    CONSTR        coeffs of tot heat transport vect CC, CC
                    in AA (Gov equ 4)
      CALL TRANS    to transfer prods HG*TDOM for known bound
                    vals into CC
      CALL SOLVE    to find temp vals T at curr day (Gov equ 4)
      CALL WRITET   to print out temp vals at all nod pts for
                    curr day
```

Stress analysis

```
      CALL STRAIN   to determ temp rise at glob nod pts, temp
                    rise + strain increms at centroids of elmts
      CALL MODUL    to determ consts for mat stiffn matr
      CLEAR STORE   to obtain init zero information in glob
                    stiffn, stress + strain matrs
      DO  100       I  =  1, NMAX
      CALL DUMMY    to relate loc displ comps to glob ones
      CALL STIFF    to constr loc stiffn matr
100   CALL GLOBAL   to constr glob stiffn matr K (Gov equ 5)
      CALL VISCO    to weight K using therm relax factor W
                    (Gov equ 5)
      CALL TFORC    to find coeffs of glob therm load vect F2 (=RΘ)
      CALL WEIGHT   to weight F2 using therm relax factors
      CALL SOLVE    to find glob displ comps u
      DO  110       I  =  1, NMAX
      CALL DUMMY    to find loc displ comps
110   CALL STRESS   to find stresses in elmt under considn
      CALL WRITE1   to print out vals of nod displ comps
      CALL WRITE2   to print out stresses SIG + princ stress
                    SIG1, SIG2
```

```
      DO   5        I = 1,8
      SELECT        temp or stress surface to be plotted
      CALL MESH     to allocate fin elmt sol to pts of rectang
                    grid
      CALL CONTRS   to draw surface contours
      CALL TURN     to determ view pt + min + max val of surface
    5 CALL SURPLT   call from TURN to plot isometric surface
      DEFINE        curr DTDT, TO + T as DTUDT, TU + TO  of next
                    cycle
1001  CONTINUE

for stationary bound condns, sol of
steady state temp distr + corr stress
surfs may be requested at this point

      STOP

      END
```

APPENDIX III

LIST OF ITEMS OF CREEP TESTING MACHINE

Main frame

(1) Front post - 7,6 mm sq. x 1980 mm hollow section
(2) Rear column - 3,8 mm sq. x 1980 mm hollow section
(3) Bottom plate - 634 x 762 x 38 mm
(4) Intermediate plate - 634 x 508 x 38 mm
(5) Top plate - 634 x 399 x 38 mm
(6) Web - 482 x 82 x 38 mm
(7) Short cantilever - 69 x 82 x 38 mm
(8) Mounting - 178 x 146 x 50 mm
(9) Pulley bracket - 200 x 50 x 8 mm
(10) Column - Ø 32 x 1680 mm
(11) Pulley - Ø 160 x 16 mm
(12) Counterweight - 61 mm sq. x 900 mm

Leverarm system

(13) Leverarm - 1130 x 100 x 19 mm, Alum.
(14) Front pivot - Ø 32 x 92 mm, KE 355
(15) Pivot at fulcrum - Ø 32 x 92 mm, KE 355
(16) Rear pivot - Ø 32 x 92 mm, KE 355
(17) Clamp - 57 x 50 x 44 mm
(18) Vee at fulcrum - 50 x 32 x 19 mm, KE 355
(19) Block - 54 mm sq. x 100 mm
(20) Threaded arm - Ø 25 x 610 mm
(21) Counterweight - Ø 152 x 76 mm
(22) Bumper - 54 mm sq. x 25 mm
(23) Diafragm- 100 x 54 x 19 mm
(24) Spacer - Ø 16 x 10 G x 54 mm

Front hanger

(25) General view of front hanger
(26) Vee at front pivot - 50 mm sq. x 38 mm, KE 355
(27) Coverplate - 242 x 50 x 16 mm, BRT MS
(28) Socket head cap screw - 3/8" BSF x 85 mm
(29) Tie rod - 3/4" BSF x 220 mm, EN 24

(30) Transverse beam - 140 x 60 x 50 mm, BRT,MS
(31) Joint pin - Ø 19 x 77 mm
(32) Clip
(33) Spacer - Ø 13 x 18 G x 38 mm
(34) Socket head cap screw - 5/8" x 85 mm

Upper universal joint

(35) General view of upper universal joint
(36) Spacer - Ø 28 x 10 G x 76 mm
(37) Joint top plate - 140 x 60 x 38 mm, BRT MS
(38) Joint bottom plate - 140 x 60 x 38 mm, BRT MS
(39) Transverse beam - 140 x 60 x 50 mm, BRT MS
(40) Tie rod - 3/4" BSF x 210 mm, EN 24
(41) Bearing ball - Ø 13 mm
(42) Spacer - Ø 28 x 10 G x 76 mm

Titanium yoke system

(43) General view of yoke system
(44) Tie rod - Ø 28 x 305 mm
(45) Tie rod - Ø 19 x 475 mm
(46) Socket head cap screw - 1/8" x 57 mm
(47) Convex spherical bearing - Ø 60 x 25 mm
(48) Spacer - Ø 27 x 10 G x 342 mm
(49) Transverse beam - 165 x 70 x 50 mm
(50) Upper bearing plate - 165 x 100 x 40 mm
(51) Concave spherical bearing - Ø 60 x 25 mm
(52) Circular bearing plate - Ø 60 x 19 mm
(53) Concrete specimen - Ø 60 x 180 mm
(54) Lower bearing plate - 165 x 100 x 40 mm

Lower universal joint

(55) General view of lower universal joint
(56) Tie rod - Ø 19 x 460 mm, EN 24
(57) Spacer - Ø 16 x 10 G x 316 mm
(58) Tie rod - Ø 27 x 330 mm, EN 24
(59) Bolt - - 3/8" BSF x 100 mm

Rear hanger and suspension

(60) Rear hanger - 76 x 54 x 50 mm
(61) Cylindrical joint pin - Ø 10 x 35 mm
(62) Bracket - 25 mm sq. x 41 mm
(63) Sliding tube - Ø 13 x 14 G x 1800 mm
(64) Suspension - Ø 10 x 1950 mm
(65) Sliding weight pan - Ø 102 x 6 mm
(66) Fixed weight pan - Ø 63 x 6 mm

Furnace sliding assembly

(67) Bolt - 5/8" BSF x 65 mm
(68) Rubber pad damper
(69) General view of furnace sliding assembly
(70) Cable
(71) Sliding tube - Ø 63 x Ø 32 x 250 mm
(72) Keys
(73) Upper band - Ø 416 x 40 x 8 T mm
(74) Lower band and furnace bearing ring - Ø 416 x 40 x 8 mm

Furnace

(75) General view of furnace - Ø 381 x Ø 177 x 762 mm
(76) Caposil insulating block - Ø 380 x Ø 177 x 60 mm
(77) Coiled coil heaters
(78) Ceramic tube - Ø 210 x Ø 178 x 640 mm
(79) Inner Triton ceramic fibre blanket - 13 mm tck
(80) Outer Triton ceramic fibre blanket - 13 mm tck
(81) Vericulite insulation - 60 mm tck
(82) Heated inner space - Ø 177 x 610 mm
(83) Power supply
(84) Sindanyo asbestos cement - Ø 380 x Ø 177 x 60 mm
(85) Platinum resistance thermometer
(86) Zone III
(87) Mild steel skin - Ø 381 x 762 x 2 mm
(88) Zone II
(89) Zone I
(90) Caposil insulating cap - Ø 177 x Ø 40 x 70 mm

Strain measuring device

(91) Location of strain measuring device
(92) Upper potentiometer collar - TI
(93) Lower potentiometer collar - TI
(94) Outer potentiometer leg - Ø 5 x 71 mm, TI
(95) Inner potentiometer leg - Ø 5 x 56 mm, TI
(96) Micrometer head - 13 mm travel
(97) Upper potentiometer plate - 152 x 25 x 6 mm, Alum.
(98) Lower potentiometer plate - 152 x 38 x 6 mm, Alum.
(99) Sangamo displacement transducer - Type ER/± 0.2"

Loading jack

(100) Slotted 57 kg weight - Ø 300 x 100 mm
(101) Loading platform
(102) Power supply
(103) Reversing switch - Neco Electronics no. ST 27497
(104) Speed control - Neco Electronics no. ST 27497
(105) Couplings - Picador 7/8" to 3/8" & 3/8" to 3/8"
(106) Output shaft - 7/8"
(107) Motor - Neco geared motor, type SW, 1/4 hp.
(108) Rotation pod
(109) Microswitch
(110) Height indicator
(111) Jactuator - Duff-Norton, capacity 500 lbs, 6" raise
(112) Weight bearing ring - Ø 200 x Ø 80 x 13 mm
(113) Power connections
(114) Adjustment screw
(115) Rubber pads
(116) Draft protection

APPENDIX IV

FORMATION OF THE STIFFNESS MATRIX FOR THE TRIAX 3 AND THE TRIAX 6 ELEMENT

$$\underline{M} = \left[(1\ r-r_1\ z-z_1)\ \underline{I}_3 \quad (1\ r-r_1\ z-z_1)\ \underline{I}_3 \right] \tag{A4.1}$$

$$\underline{Q}^i = \{ q_1\ q_2\ q_3\ q_4\ q_5\ q_6 \} \tag{A4.2}$$

$$\underline{M}^i = \begin{bmatrix} 1 & 0 & 0 & & & \\ 1 & b_1 & b_4 & & \underline{0} & \\ 1 & -b_3 & -b_6 & & & \\ & & & 1 & 0 & 0 \\ & \underline{0} & & 1 & b_1 & b_4 \\ & & & 1 & -b_3 & -b_6 \end{bmatrix} \tag{A4.3}$$

where

$$b_1 = r_2 - r_1 \qquad b_4 = z_2 - z_1$$
$$b_2 = r_3 - r_2 \qquad b_5 = z_3 - z_2$$
$$b_3 = r_1 - r_3 \qquad b_6 = z_1 - z_3$$

$$\underline{u}^i = \{ u_1\ v_1\ u_2\ v_2\ u_3\ v_3 \} \tag{A4.4}$$

$$B^i = \frac{1}{2A} \begin{bmatrix} 2A & 0 & 0 & & & \\ -b_5 & -b_6 & -b_4 & & \underline{0} & \\ b_2 & b_3 & b_1 & & & \\ & & & 2A & 0 & 0 \\ & \underline{0} & & -b_5 & -b_6 & -b_4 \\ & & & b_2 & b_3 & b_1 \end{bmatrix} \tag{A4.5}$$

Reference is made to def. (A5.3)

$$\underline{dM} = \begin{bmatrix} o & o & o & o & o & 1 \\ o & 1 & o & o & o & o \\ \frac{1}{r} & (1-\frac{r1}{r}) & (\frac{z}{r}-\frac{z1}{r}) & o & o & o \\ o & o & 1 & o & 1 & o \end{bmatrix} \qquad (A4.6)$$

$$\underline{A}^i = \begin{bmatrix} o & o & o & o & o & 1 \\ o & 1 & o & o & o & o \\ \frac{1}{r_m} & (1-\frac{r1}{r_m}) & (\frac{z_m}{r_m}-\frac{z1}{r_m}) & o & o & o \\ o & o & 1 & o & 1 & o \end{bmatrix}$$

$$\underline{A}^i\underline{B}^i = \frac{1}{2A}\begin{bmatrix} o & o & o & b_2 & b_3 & b_1 \\ -b_5 & -b_6 & -b_4 & o & o & o \\ c_1 & c_2 & c_3 & o & o & o \\ b_2 & b_3 & b_1 & -b_5 & -b_6 & -b_4 \end{bmatrix} \qquad (A4.8)$$

where

$$c_1 = \frac{2A}{r_m} - b_5(1-\frac{r_1}{r_m}) + b_2(\frac{z_m}{r_m} - \frac{z_1}{r_m})$$

$$c_2 = b_6(1-\frac{r_1}{r_m}) + b_3(\frac{z_m}{r_m} - \frac{z_1}{r_m}) \qquad (A4.9)$$

$$c_3 = -b_4(1-\frac{r_1}{r_m}) + b_1(\frac{z_m}{r_m} - \frac{z_1}{r_m})$$

With $r_m = (r_1 + r_2 + r_3)/3$ and $z_m = (z_1 + z_2 + z_3)/3$, thus

$$c = c_1 = c_2 = c_3 = \frac{2A}{3r_m} \qquad (A4.10)$$

$$\underline{F}^i = \frac{1}{E}\begin{bmatrix} 1 & -\mu & -\mu & 0 \\ -\mu & 1 & -\mu & 0 \\ -\mu & -\mu & 1 & 0 \\ 0 & 0 & 0 & 2(1+\mu) \end{bmatrix} \qquad \text{(A4.11)}$$

where E = elastic modulus

μ = Poisson ratio

$$\underline{D}^i = \frac{E(1-\mu)}{(1+\mu)(1-2\mu)}\begin{bmatrix} 1 & \frac{\mu}{1-q} & \frac{\mu}{1-\mu} & 0 \\ \frac{\mu}{1-\mu} & 1 & \frac{\mu}{1-\mu} & 0 \\ \frac{\mu}{1-\mu} & \frac{\mu}{1-\mu} & 1 & 0 \\ 0 & 0 & 0 & \frac{1-2\mu}{2(1-\mu)} \end{bmatrix} \qquad \text{(A4.12)}$$

Introducing

$$FF = \frac{E(1-\mu)}{(1+\mu)(1-2\mu)} \qquad FC = \frac{1-2\mu}{2(1-\mu)} \qquad \text{(A4.13)}$$

$$FB = \frac{\mu}{1-\mu} \quad \text{and} \quad FA = r_m A.FF/4A^2$$

thus

$$\underline{K}^i = FA\begin{bmatrix} 0 & -b_5 & c & b_2 \\ 0 & -b_6 & c & b_3 \\ 0 & -b_4 & c & b_1 \\ b_2 & 0 & 0 & -b_5 \\ b_3 & 0 & 0 & -b_6 \\ b_1 & 0 & 0 & -b_4 \end{bmatrix}\begin{bmatrix} 1 & FB & FB & 0 \\ FB & 1 & FB & 0 \\ FB & FB & 1 & 0 \\ 0 & 0 & 0 & FC \end{bmatrix}\begin{bmatrix} 0 & 0 & 0 & b_2 & b_3 & b_1 \\ -b_5 & -b_6 & -b_4 & 0 & 0 & 0 \\ c & c & c & 0 & 0 & 0 \\ b_2 & b_3 & b_1 & -b_5 & -b_6 & -b_4 \end{bmatrix} \qquad \text{(A4.14)}$$

Expanding (IV.14), thus

$$
\begin{aligned}
k_{11} &= FA(b_5^2 - 2b_5FBc + c^2 + b_2^2FC) \\
k_{12} &= FA(b_5b_6 + FBcb_4 + c^2 + b_2b_3FC) \\
k_{13} &= FA(b_4b_5 + FBcb_6 + c^2 + b_1b_2FC) \\
k_{14} &= FA(FBb_2(c - b_5) - b_2b_5FC) \\
k_{15} &= FA(FBb_3(c - b_5) - b_2b_6FC) \\
k_{16} &= FA(FBb_1(c - b_5) - b_2b_4FC) \\
k_{22} &= FA(b_6^2 - 2b_6FBc + c^2 + b_3^2FC) \\
k_{23} &= FA(b_4b_6 + FBc(-b_6 - b_4) + c^2 + b_1b_3FC) \\
k_{24} &= FA(FBb_2(c - b_6) - b_3b_5FC) \\
k_{25} &= FA(FBb_3(c - b_6) - b_3b_6FC) \\
k_{26} &= FA(FBb_1(c - b_6) - b_3b_4FC) \qquad \text{(A4.15)} \\
k_{33} &= FA(b_4^2 - 2b_4FBc + c^2 + b_1^2FC) \\
k_{34} &= FA(FBb_2(c - b_4) - b_1b_5FC) \\
k_{35} &= FA(FBb_3(c - b_4) - b_1b_6FC) \\
k_{36} &= FA(FBb_1(c - b_4) - b_1b_4FC) \\
k_{44} &= FA(b_2^2 + b_5^2FC) \\
k_{45} &= FA(b_2b_3 + b_5b_6FC) \\
k_{46} &= FA(b_1b_2 + b_4b_5FC) \\
k_{55} &= FA(b_3^2 + b_6^2FC) \\
k_{56} &= FA(b_1b_3 + b_4b_6FC) \\
k_{66} &= FA(b_1^2 + b_4^2FC)
\end{aligned}
$$

$$
\underline{H} = \begin{bmatrix} m_i & m_j & m_k & 0 \\ n_i & n_j & n_k & 0 \\ 2m_in_i & 2m_jn_j & 2m_kn_k & 0 \\ 0 & 0 & 0 & 0 \end{bmatrix} \qquad \text{(A4.16)}
$$

$$\underline{G}^{-1} = \begin{bmatrix} 1 & \cos^2\gamma & \cos^2\beta & 0 \\ & 1 & \cos^2\alpha & 0 \\ & & 1 & 0 \\ \text{sym.} & & & 1 \end{bmatrix} \tag{A4.17}$$

$$\int e_i^m e_j^n \, ds = 2A \int e_i^m e_j^n \, de_i de_j$$

$$2A \int_0^1 e_i^m \left(\int_0^{1-e_i} e_j de_j \right) de_i$$

$$2A \int_0^1 e_i^m \frac{1}{n+1} (1-e_i)^{n+1} \, de_i$$

$$\frac{2A}{n+1} \left| \frac{1}{m+1} e_i^{m+1} (1-e_i)^{n+1} \right|_0^1 \tag{A4.18}$$

$$\int + \frac{1}{m+1} e_i^{m+1} (n+1)(1-e_i)^n \, de_i$$

$$\frac{2A}{n+1} \left| 0 + \int \frac{1}{m+1} e^{m+1} (n+1)(1-e_i)^n \, de_i \right|$$

$$\frac{2A}{m+1} \int e_i^{m+1} (1-e_i)^n \, de_i$$

$$\frac{2A}{(m+1(m+2)\ldots(m+n+1)} \int e_i^{m+n+1} \, de_i$$

$$\underline{b}_1 = \frac{A}{3} \begin{bmatrix} 3 & -1 & 0 \\ 1 & 3 & 0 \\ 0 & 0 & 8 \end{bmatrix} \qquad \underline{b}_2 = \frac{A}{3} \begin{bmatrix} -1 & -1 & 4 \\ 3 & -1 & 0 \\ 0 & 4 & 4 \end{bmatrix} \tag{A4.19}$$

$$\underline{c}_{11} = \frac{1}{15} \begin{bmatrix} 3 & -1 & -2 \\ -1 & 3 & -2 \\ -2 & -2 & 24 \end{bmatrix} \qquad \underline{c}_{12} = \frac{1}{15} \begin{bmatrix} -1 & -2 & 3 \\ 3 & -2 & -1 \\ -2 & 14 & 8 \end{bmatrix}$$

$$\underline{c}_{13} = \frac{1}{15}\begin{bmatrix} -2 & -2 & 14 \\ 3 & -1 & -2 \\ -1 & 3 & 8 \end{bmatrix} \qquad \underline{c}_{22} = \frac{1}{15}\begin{bmatrix} 3 & -2 & -1 \\ -2 & 9 & 3 \\ -1 & 3 & 8 \end{bmatrix} \tag{A4.20}$$

$$\underline{c}_{23} = \frac{1}{15}\begin{bmatrix} -2 & -1 & 3 \\ 9 & -2 & 3 \\ 3 & 3 & 4 \end{bmatrix} \qquad \underline{c}_{33} = \frac{1}{15}\begin{bmatrix} 9 & -2 & 3 \\ -2 & 3 & -1 \\ 3 & -1 & 8 \end{bmatrix}$$

$$\underline{A}^t \underline{K}_{NN} e_3 \underline{A} = \begin{bmatrix} k_{11}c_{11} & k_{12}c_{12} & k_{13}c_{13}^t \\ & k_{22}c_{22} & k_{23}c_{23} \\ \text{sym.} & & k_{33}c_{33} \end{bmatrix}$$

$$\underline{A}^t \underline{K}_{NN} e_1 \underline{A} = \begin{bmatrix} k_{11}c_{33} & k_{12}c_{13} & k_{13}c_{23}^t \\ & k_{22}c_{11} & k_{23}c_{12} \\ \text{sym.} & & k_{33}c_{22} \end{bmatrix}$$

$$\underline{A}^t \underline{K}_{NN} e_2 \underline{A} = \begin{bmatrix} k_{11}c_{22} & k_{12}c_{23} & k_{13}c_{12}^t \\ & k_{22}c_{33} & k_{23}c_{13} \\ \text{sym.} & & k_{33}c_{11} \end{bmatrix}$$

$$\{ \; u_1 \; v_1 \; u_4 \; v_4 \; u_2 \; v_2 \; u_5 \; v_5 \; u_3 \; v_3 \; u_6 \; v_6 \; \}$$

$$\underline{o}^i = \begin{bmatrix} - & - & + & + & 0 & 0 & 0 & 0 & 0 & 0 & 0 & 0 \\ 0 & 0 & - & - & + & + & 0 & 0 & 0 & 0 & 0 & 0 \\ 0 & 0 & 0 & 0 & 0 & 0 & + & + & 0 & 0 & - & - \\ 0 & 0 & 0 & 0 & - & - & + & + & 0 & 0 & 0 & 0 \\ 0 & 0 & 0 & 0 & 0 & 0 & - & - & + & + & 0 & 0 \\ 0 & 0 & - & - & 0 & 0 & 0 & 0 & 0 & 0 & + & + \\ 0 & 0 & 0 & 0 & 0 & 0 & 0 & 0 & - & - & + & + \\ + & + & 0 & 0 & 0 & 0 & 0 & 0 & 0 & 0 & - & - \\ 0 & 0 & + & + & 0 & 0 & - & - & 0 & 0 & 0 & 0 \end{bmatrix} \begin{bmatrix} u_{14} \\ u_{42} \\ u_{65} \\ u_{25} \\ u_{53} \\ u_{46} \\ u_{36} \\ u_{61} \\ u_{54} \end{bmatrix}$$

C_i =	e_i =
0.064742483	-0.949107912
0.139852695	-0.741531185
0.190915025	-0.405845151
0.208979591	0.000000000
0.190915025	0.405845151
0.139852695	0.741531185
0.064742483	0.949107912

(A4.23)

$$\underline{T} = \begin{bmatrix}
1^2 & 0 & 1.4 & 0 & 1.2 & 0 & 1.5 & 0 & 1.3 & 0 & 1.6 & 0 \\
 & 0 & 0 & 0 & 0 & 0 & 0 & 0 & 0 & 0 & 0 & 0 \\
 & & 4^2 & 0 & 4.2 & 0 & 4.5 & 0 & 4.3 & 0 & 4.6 & 0 \\
 & & & 0 & 0 & 0 & 0 & 0 & 0 & 0 & 0 & 0 \\
 & & & & 2^2 & 0 & 2.5 & 0 & 2.3 & 0 & 2.6 & 0 \\
 & & & & & 0 & 0 & 0 & 0 & 0 & 0 & 0 \\
 & & & & & & 5^2 & 0 & 5.3 & 0 & 5.6 & 0 \\
 & & & & & & & 0 & 0 & 0 & 0 & 0 \\
 & & & & & & & & 3^2 & 0 & 3.6 & 0 \\
 & & & & & & & & & 0 & 0 & 0 \\
 & & & & & & & & & & 6^2 & 0 \\
\text{sym.} & & & & & & & & & & & 0
\end{bmatrix} \quad \text{(A4.24)}$$

where

$$1^2 = 4(1^4,2^0) - 4(1^3,2^0) + (1^2,2^0)$$

$$2^2 = 4(2^4,3^0) - 4(2^3,3^0) + (2^2,3^0)$$

$$3^2 = 3(3^4,1^0) - 4(3^3,1^0) + (3^2,1^0)$$

$$4^2 = 16(1^2,2^2)$$

$$5^2 = 16(2^2,3^2)$$

$$6^2 = 16(3^2,1^2)$$

$$1.2 = 4(1^2,2^2) - 2(1^2,2^2) - 2(1^2,2^2) + (1,2)$$

$$2.3 = 4(2^2,3^2) - 2(2^2,3^2) - 2(2^2,3^2) + (2,3)$$

$$1.3 = 4(3^2,1^2) - 2(3^2,1) - 2(3,1^2) + (3,1)$$

$$1.4 = 8(1^3,2) - 4(1^2,2)$$

$$2.5 = 8(2^3,3) - 4(2^2,3)$$

$$3.6 = 8(3^3,1) - 4(3^2,1)$$

$$1.5 = 12(3,1^2) - 8(3,1^3) - 8(3^2,1^2) - 4(3,1) + 4(3^2,1)$$

$$2.6 = 12(1,2^2) - 8(1,2^3) - 8(1^2,2^2) - 4(1,2) + 4(1^2,2)$$

$$3.4 = 12(2,3^2) - 8(2,3^3) - 8(2^2,3^2) - 4(2,3) + 4(2^2,3)$$

$$4.5 = 16(1,2^2) - 16(1^2,2^2) - 2(1,2^2) + (1,2)$$

$$5.6 = 16(2,3^2) - 16(2^2,3^2) - 16(2,3^2)$$

$$4.6 = 16(3,1^2) - 16(3^2,1^2) - 16(3,1^3)$$

$$\underline{S} = \frac{1}{15}\begin{bmatrix}
2 & 0 & 3 & 0 & -1 & 0 & -1 & 0 & -1 & 0 & 3 & 0 \\
-1 & 0 & 3 & 0 & 2 & 0 & 3 & 0 & -1 & 0 & -1 & 0 \\
-1 & 0 & 4 & 0 & -1 & 0 & 8 & 0 & 2 & 0 & 8 & 0 \\
-1 & 0 & 3 & 0 & 2 & 0 & 3 & 0 & -1 & 0 & -1 & 0 \\
-1 & 0 & -1 & 0 & -1 & 0 & 3 & 0 & 2 & 0 & 3 & 0 \\
2 & 0 & 8 & 0 & -1 & 0 & 4 & 0 & -1 & 0 & 8 & 0 \\
-1 & 0 & -1 & 0 & -1 & 0 & 3 & 0 & 2 & 0 & 3 & 0 \\
2 & 0 & 3 & 0 & -1 & 0 & -1 & 0 & -1 & 0 & 3 & 0 \\
-1 & 0 & 8 & 0 & 2 & 0 & 8 & 0 & -1 & 0 & 4 & 0
\end{bmatrix} \qquad \text{(A4.25)}$$

APPENDIX V

FORMATION OF THE THERMAL CONDUCTIVITY MATRIX FOR THE TRIAX 3 ELEMENT

$$\underline{M} = \begin{bmatrix} 1 & r-r_1 & z-z_1 \end{bmatrix} \tag{A5.1}$$

$$\underline{M}^i = \begin{bmatrix} 1 & 0 & 0 \\ 1 & b_1 & b_4 \\ 1 & -b_3 & -b_6 \end{bmatrix} \tag{A5.2}$$

where the b_i follow def. (A4.3)

$$\underline{B}^i = \frac{1}{2A} \begin{bmatrix} 2A & 0 & 0 \\ -b_5 & -b_6 & -b_4 \\ b_2 & b_3 & b_1 \end{bmatrix} \tag{A5.3}$$

where

$2A = b_3b_4 - b_1b_6$ $\qquad -b_5 = b_4 + b_6$

A = area of element $\qquad b_2 = -b_3 - b_1$

$$\underline{A}_r^i = \begin{bmatrix} 0 & 1 & 0 \end{bmatrix} \tag{A5.4}$$

$$\underline{A}_z^i = \begin{bmatrix} 0 & 0 & 1 \end{bmatrix}$$

$$\underline{A}_r^i\underline{B}^i = \frac{1}{2A} \begin{bmatrix} -b_5 & -b_6 & -b_4 \end{bmatrix} \tag{A5.5}$$

$$\underline{A}_r^i\underline{B}^i = \frac{1}{2A} \begin{bmatrix} b_2 & b_3 & b_1 \end{bmatrix}$$

$\underline{M}^i\underline{B}^i$ is a (3x3) identity matrix

$$(\underline{A}_r^i\underline{B}^i\underline{C}^i) = \frac{1}{2A} \begin{bmatrix} 1 & 0 & 0 \\ 0 & 1 & 0 \\ 0 & 0 & 1 \end{bmatrix} \begin{bmatrix} -b_5 \\ -b_6 \\ -b_4 \end{bmatrix} \tag{A5.6}$$

$$(\underline{A}^i \underline{B}^i \underline{C}^i) = \frac{1}{2A} \begin{bmatrix} 1 & 0 & 0 \\ 0 & 1 & 0 \\ 0 & 0 & 1 \end{bmatrix} \begin{bmatrix} b_2 \\ b_3 \\ b_1 \end{bmatrix}$$

$$\underline{K}^i = \frac{r_m^i}{4A} i \quad k_r \begin{bmatrix} -b_5 \\ -b_6 \\ -b_4 \end{bmatrix} \begin{bmatrix} 1 & 0 & 0 \\ 0 & 1 & 0 \\ 0 & 0 & 1 \end{bmatrix} \begin{bmatrix} -b_5 & -b_6 & -b_4 \end{bmatrix}$$

$$k_z \begin{bmatrix} b_2 \\ b_3 \\ b_1 \end{bmatrix} \begin{bmatrix} 1 & 0 & 0 \\ 0 & 1 & 0 \\ 0 & 0 & 1 \end{bmatrix} \begin{bmatrix} b_2 & b_3 & b_1 \end{bmatrix} \tag{A5.7}$$

$$\underline{K}^i = \frac{r_m^i}{4A} i \quad k_r \begin{bmatrix} b_5b_5 & b_5b_6 & b_5b_4 \\ & b_6b_6 & b_6b_4 \\ \text{sym.} & & b_4b_4 \end{bmatrix}$$

$$+ \quad k_z \begin{bmatrix} b_2b_2 & b_2b_3 & b_5b_4 \\ & b_3b_3 & b_3b_1 \\ \text{sym.} & & b_1b_1 \end{bmatrix} \tag{A5.8}$$

$$\underline{F}^i = r^i A^i \, (q + o\Theta' - \rho c \, \Theta'_t) \begin{bmatrix} 1 \\ 1 \\ 1 \end{bmatrix} \tag{A5.9}$$

APPENDIX VI

TABLE OF CREEP DATA

Table A6.1. Thermal creep strains for s = 0.2 in 100μ

T / t	20	40	60	80	110	140	200	250	300	350	400	450	500°C
0 h	3.2	3.4	4.0	3.8	3.6	3.8	4.2	4.6	5.2	6.8	9.2	38.0	*
¼	3.4	3.5	4.2	3.9	3.8	4.0	4.5	5.2	6.0	7.2	12.2	48.2	
½	3.5	3.6	4.3	4.0	4.0	4.2	4.6	5.6	6.4	7.4	13.2	50.6	
1	3.6	3.8	4.4	4.1	4.2	4.3	4.7	6.2	6.6	7.6	14.4	54.1	
2	3.7	4.0	4.5	4.2	4.3	4.4	4.8	6.6	6.8	8.4	16.4	59.2	
3	3.7	4.2	4.5	4.2	4.4	4.6	5.0	7.0	7.2	9.0	17.4	61.4	
6	3.8	4.3	4.6	4.3	4.5	4.8	5.5	7.4	7.6	10.6	18.6	66.8	
12	3.8	4.4	4.6	4.4	5.0	5.0	6.0	7.8	8.0	12.4	20.8	71.8	
18	3.9	4.5	4.7	4.5	5.2	5.5	6.6	8.2	8.6	13.2	22.6	75.2	
1 d	4.0	4.6	4.8	5.4	5.9	7.2	8.6	8.8	9.0	14.0	24.2	78.6	
1.5	4.1	4.8	5.0	4.7	5.7	6.2	8.0	9.6	9.7	15.0	26.0	80.8	
2	4.2	5.0	5.2	4.8	5.9	6.8	8.4	10.2	10.4	15.6	28.6	84.2	
2.5	4.2	5.1	5.3	5.0	6.1	7.0	9.0	10.4	10.9	16.4	29.4	86.6	
3	4.2	5.2	5.4	5.2	6.8	8.2	9.4	10.7	11.4	17.2	29.8	88.4	
3.5	4.3	5.3	5.4	5.3	6.4	7.3	9.5	11.0	11.8	17.5	30.2	90.4	
4	4.4	5.4	5.5	5.4	6.6	7.4	9.6	11.4	12.2	17.6	30.5	92.0	
4.5	4.4	5.5	5.6	5.5	6.8	7.5	9.7	11.7	12.6	18.0	31.0	93.3	
5	4.4	5.6	5.8	5.6	6.9	7.6	9.8	12.0	13.0	18.2	31.4	94.6	
5.5	4.4	5.6	6.0	5.7	7.0	7.7	9.9	12.2	13.3	18.4	32.0	95.8	
6	4.4	5.7	6.1	5.8	7.1	7.8	10.0	12.4	13.6	18.6	32.6	97.0	
6.5	4.5	5.7	6.2	6.0	7.2	7.8	10.1	12.5	14.0	18.8	33.2	98.2	
7	4.5	5.8	6.2	6.1	7.3	7.9	10.2	12.6	14.2	19.2	33.6	99.0	
Δ	3.2	3.3	3.4	3.4	3.2	3.3	3.5	4.0	4.7	5.7	7.3	9.2	

Table A6.2. Thermal creep strains for s = 0.4 in 100 μ

t \ T	20	40	60	80	110	140	200	250	300	350	400	450°C
0 h	6.4	7.0	8.8	9.2	7.4	8.0	8.6	11.3	12.3	12.3	17.4	*
¼	6.6	7.2	9.1	9.5	7.5	8.4	9.1	13.1	14.1	19.3	31.4	
½	6.7	7.4	9.3	9.7	7.6	8.6	9.4	13.3	14.5	20.1	33.0	
1	6.8	7.6	9.5	9.9	7.8	8.8	9.6	13.5	15.0	21.3	35.2	
2	6.9	7.8	9.6	10.1	7.9	9.2	10.0	13.7	15.5	22.6	37.3	
3	7.0	8.0	9.7	10.3	8.0	9.4	10.3	13.9	15.9	23.2	39.4	
6	7.2	8.7	10.2	10.9	8.2	10.1	11.1	14.8	16.7	24.4	42.6	
12	7.6	9.4	10.9	11.6	8.4	10.7	12.2	15.8	17.8	26.1	48.5	
18	7.9	10.0	11.2	11.9	9.1	11.1	12.8	16.4	18.7	27.6	54.7	
1 d	8.1	10.4	11.5	12.2	9.8	11.3	13.2	17.0	19.5	28.6	60.5	
1.5	8.4	11.1	11.8	12.6	10.6	11.9	13.8	18.6	20.3	30.2	67.1	
2	8.6	11.7	12.2	13.1	11.2	12.3	14.2	20.3	21.7	31.4	73.4	
2.5	8.7	12.0	12.5	13.4	11.8	12.9	15.6	21.5	22.5	32.6	76.8	
3	8.9	12.3	12.7	13.7	12.2	13.3	16.2	21.9	23.2	33.7	79.5	
3.5	9.0	12.6	12.9	13.8	12.6	13.7	16.6	22.1	23.8	34.7	81.5	
4	9.1	12.9	13.2	14.1	13.2	14.1	16.8	22.4	24.6	36.6	83.6	
4.5	9.2	13.1	13.4	14.3	13.2	14.3	17.1	23.0	25.6	37.9	86.0	
5	9.3	13.3	13.6	14.5	13.2	14.5	17.8	23.2	26.4	38.7	88.0	
5.5	9.4	13.5	13.7	14.7	13.6	14.8	18.1	23.6	26.5	38.9	90.3	
6	9.5	13.7	13.8	14.8	14.2	15.0	18.4	23.8	26.8	39.2	92.5	
6.5	9.6	13.8	14.0	15.0	14.6	15.3	18.8	24.1	26.8	39.4	96.0	
7	9.6	13.9	14.1	15.2	14.9	15.6	19.8	24.3	26.8	39.5	97.6	
Δ	5.7	6.7	7.2	7.2	6.7	6.8	7.6	8.8	10.2	12.0	14.0	

Table A6.3. Thermal creep strains for s = 0.66 in 100 μ

T / t	20	40	60	80	110	140	200	250	300	350	400°C
0 h	10.6	11.6	13.6	13.8	11.2	12.6	17.0	16.8	22.6	32.0	*
¼	11.0	13.0	15.2	15.5	12.8	13.4	18.6	18.2	25.8	38.4	
½	11.3	13.6	16.0	15.7	13.0	13.9	19.0	18.8	27.0	40.4	
1	11.6	14.0	16.3	16.2	13.6	14.4	19.6	19.4	28.2	43.2	
2	11.7	14.2	17.0	16.8	14.2	15.0	20.4	20.2	29.4	44.8	
3	11.8	14.5	17.4	17.5	14.6	15.4	21.0	21.2	30.4	48.6	
6	12.0	15.0	18.2	18.2	15.6	15.8	21.8	24.0	32.6	53.4	
12	12.2	16.5	19.6	19.5	15.7	16.2	23.0	27.5	34.8	58.4	
18	12.7	17.0	20.2	20.3	15.8	16.6	25.2	29.0	37.2	64.8	
1 d	13.2	17.6	20.6	21.0	16.8	17.0	26.4	30.6	39.0	68.4	
1.5	13.3	18.2	21.8	21.9	17.4	17.4	27.8	32.5	39.8	75.6	
2	13.4	18.3	22.4	22.4	17.6	17.8	29.0	33.8	41.4	85.0	
2.5	13.5	18.4	23.0	22.8	17.0	18.1	30.4	35.0	42.8	*	
3	13.6	18.7	23.4	23.6	17.4	18.4	31.4	35.4	43.2		
3.5	13.7	18.9	23.6	23.7	17.6	18.8	31.6	36.2	43.4		
4	13.8	19.0	24.0	24.0	17.8	19.2	32.0	37.0	43.6		
4.5	13.9	19.2	24.2	24.2	18.0	19.4	32.6	37.5	43.8		
5	14.0	19.5	24.6	24.8	18.2	19.5	33.4	38.1	43.9		
5.5	14.1	19.5	24.8	24.8	18.4	19.6	33.8	38.6	44.0		
6	14.2	19.6	25.2	25.0	18.6	19.8	34.0	39.0	44.4		
6.5	14.2	19.6	25.4	25.2	18.8	20.0	34.2	39.2	45.6		
7	14.2	19.7	25.6	25.3	19.0	20.0	34.2	39.6	46.0		
Δ	9.2	10.0	10.5	10.6	10.1	11.0	13.0	15.0	17.2		

Table A6.4. Normalized thermal relaxation weighting factors

T / t	20	40	60	80	110	140	200	250	300°C
0 d	1.0	1.0	1.0	1.0	1.0	1.0	1.0	1.0	1.0
0.1	0.68	0.71	0.88	0.86	0.62	0.57	0.49	0.42	0.38
0.2	0.66	0.65	0.81	0.79	0.56	0.52	0.44	0.38	0.34
0.3	0.64	0.62	0.77	0.75	0.53	0.49	0.41	0.36	0.32
0.4	0.63	0.60	0.74	0.72	0.51	0.47	0.39	0.35	0.31
0.5	0.62	0.58	0.72	0.70	0.49	0.45	0.38	0.34	0.30
0.6	0.61	0.57	0.70	0.68	0.48	0.44	0.37	0.33	0.28
0.7	0.60	0.56	0.68	0.67	0.46	0.43	0.36	0.32	0.28
0.8	0.60	0.55	0.67	0.65	0.45	0.42	0.35	0.31	0.27
0.9	0.59	0.54	0.66	0.64	0.44	0.41	0.34	0.30	0.26
1	0.59	0.53	0.65	0.63	0.43	0.40	0.33	0.29	0.26
2	0.56	0.48	0.58	0.55	0.38	0.35	0.29	0.25	0.22
3	0.55	0.45	0.54	0.51	0.35	0.32	0.27	0.23	0.20
4	0.54	0.43	0.51	0.48	0.33	0.30	0.25	0.21	0.18
5	0.52	0.41	0.49	0.46	0.31	0.28	0.23	0.19	0.17
6	0.51	0.39	0.47	0.44	0.30	0.27	0.22	0.19	0.16
7	0.50	0.38	0.45	0.42	0.28	0.26	0.21	0.18	0.15
8	0.50	0.38	0.44	0.40	0.27	0.25	0.20	0.17	0.15
9	0.49	0.37	0.43	0.39	0.26	0.24	0.19	0.16	0.14
10	0.49	0.36	0.42	0.39	0.25	0.23	0.19	0.15	0.13
15	0.48	0.33	0.38	0.34	0.22	0.20	0.16	0.13	0.11

Errata

pg. ii : Professor Dr. Ing. TH. Jaeger

pg. viii : Fig. 6.7 ... a __ plane

pg. 1 : aerial

pg. 10 : in a meaningful manner

pg. 37 : in and out

pg. 60 : cold

pg. 66 : + sign instead of - sign

pg. 67 : temperatures higher than or equal to ...

: where $e(s,T) = 1.5\ (0.001\ T - 0.18)\ (\frac{s}{0.1} - 1)$

pg. 73 : Thermoelasto-Plasticity

: the collapse of the specimens

pg. 77 : and the reference value by

pg. 97 : they

: $d\beta_j$

pg. 98 : (6.16)

pg. 102 : repeatedly

pg. 117 : last strain

pg. 125 : quantities

pg. 126 : (7.34)

pg. 127 : describe_

pg. 135 : (7.57)

pg. 137 : 7.3.4.1 to

: in eq. (7.63) comma missing

: in (7.65) check subscript

: differential equation

pg. 149 : eq. (A4.11)

pg. 150 : eq. (A4.13)

pg.151 : is that they

pg. 175 : (A4.25)